INTERNATIONAL COLLOQUIUM

STABILITY OF STEEL STRUCTURES

HUNGARY, BUDAPEST 1990

PRELIMINARY REPORT

VOLUME IV.

TECHNICAL UNIVERSITY OF BUDAPEST

HUNGARIAN ACADEMY OF SCIENCES

STRUCTURAL STABILITY RESEARCH COUNCIL

INTERNATIONAL ASSOCIATION FOR BRIDGE
AND STRUCTURAL ENGINEERING

INTERNATIONAL COLLOQUIUM
EAST-EUROPEAN SESSION

STABILITY OF STEEL STRUCTURES

PRELIMINARY REPORT

VOLUME IV.

EDITED BY
M. IVÁNYI
B. VERŐCI

HUNGARY, BUDAPEST
APRIL 25-27, 1990

Címlap
részlet Somogyi Győző
rajzából

Cover
a piece of Győző Somogyi's
drawing

ISBN 963-421-487-8 ö

ISBN. 963.420.221.7 IV

Felelős szerkesztők: Dr. Iványi Miklós
Dr. Verőci Béla

1990

Kiadja: a Budapesti Műszaki Egyetem
Acélszerkezetek Tanszék

A kiadásért felelős: az Acélszerkezetek
Tanszék vezetője

Készült: a Budapesti Műszaki Egyetem
Sokszorosító Üzemében
Felelős vezető: Miszori Sándor

Példányszám: 350, Méret: B/5

SESSION 13

COMPOSITE MEMBERS

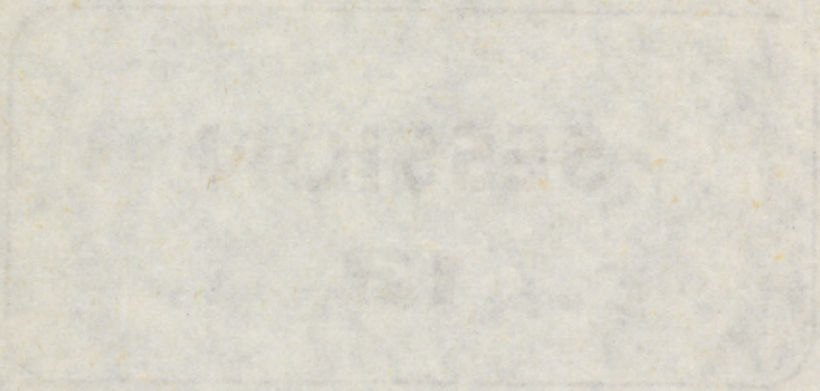

(1)
ALTMANN, Roland (1)
MAQUOI, René (2)
JASPART, Jean-Pierre (3)

EXPERIMENTAL STUDY OF THE NON-LINEAR BEHAVIOUR OF BEAM-TO-COLUMN COMPOSITE JOINTS.

INTERNATIONAL COLLOQUIUM
STABILITY OF STEEL STRUCTURES
BUDAPEST, HUNGARY, 1990
PRELIMINARY REPORT

Summary : This paper presents the main results of an experimental research recently performed at the University of Liège, the aim of which was to analyse the behaviour till collapse of strong axis beam-to-column composite joints commonly used in practice.

1. INTRODUCTION

Many multi-storey frames are built now in such a way that the concrete floors contribute to the strength of the steel skeleton and participate to the structural behaviour of the framing.
Work performed in this field has however principally focused on the study of the individual frame components (columns and composite floors) and not so much on that of the connections between these elements. This has led the departments RPS of ARBED-Recherches (Luxemburg) and MSM of the University of Liège (Belgium) to introduce a two and a half years research project (01.07.87 to 31.12.89) to the Commission of the European Communities (agreement N° 7210-SA/507 C.E.C.-ARBED) in view to :

- investigate experimentally the behaviour under static loading and until collapse of 38 interior composite joints between a steel column and a floor composed of steel beams surmounted by a reinforced concrete slab on the one hand, and of 18 interior and exterior bare steel joints on the other hand;
- develop mathematical methods for the prediction of the non linear response till collapse of these joints on base of the knowledge of their mechanical and geometrical properties;
- develop a program for the non linear calculation of steel and composite frames with semi-rigid joints.

---

(1) Engineer at ARBED-Recherches, Luxemburg
(2) Professor of Civil Engineering, University of Liège, Belgium
(3) Assistant, University of Liège, Belgium.

(2)
This paper presents the main results of the experimental part of the research dealing with the composite joints. Another paper is aimed at presenting the mathematical modelling of the behaviour of these joints.

Two types of cleat connections between steel beams and columns are considered; they only differ by the presence or not of one cleat connecting the upper beam flange to the column flange (figure 1).
All the connections use bolts of quality 8.8 (H.S.bolts) preloaded with a specified torque moment associated to a not-controlled hand tightening.

A clearance of 1 mm is adopted between bolts and their holes while the clearance between the beam and the adjacent column flange is 15 mm.

The slab thickness is kept constant : 12 cm. It breadth is fixed to 120 cm because of considerations dealing with the slab effective width.

Concrete strength has been kept as constant as possible and corresponds to normal concrete.

The concrete slab is connected to the steel beam by means of shear stud connectors allowing for a full interaction.

The continuity of the concrete slab at the column support is achieved by means of two layers of six rebars each.

All the mechanical and geometrical properties of the specimens have been measured but are not listed here.

The following parameters have been investigated :

- the type of sections used as column and beams: it was decided to use a single HE section (HEB 200) as column and IPE sections as beams, in accordance with a current practice for multi-storey buildings;

- the relative beam-to-column stiffness: because of the role played by the beam depth in the force distribution between the steel and concrete components of a composite joint (with a specified column section), three different beam depths are chosen : IPE 240 - 300 - 360.

- the sizes of the connecting cleats: for constructional and structural reasons, unequal leg 150 X 90 mm cleats are used, the larger leg being in contact with the beam. For sake of simplicity, all the cleats in a specified connection are identical. Two different values of thickness are considered with a view to assess the influence of the cleat flexibility:
  a) 150 x 90 x 10 mm cleats
  b) 150 x 90 x 13 mm cleats

- the percentage of steel reinforcement in the slab : three different bar diameters (10,14 and 18 mm) have been selected in order to cover the current range : 0,67 % -1,3 % -2,1 %.

The collapse of the composite joints with IPE 240 beams being associated to the buckling of the lower beam flange and not to the collapse of the connection itself, therefore only the results of the test series with IPE300 and 360 beams are presented in this paper (see table 1).

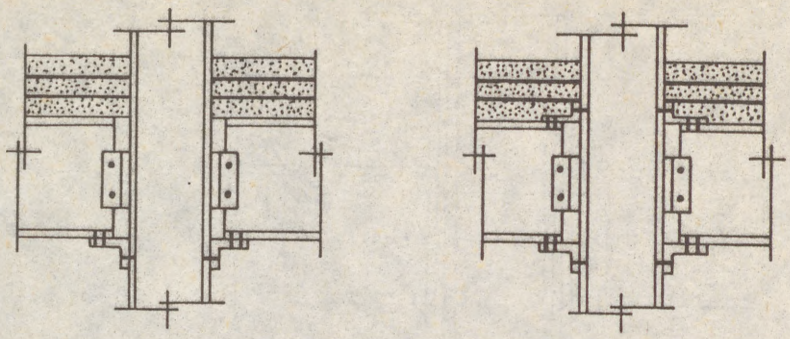

(a) composite joints with 2 cleats per connection (tests 30 x 2c or 36 x 2c)

(b) composite joints with 3 cleats per connection (tests 30 x 3c or 36 x 3c)

Figure 1 - Types of composite joints tested in laboratory.

2. TESTING ARRANGEMENT

The experimental testing arrangement is given in figure 2.
Beams and columns are guided laterally so that any displacement of the test specimen perpendicular to the plane of loading is prevented.
The test specimen is loaded by means of a 50 tons jack, permitting a maximum vertical displacement of 20 cm.

The load is increased step by step either up to the collapse of the joint, or up to the maximum vertical displacement. Unloadings are carried out during the tests.

The specimens are instrumented as described in figure 2 and 3.

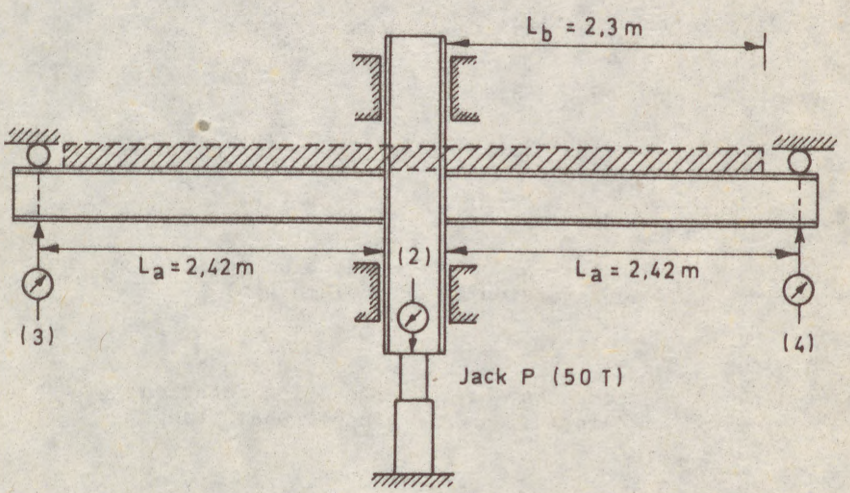

Figure 2 - Cruciform testing arrangement and location of displacement transducers.

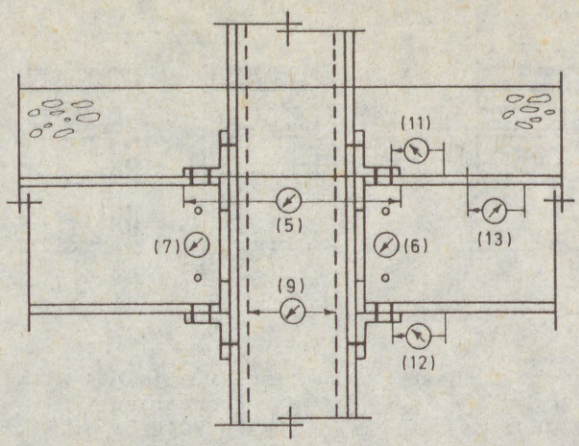

Figure 3 - Location of the displacement transducers and of rotation transducers (6-7) in the vicinity of the connections.

3. EXPERIMENTAL CURVES.

The following deformability curves have been plotted for each test performed (see figures 2 and 3):

1) M-w curve (w = vectical displacement of the column)

. $w = (2) - \frac{(3) + (4)}{2}$

2) M-ϕ curve (ϕ = relative rotation of the connection)

. $\phi = \frac{(6) + (7)}{2}$ (first assessment)

. $\phi = \frac{(5) - [(9) + 2 \cdot (12)]}{2H_b}$ (second assessment)

where H_b = depth of the beams.

3) M-ϕ_{ws} curve (ϕ_{ws} = relative rotation without slip of the connection)

. $\phi_{ws} = \frac{(5) - (9)}{2H_b}$

4) M-ϕ_{cz} curve (ϕ_{cz} = component of the connection rotation ϕ_{ws} due to the compression in the column web)

. $\phi_{cz} = \frac{(9)}{2H_b}$

5) M-ϕ_{bf} curve (ϕ_{bf} = component of the connection rotation ϕ_{ws} due to the deformation at the upper beam flange)

. $\phi_{TZ} = \frac{(5)}{2H_b}$

For each test, the strains have been measured in the beam flanges and in the rebars (20 strain gages) in view to explore the stress distribution in

(5) the two beam sections located just near the steel connections. This has enabled to report for each test :

(6) the mean values of the strains in the steel reinforcement of the concrete slab;

(7) the mean values of the stresses in the steel reinforcement of the concrete slab;

(8) the mean values of the stresses in the beam flanges.

It must be noted that the "connection relative rotation M-ϕ_{ws} curve without slip" obtained by combination of the measurements n° 5 and 9 (figure 3) differs from the one which would result from another test on an equivalent connection but actually with no slip (cleats welded to the beam for instance); this may be explained by the dependence of the measurement n° 5 upon the slip value at the lower beam flanges.

4. INTERPRETATION OF THE EXPERIMENTAL RESULTS.

4.1. General description of the results.

The nature of the collapse for each specimen tested as well as the ultimate bending moment supported by the connections are presented in table 1. It may be seen that these maximum moments represent an appreciable percentage of the theoretical plastic moment of the composite beam sections.

The collapse of the partial-strength connections tested is linked up to the buckling of the transversally compressed column web or to the excessive yielding of the rebars according to the percentage of reinforcement in the concrete slab.
A brittle failure of sheared bolts has only been encountered for the test 30x2c.1; it seems to result more from a local problem of load distribution between the bolts connecting the lower cleats to the flange of the left beam than from an excess of stress in the bolts.

The test results highlight the importance of the flexibility of the connections due to the slip between the lower cleat and the beam flange.
It is not very difficult and expensive to prevent such slip with the result of improved rotational characteristics of the composite connections tested in the frame of this research.

The two other components of the connection deformability registered during the tests in laboratory are related to :

- the compression in the column web ;
- the variation of the distance between the upper flanges of left and right beams (this measurement gives an idea of the concrete slab axial deformation).

The relative importance of these two sources of flexibility is strongly dependent on the percentage of reinforcement in the concrete slab.

Test number	Thickness of the cleats (mm)	Diameter of rebars (mm)	Type of collapse [x]	M_{max}/M_p (%)	Test number	Thickness of the cleats (mm)	Diameter of rebars (mm)	Type of collapse	M_{max}/M_p (%)
30x3c.2	10	10	a, c	99	36x3c.1	10	10	a	77
30x3c.3	10	14	a	98	36x3c.2	10	14	a	80
30x3c.1	10	18	a	94	36x3c.3	10	18	a	79
30x3c.6	13	10	c (a)	114	36x3c.5	13	10	a	79
30x3c.8	13	14	a	95	36x3c.6	13	14	a	85
30x3c.7	13	18	a	95	36x3c.7	13	18	a	84
30x2c.2	10	10	c	81	36x2c.2	10	10	b	67
30x2c.1	10	14	d	89	36x2c.1	10	14	a	82
30x2c.3	10	18	a	94	36x2c.3	10	18	a	78
30x2c.5	13	10	c	79	36x2c.7	13	10	c	67
30x2c.6	13	14	a	99	36x2c.6	13	14	a	83
30x2c.7	13	18	a	94	36x2c.5	13	18	a	77

[x] a: buckling of the column web at the level of the lower cleats ;

b: collapse (in tension) of the reinforcements in the concrete slab ;

c: attaintment of the maximum permissible vertical displacement of the column (20 cm) due to the excessive yielding of the reinforcements in the concrete slab ;

d: collapse (in shear) of the bolts connecting the lower cleats and the beam flanges.

Table 1 - Description of the collapse for the performed tests.

4.2. Influence of the parameters choosen for the tests.

The parameters investigated in the experimental part of this research are the following :
- the thickness of the cleats ;
- the number of cleats ;
- the percentage of reinforcement in the slab.

The results of both presented test series (connections with IPE300 and 360 beams) lead to conclude to a similar influence of the here above recalled parameters according to the type of beam. Only the "IPE360 serie" will consequently be discussed in this paper.

Figure 4 for instance shows clearly the benefical influence of the percentage of reinforcement on the rigidity and on the ultimate strength of the connections. The substantial rotation capacity of the composite connections with bars of 10 mm in the concrete slab is linked up to the tensile yielding of the rebars.

Figures 5 to 7 allow to highlight the influence of the cleat thickness on the semi-rigid behaviour of the composite connections. It may be seen that the rotational rigidity and the ultimate capacity of the connections are not strongly affected by this factor, more especially as the differences registered may be partly explained by :
- the relative importance of the slip between cleats and beam flanges ;
- the buckling direction of the column web, which influences the value of the collapse buckling load, and which is dependent on the initial out-of-plane deformation of the web, on its direction, and on the

(7)
position of the cleats connecting the beam web to the column (they are submitted to compression during the test and tend consequently to produce small bending moments in the column web).

The necessity to connect the upper flange of the beam to the column by means of a third cleat may be discussed on base of the diagrams of figures 5 to 7 too. The upper cleat do not affect significantly the behaviour of the connection (figures 6 and 7) as far as the plastic resistance of the rebars is not reached in the section of the connection and the associated plastic deformation has not developed. In the other cases (figure 5), an additional bending moment related to the resistance of the upper cleat submitted to tension forces is carried over to the column by the composite beams.

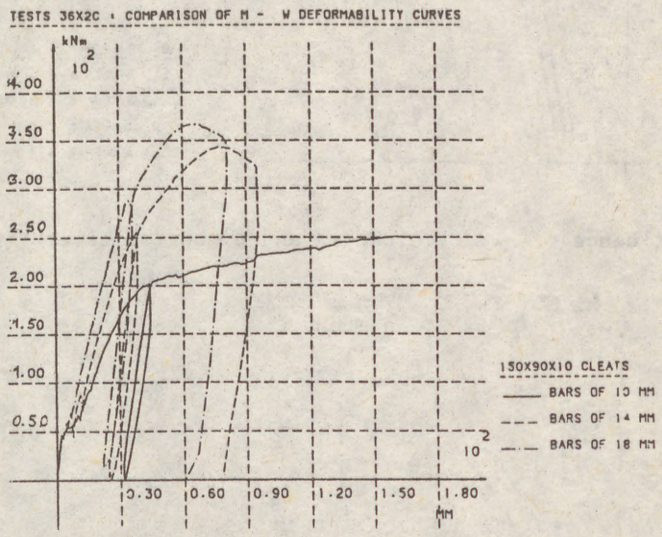

Figure 4-Influence of the percentage of reinforcement in the concrete slab.

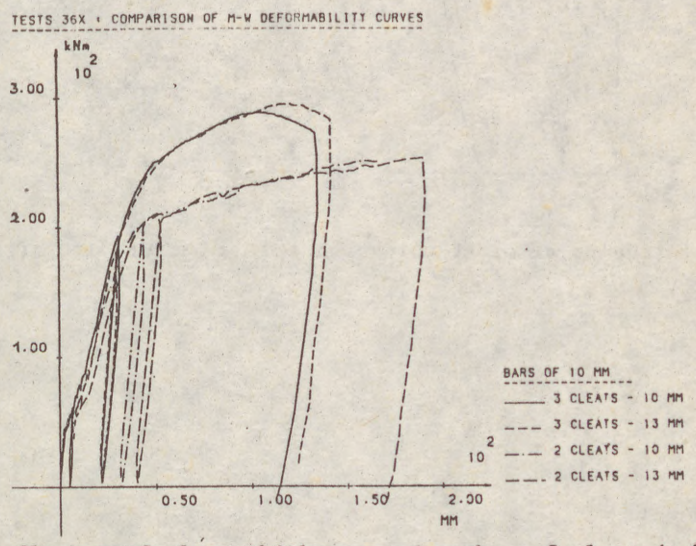

Figure 5-Influence of cleat thickness and number of cleat (rebars of 10mm)

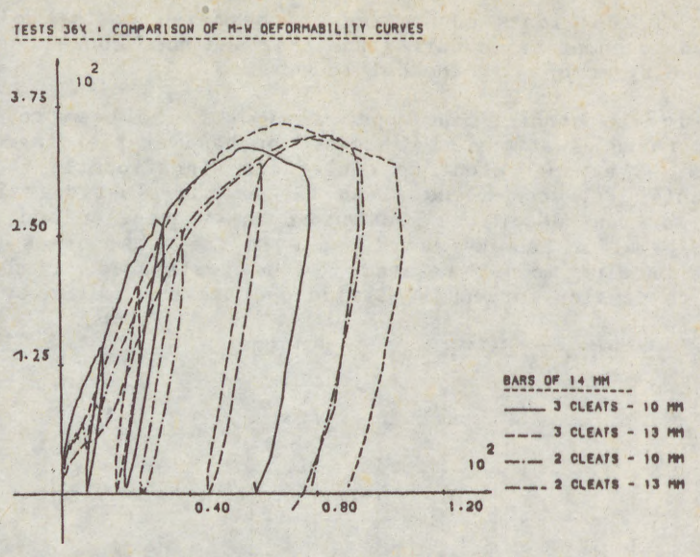

Figure 6-Influence of cleat thickness and number of cleats (rebars of 14mm)

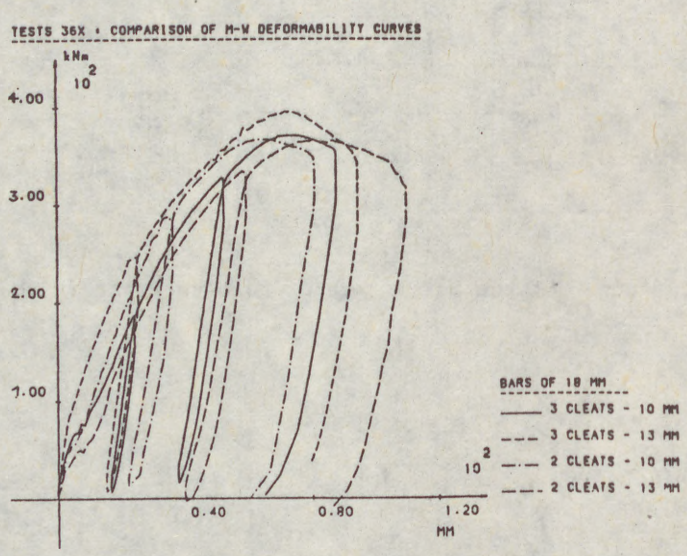

Figure 8-Influence of cleat thickness and number of cleats(rebars of 18mm)

(1)
DAVIES, J Michael (1)
HAKMI, Raheef (2)

POST-BUCKLING BEHAVIOUR OF FOAM-FILLED, THIN-WALLED STEEL BEAMS

INTERNATIONAL COLLOQUIUM
STABILITY OF STEEL STRUCTURES
BUDAPEST, HUNGARY, 1990
PRELIMINARY REPORT

Summary: Sandwich construction is increasingly used as wall and roof cladding for building structures. Typically, a cladding panel may consist of two plane or profiled metal faces with a foamed plastic core. The core may be polyurethane, polyisocyanurate, polystyrene or phenolic resin. When such a panel is subject to static loading due, for instance, to wind, snow or temperature gradient, one face is compressed and becomes liable to local buckling. If this face has a trapezoidal or similar profile the failure mode is similar to that for profiled steel sheeting though the failure stress is enhanced by the presence of the core. The compressed face element first forms a series of buckling waves which increase in amplitude in the post-buckling phase. Failure takes place when one buckle in the region of maximum bending moment cripples.

In light gauge steel applications, the conventional design treatment for this phenomenon utilises the concept of "effective width". In order to investigate the extension of the effective width concept to plate elements supported by plastic foam material a series of tests were undertaken on foam-filled steel beams. This paper describes these tests and their interpretation in terms of an enhanced effective width formula.

General Arrangement for tests

The tested beams were folded from galvanised steel sheet to the dimensions shown in Fig. 1. All dimensions were kept constant except for the width b which was varied to allow breadth to thickness ratios for the compression flange in the range 70 to 250. Both plain steel and foam-filled beams were tested. The density of the foam, and therefore its mechanical properties, were also varied as described later. A total of 18 beams were tested of which 13 were foam-filled. The details of the tests are given, together with the summarised results, in Table 1.

(1) Professor of Civil Engineering and Head of Department
Department of Civil Engineering
University of Salford
Salford M5 4WT, England.
(2) Research Assistant, address as above

(2)

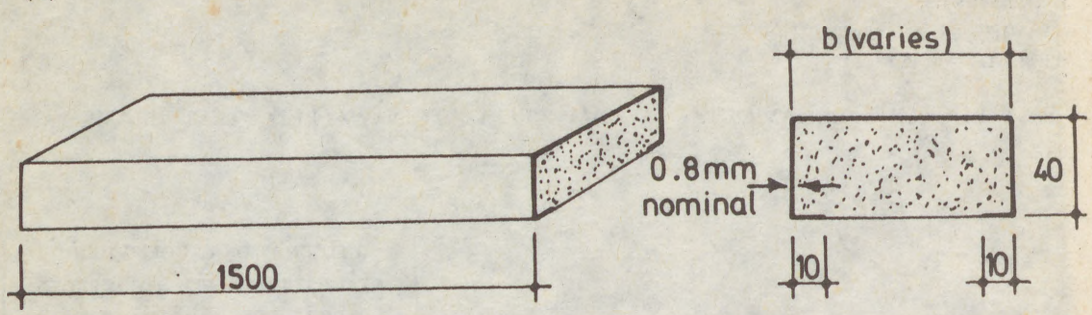

Fig. 1. Dimensions of tested beams.

For each steel beam, the material thickness was measured, net of galvanising, and the mechanical properties determined by testing according to BS 18. The measured properties were used in the interpretation of the test results. The yield stress was reasonably constant with an average value of 281 N/mm^2.

The beams were tested under four-point loading as shown in Fig. 2. Load was applied in increments by adding weights to hangars and, at each load level, the deflection at salient points was measured using dial gauges. A typical beam under test is shown in Fig. 3.

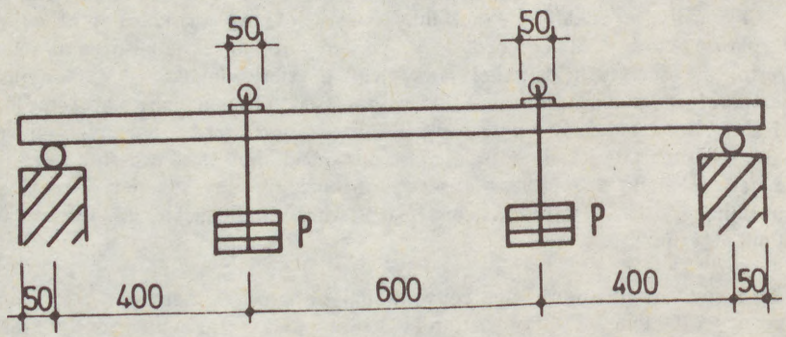

Fig. 2. Diagram of loading system

Foam core material

13 of the tested beams were filled with rigid polyurethane foam. The constituent chemicals for this foam were supplied by Imperial Chemical Industries plc. The foam was produced in the laboratory by mechanically mixing carefully weighed quantities of the three constituent materials, namely Datolac K1335, Suprasec DND and Refrigerant 11. The first two components form the bulk of the foam while Refrigerant 11 acts as a blowing agent which controls the density. For each beam, the total quantity of material to fill the mould at the required density was calculated and this was increased by an overpacking factor which was found by trial and error. The beams were made in a sturdy mould into which the inverted steel member was placed. The beams were first degreased and then both beams and mould were preheated to about 40°C prior to foaming. The measured materials were mixed for 30 seconds and, before the foam started to rise, the mixture was poured evenly along the centre line of the mould. The mould was then closed with a weighted lid and left for approximately 15 minutes for the foam to rise and harden before the beam was removed from the mould

and left to cure under laboratory conditions.[3]

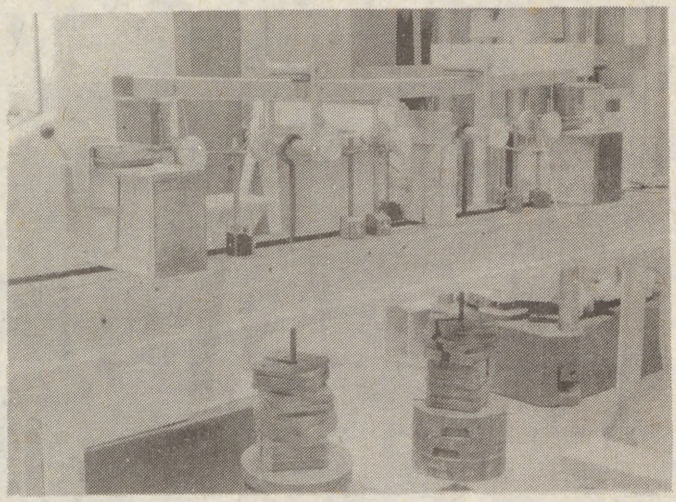

Fig. 3. Typical beam under test

After a little practice, the foam produced was found to be of consistent good quality and no defects in its adhesion were found during testing.

For each of the tested beams, the density and compression modulus of the core material were determined by testing according to ISO standards. The shear strength and modulus were determined using the test described in Fig. 4. It has been found (Basu, 1976) that the more conventional lapped tests, such as that required by ISO 1922, give low results. The test shown in Fig. 4 is a development of an alternative test proposed by Basu. It is the moduli that govern the buckling behaviour and the variation of the compression modulus E_c and shear modulus G_c with the density D_c is shown in Fig. 5. The relationships are approximately linear, the lines shown on Fig. 5 having the following equations:

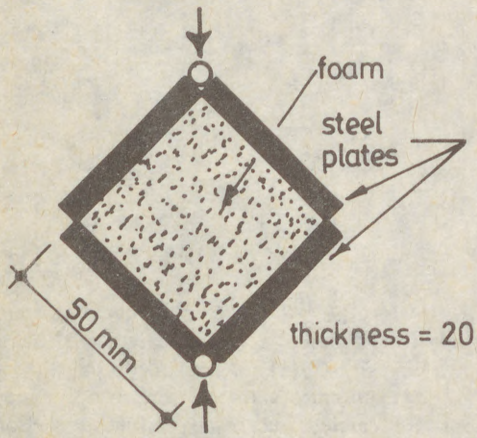

$$\left.\begin{aligned} E_c &= (D_c - 20)/5.4 \\ G_c &= (D_c - 10)10.4 \end{aligned}\right\} \quad \ldots\ (1)$$

Fig. 4. Test for shear strength and modulus of foam

(4)

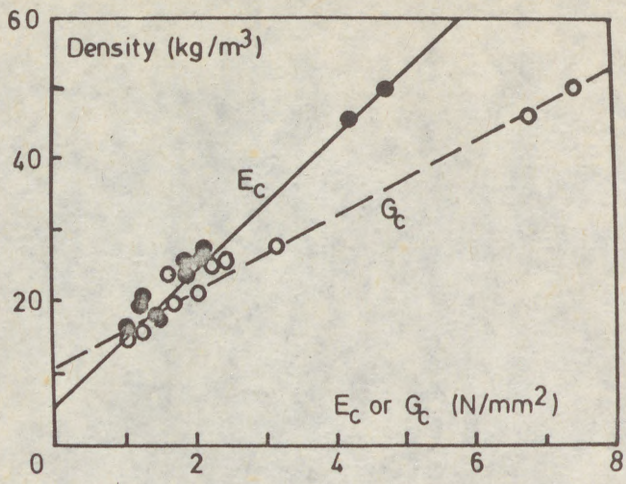

Fig. 5. Compression and shear moduli of laboratory produced foam

Results of beam tests

The results of the tests are summarised in Table 1. In each case the quoted failure load is the maximum load carried and corresponded to local buckling of the compressed flange. The effective width of the compression flange was determined by equating this load to the moment of resistance of the reduced cross-section shown in Fig. 6.

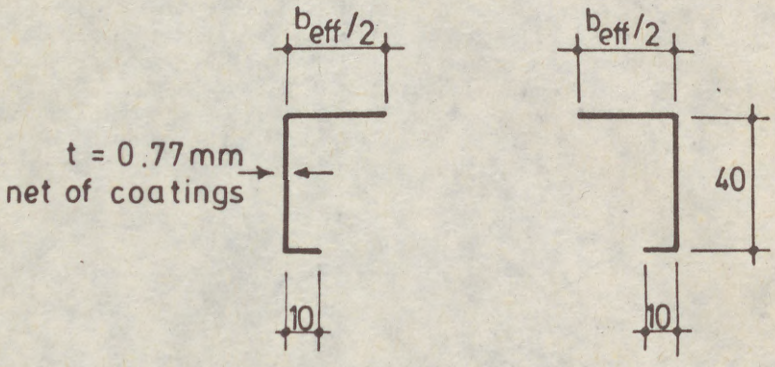

Fig. 6. Cross-section for effective width calculation

Effective width formulae for steel plates

The basis of effective width formulae is shown in Fig. 7. In the post-buckling range of loading, the stress distribution in a compressed steel plate is complicated. For design purposes, the actual distribution of stress shown in Fig. 7(a) is replaced by the simple equivalent shown in Fig. 7(b) which has the same maximum value at the simply supported edges and the same resultant. Design calculations are carried out using "effective sections" in which the actual width 'b' of each element in compression is replaced by its effective width b_{eff}.

(5)

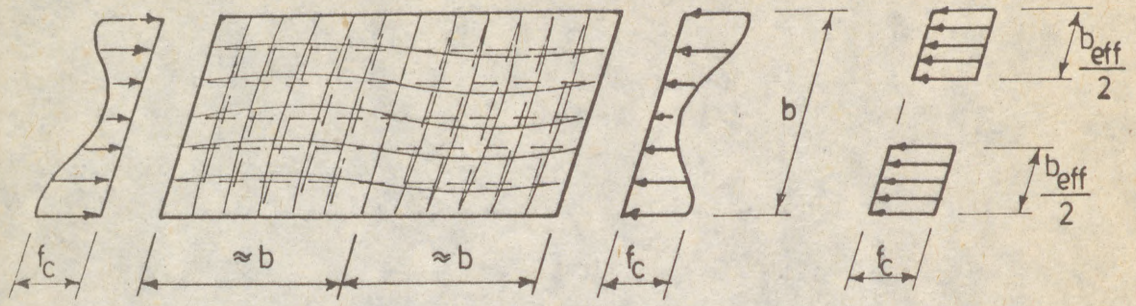

(a) Actual stress distribution (b) Equivalent stresses

Fig. 7. Illustrating the effective width, b_{eff}, in plain steel plates

Test number	b/t	Core density (kg/m³)	Compression modulus E_c (N/mm²)	Shear modulus G_c (N/mm²)	Failure load (P) (kg)	Effective width $\rho = b_{eff}/b$
1a	73	0	0	0	103.2	0.682
1b	73	36	2.4	2.1	115.2	0.809
2a	104	0	0	0	108.8	0.519
2b	104	29	1.5	1.3	112.8	0.549
2c	104	28	1.5	1.3	117.2	0.581
2d	104	38	3.2	2.2	125.2	0.641
2e	104	60	7.4	4.7	135.2	0.715
3a	156	0	0	0	106.8	0.336
3b	156	26	1.4	1.3	125.2	0.427
3c	156	30	1.7	1.3	125.2	0.427
3d	156	31	2.0	1.2	128.8	0.445
3e	156	31.5	2.1	1.3	135.2	0.447
3f	156	56	6.7	4.2	150.2	0.552
3g	156	95	9.1	7.4	172.2	0.661
4a	208	0	0	0	110.2	0.265
4b	208	34	1.4	1.9	143.2	0.387
5a	260	0	0	0	115.2	0.226
5b	260	36	2.0	1.9	149.2	0.328

Table 1. Dimensions, material properties and test results

There are numerous effective width formulae in the literature but only one or two have any practical significance. Internationally, the most commonly used is the Winter formula which is found, for instance, in the European Recommendations which also provide the basis for the current draft of Eurocode 3 (Eurocode 3, 1988). When f_c is equal to the yield stress, Y_s, this takes the form:

(6)

$$b_{eff} = \rho b$$

where,

$$\rho = \frac{1}{\lambda_p}\left[1 - \frac{0.22}{\lambda_p}\right] \quad \text{for} \quad \lambda_p > 0.673$$

$$\rho = 1.0 \quad \text{for} \quad \lambda_p \leq 0.673 \qquad \ldots\ldots\ldots \quad (2)$$

$$\lambda_p = 1.052 \, \frac{b}{t}\sqrt{\frac{Y_s}{E_s K}}$$

Y_s = yield stress of steel

E_s = Young's modulus for steel (205 N/mm^2)

t = thickness, net of coatings

K = buckling coefficient
= 4.0 with simply supported longitudinal edges

The current British Standard, BS 5950 : Part 5 (1987), recognises that the Winter formula can be unconservative and gives the alternative expression

$$\rho = \left[1 + 14\left[\left[\frac{f_c}{p_{cr}}\right]^{\frac{1}{2}} - 0.35\right]^4\right]^{-0.2} \quad \text{for} \quad \frac{f_c}{p_{cr}} \geq 0.123$$

$$\rho = 1.0 \quad \text{for} \quad \frac{f_c}{p_{cr}} < 0.123 \qquad \ldots\ldots \quad (3)$$

where $p_{cr} = 185000 \, K \left[\frac{t}{b}\right]^2$ = local buckling stress

These two formulae, together with the five test results for beams without foam infill are shown in Fig. 8. It may be noted that most National and International Standards allow values of $K > 4.0$ to be used in order to take account of the restraint that the compression flange receives from the supporting webs. The curves in Fig. 8 are drawn on this basis and it is in this context that the Winter formula may be unconservative. However, in the practical situations considered in this paper, the benefit from the foam core is likely to exceed that from the supporting webs and in the analysis which follows the influence of the webs is neglected.

Effective width formulae with foam stiffening

The above effective width formulae both include the bucklin coefficient K. An obvious initial approach to the derivation of an effective width formula suitable for plate elements stiffened by foam is simply to replace K = 4.0 by a modified buckling coefficient which takes account of the foam core material.

Hakmi (1988) has given an analysis for the buckling of simply supported plate elements stiffened by an isotropic medium of infinite depth. His equations do not have an explicit

(7)
solution but, within the practical range of values of the mechanical properties of the core and face materials, the following equation is adequate for the purposes of design:

$$K = 4.0 + R^{1/3}\left[R^{1/3} - 0.5 - 10000\sqrt{\frac{G_c E_c}{E_s}}\right] \quad \ldots\ldots\ldots\ldots\ldots \quad (4)$$

where $$R = \left[\frac{b}{t}\right]^3 \sqrt{\frac{G_c E_c}{E_s}}$$

G_c = shear modulus of core material

E_c = compression modulus of core material

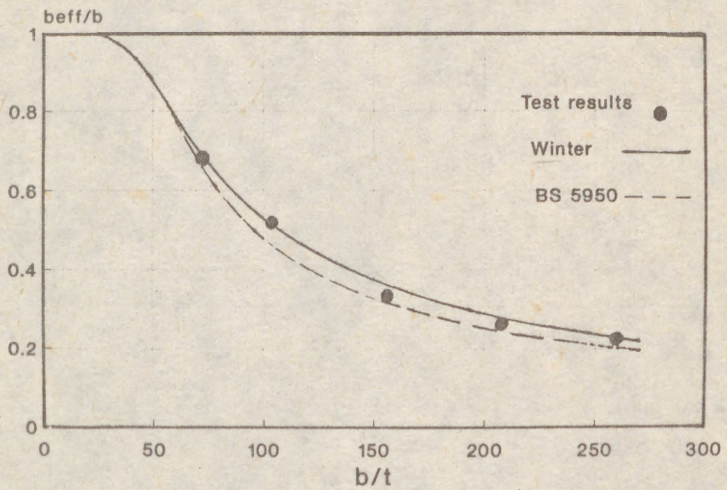

Fig. 8. Effective width of plain steel elements

Comparison between experimental and theoretical effective widths

Effective widths given by the above approach are shown, together with the test results, in Fig. 9.

In Fig. 9, the basis of the theoretical evaluation is the Winter effective width formula with K according to equation (4). However, generally similar results are obtained using the alternative formula from the British Standard. The numerical values alongside the test results are the values of the foam stiffness parameter $\sqrt{G_c E_c}$. As might be expected, the correlation between the experimental and theoretical values of ρ is far from perfect but, at low values of b/t, it is adequate for all practical purposes. With higher plate slenderness, the approach tends to become unconservative.

A reason for this tendency can be suggested. Conventional effective width formulae utilise the post-buckled strength of the steel and reflect the relationship between the elastic buckling stress p_{cr} and the failure stress. With increasing plate slenderness and foam stiffness, the buckling stress and the failure stress become closer together. It follows that effective width formulations based on elastic buckling are likely to become increasingly unconservative with increasing plate slenderness when conventional formulations for plain plates are extrapolated to

(8)
plates stiffened by foam. It further follows that more accurate formulations for plate elements stiffened by foam require consideration of the post-buckling behaviour of the composite. This makes the analysis an order of magnitude more difficult and also makes the presentation of the results in the form of conventional effective width expressions more problematical. This will be considered in a later paper.

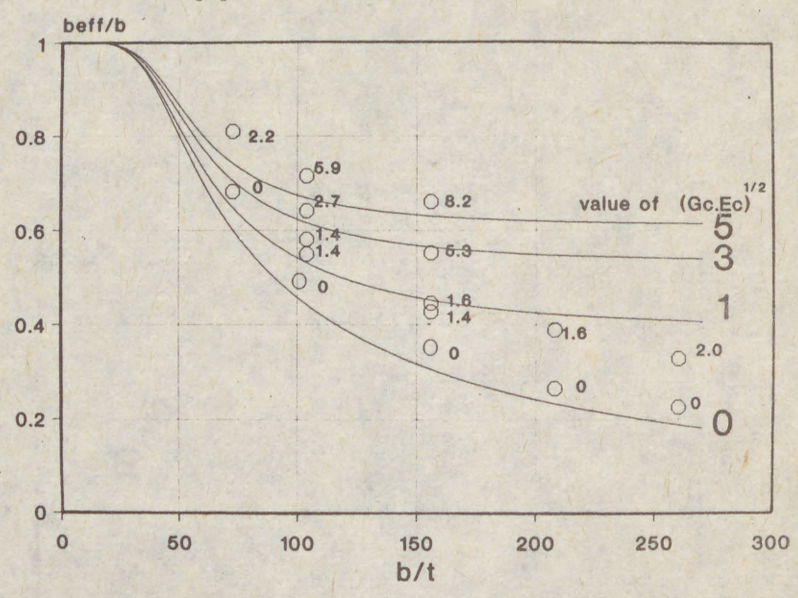

Fig. 9. Effective width of steel elements stiffened by foam

Conclusions

For plate elements of relaltively low slenderness (b/t less than about 120), the design expressions given in the paper may be used to predict the effective width of thin metal plates stiffened by rigid plastic foam. For plates of higher slenderness, a more rigorous analysis is required.

References

A K Basu "Zur Herstellung und zum Werkstoffverhalten von Sandwichtragwerken des Werkstoffverbundsystems Stahlfeinblech-Polyurethan-Hartschaum". ("The manufacture and material properties of sandwich panels made of the material combination of thin steel sheet and rigid polyurethane foam". Dr Ing dissertation, Technischen Hochschule Darmstadt, D17, 1976 (In German).

BS 5950 : Part 5 : 1987 "British Standard : Structural use of steelwork in building : Part 5; Code of practice for design of cold formed sections". British Standards Institution, June 1987.

Eurocode No 3 "Design of Steel Structures : Part 1 - General Rules and Rules for Buildings". Eurocode 3 Editorial Group, Final Draft (December 1988).

M R Hakmi "Local buckling of sandwich panels". PhD Thesis, University of Salford, October 1988.

(1)
LAPOS, Jozef (1)

EFFECTIVE MODULUS OF CONCRETE FOR COMPOSITE COLUMNS

INTERNATIONAL COLLOQUIUM
STABILITY OF STEEL STRUCTURES
BUDAPEST, HUNGARY, 1990
PRELIMINARY REPORT

Summary: The paper deals with the problem of the effective modulus of elasticity of concrete,for composite steel-concrete beam-columns.The modulus of conrete is derived by equating of the elastic end plastic axial strength of composite cross-section,taking into account the triaxial effect in circular filled tubes and the eccentricity of loading as well.The computed values are compared with the values given by different standards.

1.Introduction

The design of composite steel-concrete beam-columns is much influenced by the fundamental difference between the stress-strain curve for steel and concrete.Thus,there exist great differences,particularly in the value of the modulus of elasticity of concrete,given by standards in different countries.The variations are mainly due to two approaches,concerning the influence of the creep of concrete.Some standards take into account the time-dependent changes of the strain of concrete and give high values of the modulus E_c.The other approach avoiding the problem of creep,gives

(1) Assoc.Prof.,Slovak Technical University,Bratislava

[2]

essentially lower values.The present paper derives the value of effective modulus of concrete from the equality of the elastic axial strength and the squash load of infilled or encased composite columns,in terms of their slenderness ratio λ .

2.The effective modulus E_{ce}

Using similar symbols as in Eurocode 4,the elastic axial strength and the squash load of a composite cross-section can be given by formulas

$$N_{el} = \left(A_s + A_c \frac{E_{ce}}{E_s} + A_r \right) R_{sd} \qquad (1)$$

$$N_{pl} = A_s R_{sd} \gamma_{rs} + A_c R_{cd} \gamma_{rc} + A_r R_{rd} \qquad (2)$$

where the design strengths of steel,concrete and reinforcement are

$$R_{sd} = \frac{f_y}{\gamma_a} , \quad R_{cd} = \frac{0,85\, f_{ck}}{\gamma_c} \quad \text{and} \quad R_{rd} = \frac{f_{sk}}{\gamma_s}$$

To determine the coefficient of confined compressive strength of concrete,the authors of paper[5]recommend the expression

$$\gamma_{rc} = 2,254 \sqrt{1 + 7,94\, \varsigma} - 2\varsigma - 1,254 \qquad (3)$$

$$\varsigma = \varkappa \frac{t}{d} \frac{f_y}{f_c} \left(1 - \frac{8e}{d} \right) \qquad (4)$$

where e = M/N is the eccentricity of the loading

$f_c = 0,85\, f_{ck}$

The slenderness parameter $\varkappa$ for circular filled tubes can be given as [4]

(3)

$$\varkappa = 0{,}5\left(1 + \cos\frac{\pi}{75}\lambda\right) \qquad (5)$$

Considering the Huber-Mises-Hencky theory, the corresponding coefficient of the reduced axial strength of the steel tube is

$$\gamma_{rs} = 0{,}25\left(\sqrt{16 - 3\varkappa^2} - \varkappa\right) \qquad (6)$$

For a homogenous non-composite cross-section it is a matter of course, that

$$N_{e\ell} = N_{p\ell}. \qquad (7)$$

Idealizing this equality for composite columns, the substitution of (1) and (2) in (7) gives the effective modulus of concrete

$$E_{ce} = \left[\gamma_{rc}\frac{R_{cd}}{R_{sd}} - \left(1 - \gamma_{rs}\right)\frac{A_s}{A_c} - \left(1 - \frac{R_{rd}}{R_{sd}}\right)\frac{A_r}{A_c}\right]E_s \qquad (8)$$

where E_s is the modulus of elasticity of steel and reinforcement.

The formula (8) can be applied for all commonly used composite cross-sections. The effective modulus E_{ce} is given in terms of mechanical properties of steel, concrete and reinforcement. It includes the effect of creep and gives reliable values, because the strength of concrete do not decrease with the time-dependent strain of concrete. For circular filled tubes the modulus E_{ce} depends on the slenderness ratio as well, when $\lambda < 75$. Since γ_{rs} and γ_{rc} depend on the slenderness ratio, it is not possible to calculate the E_{ce} directly. Therefore a short iterative calculation is necessary. It has been proved as suitable, to begin the iteration with the following estimated radius of gyration

$$r_e = 0{,}3d \qquad (9)$$

where d is the diameter of the steel tube

(4)

Then after calculating the E_{ce}, the radius of gyration is

$$r = \sqrt{\frac{I_s + I_r + \omega I_c}{A_s + A_r + \omega A_c}} \qquad (10)$$

where $\omega = E_{ce}/E_s$

Usually it is enough to perform only two iterations, to obtain the correct result.

3. Numerical example

As a numerical example is considered a concentrically loaded pin-ended composite column shown in Fig.1. It is required to calculate the E_{ce} for the effective length L=6,0 m. The properties of the cross-section and the strengths of materials – structural steel of Grade 37 and concrete C 30.

A_s = 15 966 mm^2
A_c = 95 662 mm^2
I_s = 263,4.10^6 mm^4
I_c = 728,2.10^6 mm^4
f_y = 240 MPa
f_{ck} = 30 MPa
f_c = 0,85.30 = 25,5 MPa
R_{sd} = 240/1,15 = 210 MPa
R_{cd} = 0,85.30/1,5 = 17 MPa
E_s = 210 000 MPa

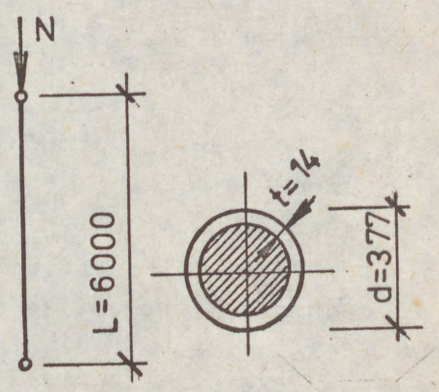

Fig.1

Besides this is to calculate the E_{ce} for λ = 0,15,30 ... 75

Calculation of E_{ce} for L = 6,0 m

$$r_e = 0{,}3 \cdot 377 = 113{,}1 \text{ mm}, \quad \lambda = \frac{6000}{113{,}1} = 53{,}05$$

$$\varkappa = 0{,}5\left(1 + \cos\frac{\pi}{75} \cdot 53{,}05\right) = 0{,}197$$

(5)

$$\gamma_{ra} = 0{,}25\left(\sqrt{16 - 3.0{,}197^2} - 0{,}197\right) = 0{,}947$$

$$\rho = 0{,}197 \frac{14}{377} \cdot \frac{240}{25{,}5} = 0{,}0689$$

$$\gamma_{rc} = 2{,}254 \cdot \sqrt{1 + 7{,}94.0{,}0689} - 2.0{,}0689 - 1{,}254 =$$

$$= 1{,}412$$

$$E_{ce} = \left[1{,}412 \frac{17}{210} - (1 - 0{,}947) \frac{15966}{95\,662}\right] \cdot 210\,000 =$$

$$= 22\,146 \text{ MPa}, \quad \omega = 22146/210\,000 = 0{,}10546$$

$$r = \sqrt{\frac{263{,}4.10^6 + 0{,}10546.728{,}2.10^6}{15\,966 + 0{,}10546.95\,662}} = 114{,}27 \text{ mm}$$

The modulus obtained from the second iteration is E_{ce} = 22 327 MPa. Since the difference is small, no subsequent iteration is necessary.

The results for λ = 0, 15, 30 ... 75 are given in the table

λ	E_{ce} [MPa]
0	29 010
15	28 987
30	28 039
45	24 820
60	19 779
75	17 000

4. Comparison with standards

The results for the assumed class of concrete C 30 are compared, with values given by several standards for short-time and long-time loading.

ČSN 73 1201 - Czechoslovakia

E_c = 32 500 MPa for short-time loading

The creep factor for long - time loading is usually gi-

(6)
ven as $\varphi \triangleq 1{,}0$. The corresponding modulus for long-time loading $E_c = 0{,}5.32\,500 = 16\,250$ MPa.

Eurocode 4

$E_c = 600\, f_{ck} = 600.30 = 18\,000$ MPa

ISO proposal [1]

$E_c = 2.2500\sqrt{f_{ck}} = 5000\sqrt{30} = 27\,386$ MPa for short-time loading.

$E_c = 0{,}5.27\,386 = 13\,693$ MPa for long-time loading.

DIN 18 806

$E_c = 500\,\beta_{wn} = 500.30 = 15\,000$ MPa for short-time loading.

$E_c = 0{,}5.15\,000 = 7\,500$ MPa for long-time loading.

ACI 318 - 83 - USA

Taking the density of concrete $w = 2\,200$ kg/m^3

$E_c = 0{,}043\sqrt{w^3 f_{ck}} = 0{,}043\sqrt{2200^3.30} = 24\,303$ MPa for short-time loading.

$E_c = 0{,}2.24\,303 = 4861$ MPa for long-time loading.

The comparison of values calculated by formula (8), with values given by several standards for long-time loading is ilustrated in terms of the slenderness ratio in Fig.2.

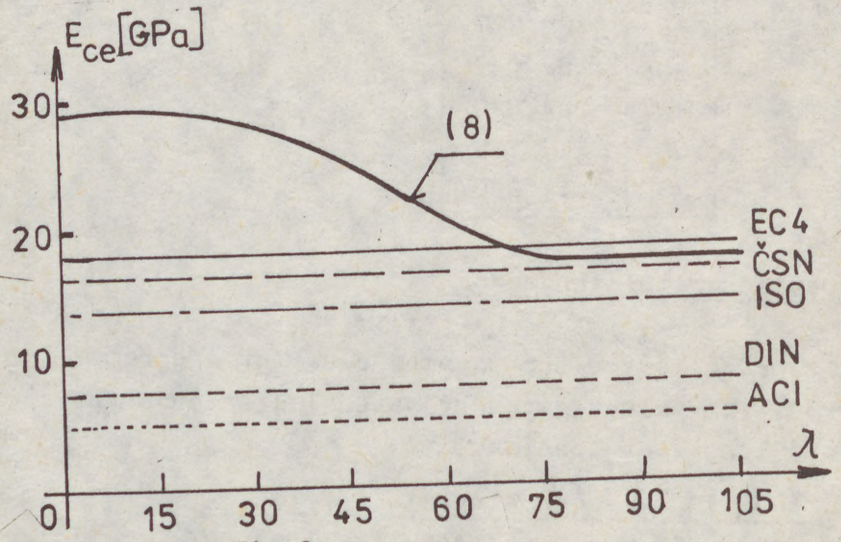

Fig.2

(7)

5.Conlusions

The effective modulus of concrete given by formula (8) enables to calculate increased values of modulus E_{ce}, due to triaxial effect in short circular filled tubes. For slender columns, there is a good conformity with Eurocode 4 and ČSN. On the other hand, the values given by DIN for short and long-time loading and particularly by ACI for long-time loading, seem to be deliberately low.

References

[1] Canadian Delegations Submission to SC1:Composite Structures.Secretariat of ISO/TC,167/SC2,1988.

[2] Dowling,P.J.-Janss,J.-Virdi,K.S.:The design of composite steel concrete columns.Introductory Report of II.International Collqium on Stability of Steel Structures, Liege,1977.

[3] Kikin,A.I.-Sanzharovsky,R.S.-Trull,V.A.:Concrete filled tubular steel structures.Stroyisdat,Moscow,1974,/ In Russian/.

[4] Lapos,J.:Steel columns filled with concrete subjected buckling and bending.Pozemní stavby 2/1988,/In Slovak/.

[5] Mander,J.B.-Priestley,M.J.N.-Park,R.:Theoretical Stress-Strain Model for Confined Concrete.J.Struct.Engrg.,ASCE, 114/8/,1804 - 1826,/1988/.

[6] Roik,K.-Bode,H.-Bergmann,R.:Zur Traglast von betongefüllten Hohlprofilstützen unter Berücksichtigung des Langzeitverhaltens des Betons.Der Stahlbau 7/1982.

[7] Stability of Metal Structures.A World Wiew - 2nd Edition.Introductory Document,Vol.2,Chapter 12 - Composite members,p.529 - 586,SSRC 1989.

[1]
H. SH

On:

SYNOP
Te
view to
cross-s
space
bucklin
failure
against

NOTAT
A_c , A
A_{si} ,A_s
D_{ci} ,D_c
D_i , D
E_c , E
e
$\bar{e}$
F_c
F_s

F_{s1}
f_{cd} ,f_{sd}

f_{cu} ,f_{cy}
f_{sdi},f_{sdo}
f_{sdr},f_{sdt}
L_e
M , N
M_u
N_e
N_{fe}
N_p

(1) Civi

[1]

H. SHAKIR-KHALIL (1)

On: COLUMNS OF COMPOSITE SHELLS

INTERNATIONAL COLLOQUIUM
STABILITY OF STEEL STRUCTURES
BUDAPEST, HUNGARY, 1990
PRELIMINARY REPORT

SYNOPSIS

Tests were carried out on twelve hollow circular columns of composite shell walls with a view to investigating their behaviour when subjected to eccentric end compressive forces. The cross-section of the columns consists of two concentric thin steel shells, and the ring-shaped space between them is filled with either grout or micro-concrete. The columns have a buckling length of about 4m, and the results of the tests are reported here. The experimental failure loads are compared against the predictions of the British Standard BS5400, and also against the results of a finite element analysis.

NOTATION

A_c , A_s	Areas of concrete (or grout) and steel respectively.
A_{si} , A_{so}	Areas of the inner and outer steel shells.
D_{ci} , D_{co}	Inner and outer diameters of the hollow concrete cylinder.
D_i , D_o	Respective inner and outer diameters of composite shell.
E_c , E_s	Elastic moduli of concrete and steel respectively.
e	Eccentricity at which end compressive load is applied.
$\bar{e}$	Eccentricity ratio, given by e/D_o
F_c	Force in the compressive area of concrete at failure of composite section.
F_s	Concentric compressive force to cause yielding of the total area of steel of the composite section, given by: $f_{sd}.(A_{si} + A_{so})$
F_{s1}	Twice the force in the compressive area of steel at failure of composite section.
f_{cd} , f_{sd}	Design strengths of concrete and steel respectively, taken as the respective characteristic strength divided by the material partial safety factor.
f_{cu} , f_{cy}	Characteristic 28 day cube and cylinder strengths of concrete.
f_{sdi}, f_{sdo}	Design strengths of the steel of the inner and outer shells.
f_{sdr}, f_{sdt}	Design strengths of steel plates in direction of rolling and in transverse direction.
L_e	Effective buckling length of column.
M , N	Applied end moment and axial compressive force on column.
M_u	Ultimate moment of resistance of composite section.
N_e	Experimental failure load of column.
N_{fe}	Failure load as predicted by finite element analysis
N_p	Predicted failure load of column in accordance with BS5400.

(1) Civil Engineering Department, University of Manchester, England, U.K.

[2]

N_u Squash load of column.
t_c Thickness of concrete, i.e spacing between steel shells.
t_i , t_o Thicknesses of inner and outer steel shells, respectively.

y_c , y_s Respective distance from the centre of gravity of the compressive force in concrete and steel to the X axis.
α_c Concrete contribution factor, given by the portion of the squash load carried by the concrete.
γ_{mc}, γ_{ms} Material partial safety factors of concrete and steel respectively, taken equal to unity when comparing predicted with experimental failure loads.

INTRODUCTION

The columns tested in this study employed a new type of sandwich cylinder construction which had been developed in the Civil Engineering Department, University of Manchester, U.K. [2,3]. Such shells were originally investigated for use as compression chambers in deep-sea pressure vessels. The columns are a natural development of the previous work, in which the diameter and length of the chambers were respectively decreased and increased. The cross-section of all columns tested in this investigation has an internal diameter of 172mm, a 1mm thick internal steel shell and a clear spacing of 12mm between the inner and outer steel shells. Two series of tests were carried out in this work. Six columns were tested in series 'A', in which grout was used as the filler material, and the outer steel shell was only 1mm thick [5,6]. Owing to the unsatisfactory results of this series, six more columns were tested in series 'B' in which micro-concrete was used as the filler material, and the thickness of the outer steel shell was increased to 2mm [4].

Although not strictly applicable to this type of composite columns, the British Standard BS5400 [1] was used to predict the failure loads of the tested columns. It should be stated that the section of the columns investigated here is not listed amongst the types of columns to which BS5400 is applicable, and that the thickness of the steel shells used in this investigation violates the specified minimum wall thickness requirement of the Standard. Furthermore, BS5400 is only applicable when normal density concrete is used, with no reference being mentioned when either grout or micro-concrete is used.

Use was also made of a finite element computer programme developed in the Department for the analysis of concrete-filled hollow rectangular steel section columns [7]. The programme was later modified in order to take into account the more complicated column section used in this work [4]. The numerical analysis is, however, only applicable to series 'B' in which micro-concrete was used as the filler material. The unavailability of a generally standard stress-strain relationship for grout precluded the possibility of applying the numerical analysis to the series 'A' columns.

PROPERTIES OF MATERIALS

The mix of both the grout and micro-concrete used were so chosen such that a characteristic 28-day cube strength, f_{cu} , of about 40N/mm^2 was obtained. At least four 100mm cubes and two 150x300mm cylinders were tested with each column, and the respective cube strengths are given later together with the properties of the column specimens.

The columns were manufactured out of 1220mm wide steel sheets. Each column required three steel cylinders for each of its outer and inner shells. Four coupon specimens were taken from each sheet used, two in the direction of rolling, and two in the transverse direction. The design strengths, f_{sd} , of the steel used for each column were thus established in both the rolling and transverse directions, f_{sdr} and f_{sdt} respectively. It should be noted, however, that the column shells were rolled in the same direction in which the steel sheets had originally been rolled, and the end compressive forces were therefore applied in the direction transverse to the direction of rolling. The design strength transverse to rolling, f_{sdt} , was therefore taken as the basis of the predictions and numerical work reported later. The design strength values for each column were taken as the average of the results obtained from the

[3]

coupon specimens taken from the six steel sheets from which each column was made. The elastic modulus of steel, E_s , was also similarly evaluated for each column.

PRELIMINARY TESTS

Tests were carried out in series 'A' columns on short specimens in order to establish the grout–steel bond strength, and also the mode of load transfer from one steel cylinder to the other by shear through the filler material. The bond strength was found to vary between 0.1 and 0.13N/mm², which is much lower than values obtained for concrete–encased bars and structural sections. Failure took place by slip occurring between the outer steel shell and the grout filling, despite the fact that this is the larger of the two grout–steel interfaces. The fact that any shrinkage of the grout would cause some separation between the filling and the outer steel shell seems to be the most likely explanation for the above results. The shrinkage would result in the filling clinging to the inner steel shell, causes partial separation between the grout and the outer shell and results in a drop in the bond strength value.

Short composite cylinders were also tested in both series in order to establish the squash load of these cylinders, and also to compare the experimental values with the predictions given in BS5400 [6]. Some of the specimens were provided with special end rings and/or end tension rings in order to avoid any premature failure due to local buckling at the loading platens. Other specimens had their ends either machined after casting or left as cast. The types of end conditions used had very little effect on the failure load of the specimens. Provided that the outer and inner steel shells are machined to the same height, it seems that after casting the filler material, such specimens would only need their ends to be smoothed with plaster before being tested.

The squash load, N_u , is defined as the ultimate load carrying capacity of a short column subjected to a concentric compressive load. It is given in BS5400 as follows:

$$N_u = f_{sd} A_s + 0.67 f_{cu} A_c \qquad (1)$$

where the terms in the above equation are as defined in the notation. It should be noted that in the work presented here, the material partial safety factors, γ_m , given in BS5400 for both the steel element, γ_{ms} , and the filler material, γ_{mc} , are taken equal to unity so that the experimental and predicted values may be compared on an equal footing.

Table 1 Results of tests on short composite tubes

Sp. No.	Height (mm)	t_i (mm)	t_o	A_{si} (	A_{so} mm²	A_s)	f_{sdi} (	f_{sdo} N/mm²	f_{cu})	N_u (kN) Exp.	BS	Exp / BS
1A	100	1.02	1.02	554	638	1192	245	245	48.0	470	518	0.91
2A	200	1.02	1.02	"	"	"	"	"	48.0	445	518	0.86
3A	300	1.02	1.02	"	"	"	"	"	48.0	370	518	0.71
4A	400	1.02	1.02	"	"	"	"	"	48.0	377	518	0.73
5A	400	1.18	1.18	641	738	1379	230	230	42.0	490	514	0.95
6A	400	1.18	1.18	"	"	"	236	236	42.0	480	523	0.92
7A	400	1.04	1.04	565	650	1215	232	232	40.5	440	472	0.93
8A	400	1.04	1.04	"	"	"	"	"	40.5	380	472	0.81
9A	400	1.04	1.04	"	"	"	"	"	35.0	360	446	0.81
1B	200	1.02	1.93	554	1213	1767	223	219	46.3	758	607	1.25
2B	200	1.02	1.93	"	"	"	"	"	45.1	710	601	1.18
3B	200	1.02	1.93	"	"	"	"	"	46.2	660	606	1.09
4B	200	1.04	1.97	565	1238	1803	234	186	48.2	590	578	1.02
5B	200	1.05	1.98	571	1244	1815	218	193	43.0	620	567	1.09
6B	200	1.03	1.98	560	1244	1804	236	178	43.4	640	579	1.11
7B	200	1.04	1.97	565	1238	1803	255	178	44.0	610	600	1.02

[4]

The results of the tests on the squash specimens are given in Table 1 together with the predictions of BS5400. As can be seen from the table, all grout-fil'ed specimens failed to reach their predicted loads, whereas the concrete-filled specimens exceeded their predicted values by between 2 and 25%. Specimens 4B-7B were made from the same steel sheets and concrete mix as columns B3-B6.

COMPOSITE COLUMNS

Properties of section

In addition to the squash load defined above, two more properties of the column cross-section need to be evaluated in order that the column failure load may be calculated in accordance with BS5400. These are the concrete contribution factor, α_c , and the ultimate moment of resistance of the section, M_u.

The concrete contribution factor is defined as the portion of the squash load carried by the concrete, and is given by:

$$\alpha_c = 0.67 f_{cu} . A_c / N_u \qquad (2)$$

The ultimate moment of resistance of the section is defined as the moment which when applied to the section would cause the steel to reach its design strength both in tension and compression, and causes the concrete to reach its bending compressive strength. It should be noted that the standard rectangular stress blocks are used in this analysis, and that the strain hardening of steel and tension in concrete are both ignored, Fig.1. The bending compressive strength of concrete is taken here as $0.6f_{cu}$ in accordance with BS5400 when the partial safety factor of concrete, γ_{mc} , is taken equal to unity.

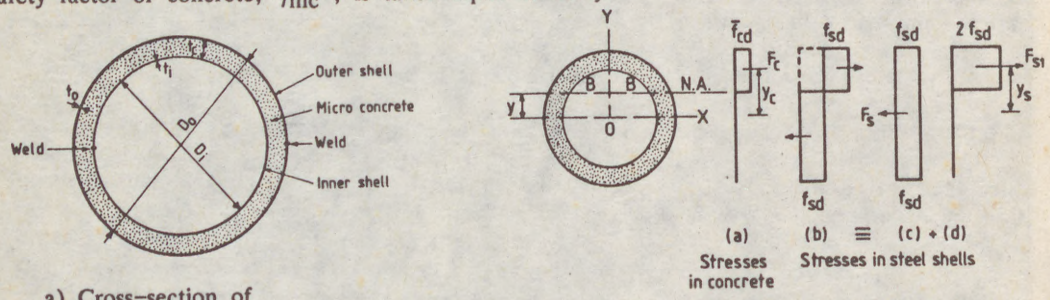

a) Cross-section of Series 'B'columns

b) Stress block diagram of section

Fig.1 Column section and stress block analysis

Details of specimens

As mentioned earlier, each column was assembled from six steel cylinders, three for each of the inner and outer shells. The details of the columns of both series are shown in Fig.2. The columns of series 'A' were assembled by the use of slotted intermediate rings at the third points, a solid ring at one end and a slotted ring at the other end; the slots were provided for the purpose of casting the grout.

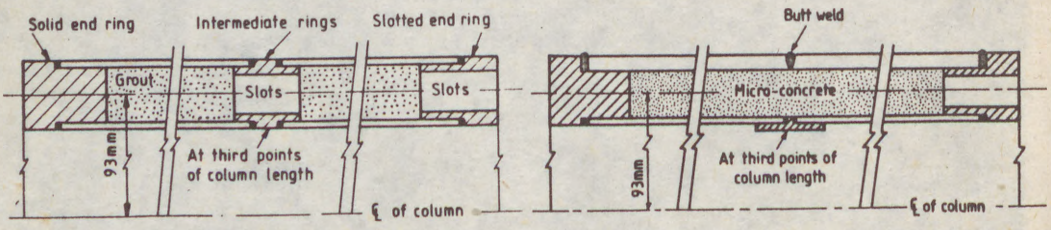

a) Series 'A' columns

b) Series 'B'columns

Fig.2 Details of columns

[5]

In series 'B' in which micro-concrete was used, the end rings were the same as for series 'A', but the intermediate rings were replaced by backing plates to which the inner cylinders were welded. Spacers were used at the third points to maintain the spacing between the inner and outer shells at 12mm, and the outer steel cylinders were butt welded together at these locations. The slotted intermediate rings were dispensed with in series 'B' in order to facilitate the casting of the micro-concrete over the full length of the columns. The dimensions and material properties of all columns tested in both series 'A' and 'B' are given in Table 2.

Table 2 Properties of tested columns

Col. No.	e_1 mm	e_2 mm	t_i mm	t_o mm	A_s mm²	f_{sd} N/mm²	f_{cu} N/mm²	E_s kN/mm²	(BS5400) N_u(kN)	M_u(kNm)
A1	0	0	1.05	1.05	1227	261	50.0	N/A	555	23.2
A2	25	25	1.05	1.05	1227	263	44.7	"	533	23.0
A3	50	50	1.03	1.03	1204	250	36.0	"	470	22.2
A4	75	75	1.03	1.03	1204	236	40.0	"	472	20.5
A5	100	100	1.03	1.03	1204	253	45.0	"	516	22.3
A6	150	150	1.04	1.04	1215	259	42.0	"	512	22.5
B1	10	10	1.02	1.97	1792	196	44.1	197	555	25.5
B2	25	25	1.02	1.96	1786	216	44.0	195	592	28.0
B3	75	75	1.04	1.97	1803	210	48.2	190	578	25.9
B4	150	150	1.05	1.98	1815	205	43.0	194	567	26.2
B5	75	25	1.03	1.98	1804	207	43.4	194	579	27.1
B6	150	75	1.04	1.97	1803	217	44.0	194	600	28.1

Instrumentation

All columns of series 'A' and the first four columns of series 'B' were subjected to equal end eccentricities. These columns were instrumented with strain gauges at the mid-length section, and also at two more sections along one half of the column length; sections I, II and III in Figs.3 and 4. Columns B5 and B6 were subjected to unequal end eccentricities, and were therefore instrumented at two more sections (IV and V) along the other half of the column length. In order to monitor the strains in the inner steel shell,strain gauges were also fixed at section II to the inside of the middle inner steel cylinder prior to assembling the inner column shell. The column deflections were measured by displacement transducers placed at the locations marked 'T' in Fig.3. The displacements were measured both in the plane of bending and transverse to it. The displacements at the column ends were also monitored, but were ignored in the analysis as they were of negligible value.

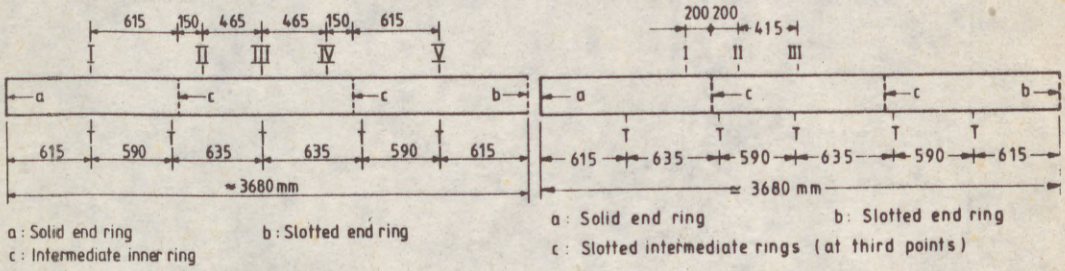

a) Series 'A' columns b) Series 'B' columns

Fig.3 Composite column specimens

[6]

Test rig

The columns were tested in the horizontal position in a 3000kN capacity test rig, Fig.5. The test rig is securely bolted to the strong floor of the laboratory, and the bulk heads are laterally restrained to ensure the stability of the loading arrangement. The load is applied through thick end loading plates which form cross knife edges in order to permit the tested columns to rotate freely at both ends. The test rig is self contained, and the movable bulkhead is seated on rollers which allow it freedom of movement in the longitudinal direction.

Throughout the test procedure, the load cell, strain gauges and displacement transducers were all connected to a data logging equipment. All data was stored on disk and a hard copy was printed during the course of the test. The strains at the mid-span section were simultaneously viewed on a monitor to help determine the loading increments to be applied to the column at a particular stage of loading, and also in the post failure stage.

Fig.4. Instrumentation of columns

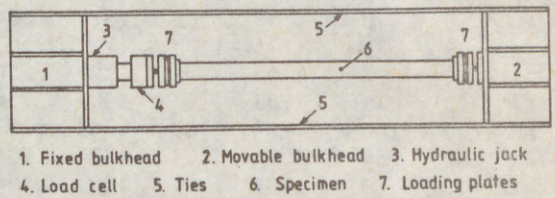

Fig.5 Plan view of test rig

a) Series 'A' columns

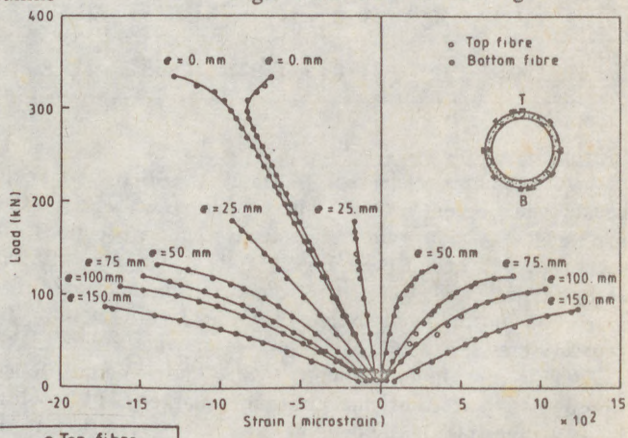

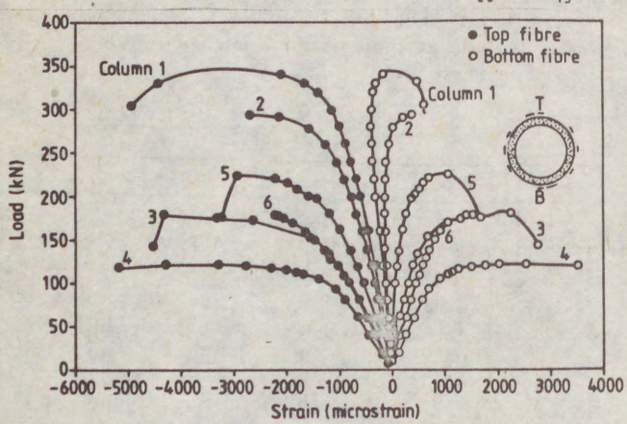

b) Series 'B' columns

Fig.6 Strains in extreme fibres at mid-length of columns

[7]

TEST RESULTS

Strains

The extreme mid-length strains in the columns in the top and bottom fibres are given in Fig.6 for both series of tests. In series 'A', it was not possible to follow the descending branch of the relationship when the columns should have been shedding their loads in the post failure stage. Although most of the extreme compressive strains at failure reached the yield strain of the steel used, the maximum recorded tensile strains were much lower than these values.

In all columns of series 'A', failure took place by the formation of short compression buckles in the outer steel shell in the vicinity of one of the intermediate rings. The strapping of a tension stiffener around the buckle only caused the compression buckle to shift slightly to one side, or to form either on the other side of the ring or at the other intermediate ring. It may be stated that the columns of this series failed prematurely as a result of local buckling of the outer shell. The buckles had a halfwave length of about 20mm, and probably resulted from the combined effect of a low grout-steel bond strength and the very thin outer shell used in this series.

The load-strain graphs of series 'B' are a marked improvement relative to those of the previous tests. The relationships show ascending as well as descending branches, and seem to show that, unlike series 'A', the columns of this series suffered an overall type of failure. The tensile strains in the post failure stage are also seen to be much higher than in the previous series, and are also in excess of the yield strain of the steel used.

Deflections

The mid-length load-displacement relationships of the columns of both series are shown in Fig.7. The graphs exhibit similar characteristics to those of the load-strain relationships as far as the lack, or presence, of the descending portion of the column response is concerned. Most of the columns of series 'B' show a plateau in the load-deflection relationship, and thus indicate an overall type of failure. The actual failure loads of the columns of this series are clearly identified by the plateau in this type of load-deflection relationship.

Failure loads

The experimental failure loads, N_e , and the predicted failure loads in accordance with BS5400, N_p , are shown in Table 3. The table gives these values for the columns in series 'A' and 'B', and also the failure loads, N_{fe} , of columns B1-B4 of series 'B' as predicted by a finite element analysis. The table shows that the experimental failure loads of the columns of series 'A' are much lower than those predicted by BS5400, and that the ratio N_e to N_p varies between 63% and 78%. In series 'B', the failure loads of columns B1-B4 which were subjected to equal end eccentricities, are seen to be still lower than those predicted by BS5400, but the N_e to N_p ratio is seen in this case to vary between 82% and 91%. Columns B5 and B6, which were subjected to unequal end eccentricities, give N_e to N_p ratios of 90% and 111% respectively. It should be noted that the 2mm thickness of the outer shell in series 'B' still violates the minimum wall thickness requirement of BS5400, and that the micro-concrete used in the tests does not satisfy the 'normal density concrete' specification stated in the Standard.

The finite element analysis predictions given in Table 3 for columns B1-B4 to which the analysis is applicable, show that the columns had practically reached the predicted failure values since the N_e to N_{fe} ratios are seen to vary between 97 and 103%. This seems to indicate that designing such columns by BS5400 generally overestimates the failure loads of these columns. It should be stated that the BS5400 predictions reported here are based on the use of curve 'a' of the European buckling curves. In view of the test results reported here, it seems that a lower design curve should be used in the design of these columns in order that lower failure load predictions may be obtained.

[8]

a) Series 'A' columns

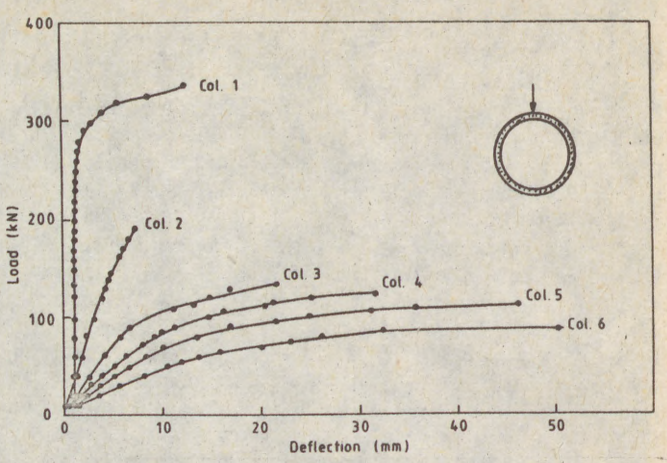

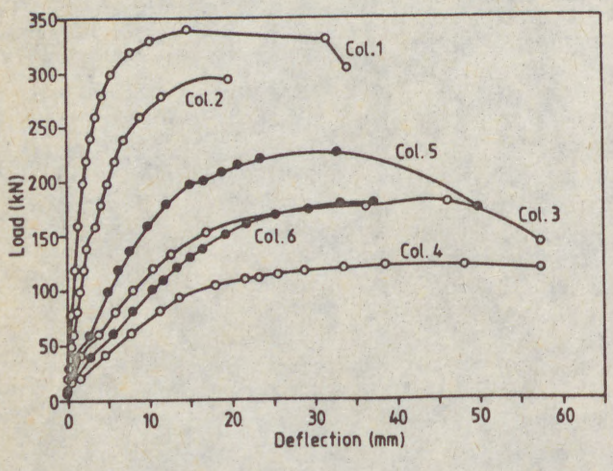

b) Series 'B' columns

Fig.7 Mid-length displacements of columns

Table 3 Results of tests on columns

Col. No.	N_e (kN)	N_p (kN)	N_{fe} (kN)	N_e/N_p	N_e/N_{fe}	N_e/N_u
A1	335	461	N/A	0.73	N/A	0.60
A2	191	302	"	0.63	"	0.36
A3	133	211	"	0.63	"	0.28
A4	123	163	"	0.75	"	0.26
A5	111	147	"	0.75	"	0.22
A6	87	112	"	0.78	"	0.17
B1	340	423	330	0.80	1.03	0.58
B2	294	360	303	0.82	0.97	0.49
B3	179	207	181	0.86	0.99	0.30
B4	119	130	118	0.91	1.01	0.19
B5	225	249	N/A	0.90	N/A	0.35
B6	161	179	"	1.11	"	0.29

[9]

DISCUSSION and CONCLUSIONS

The results of the tests on the columns of series 'A' show that the experimental failure loads are much lower than predicted by BS5400. This resulted from several factors including the use of grout as the filler material, and also the use of outer steel shells which are less than half the minimum wall thickness of 2.5mm in accordance with the Standard. The use of micro-concrete as the filler material and increasing the wall thickness of the outer shell in the columns of series 'B' improved the performance of the columns. However, the experimental failure loads of the columns are still below the predictions of BS5400 except for column B6 which was subjected to large unequal end eccentricities. It should be stated that the columns of series 'B' satisfy neither the BS5400 requirement regarding the type of concrete used nor the minimum wall thickness of the steel section. Although columns B1-B4 failed to reach the predictions of BS5400, they are seen to be within ±3% of the finite element analysis predictions. This seems to indicate that the BS5400 predictions for this type of composite column are on the unconservative side, and that perhaps a lower design curve (either 'b' or 'c') of the column buckling curves should be selected for the design of these columns.

The test results show a marked improvement in the load carrying capacity of the series 'B' columns as compared to series 'A', and clearly indicate that such composite columns have potential for use in practice. The behaviour of such columns would be greatly enhanced for larger sections which would allow the use of normal density concrete in the relatively wider annular cavity thus improving the filler-steel bond strength. The structural steel sections used would also be relatively free from the built-in residual stresses due to welding which must have had an adverse effect on the tested columns since failure was always accompanied by buckling of the outer shell in the vicinity of the weld at the intermediate ring.

Although more tests are required to fully investigate the behaviour of this type of column, the tests reported here illustrate the practical potential of such columns. The results also indicate that intensive investigations are required before the application of BS5400 to the design of columns of unusual dimensions and cross-sections.

REFERENCES

1. British Standards Institution: "Steel, concrete and composite bridges, Part 5: Code of practice for design of composite bridges". BS5400, 1979.

2. Montague, P. (1975): "A simple composite construction for cylindrical shells subjected to external pressure". Journal of Mechanical Engineering Science, vol. 17, No. 2, Feb. 1975, pp. 105-113.

3. Montague, P. (1978): "The experimental behaviour of double-skinned composite, circular, cylindrical shells under external pressure". Journal of Mechanical Engineering Science, vol. 20, No. 1(b), Feb. 1978, pp. 21-34.

4. Shakir-Khalil, H. and Boufennara, K.: "Columns of concrete-filled concentric steel shells". Accepted for publication, Structural Engineering Review.

5. Shakir-Khalil, H. and Illouli, S. (1987): "Composite columns of concentric steel tubes". Proceedings, "Non-conventional structures", Conference, London, Dec. 1987, vol. 1, pp. 73-82.

6. Shakir-Khalil, H. and Illouli, S. (1988): "Columns of composite cylindrical shells". Structural Engineering Review, vol. 1, 1988, pp. 113-118.

7. Shakir-Khalil, H. and Zeghiche, J.: "Experimental behaviour of concrete-filled rolled rectangular hollow section columns". Accepted for publication. The Structural Engineer, London.

(1)
ŠOLTÉSZ, JÚLIUS (1)

ANALYSIS OF SLENDER STEEL REINFORCEMENT CONCRETE COLUMNS UNDER EXTREME THERMAL CONDITIONS

INTERNATIONAL COLLOQUIUM
STABILITY OF STEEL STRUCTURES
BUDAPEST, HUNGARY, 1990
PRELIMINARY REPORT

SUMMARY: Behaviour of steel reiforced concrete (SRC) columns in elastic-plastic range. Analysis based on synthesis of method of transfered matrices (MTM) and method of step-by-step plastification in an incremental loading cycle. Interaction curves of SRC columns with consideration of buckling. Traceing of cracking and plastification. Comparison with test results and BS 5400/1979. Secondary stressing due to thermal shock.

INTRODUCTION

The SRC systems are mainly applied to tall buildings. A good earthquake-resistance ability of SRC systems was proved for example at the great Kanto earthquake in 1923. For example in Japan a half of building structures taller then 6-stories are presently constructed by SRC systems. A good fire resistance of SRC systems is well known as well. Increase of cross-section's stressing due to non-uniform distribution of temperature over the cross-section is required to calculate in order to check a fire resistance ability of a structure.

AIM AND INITIAL ASSUMPTIONS

The aim of the contribution is to present the theoretical basis of a numerical approach, takeing full account of the recomendations of the cs-standards CSN 731401-Design of steel structures and CSN 731201-Design of concrete structures to topics as follows:

---

(1) Senior lecturer, Department of Concrete Str. and Bridges, Slovak Technical University, Bratislava

(2)

a: Actual interaction curve for uniaxial bending of composite columns with consideration of buckling. It means to solve the task as a parametric study with $\lambda = l/r_i$ as a parameter, where l is a critical buckling length from an elastic solution and r_i is a transformed cross-sections radius of gyration:

$$N = f(M, \lambda = \text{parameter}) \qquad (1)$$

b: Tracking of plastification and cracking in a critical cross-section and over the whole column length.

c: Comparison with test results and BS 5400/1979.

d: Secondary stressing due to extreme thermal shock.

A complete strength analyses even for a apparently simple case of loading, takeing full account of the effects of the plasticity, cracking, structural and geometrical imperfections, involves great computational effort. For the present problem, therefore , certain simplifying assumptions are made in agreement with [4,5]. The most important assumptions are as follows:

1. The cross-section is divided by a net into elements $dA_{i...n}$, and the column length into polygonal equidistant sections Δl on account of the numerical analysis. The cross-section does not vary over the column length.

2. The strain distribution over the cross-section depth is linear.

3. The moment and curvature are supposed constant over the section length Δl.

4. The residual stresses are taken in consideration in accordance with CSN 731401. By means of the relative eccentricity m_o and through e_o is the effect of residual stresses together with geometrical imperfection, expressed as an equivalent geometrical imperfection in the form of the initial curvature. The shape of the initial curvature is considered in the first eigenfunction of an ideal elastic column and e_o is its characteristical amplitude.

5. Pin-ended columns are analysed.

6. Perfect bond and no slip is assumed.

7. The concrete is assumed to have no tensile strength and a trapezoidal stress-strain relationship in compression. The stress-strain relationship for steel is taken as elastic-perfectly plastic.

8. Creep and shrinkage effects are neglected in presented results but they could be treated in accordance with CEB-FIP Recomendations by means of time-stepping method.

9. Repeated loading is not treated.

10. Validity of superposition of primary and secondary stressing is assumed.

11. Primary stressing of SRC column is calculated in elastic-plastic range and the secondary stressing in elastic one.

12. Basic material properties are supposed constant within the increase of temperature.

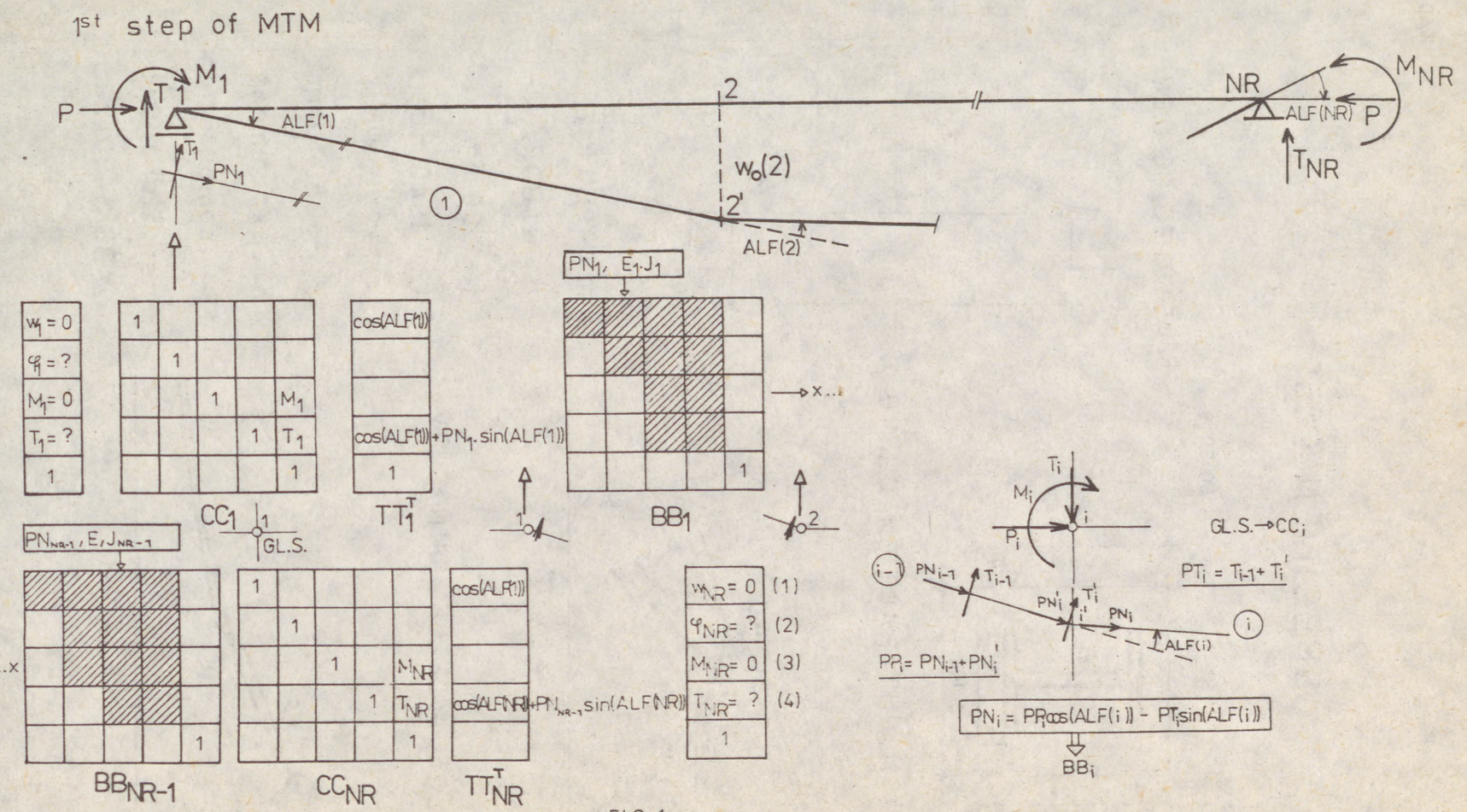
1st step of MTM
P
M1
T1
T1
ALF(1)
PN1
1
2
2'
w0(2)
ALF(2)
NR
MNR
ALF(NR)
P
TNR
PN1, E1·J1
w1 = 0
φ1 = ?
M1 = 0
T1 = ?
1
CC1
1
GL.S.
TT1T
cos(ALF(1))
cos(ALF(1))+PN1·sin(ALF(1))
BB1
x...
PNNR-1 / ENR-1 JNR-1
BBNR-1
CCNR
TTNRT
cos(ALF(NR))+PNNR-1·sin(ALF(NR))
wNR = 0 (1)
φNR = ? (2)
MNR = 0 (3)
TNR = ? (4)
Ti
Mi
Pi
i
GL.S.→CCi
i-1
PNi-1
Ti-1
PTi = Ti-1 + Ti'
PNi'
Ti'
PNi
ALF(i)
PRi = PNi-1 + PNi'
PNi = PRi cos(ALF(i)) - PTi sin(ALF(i))
BBi

FIG. 1

SPECIMEN C050

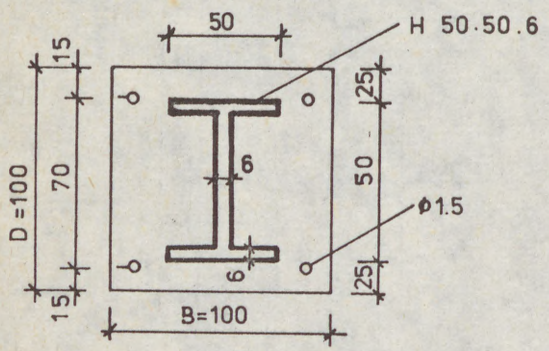

M-N INTERACTION CURVE

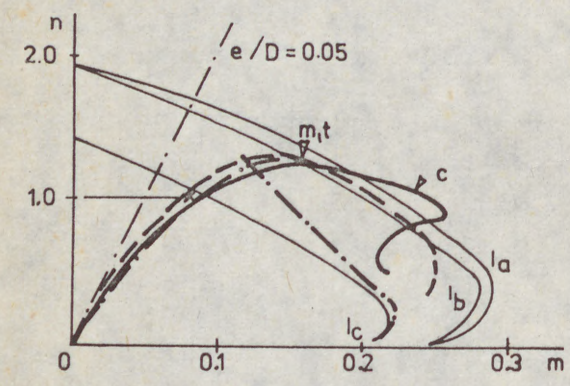

LOAD - DEFLECTION CURVE

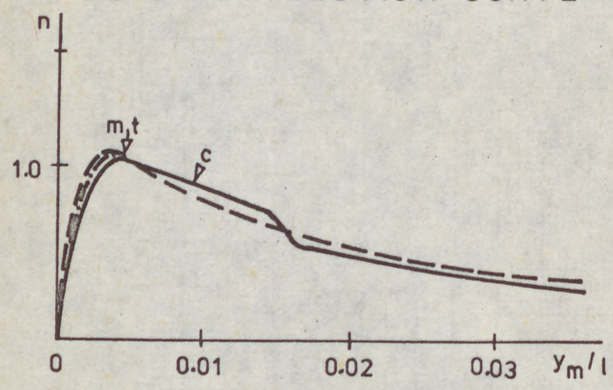

FIG. 2

ASSUMED DEFL.CURVE

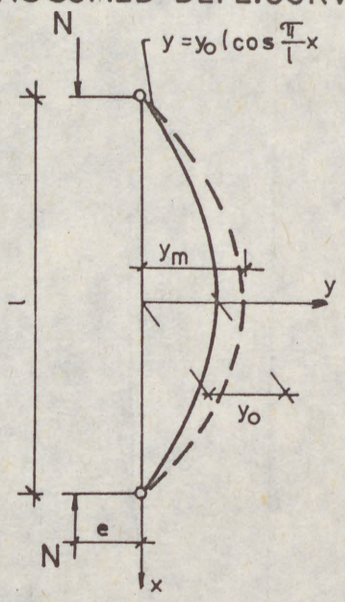

$m = M / BD^2 R_{cd}$

$n = N / BDR_{cd}$

$l = 1500$ mm

$l_{ef} = 1640$ mm

$R_{cd} = 22.5$ N/mm²

$R_{sd} = 280$ N/mm²

— experiment

-- computation

-·-J.S. analysis

× BS 5400/79

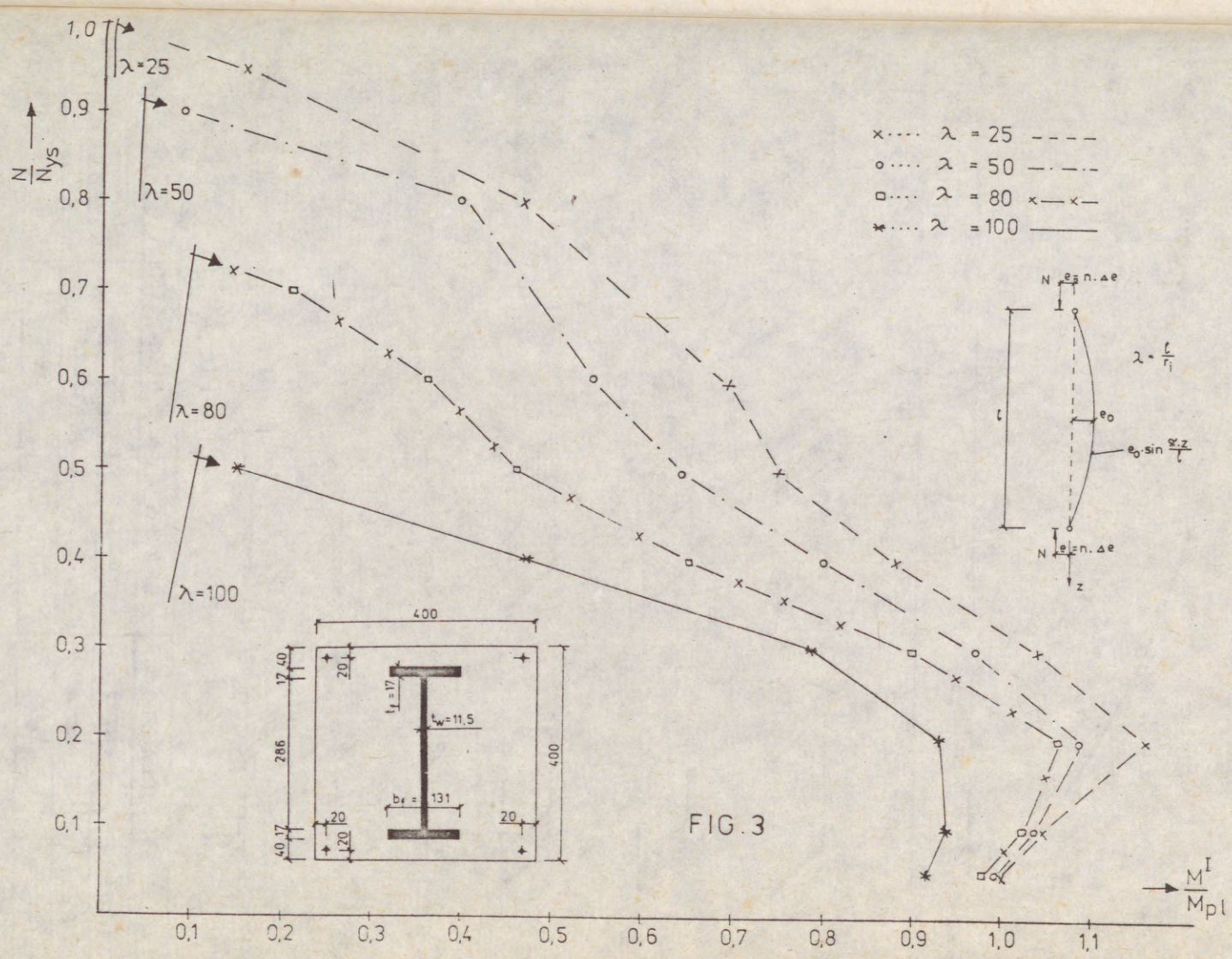
1,0
0,9
0,8
0,7
0,6
0,5
0,4
0,3
0,2
0,1
N/Nys
λ=25
λ=50
λ=80
λ=100
× ···· λ = 25 ----
○ ···· λ = 50 —·—·—
□ ···· λ = 80 ×—×—
✱ ···· λ = 100 ——
N e = n.Δe
λ = l/i
l
e0
e0·sin πz/l
z
400
17 40
286
20
tf = 17
tw = 11,5
bf = 131
400
0,1 0,2 0,3 0,4 0,5 0,6 0,7 0,8 0,9 1,0 1,1
M^I/Mpl

FIG. 3

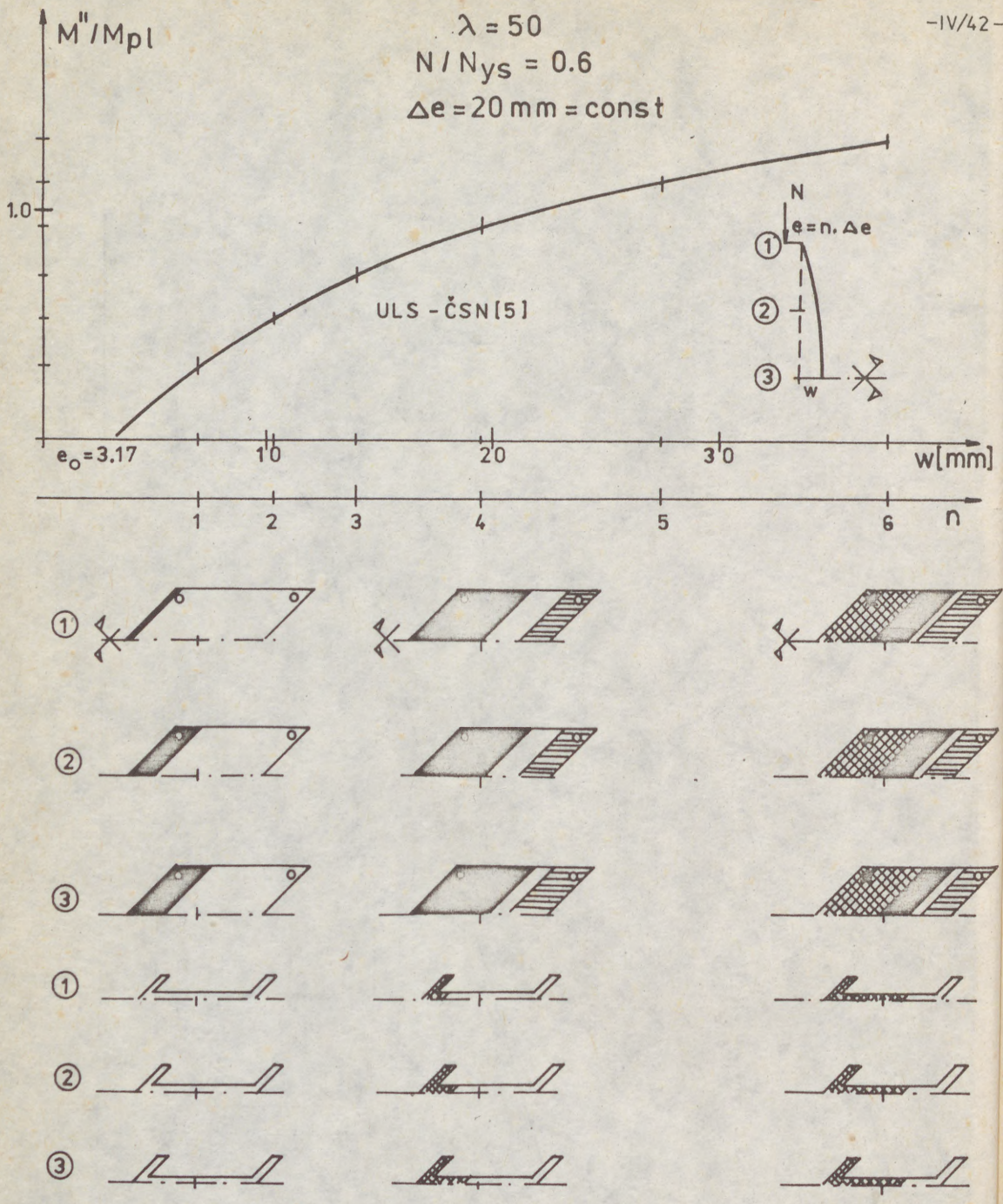

FIG.4

	PLASTIC	CRACKS	NOT PERMITTED	ELASTIC
CONCRETE	▬	▬	▬	═
STEEL	▬		▬	═
REINFOR.	●		■	○

ISOTHERMAL LINES

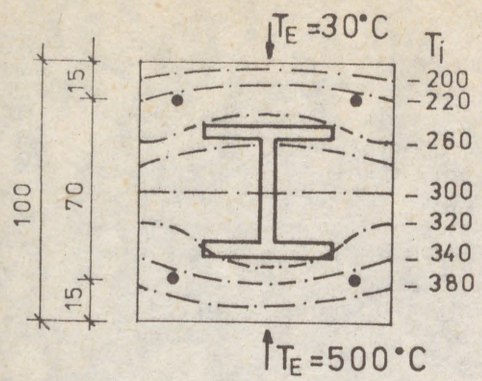

THERMAL LOADING

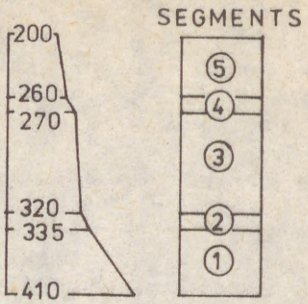

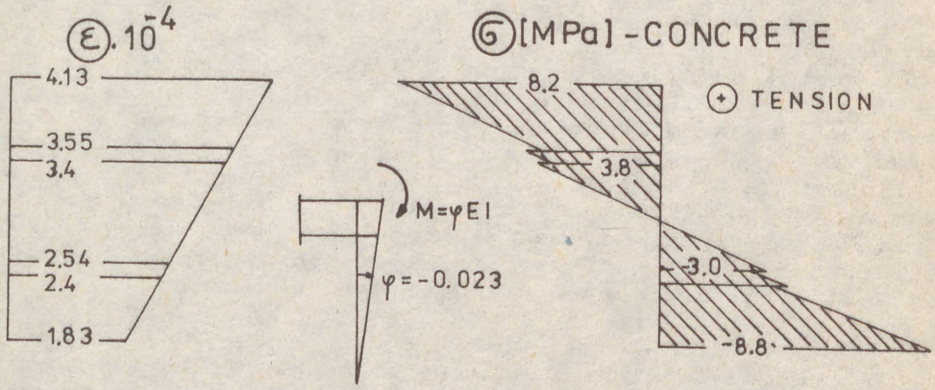

CONCRETE

STEEL

REINFORCEMENT

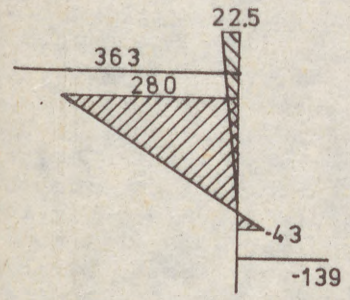

PRIMARY STRESSING

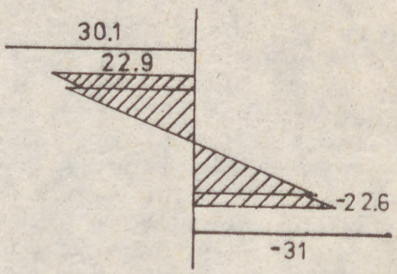

SECONDARY STRESSING

FIG.5

(8)

METHOD OF ANALYSIS

The analysis of tasks a, and b, described in above paragraph is made in incremental loading cycle. This approach is correct when the real construction is analysed, and its load carrying capacity is not necessary to define as an extremum of the load-deflection diagram. The method is a combination of two numerical methods: MTM and step-by-step plastification. The check of the ULS is made in every loading cycle and in every nodal point of the theoretical polygonal simulation of the deformed column. The application of MTM to the treated problem (due to lack of space first step only) is plotted schematically in Fig.1.

The task d, is solved in a following way. First, the distribution of isothermal lines over the cross-section for a steady heat flow is computed. Than the SRC cross-section is treated. The solution of B.Búci [2] is applied. This 'general' solution, supposing a common center of curvature for all layers, allows to analyse composite cross-sections consisting of not age equal concrete layers, steel layers, reiforcement bars and prestressing tendons. The thermal loading determined by distribution of isothermal lines and the resulted secondery stressing over the cross-section are plotted in Fig.5. The analysed section is identical with the cross-section of specimen C050.

COMPARISON

The theoretical results were compered with test results carried out in Japan by Prof.Wakabayashi. The comparison is plotted in Fig.2 for specimen C050 [7]. Parameters of specimen C050 and the ultimate moment of resistance about major axis for n=1.0, which was calculated in accordance with BS 5400/79 are shown in Fig.2 as well.

CONCLUSION

By means of the presented incremental numerical method it is possible to analyse beam columns subjected to arbitrary loading case. The plastification and development of cracks is shown in Fig.4. The method permits a development of local plastification over the cross-section as well. The output(Fig.3) is an adviseble design aid, because of a simple check of ULS for arbitrary M,N combination. A good agreement with test results is evident from Fig.2. The secondary stressing of SRC column due to 'thermal shock' could be significant. The analysed example, when the difference of external temperatures over the cross-section is assumed 470°C, shows that the secondary stressing in concrete is 38% .

REFERENCES: [1] BS 5400/79 Part 5; [2] Búci,B.:Reológia,ES SvF SVŠT,Bratislava,1989; [3] CEB/FIP-Design manual on buckling and instability,1978,The Constuction Press; [4] CEB/FIP MC for concrete structures,N°124/125; [5] ČSN 731201; [6] Šoltész,J.: Load carrying capasity of SRC columns, Stavebnícky časopis 4/87; [7] Wakabayashi et al: Recomendation for SRC structures..,Ass. of Japanese architects,Hokkaido, parts 2713,2714, 1978

SESSION 14

EARTHQUAKE ENGINEERING & DYNAMIC BEHAVIOUR

/1/
GYÖ

DYN
OF

Su
dyn
sta
tic
loa
abo
exp

1.

1.1

(1)

/1/
GYÖKÖS, Ferenc (1)

DYNAMIC TEST OF EQUILIBRIUM STATE OF ECCENTRIC LOADED THIN-WALLED STEEL I-BEAMS

INTERNATIONAL COLLOQUIUM
STABILITY OF STEEL STRUCTURES
BUDAPEST, HUNGARY, 1990
PRELIMINARY REPORT

Summary: The "perturbational method" -though it is a dynamic one essentially- can be used as well to identify statically loaded structures. This paper is about the theoretical investigation of undamped free vibration of eccentric loaded thin-walled steel I beams with closed flanges and about adoption of "perturbational method" during buckling experiment of such kind of beams.

1. THEORETICAL INVESTIGATION

1.1. Basic equations of equilibrium

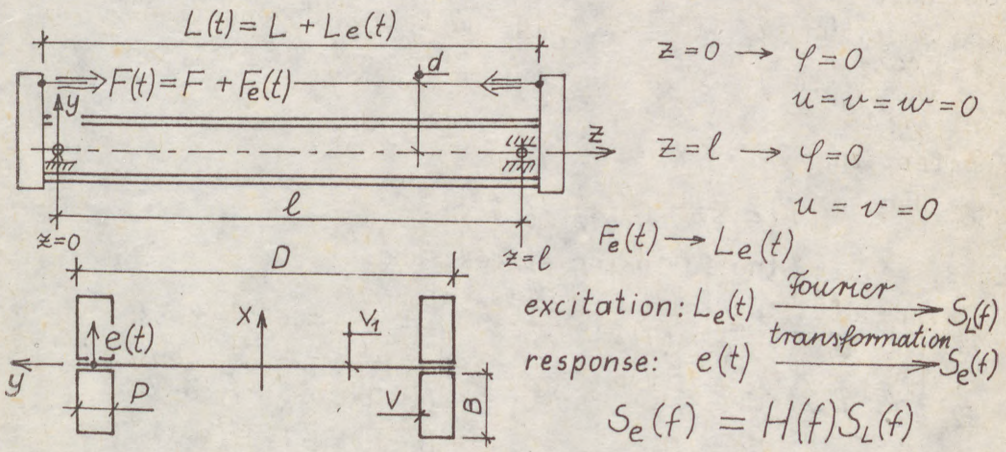

Fig.1.

(1) Head of the Structural Laboratory
of Hungarian Institute for Building Science (HIBS)

/2/
Fig.1. shows the cross section and the scheme of the support and the loading of the beam. The eccentric load functions in the symmetry plane of the beam.
The basic equations of equilibrium are the followings:

1. $K_\omega \varphi^{IV} - K_c \varphi'' = m - K_p m''$

2. $K_y u^{IV} = f_x$ 3. $K_x v^{IV} = f_y$

The buckling of the beam can be discussed according to the system of equations including Eq.1. and 2.
Intensities of the distributed torsional moment m and lateral load f_x by the length of the beam are as follows:

4. $m = F d u'' - F \frac{J_p}{A} \varphi'' - v \ddot{\varphi}$

5. $f_x = -F u'' + F d \varphi'' - \varrho \ddot{u}$

Introducing relations 4. and 5. into Eq.1. and 2., the basic system of equilibrium equations are the followings:

6. $\varphi^{IV}(K_\omega - F K_p J_p \frac{1}{A}) + \varphi''(F J_p \frac{1}{A} - K_c) + u^{IV} K_p d F - u'' F d - K_p v \ddot{\varphi}'' + v \ddot{\varphi} = 0$

7. $u^{IV} K_y + u'' F - \varphi'' F d + \varrho \ddot{u} = 0$

1.2. Free vibration of the unloaded beam

From Eq.6. and 7. if $F=0$ yield the following equations.

8. $K_\omega \varphi^{IV} - K_c \varphi'' = -v \ddot{\varphi} + K_p v \ddot{\varphi}''$

9. $K_y u^{IV} = -\varrho \ddot{u}$

Provided that

10. $\varphi(z,t) = \phi(z) \cdot \tau(t)$

Eq.8. results the following expressions:

11. $(K_\omega \frac{\phi^{IV}}{\phi} - K_c \frac{\phi''}{\phi}) : (K_p v \frac{\phi''}{\phi} - v) = \frac{\ddot{\tau}}{\tau} = -\alpha^2 = const.$

12. $\ddot{\tau} + \alpha^2 \tau = 0 \quad \rightarrow \quad \tau = Q \cdot \sin \alpha t + R \cos \alpha t$

13. $K_\omega \phi^{IV} - K_c \phi'' = -\alpha^2 (K_p v \phi'' - v \phi)$

14. $k^2 = \frac{\alpha^2 K_p v - K_c}{K_\omega}$, $\lambda = \alpha^2 \frac{v}{K_\omega}$

/3/

The characteristic equation, if $\phi = e^{qz}$, is the next:

15. $$q^4 + k^2 q^2 - \lambda = 0$$

The roots are:

16. $$q_1 = \left[\frac{k^2 + \sqrt{k^4 + 4\lambda}}{2}\right]^{1/2} = -q_3$$

17. $$q_2 = \left[\frac{-k^2 + \sqrt{k^4 + 4\lambda}}{2}\right]^{1/2} = -q_4$$

The general solution for Eq.15. is the following:

18. $$\phi = C_1 \sin q_1 z + C_2 \cos q_1 z + C_3 \operatorname{sh} q_2 z + C_4 \operatorname{ch} q_2 z$$

The boundary conditions according to Fig.1. are as follows:

$$\phi(0) = 0 \rightarrow C_2 + C_4 = 0$$

$$\phi''(0) = 0 \rightarrow -q_1^2 C_2 + q_2^2 C_4 = 0 \Rightarrow C_2 = C_4 = 0$$

From these equations results the following system of equations:

19. $$\begin{bmatrix} \sin q_1 l & \operatorname{sh} q_2 l \\ -q_1^2 \sin q_1 l & q_2^2 \operatorname{sh} q_2 l \end{bmatrix} \begin{bmatrix} C_1 \\ C_2 \end{bmatrix} = \underline{0}$$

The condition of its nontrivial solution is given by

20. $$\sin q_1 l \operatorname{sh} q_2 l \,(q_1^2 + q_2^2) = 0$$

if $q_2 \neq 0$

21. $$\sin q_1 l = 0 \rightarrow q_1 l = n\pi \qquad n = (1, 2, \ldots)$$

22. $$q_1 = \frac{n\pi}{l}$$

From Eq.16. and 22. is obtained:

23. $$\frac{n^4 \pi^4}{l^4} - \frac{n^2 \pi^2}{l^2} k^2 = \lambda$$

The Eq.14. and 23. result:

24. $$\frac{n^4 \pi^4}{l^4} - \frac{n^2 \pi^2}{l^2} \frac{v}{G J_p^*} \alpha_n^2 - \frac{n^2 \pi^2}{l^2} \frac{K_c}{K_\omega} = \frac{v}{K_\omega} \alpha_n^2$$

/4/
The square of the n-th rotational eigenfrequency from this equation is:

$$25.\quad \alpha_n^2 = \frac{n^2\frac{\pi^2}{\ell^2}\left(n^2\frac{\pi^2}{\ell^2}K_\omega + K_c\right)}{\nu\left(1+\frac{n^2\pi^2}{\ell^2}K_p\right)}$$

The square of the smallest rotational eigenfrequency is:

$$26.\quad \alpha^2 = \frac{\frac{\pi^2}{\ell^2}\left(\frac{\pi^2}{\ell^2}K_\omega + K_c\right)}{\nu\left(1+\frac{\pi^2}{\ell^2}K_p\right)}\,, \qquad \nu = \rho\frac{J_p}{A}$$

$$27.\quad \alpha^2 = \frac{1}{\rho}\frac{\pi^2}{\ell^2}F_\varphi \qquad 28.\quad F_\varphi = \frac{K_c + K_\omega\frac{\pi^2}{\ell^2}}{\left(1+K_p\frac{\pi^2}{\ell^2}\right)\frac{J_p}{A}}$$

Similarly to the previous ones, provided that

$$u(z,t) = U(z)\,T(t)$$

the following expressions give the square of radian frequencies of free lateral vibration which is perpendicular to the web plane.

$$29.\quad \beta_n^2 = \frac{1}{\rho}K_y\frac{n^4\pi^4}{\ell^4} \qquad n=(1,2,\dots)$$

$$30.\quad \beta^2 = \frac{1}{\rho}K_y\frac{\pi^4}{\ell^4} \qquad 31.\quad \beta^2 = \frac{1}{\rho}\frac{\pi^2}{\ell^2}F_y$$

$$32.\quad F_y = K_y\frac{\pi^2}{\ell^2}$$

These relations are quite remarkable as they reveal a connection between the smallest radian eigenfrequencies (α , β) of free vibrations of unloaded beams and the smallest bifurcational critical loads of axial compression beam (F_φ , F_y) being in static equilibrium state. That is the special marginal case of the static loading capacity can be determined by means of dynamic tests.

/5/

1.3. Free vibration of eccentric compression beams

Presumed that

33. $$\varphi = \phi(z) \cdot \sin \omega t$$

34. $$u = U(z) \cdot \sin \omega t$$

and substituting these for Eq.6. and 7., yield the following equations:

35. $$\phi^{IV} p_4 + \phi'' p_2 + U^{IV} r_4 - U'' r_2 + t_4 \phi'' \omega^2 - \nu \phi \omega^2 = 0$$

36. $$U^{IV} s_4 + U'' s_2 - r_2 \phi'' - \varrho U \omega^2 = 0$$

From Eq. 36. is obtained:

37. $$\phi'' = (U^{IV} s_4 + U'' s_2 - \varrho U \omega^2) : r_2$$

38. $$\phi^{IV} = (U^{VI} s_4 + U^{IV} s_2 - U'' \varrho \omega^2) : r_2$$

The constants can be written as the followings:

39.
$$p_2 = F \frac{J_p}{A} - K_c \qquad p_4 = K_\omega - F K_p \frac{J_p}{A}$$
$$r_2 = F d \qquad r_4 = K_p F d$$
$$s_2 = F \qquad s_4 = K_y, \quad t_4 = K_p \nu$$

Eq.40. follows from Eq. 37., 38., and 35.

40. $$U^{VIII} b_8 + U^{VI} b_6 + U^{IV} b_4 + U'' b_2 + U b_0 = 0$$

$$b_0 = \varrho \nu \omega^4, \quad b_2 = -\varrho p_2 \omega^2 - t_4 \varrho \omega^4 - s_2 \nu \omega^2$$

$$b_4 = s_2 p_2 - p_4 \varrho \omega^2 - r_2^2 + s_2 t_4 \omega^4 - s_4 \nu \omega^2$$

$$b_6 = s_2 p_4 + s_4 p_2 + r_4 r_2 + s_4 t_4 \omega^2, \quad b_8 = s_4 p_4$$

Provided that

41. $$U = \mathcal{U} \cdot \sin \frac{\pi z}{l}$$

Eq. 40. results:

42. $$b_8 \frac{\pi^8}{l^8} - b_6 \frac{\pi^6}{l^6} + b_4 \frac{\pi^4}{l^4} - b_2 \frac{\pi^2}{l^2} + b_0 = 0$$

/6/
Without the details from the Eq.42., the relation between the eccentric load F and the smallest radian frequency ω is as follows:

$$43.\quad F_y F_\varphi \frac{\pi^4}{\ell^4} - \rho\omega^2(F_y+F_\varphi)\frac{\pi^2}{\ell^2} + (\rho\omega^2)^2 - F(F_y+F_\varphi)\frac{\pi^4}{\ell^4} + F^2\left(1-\frac{A}{J_p}d^2\right)\frac{\pi^4}{\ell^4} = 0$$

$$44.\quad (\rho\beta^2)(v\alpha^2) - \rho v\omega^2(\beta^2+\alpha^2) + \rho v\omega^4 - Fv(\beta^2+\alpha^2)\frac{\pi^2}{\ell^2} + F^2\left(\frac{J_p}{A}-d^2\right)\frac{\pi^4}{\ell^4} = 0$$

Eq. 44. is an analogous form to Eq. 43. expressing the equation with frequencies of free vibrations of unloaded I-beams.
The diagrams of the analogous relations, Eq. 43. and 44. demonstrate well, that while the axial compression is increasing, the radian frequency of free vibration is decreasing.
When the axial load reaches the buckling critical value F_c, the natural frequencies become zero.
When $F=0$, the frequency is ν_0, which is the resonance frequency of free vibration of unloaded beam. Fig.2. represents the function $F(\nu^2)$ in a concrete case. In this case the characteristics of the beam are:

$$v = 3mm,\ v_1 = 5mm,\ D = 600mm,\ P = 50mm,\ \ell = 9600mm,\ d = 600mm$$

$$\nu = \frac{1}{2\pi}\omega \qquad [\nu] = [\omega] = Hz = \frac{1}{s}$$

This case represents well that the relation between the F and ν^2 is nearly linear although the eccentricity of load is relatively big in terms of to the size of the cross section of beam.

In case of small eccentricity of the load the function $F(\nu^2)$ can be considered practically linear.
It has a great importance in the experiments with the loadbearing structures.

It is impossible to determine directly the load of bifurcation of the equilibrium of the beam.

It is enough to measure frequencies of the beam on two load levels.

/7/
The linear function gives critical load indirectly.

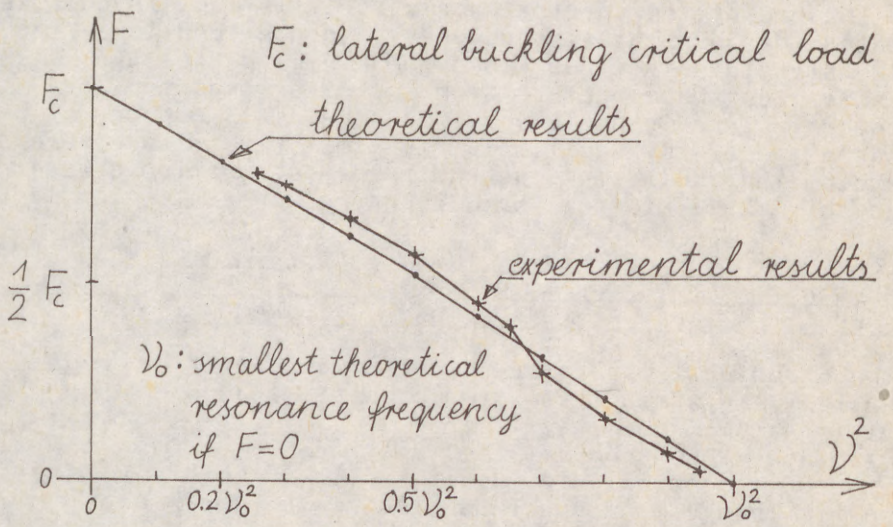

Fig.2.

2. EXPERIMENTS FOR TESTING OF VIBRATIONS OF ECCENTRIC LOADED THIN-WALLED I-BEAMS.

2.1. Substance of the applied perturbational method".

The "perturbational method" is the most convenient one in the laboratory for experimental identification of loadbearing structures.
The substance of this method is the following:
First we originate the static equilibrium state of the structure with loading actuators and afterwards we originate the small random perturbation of this equilibrium state with one of the loading actuators.

This way the perturbating actuator provides the input signal, the measuring system provides the output signal.

From the aspect of the structure, the controlled load or motion is input signal, but any of the measured mechanical responses of the structure is the output signal.

The controlled loading actuator drived by a noisegenerator provides a noise excitation of limited frequency range as input signal.
The two-channel signal analyzer executes the spectral analyzis of the input and output signals.

/8/
Thus the dynamic behaviour of the tested structure can be evaluated provided that the analyzis is carried out with well selected excitation and response processes.

With the use of the spectral analyzis it is most favourable to determine any typical frequency response functions /F.R.F./. If the structure is linear than the F.R.F. perfectly characterizes the structure from the given aspect. If the structure is nonlinear, than the small degree perturbation of the equilibrium is similarly a linear process regarding the excitation and the response function characterizes this state of equilibrium under given static loading.

2.2. Adoption of the "perturbational method" for dynamic test of eccentric loaded thin-walled steel I-beams

In the Structural Laboratory of HIBS was performed several experimental dynamic test with eccentric loaded thin-walled steel I-beams.
Fig 1. shows the scheme of the test.
The feedback-controlled actuator provided the static eccentric load F and superposed on F the small perturbation $F_e(t)$.
In this test the input signal was $F_e(t)$ or $L_e(t)$, output signal was $e(t)$ (see Fig.1.)
The two-channel signal analyser executed the spectral analyzis of the input and output signals.
The result of the analys is the Frequency Response Function $H(f)$.

$$H(f) = K(f)\, e^{i\psi(f)}$$

Fig.3. shows the $K(f)$ function if the static load $F = 120\,kN$

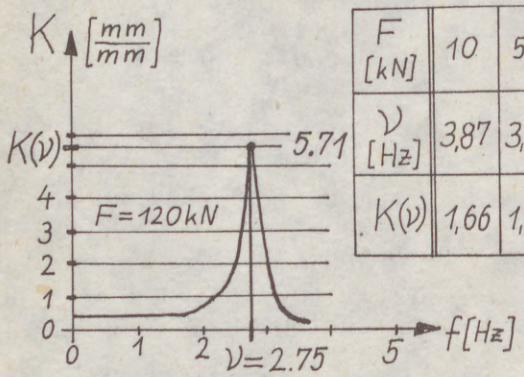

F [kN]	10	50	80	100	120	140	150	158
ν [Hz]	3,87	3,31	3,19	3,00	2,75	2,38	2,12	2,00
K(ν)	1,66	1,49	3,52	4,70	5,71	7,72	15,4	36,5

Fig.3.

/9/ The $H(f)$ function characterizes the mechanical state of the beam on this load level.
If we change the static load F the dynamic properties of the beam will change.
These changes are shown by the Frequency Response Functions.
The $H(f)$ function precisely shows the smallest resonance frequency of the beam on this load level.
If the static load F increases, the smallest resonance frequency $f=\nu$ decreases and the amplitude $K(\nu)$ increases, too.
These phenomena are in accordance with the theoretical results which are shown in Fig.2.
If we cant determine the critical load of the bifurcation of the equilibrium theoretically,we can measure the frequency of the free vibration under various loading forces. Then the experimental graph indicates the critical load in abscissa.
Fig.2. shows the experimental results, too.
The Fig.2. shows that the theoretial results in this case correspond well with experimental results.

NOTATION:

x, y, z : rectangular coord.system
u, v, w : displacement components to x, y, z directions
$\varphi(z,t)$: rotation around z axis
F : eccentric static load d : eccentricity of loading
$F_e(t)$: random force excitation t : time
$L_e(t)$: random displacement excitation
$e(t)$: random displacement of the upper flange of the beam (Fig.1.)
$S_L(f)$: complex spectrum of displacement excitation (Fig.1.)
$S_e(f)$: complex spectrum of displacement response (Fig.1.)
$H(f)$: complex frequency response function, f : frequency
E : Young modulus, G : shear modulus
$K_\omega = EJ_\omega$, $K_c = GJ_c$, $K_p = K_\omega : GJ_p^*$, $K_y = EJ_y$, $K_x = EJ_x$
$J_\omega, J_c, J_p^*, J_x, J_y, A$: cross sectional geometric quantities
m and f_x : distributed torsional moment and lateral load
ν : moment of inertia per unit length of the beam-column
ρ : mass per unit length of the beam-column
α : smallest radian frequency of rotational free vibration if
β : smallest radian frequency of lateral bending free vibration if

/10/ F_φ : centric rotational critical load

F_y : centric bending critical load (Euler force)

ω : smallest radian frequency of free vibration if and lateral bending is with rotation

$K(f)$: magnitude of $H(f)$ function

$\Psi(f)$: phase of $H(f)$ function

$K(\nu)$: first maximum value of $K(f)$ function

REFERENCES:

- Chen,W.F. and Atsuta, T. 1976. "Theory of Beam Columns"
- Lurie, H. 1952. "Lateral Vibrations as Related to Structural Stability", Journal of Applied Mechanics. June, 1952.p.10, 195-204
- Massonnet,C. 1940. "Les Relations Entre Les Modes Normaux De Vibration Et La Stabilité Des Systémes Élastiques"
- Souza,M.A., Fok,W.C., Walker, A.C. 1983. "Review of Experimental Techniques for Thin-walled Structures Liable to Buckling" Part I and Part II, Experimental Techniques September, 1983. p. 4, 21.-24. and October, 1983. p.4,36.-39.
- Timoshenko,S.P. and Gere, I.M. 1961. "Theory of Elastic Stability"

Kozarov, Marin (1)
Chong, N. (2)

DYNAMIC STABILITY OF ELASTIC ELLIPTIC CYLINDRICAL SHELLS AND PANELS

INTERNATIONAL COLLOQUIUM
STABILITY OF STEEL STRUCTURES
BUDAPEST, HUNGARY, 1990
PRELIMINARY REPORT

Summary: The paper is concerned with the dynamical stability of elastic cylindrical shells and panels of elliptic crossection, charged with axial pulsating loading. Linear as well as nonlinear vibration is investigated. Some analytical and numerical results obtained here with the aid of computer programs are compared with those known from the literature. Also, the parametric resonance of the systems is investigated and a new formula has been obtained.

Thin-walled shells and panels are basic structural elements in a broad sense of the concept of civil engineering. More then two thousend papers have appeared so far, most of them dedicated to the stability problems. Comprehensive surveys on the topic can be found in the monographs by Volimir [1], [2], [3], [4] and by Bolotin [5].

Sinse 1963 a group of researchers in the Higher Institute for Architecture and Civil Engineering in Sofia have been dealing with thin-walled elliptic cylindrical shells and panels, including statical elastic and elastoplastic instability, creep buckling, thermoinstability, hydroelastic and aeroelastic stability, dynamic stability and vibration.

I. Dynamic Stability of an Elliptic Cylindrical Shell with Axial Compression

Given an elliptic cyllindrical shell (Fig. 1) of radius of curvature and eccentricity

$$\varepsilon = \sqrt{1-(b/a)^2}\ ;\quad R = b^2(1-\varepsilon^2\cos^2\varphi)^{-3/2}/a \qquad (1), (2)$$

(1) Professor of Mechanics, Higher Institute for Architecture and Civil Engineering, Sofia, Bulgaria

(2) Researcher of Mechanics, Higher Institute for Architecture and Civil Engineering, Sofia, Bulgaria

respectively.

The classical Vlassov's linear differential equations

$$\frac{1}{E}\nabla^4\Phi = -\frac{1}{R}\frac{\partial^2 w}{\partial x^2}\ ; \tag{3}$$

$$\frac{D}{h}\nabla^4 w = \frac{\partial^2\Phi}{R\partial x^2} - p\frac{\partial^2 w}{\partial x^2} - \rho\frac{\partial^2 w}{\partial t^2} \tag{4}$$

with the boundary conditions corresponding to simply supported edges set the problem to be solved in three different variants.

First Variant: Here the approximation for the displacement is of the form

$$w(x,y,t) = f(t)R^* \sin\alpha x \cos\beta y\ ; \tag{5}$$

$$w(x,y,t) = f(t)R^* \sin\alpha x \sin\beta y\ , \tag{6}$$

where

$$R^* = R_1 + (R_2 - R_1)\sin^2\frac{y}{R_0}\ ;$$

$$\alpha = \frac{m\pi}{L}\ ;\ \beta = \frac{n}{R_0}\ ;\quad m = 1,2,3,\ldots\ ;\quad n = 0,1,2,\ldots\ ;$$

and R_1, R_2 are the largest and the smallest radius of curvature of the crossection, while R^* stands for the first approximation of the variable radius of curvature R. The latter differs slightly from R^* so that $R^* \approx R$.

The functions (5) and (6) describe the even and odd modes of postcritical shell motion with respect to the small axis of the ellipse. Applying the well-known Bubnov-Galerkin procedure consecutively to (5) and (6) one arrives at the differential equation

$$\ddot{f} + \Omega^2(1 - 2\bar{\mu}\cos\vartheta t)f = 0;\quad \Omega^2 = \frac{K_1 - P_0 K_2}{K_0}\ ;\quad \bar{\mu} = \frac{K_2 P_t}{2(K_1 - P_0 K_2)}\ , \tag{7}$$

where K_0, K_1 and K_2 are coefficients which vary depending on the approximation function.

The principal regions of instability are obtained through the Bolotin's formula [5]

$$\vartheta_{cr} = 2\Omega\sqrt{1 \pm \mu} \quad \text{or} \quad \vartheta_{cr} = 2\omega^2\sqrt{1 - \frac{P_0 \pm P_t/2}{P_{cr}}}\ , \tag{8),(9}$$

wherein $\omega^2 = K_1/K_0$; $P_{cr} = K_1/K_2$

while ω is the natural frequency and P_{cr} is the critical loading for the same postcritical mode.

It is worth noting that ϑ_{cr} is a complicated function of α and β and so it is inexpedient to obtain its extremum values analytically. Here the smallest critical frequencies have been calculated directly varying m and n. This approach is convenient for the problem at hand for it is easely seen from the

above formulae that ϑ_{cr} attains its minimum value for relatively small m and n. If these integers are large enough then we have approximately $\vartheta_{cr} = \alpha^2 + \beta^2$.

In the same manner we can establish minimum ω and P_{cr}.

Second Variant: The even and odd modes with respect to to the small axis of the crossection are respectively:

$$w = f(t)\, R \sin\alpha x \cos\beta y \; ; \tag{10}$$

$$w = f(t)\, R \sin\alpha x \sin\beta y \; . \tag{11}$$

It should be noted that the derivatives of R and R^* differ too much from each other although the radiuses themselves do not. This is the difference between the first and the second variants of the solution.

The Bubnov-Galerkin procedure leads to the same equation (7) but the coefficients (10) and (11) are different.

All the expressions have been programmed using FORTRAN-IV. Some final results are discussed after the third variant has been stated.

Third Variant: The approximation function is

$$w(x,y,t) = R\left[f(t)\sin\alpha x \cos\beta y + g(t)\sin^2\alpha x\right] , \tag{12}$$

i.e. we have chosen the expression for the static stability analysis for the circular cylindrical shell multiplied by R, which accounts for the noncircular crossection. The solution is now based on the Lagrangian's equations of the second kind

$$\frac{\partial}{dt}\frac{\partial T}{\partial \dot{q}_i} - \frac{\partial (T-\Pi)}{\partial q_i} = Q_i \tag{13}$$

or in matrix definition

$$A\ddot{\vec{F}} + B\vec{F} - P(t)\,C\vec{F} = 0 \; . \tag{14}$$

The critical frequences in the principal instability region are obtained approximately using the trigonometric series method [5]:

$$\mathrm{Det}\left[-\frac{\theta^2}{4}A + B - \left(P_0 \pm \frac{1}{2}P_t\right)C\right] = 0 \; . \tag{15}$$

The equation for the natural frequency is

$$\mathrm{Det}\left[-\omega^2 A + B\right] = 0 \; , \tag{16}$$

while the frequency when an axial compression is applied is obtained from the equation

$$\mathrm{Det}\left[-\bar{\omega}^2 A + B - P_0 C\right] = 0 \quad . \tag{17}$$

The critical loading, corresponding to the mode of vibration follows from the equation

$$\mathrm{Det}\left[B - P C\right] = 0 \quad . \tag{18}$$

Figures 2 and 3 show some numerical results obtained with the aid of a computer program.

II. Dynamic Stability of an elliptic cylindrical panel with axial loading

Linear as well as nonlinear problems will be considered for the panel given in Fig. 4.

Linear problem: The solution is based on the Lagrange's equations of the second kind. The displacement $w(x,y,t)$ is of the form

$$w(x,y,t) = R(y)\, f(t) \sin \alpha x \sin \beta y \tag{19}$$

thus satisfying the boundary conditions for simply supported edges. The Lagrange's equations mentioned above lead to

$$\ddot{f} + \Omega^2 (1 - 2\bar{\mu}\cos\theta t) f = 0 \; ; \tag{20}$$

$$\Omega^2 = \frac{C_2 - P_0 C_3}{C_1} \; ; \quad \bar{\mu} = \frac{P_t C_3}{2(C_2 - P_0 C_3)} \quad . \tag{21}$$

The critical frequencies of the principal region of instability are determined by the Bolotin's formula. As for the natural frequency and the upper critical loading they are calculated through the expressions

$$\omega = \sqrt{\frac{C_2}{C_1}} \; ; \quad P_{cr} = \frac{C_2}{C_3} \quad . \tag{22}$$

Some numerical results are plotted in Fig. 5.

Nonlinear problem: This solution appeared to be cumbersome and complicated from mathematical point of view. On the basis of the classical system of the Vlassov's nonlinear differential equations with respect to the displacement W and the function Φ and applying the Bubnov-Galerkin procedure along with the Lagrange's differential equations, one arrives at the Mathieu nonlinear equation

$$\ddot{f} + \Omega^2 (1 - 2\mu\cos\theta t) f - C_2 f^2 + C_3 f^3 = 0 \; ; \tag{23}$$

$$\mu = P_t/(2(P_{cr}-P_0)) \; ; \; P_{cr} = \omega^2/C_1 \; ;$$
$$C_1 = K_P/K_0 \; ; \; C_2 = h K_2/K_0/H_n \; ; \; C_3 = h^2 K_3/K_0/H_n^2 .$$

Here f is a dimensionless parameter and H_n is a norm of the coordinate function.

The differential equation (23) governs the dynamical process into consideration. As an analytic solution is hardly possible we rely on a numerical solution. For this purpose a computer program has been made which enables the user to consider some particular cases as well, including chaotic motion. However the latter is beyond the scope of the present paper and will not be discussed here.

III. After having investigated the dynamical stability of elliptic sylindrical shell and panel thoroughly let us further study the parametric resonance of the nonlinear system. The governing differential equation is of the form

$$\ddot{f} + \Omega^2(1 - 2\mu\cos\vartheta t)f - C_2 f^2 + C_3 f^3 = 0 \; . \qquad (24)$$

According to the Lyapunov's theory we study the stability of an initial equilibrium position of the system acted upon by a parametric excitation. In that sense the critical frequencies of the principal parametric resonance can be obtained by the Bolotin's formula. Some other authors have considered an analogous problem concerned with a circular cylindrical panel under pulsating load using the small parameter method. However the coefficients C_2 and C_3 are large so that it may not be applied here.

Before studying the parametric resonance let us admit that

1) For $\mu = 0$ the initial conditions are chosen such that the amplitude of vibration is A_0 ;

2) For $\mu \neq 0$ and the same initial conditions parametric resonance is said to appear when the amplitude of vibration is greater then A_0 . Besides we restrict ourselves to the case of an autonomous system which vibrates in the vicinity of its equilibrium position. The first approximation of the solution obtained through the harmonic balance method is

$$f(t) = \bar{a}_0 + \bar{a}_1 \cos\Omega_N t + \bar{b}_1 \sin\Omega_N t \; , \qquad (25)$$

where Ω_N is the nonlinear natural frequency.

Inserting (25) into (24) for $\mu = 0$ and using again the harmonic balance method we have the system

$$\begin{aligned}
&\bar{a}_0 + \sqrt{\bar{a}_1^2 + \bar{b}_1^2} = A_0 \; ; \\
&2C_3\bar{a}_0^3 - 2C_2\bar{a}_0^2 + [2\Omega^2 + 3C_3(\bar{a}_1^2 + \bar{b}_1^2)] - C_2(\bar{a}_1^2 + \bar{b}_1^2) = 0 \; ; \\
&\cdots\cdots\cdots\cdots\cdots \qquad (26) \\
&\cdots\cdots\cdots\cdots\cdots .
\end{aligned}$$

Next we are looking for a solution of the principal para-

metric resonance in the form

$$f(t)=a_0+a_1\cos\frac{\theta}{2}t+b_1\sin\frac{\theta}{2}t\ . \qquad (27)$$

Inserting now (27) into (24) for $\mu\neq 0$ and applying the harmonic balance method we derive an analogous system

$$a_0+\sqrt{a_1^2+b_1^2}=A_0\ ;$$
$$2C_3a_0^3-2C_2a_0^2+\left[2\Omega^2+3C_3(a_1^2+b_1^2)\right]-C_2(a_1^2+b_1^2)=0; \qquad (28)$$

- - - - - - - - - - - - - - - - ;

- - - - - - - - - - - - - - - - .

Some relations exist between the solutions of the last two systems, namely

$$\frac{\theta^2}{4}+\mu\Omega^2=\Omega_N^2\ ; \qquad (29)$$

$$\frac{\theta^2}{4}-\mu\Omega^2=\Omega_N^2\ . \qquad (30)$$

or

$$\theta_{cr}^N=2\Omega_N\sqrt{1\pm\mu_N}\ ; \qquad (31)$$

$$\mu_N=\left(\frac{\Omega}{\Omega_N}\right)^2\mu\ .$$

The formula (31), derived here gives the critical frequency for the principal parametric resonance of the system (24) for a prescribed amplitude A_0. As for the nonlinear natural frequency of the system Ω_N it may be obtained solving (26). Also the formula (31) possesses the following features:

1) When $A_0=0$ and a linear system it reduces to the Bolotin's formula;

2) The numerical examples show that in comparison with the Bolotin's formula (31) leads to more accurate results for the critical frequencies;

3) It may be applied when considering other problems of dynamical stability;

4) On the basis of the results obtained here one concludes that the parametric resonance can occur regardless of whether the elastic force graws monotonically or not. In the latter case the parametric resonance can appear both on the increasing and on the decreasing branch of the force. Consequently the presence of a decreasing branch of the elastic force is not necessary condition for parametric instability.

References:

1. Volimir, A.C., Stability of elastic systems, Moscow, 1967 (in Russian)

2. Volimir, A.C., Nonlinear Dynamics of Plates and Shells, Moscow, 1972 (in Russian)

3. Volimir, A.C., Problems of Aeroelasticity, Moscow, 1976, (in Russian)

4. Volimir, A.C., Problems of Hydroelasticity, Moscow, 1979, (in Russian)

5. Bolotin, V.V., Dynamic Stability of Elastic Systems, Moscow, 1956, (in Russian)

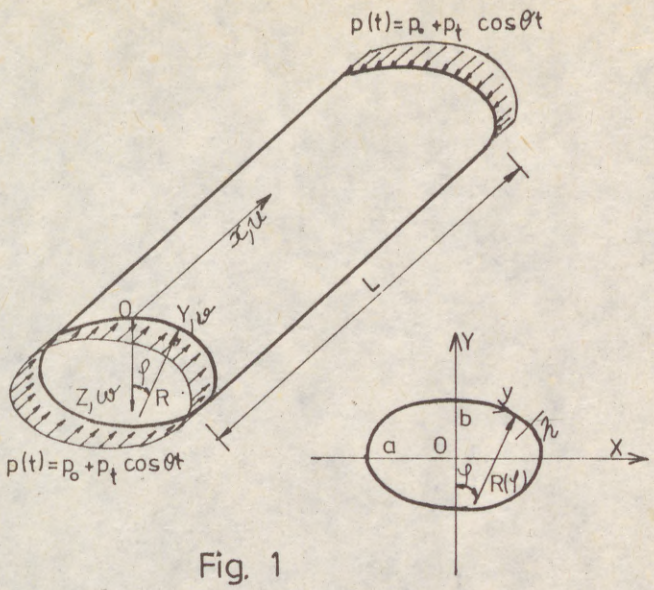

Fig. 1

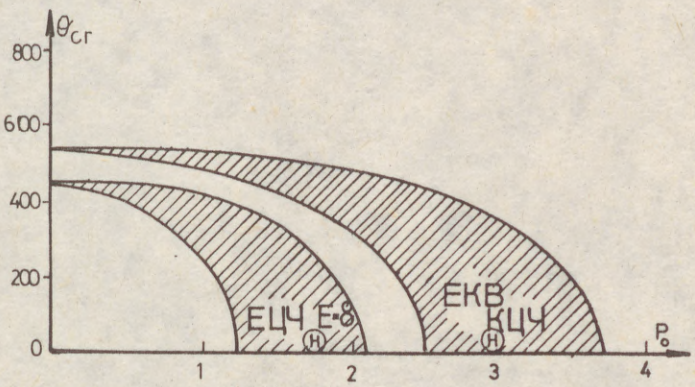

Fig. 2

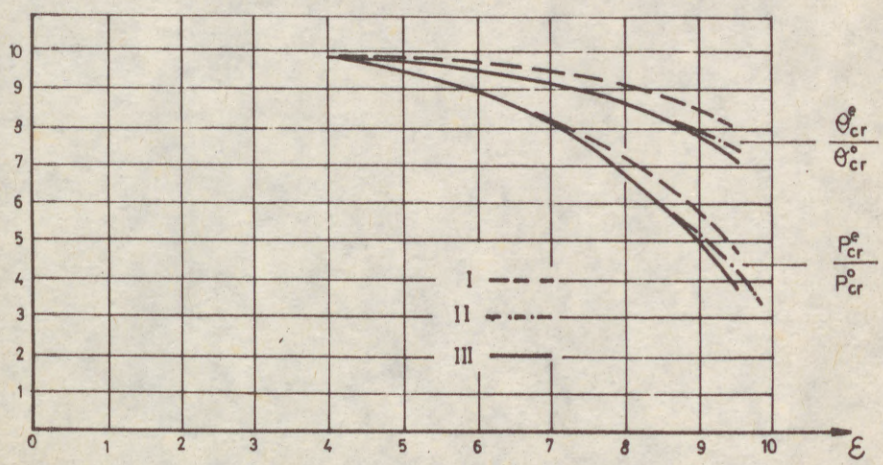

Fig. 3

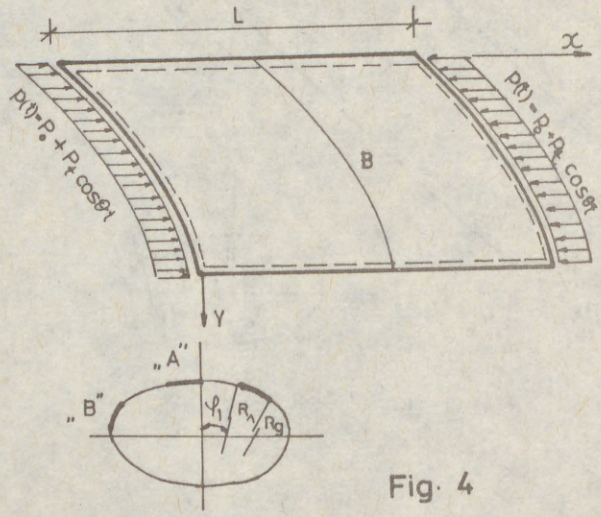

Fig. 4

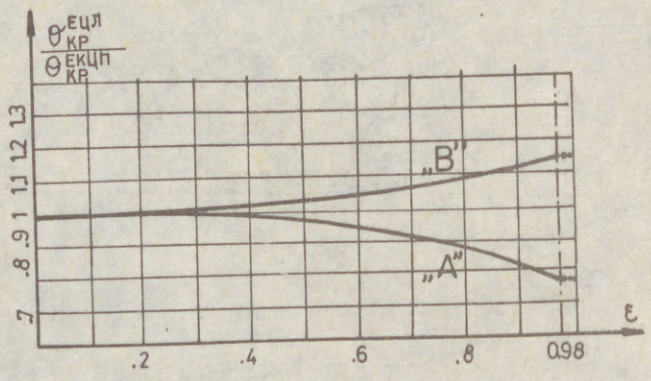

Fig. 5

(1)
MAZZOLANI, Federico M. (*)

THE EUROPEAN RECOMMENDATIONS FOR STEEL STRUCTURES IN SEISMIC AREAS.

INTERNATIONAL COLLOQUIUM
STABILITY OF STEEL STRUCTURES
BUDAPEST, HUNGARY, 1990
PRELIMINARY REPORT

Summary: The basic principles, which have inspired the preparation of the European Recommendations for Steel Structures in Seismic Zones (ERSSSZ), are presented here. A short survey on the contents of these Recommendations is also given, by emphasizing the subjects of main interest in the calculation and design of seismic-resistant structures.

1. INTRODUCTION: The interest of the European Convention for Constructional Steelwork in the problem of earthquake engineering has by now an established tradition of more than twenty years.

In the last years the ECCS - Committee "Seismic design" honoured this tradition by carrying out studies and researches on the behaviour of the steel structures and their component under seismic actions [Mazzolani, 1988].

With the publication of the European Recommendations for Steel Structures in Seismic Zones [ECCS, 1988], the already existing "seismic culture" reached a very significant stage which merits to be emphasized from the scientific and technical point of view.

The eighties will be remembered by historians as the "golden years" of Eurocodes and now the unification at European level is a driving necessity. This climate influenced the last period of activity of the ECCS Committee, which developed the main part of its work as a consulting body of the drafting panel of EC8 "Structures in seismic regions",

---

(*) Full Professor of Structural Engineering,
University of Naples (I).

(2)

with particular reference to its Chapter 3, which is directly devoted to steel structures. The pressing deadlines for the issue of EC8 forced the ECCS Committee to accelerate in a very short time the preparation of its Recommendations (ERSSSZ).

2.THE CONTENTS OF THE ECCS RECOMMENDATIONS: The matter is basically subdivided into three parts:

Part 1: General principles and seismic actions.

Part 2: Rules for structural analysis.

Part. 3: Rules for structural design.

The first part has a general character, because it contains the safety principles for designing steel structures in seismic zones. Seismic actions and their combinations with the design load are given here in qualitative way, on the hypothesis that each national territory is subdivided into three areas of different seismicity. The task to quantify the seismic parameters is left to the national Authorities of each Country.

The second part deals with the calculation methods (direct dynamic analysis, response spectrum modal analysis, static equivalent analysis). The safety verifications against collaps are given together with the limitations of damage and of unforeseen behaviour. Particular attention is paid to the definition of the structural regularity and to the effect of non structural elements on the seismic behaviour.

The third part is completely devoted to the design criteria and safety checks of seismic-resistant structures made of steel. They are classified in different types from the seismic point of view, which mainly subdivide them into dissipative or non dissipative structures. Appropriate behaviour factors are assessed for each type. Particular requirements are imposed for materials and connections belonging to dissipative zones. The given design rules are strictly correlated to EC3, which gives the basic references. The safety checks are provided for the structural elements in the main typologies.

3.DISSIPATIVE STRUCTURES: Contrary to non-dissipative structures, which must resist the most severe seismic event in elastic range, the dissipative structures can be designed by allowing the yielding of some zones of its members. During a catastrophic earthquake these zones - so called dissipative zones - dissipate the cinetic energy of the earthquake by means of a hysteretic ductile behaviour.

The dissipative structures, in the ERSSSZ as well as in EC8, are classified in the following way:

a) Frame structures, consisting in rigid joint frames which exhibit a large number of dissipative zones.

(3)

They resist the horizontal forces in an essentially bending manner. The dissipative zones are mainly located near the beam-to-column joints and energy can be dissipated by means of cyclic bending behaviour. Plastic hinges must lie in the beams rather than in the columns.

b) Concentric truss bracings, in which horizontal forces are mainly resisted by bars subjected to axial actions. In these structures the dissipative zones are mainly located in the tensile diagonals. They are dubdivided in:
   - diagonal bracings, in which the horizontal forces can be resisted by the tension diagonals only, neglecting the compression diagonals;
   - V-bracings, in which the horizontal forces can be resisted by considering both tension and compression diagonals;
   - K-bracing, cannot be considered as dissipative when the diagonals intersect the column in an intermediate point, by producing the participation of the column to the yielding mechanism.

c) Eccentric truss bracings, which combine the ductility of the frame structures with the lateral stiffness typical of bracings. The horizontal forces are mainly absorbed by axially loaded members, but the eccentricity of the layout allows the energy dissipation by means of a cyclic bending or/and shearing behaviour of the beams. They belong to the group of dissipative structures provided that the bending or shear limit strength of the beams or part of them precedes the attainment of the tension or compression limit strength of the other bars.

d) Cantilever structures, which act essentially as beam-columns where the dissipative zones are mainly located at the base.

e) Braced frame structures, in which horizontal forces are resisted by both frames and bracings acting in the same plane.

f) Structures with reinforced concrete cores or walls, which mainly resist the horizontal forces with dissipative zones located at the base.

g) Mixed structures in steel and reinforced concrete, in which the horizontal forces are resisted by both reinforced concrete structures and steel frameworks or truss bracings.

4. STRUCTURAL REGULARITY: The experience of the past earthquakes demonstrate that regular buildings behave much

(4)

better than non regular ones. The problem of a correct definition of "what regular building means" is up-to-now very far from a satisfactory solution. Nevertheless, a distinction between regular and irregular buildings must be made in the codes in order to establish the corresponding behaviour factor q.

Both in ERSSSZ and in EC8, a building is referred to as "regular", when the following conditions are satisfied.

Plan configuration: The building has a significant symmetry of structure and mass with regard to at least two orthogonal axes. When re-entrant corners or recesses exist, their dimension does not exceed 25% of the external size of the building in the corresponding direction.

The distance (as measured perpendicularly to the direction of the seismic action) between the centre of gravity of the mass and the centre of stiffness does not exceed, at each floor, 15% of the "torsional stiffness distance", defined as the square root of the ratio between the torsional stiffness and the translational stiffness of the building at the considered floor.

Vertical configuration: The stiffness and mass properties must be approximately uniform along the building height.

In case of gradually tapering buildings with symmetry about the vertical axis, the extent of setback at each floor must not exceed 20% of the previous plan dimension.

The above limit may be exceed up to 50%, if the setback stops at a level 15% below the top of the building.

In case of only one tapered facade, the setback at each floor must not exceed 10% and the overall setback must not be greater than 30% of the plan dimension at the first floor.

5.BEHAVIOUR FACTORS: For the above-mentioned typological **classes** of dissipative steel structures (see para 3.), the corresponding q-factors values, which account for energy dissipation capacity and post-elastic resistance, are given as a function of the ratio α_u / α_1, being:

α_1 the multiplier of the horizontal seismic actions, by keeping constant the other design loads, which corresponds to the point where the structure reaches its elastic limit in one section;

α_u the multiplier of the horizontal seismic actions, by keeping constant the other design loads, which corresponds to the point where the structure reaches the maximum load bearing capacity due to the formation of plastic hinges in the assumed dissipative zones in a sufficient number to transform the structure

(5)

in to a mechanism or/and due to the presence of some element which becomes unstable.

Referring to the behaviour factors, the structural types can be grouped as follows:

Concentric truss bracings:	
. diagonal bracings	$q = 4\,\alpha_u/\alpha_1$
. V-bracings	$q = 2\,\alpha_u/\alpha_1$
Cantilever structures:	$q = 3\,\alpha_u/\alpha_1$
Mixed structures:	$q = 2$
Structures mainly resisting in bending (frame structures, eccentric truss bracings, braced frame structures)	$q = 5\,\alpha_u/\alpha_1 \leq 8$

As simplified rule, in regions of low seismicity $q = 2$ may be adopted without taking into account any further ductility requirement in case of highly regular buildings with frame or truss structures made of rolled sections.

The above values of q are valid provided that:

a) appropriate "regularity" requirements are strictly respected in the building;

b) appropriate detailing rules for connections assure sufficient local ductility;

c) appropriate design rules guarantee the formation of a global collapse mechanism;

d) appropriate limitations of the b/t ratios of the cross-sections are fulfilled.

If the requirements given in para 3 are not respected, the building is irregular, so the above q-factors must be multiplied by 0.75 (point a).

According to point b), the code gives special requirements for connections (see para 7).

The achievement of a global collapse mechanism is governed by the use of an appropriate method based on amplification factors (see para 8).

The assessment of local ductility is also given in the code by means of ductility classes which generally refer to the b/t ratios of Eurocode n. 3 (see para 6).

6. ASSESSMENT OF LOCAL DUCTILITY: Sufficient local ductility is assured by limiting the width-thickness ratio b/t in compressed parts of the cross-sections. In non-dissipative zones ($q = 1$) the b/t ratios should respect the limits given in the Eurocode n. 3. In dissipative zones of structures ($q > 1$), three ductility classes have been proposed, depending on the chosen values of the q-factor:

class A	$q < 6$
class B	$q < 4$
class C	$q < 2$

(6)
Class A-values are necessary where large rotation capacity of plastic zones is required. They correspond to class 1 (plastic sections).
Class B-values must be reached where plastic resistance shall be attained. They correspond to class 2 (compact sections) of EC3.
Class C-values are necessary where the resistance is limited by the yielding of the extreme fibres. They are intermediate between class 2 and 3 of EC3.
For $q > 6$, the b/t ratios of class A can be used, provided $N/N_y + 0.8\,\lambda/\lambda_o \leq 1$, where $\lambda_o = \pi\sqrt{E/f_y}$ being N_y the squash load of the member.

7. CONNECTIONS: Connections in dissipative zones must have sufficient over-strength to allow for yielding of the connected parts.
Connections made by means of butt-welds or full-penetration groove welds do not require any particular check.
For fillet-weld or bolted connections the resistance of the connection R must be 1.2 times the resistance of the connected member R_d, by considering the upper value of its yield strength:

$$R \geq R_d\,(f_{y,max}).$$

8.AMPLIFICATION FACTORS: In order to avoid the formation of local mechanism, appropriate amplification factors are introduced in the code.
In case of framed structures the amplification factor is used in the verification of columns, in order to guarantee that the yielding of beams precedes the yielding of columns, except at the base of the frame.
The design values for the bending moments are given by the sum of the bending moments $M_{c,s}$ due to the horizontal seismic actions multiplied by the amplification factor α, plus the bending moments $M_{c,o}$ due to the other design loads:
$M_d = M_{c,o} + \alpha M_{c,s}$.
The amplification factor α is given by $\alpha = \dfrac{\sum M_R - \sum M_{c,o}}{\sum M_{c,s}}$
being: $\sum M_R$ the sum of the resisting moments of the beam connected to the columns;
$\sum M_{c,o}$ the sum of the bending moments in the columns due to non-seismic loads;
$\sum M_{c,s}$ the sum of the bending moments in the columns due to seismic loads.
At the top floor of multistorey frames $\alpha = 1$ is assumed.
At the base of the frame, the α factor must be set equal to 1.2.
In case of concentric truss bracings the amplification

(7)
factor is used in the verification of beams and columns and of diagonal member connections, in order to guarantee that the axial yielding of the tensile diagonals precedes the ultimate strength of their connections as well as the collapse of beams and columns.
Once the diagonals have been verified, one can compute the amplification factor α , equal to the smaller of the ratios between the tensile strength $N_{R,j}$ of the j-th diagonal and the corresponding force $N_j(.)$ produced in the same member by external forces:

$$\alpha = \min_j \left| \frac{N_{R,j}}{N_j(.)} \right|$$

In case of eccentric truss bracings the amplification factor is used in the verification of columns and diagonal members, in order to guarantee that the yielding in bending or in shearing of beams precedes the collapse of columns and diagonal members.
Once the beams have been verified, the value of α to be used for checking columns and diagonal members is given by:

$$\alpha = \min_{i,j} \left| \frac{V_{R,i}}{V_i} , \quad \frac{M_{R,j}}{M_j} \right|$$

where

$V_{R,i}$ and V_i are the resisting shear and the corresponding computed shear present in the i-th beam;

$M_{R,i}$ and M_i are the resisting moment and the corresponding computed bending moment present in the j-th beam.

REFERENCES

MAZZOLANI F., 1988, "The ECCS activity in the field of recommendations for steel seismic resistant structures", 9th International Conference of Earthquake Engineering, Tokyo-Kyoto.

ECCS-CECM-EKS, 1988 European Recommendations for Steel Structures in Seismic Zones, Tecnical Working Group 1.3: Seismic Design, N. 54.

COMMISSION OF EUROPEAN COMUNITIES, 1988, Eurocode n. 8: Structures in Seismic Regions.

(8)

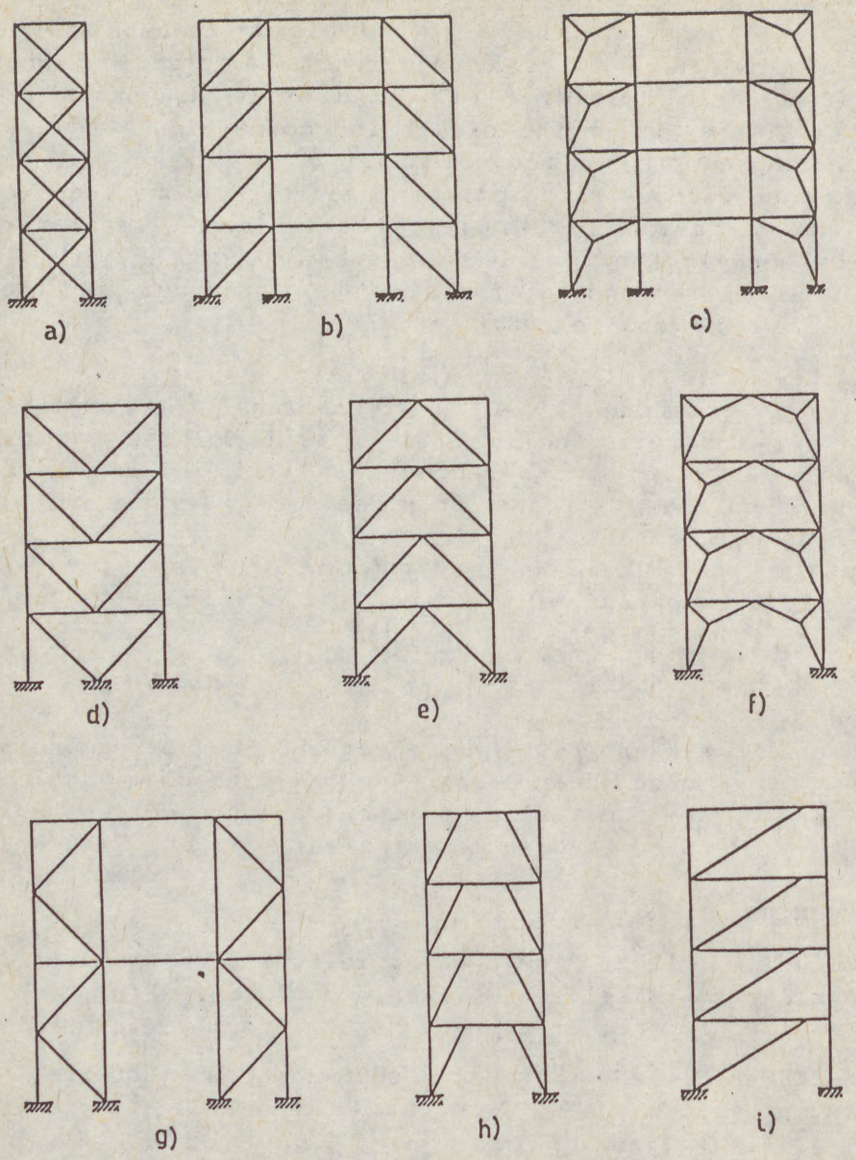

FIG.1 - Some examples of structural schemes :

(a), (b), (c)	diagonal bracings
(d), (e), (f)	V-bracings
(g)	K-bracing
(h), (i)	eccentric truss bracings

PAMMER, Zoltan (1)
RACZ, Sandor (2)

DYNAMIC ANALYSIS OF STEEL STRUCTURES USING THE P-EXTENDED FINITE ELEMENT METHOD

INTERNATIONAL COLLOQUIUM
STABILITY OF STEEL STRUCTURES
BUDAPEST, HUNGARY, 1990
PRELIMINARY REPORT

SUMMARY: This paper concentrates on the advantages of the hierarchic p-version of the finite element method in structural dynamic applications. Theoretical considerations and sample problems show that drastic reduction in human and computational labour, accompanied by increased reliability and robustness, are the most important features.

INTRODUCTION

It is well known in the engineering practice that the accuracy of a finite element (FE) solution may strongly depend on the selection and the number of basis functions. Concisely, the accuracy is discretization dependent.

The finite element mesh and type of the elements determine the discretization. Consequently, if a problem is defined by means of finite element data then the accuracy of the solution is predeterminated. However, conventional finite element programs give no quantitative indications or estimations of discretization error and reliable solution requires great effort of data preprocessing even of an experienced user.

The most expensive way to avoid large discretization error is to carry out two subsequent calculations, starting with a fine mesh first, then repeating with further uniformly refined mesh.

(1) ESTOREL , 1133 Budapest,Karpat u 17
(2) ESTOREL , 9012 Gyor , Szabo P. u. 5.

To make mesh refinement less laborious, extensive advancement of adaptive processes started from the 1970s. Research was mainly concentrated on two comprehensive topics:

1. error indicators and a-posteriori error estimations
2. development of finite element processes with adaptively controlled convergence

Next sections survey the most important definitions, principles and practical considerations in this field that were taking into account in design of the program presented here. Finally p-extended solutions to sample problems verify efficiency.

HIERARCHIC P-EXTENSION

There are two usual ways to increase the number of basis functions. In case of 'h-extension', the number of elements increased and the size of elements (h) approaches to zero through the refinement process. If the number of elements does not change but the polinomial order (p) of elements is increased, then the process is called 'p-extension'. The two type of extensions can be easily combined.

The name 'extension', proposed by Szabo[1], emphasizes systematic increase of the number of degrees of freedom (NDOF). An enrichment of the NDOF is called systematic if a certain relationship can be established between a discretization 'A' with NDOF=N and a discretization 'B' with NDOF=N+M.

In some applications of the 'h'-extension[2,3], subsequent meshes are not in strictly deterministic connection: mesh refinement changes the basic functions.

Hierarchic extension provides more systematic enrichment of NDOF. An extension is called hierarchic, if a discretization 'B', extended from discretization 'A', possesses the following property: the shape functions, used for discretization 'A', constitute a subset of the set of shape functions for discretization 'B'. Although the trial space spanned by hierarchic and non-hierarchic functions are the same, the hierarchic extension has many computational advantages. Firstly, the coefficient matrix and right hand side (rhs.) vector of discretization 'A' are simply the partitions of the matrix and rhs. vector of discretization 'B' respectively. Thus subsequent solutions with increased NDOF are computed more efficiently. The other important feature

is the better conditioning of the system of equations that reduces roundoff errors.

Hierarchic extension has both h - and p-versions. Present implementation has been based on the p- version. The hierarchic increase of the polinomial order was firstly introduced by Zienkiewicz et al.[4], nevertheless, the idea was considerably generalized and extended by Peano[5].

The hierarchic p-version has many substantial advantages over h-version. References 5-7 discuss them in details, however, some essential features should be emphasized here.

First of all, user can define a problem with minimal data preparation effort. Mesh design is essentially governed by geometry and boundary conditions. A mesh, designed for p-version, consists of a few large elements therefore pre- and postprocessing with interactive computer grafics are not so tiring. The analyst can spend more time on creative engineering.

The second important feature is that the p-version is superior in rate of convergence. Babuska's[8] theoretical studies revealed: in the p-version, the rate of convergence can not be slower than in the h-version, using quasiuniform mesh. Practical experiences showed, that the rate of convergence of the p-version is almost twice that of the h-version (see ref. 9-11).

STRUCTURAL DYNAMIC APPLICATIONS

In structural dynamic problems the efficient solution of the generalized eigenvalue problem

$$(K-\lambda M)\vec{x}=0 \qquad (1)$$

plays fundamental role (K and M are , respectively ,the stiffnes and mass matrices and $(\lambda,\vec{x})$ is an eigen pair). Our interest lies in the convergence to a number of eigenvalues computed concurently by means of the finite element method , and how this convergence compares for different refinement strategies. Ordinarily, one can obtain acceptable accuracy only for some limited number of lower eigenvalues obtained by the finite element method. Clearly, the superior refinement strategy is the one that yields the greatest accuracy for the the largest number of eigenvalues with the smallest number of degrees of freedom.

To illustrate our results, let us consider the next examples.The computations were made by PEXFE-3D·DYNAMIC, a three dimensional finite element package.The maximal value of polynomial degree was p=4.Parallelepiped elements were used. The eigenpairs were extracted by Lanczos method.

For the first example consider a cantilever beam. The beam is clamped at one end and free on the other. The first five eigenfrequencies (eigenvalue is equal to eigenfrequency squared) were computed and compared with theoretical results based on Rayleigh-Ritz beam theory and with eigenfrequencies extracted by the conventional COSMOS FE program using 8-node brick elements. The results are summoned in Table 1.

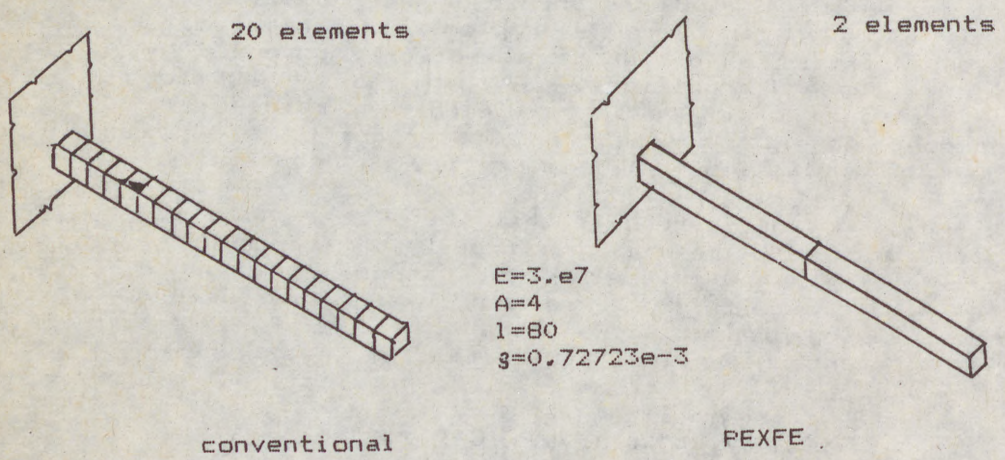

Fig.1. Uniform beam clamped at one end .

	Theory	Conventional	PEXFE-3D
1	10.26	10.24	10.25
2	65.32	63.94	64.17
3	179.92	178.38	179.60
4	352.84	348.06	358.80
5	583.22	572.63	580.32

Table 1. Eigenfrequencies (Hz) for cantilever beam.

The second example is shown in Fig.2 . We used only one three dimensional superelement. In reference solution [12]

sixten 8-noded semiloof elements were used.

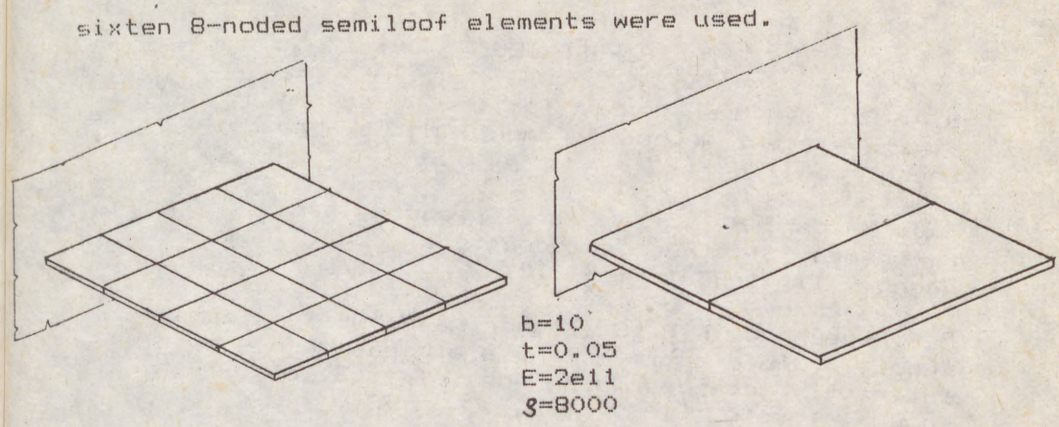

Fig.2.Cantilevered thin square plate

	Reference solution	PEXFE
1.	0.421	0.442
2.	1.029	1.06
3.	2.582	2.78

Table 2. Eigenfrequencies (Hz) for thin plate

CONCLUSION

The p-extension makes the finite element method more *user-friendly* and *efficient*. Reliable result is supplied without laborious data preprocessing and mesh refinement. The amount of effort required in defining a problem is almost minimal. *The p-extended finite element (PEXFE) method lets the analyst design coarse meshes with few elements instead of generating hundreds of elements as the conventional finite element method often requires.* A mesh is properly designed for the PEXFE method, if accurate and smooth mapping of the geometry is ensured. The element equilibrium test is proved to be useful to qualify mesh designs. Uniformly small unequilibrated forces indicate properly designed mesh.

REFERENCES

1 B.A. Szabo, Mesh design for the p-version of the finite element method , Comput. Meths.Appl.Mech. Engrg. 55 (1986)

2 R.J. Melosh, P. V. Marcal, An energy basis for mesh refinement of structural continua. , Int.J.num.Meth. Engng., 11, 1083-1091 (1977)

3 M.S. Shephard, R.H. Gallagher, J.F. Abel, The synthesis of near-optimum finite element meshes with interactive computer graphics , Int. J. num. Meth. Engng., 15, 1021-1039 (1980)

4 O.C. Zienkiewicz, B.M. Irons, F.C. Scott, J. Campbell, Three dimensional stress analysis , Proc.IUTAM Symp. on High Speed Computing of Elastic Structures, Univ. of Liege Press, 1971.

5 A. Peano, Hierarchies of confirming finite elements for plane elasticity and plate bending ,Comp. & Maths. with Appls. 2. 211-224 (1976)

6 B.A. Szabo, Some recent developments in finite element analysis . Comp.& Maths.with Appls. 5. 99-115 (1979)

7 A.Peano, A.Pasini, R.Riccioni, L.Sardella, Adaptive approximations in finite element structural analysis , Comp. & Struct. 10, 333-342 (1979)

8 I.Babuska, B.A. Szabo, On the rates of convergence of the finite element method , Int. J. num.Meth.Engng., 18, 323-341 (1982)

9 I. Babuska, B.A. Szabo, I.N. Katz, The p-version of the finite element method , SIAM J. Num. Anal. 18, 515-545 (1981)

10 S.M. Yunus, M.S. Shepard, A comment on the effectiveness of uniform finite element refinements , Int. J. num. Meth. Engng, 20, 187-194 (1984)

11 O.C. Zienkiewicz, J.P. De S.R. Gago, D.W. Kelly, The hierarchical concept in finite element analysis , Comp. & Struct. 16, 53-65 (1983)

12 F. Abbassian, N.C. Knowles, Benchmarks for Finite Elements in Free Vibration - an overview , Contribution to the NAFEMS Dynamics Workshop, Grand Hotel, Brighton , September 1988

(1)
POLISHCHUK, Nickolai (1)

LIMITING VALUE DETERMINATION OF HARMONIC LOAD FREQUENCY AFFECTING STEEL BAR STRUCTURE

INTERNATIONAL COLLOQUIUM
STABILITY OF STEEL STRUCTURES
BUDAPEST, HUNGARY, 1990
PRELIMINARY REPORT

Summary: The paper deals with a method of determining the limiting value of harmonic load frequency affecting a steel bar structure. The limiting value of harmonic load frequency is its maximum value under which constraints on dynamic displacements, speed and acceleration values of a steel bar structure are met. A steel bar structure satisfying above mentioned dynamic constraints is characterized as dynamically stable. It is proposed to make use of discussed methods in the dynamic analysis of steel bar structures under concentrated harmonic moads of identical frequency. The application of the method is extended to steel bar structures with the hinged and rigid node joint.

Introduction

When technological and transport equipment is available in buildings(structures) which causes oscillations and when there are other vibration sources it is necessary to restrict dynamic movements, speeds and accelerations of building structures.

The application of high-strength materials during the prefabrications of modern building structures results in substantial reduction of static rigidity and in sharp deterioration of their dynamic characteristics, particularly during the application of high-strength steel having insignificant dissipation properties.

(1) Assistant Lecturer, Strength of Materials and Building Mechanics Department, Ukrainian Institute of Water Management Engineers(Rovno, USSR)

(2)
If calculated structures vibrations do not meet requirements of limiting their dynamic displacements, speeds and accelerations it is necessary to apply methods of decreasing oscillations one of which consists in changing the ratio between forced vibration frequency and natural structure vibrations by increasing the cross-section of its elements or by changing forced oscillations frequency.

The Reference 1,proposes a method for determining values of cross-section areas of steel truss elements subjected to concentrated harmonic loads in its nodes taking into account constraints on node dynamic displacement. This method may be used also for similar analysis of bar structures with node rigid connection. However, the increase of cross-sections of bar structure elements leads to increasing its mass and,hence,to its higher cost and, on the other hand, is not always possible.

The present paper deals with methods of determining the limiting frequency value of concentrated harmonic load affecting the steel bar structure carrying concentrated masses. All geometric characteristics of cross-sections of bar structure elements and physico-mechanical properties of steel used for its prefabrication are supposed to be predetermined. Dynamic displacements, speeds and accelerations of steel bar system are accepted as limiting dynamic characteristics.

Problem formulation

A steel bar structure taking up harmonic loads is called dynamically stable if it meets requirements (1-3) :

$$u \leqslant U; \qquad (1)$$

$$v \leqslant V; \qquad (2)$$

$$w \leqslant W, \qquad (3)$$

where u , v , w are maximal calculated from dynamic analysis values of dynamic displacements, speeds and accelerations correspondingly; U , V , W are limiting dynamic displacements, speeds and accelerations accepted subject to structure service conditions. We consider only such conditions of dynamic loading under which harmonic loads are concentrated and have similar frequences while analyzed scheme of bar structure may be represented as a system with several dynamic degrees of freedom. This allows to take into account during dynamic analysis process established relations between quantities u , v and w :

(3)

$$v = u \cdot \theta; \qquad (4)$$

$$w = u \cdot \theta^2, \qquad (5)$$

where θ is the harmonic load frequency in sec^{-1}.

The problem consists in finding under certain amplitudes of harmonic loads affecting a given steel bar structure the maximal value of their frequency to satisfy conditions(1-3).

Problem solution

We suggest solving the problem in the following way.

1. Under a certain initial value of harmonic load frequency accepted for operation conditions of steel bar structure we make a preliminary dynamic analysis with a view of determining values of u, v, w and also values of natural vibrations frequencies.

2. We find maximum values of harmonic load frequencies under which each of requirements(1-3) is observed irrespective of other ones. To define these values the author suggests following formulas:

a) to satisfy the condition (1)

$$\theta_1 = \sqrt{\nu^2 - \frac{u\left(\nu^2 - \theta_0^2\right)}{v}}; \qquad (6)$$

b) to satisfy the condition(2)

$$\theta_2 = \frac{\sqrt{u^2(\nu^2-\theta_0^2)^2 + 4V^2\nu^2} - u(\nu^2 - \theta_0^2)}{2V}; \qquad (7)$$

c) to satisfy the condition (3)

(4)

$$\theta_3 = \sqrt{\frac{W \cdot \nu^2}{u\left(\nu^2 - \theta_0^2\right) + W}}, \qquad (8)$$

where θ_0 is the initial value of harmonic load frequency; ν is the frequency of steel bar structure natural oscillations corresponding to the discussed form. Other quantities belonging to formulas(6-8) were determined earlier.

3. We find the minimal value of harmonic load frequency from calculated values of θ_1 , θ_2 , θ_3 .

The values of harmonic load frequency thus defined is limiting for a given steel bar structure.

Here we should emphasize the following. As with a majority of problems of bar structures dynamics the presented problem is a complex one. Therefore to precisely calculate values of θ_1 , θ_2 , θ_3 is some cases we have to make approximations. For this purpose at each subsequent calculation iteration we should accept as θ_0 values of θ_1 , θ_2 , θ_3 found at previous iteration. It is necessary to complete calculations when values of θ at two contingnous iterations co - incide. The number of approximations, however, does not exceed three as a rule.

The proposed method of determining the limiting value of concentrated harmonic load frequency affecting steel bar structure may be applied for dynamic analysis of steel bar structures with hinged and rigid node joints.

References

1. Polishchuk N,,Bykovski S.,1986.,Optimal design algorithm for steel trusses of predetermined stiffness under dynamic loads taking into account compressed bar stability., Procedings and Final Report of the International Colloquium on "Stability of Steel Structures"(HUNGARY,Tihany, September 25-26,1986),V.Trusses contribution,589-593.

(1)
RAVINGER, Ján (1)

DYNAMIC POST-BUCKLING BEHAVIOUR OF THIN WALLED PANEL

INTERNATIONAL COLLOQUIUM
STABILITY OF STEEL STRUCTURES
BUDAPEST, HUNGARY, 1990
PRELIMINARY REPORT

Summary: By including the inertia forces the problem of the post-buckling behaviour of slender webs is extended into dynamics. The FEM with the modification of the transformation into the forms of buckling surfaces is used for the solution of a thin-walled panel loaded by a harmonic load.

Theoretical assumptions

The von Kármán theory for the large deflections of plates is extrapolated into dynamics by including the inertia forces

$$p_m = \varrho \ddot{w} \qquad (1)$$

where ϱ is the mass per unit volume, $\ddot{w}$ are the accelerations of the plate displacemenets functions. Using the Hamilton´s principle we have the system of conditional equations

$$K_M \ddot{\alpha}_D + K_C \dot{\alpha}_D + (K_{LD} + K_{GD} + K_{GDo}) \alpha_D + K_{DS} \alpha_S =$$

$$= P_D + P_{Do}; \; K_{SD} \alpha_D + K_{LS} \alpha_S = P_S + P_{So} \qquad (2)$$

where

K_M is the mass matrix,
K_C is the damping matrix,
K_{LD} is the linear stiffness matrix of the plate,
K_{GD} is the geometrically non-linear stiffness matrix of the plate,

1 Slovak Academy of Sciences, Institute of Building Constructions and Architecture, 842 20 Bratislava, Czechoslovakia

(2)

K_{GDo} is the matrix of the increasing of the bending stiffness of the plate due to the initial displacements, non-linear part,

K_{DS} is the non-linear stiffness matrix, the interaction between the plate and the in-plane displacements parameters,

P_D is the vector of the transform external load of the plate,

P_{Do} is the vector of the transform plate internal forces due to the initial displacements,

K_{LS} is the linear stiffness matrix of the web (in plane),

K_{SD} is the non-linear stiffness matrix, the interaction between the in-plane and the plate displacements parameters,

P_S is the vector of the transform external load of the web (in-plane forces),

P_{So} is the vector of the transform in-plane internal forces due to the initial displacements,

α_D, α_S are the parameters of the displacements functions; plate, in-plane.

The stiffness matrix of the web K_{LS} is linear a so we can arrange

$$K_M \ddot{\alpha}_D + K_C \dot{\alpha}_D + (K_{LD} + K_{GD} + K_{GDo} - K_{DS} \cdot K_{LS}^{-1} \cdot K_{SD}) \alpha_D =$$

$$= P_D + P_{Do} - K_{DS} \cdot K_{LS}^{-1} \cdot (P_S + P_{So}) \qquad (3)$$

For the next investigation we neglect damping effects

FEM with the modification into forms of buckling surfaces.

Eq. (3) represents the system of differential equations. Due to the geometric non-linear stiffness matrixes the problem is complicated and it is impossible to get the solution with a large number of parameters. One possibility how to arrange the solution is the modification of FEM by a transformation into the forms of buckling surfaces.

The way of the solution is followed as the first step is the solution of the linear problem of the web in-plane

$$K_{LS} \cdot \alpha_S = P_S \qquad (4)$$

Then the linear problem of the stability can be established

$$| K_{LD} - \lambda K_G |_{det} = 0 \qquad (5)$$

where K_G is the matrix of the increasing bending stiffness of the plate due to the action of membrane forces.

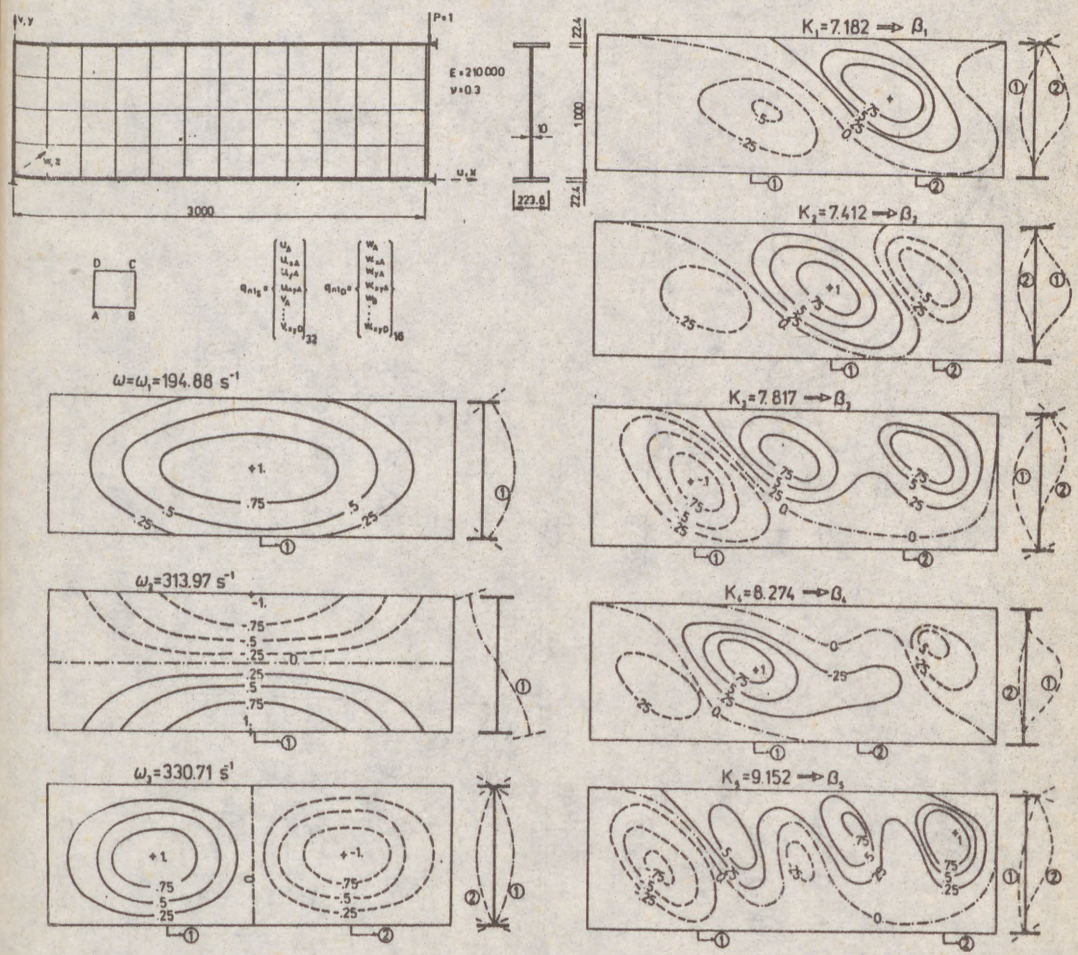

Fig. 1

Thin-walled panel - forms of free vibration and forms of buckling

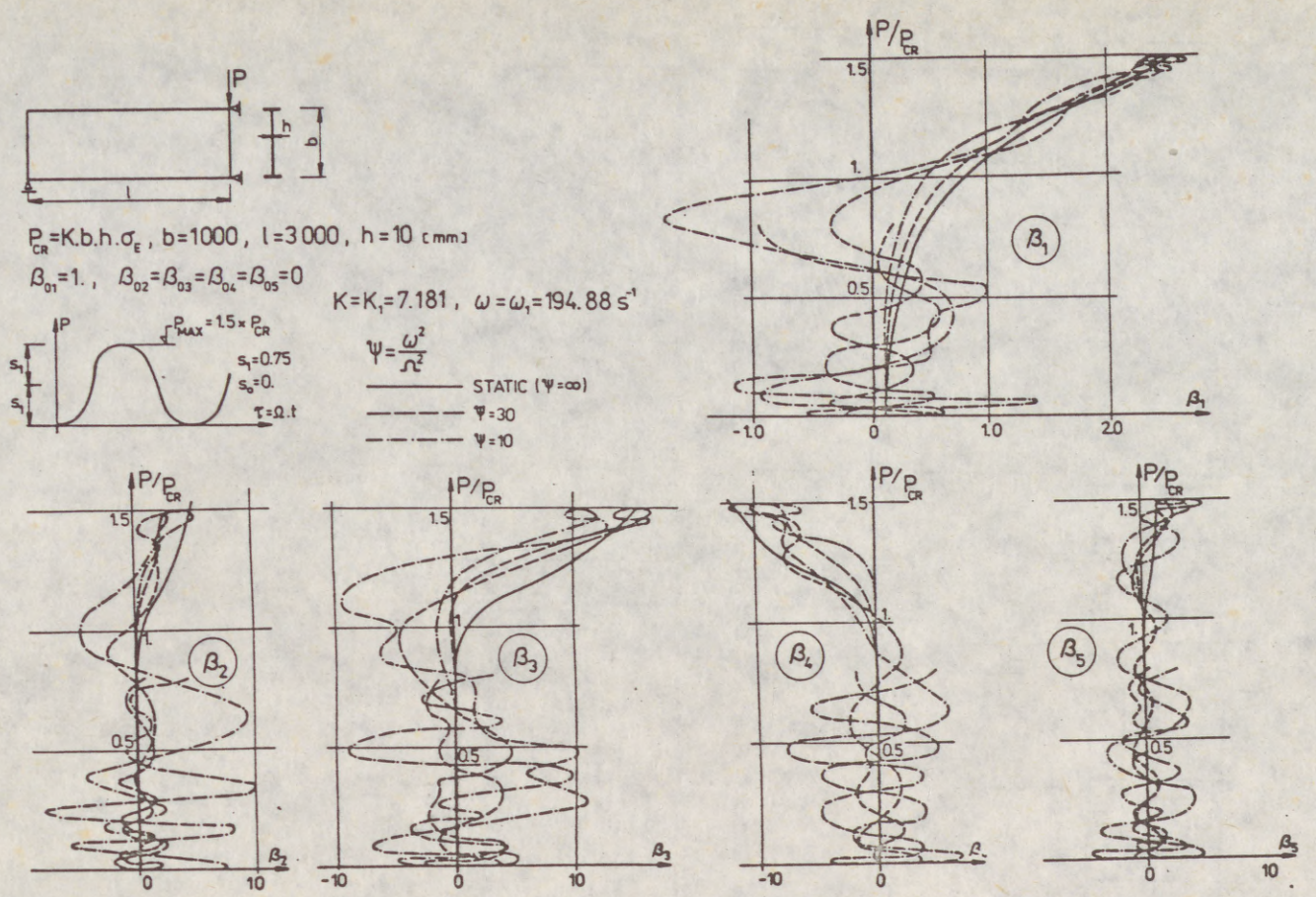

Fig. 2 Dynamic post-buckling behaviour of thin-walled panel, load vs plate displacements parameters

load vs plate displacements parameters

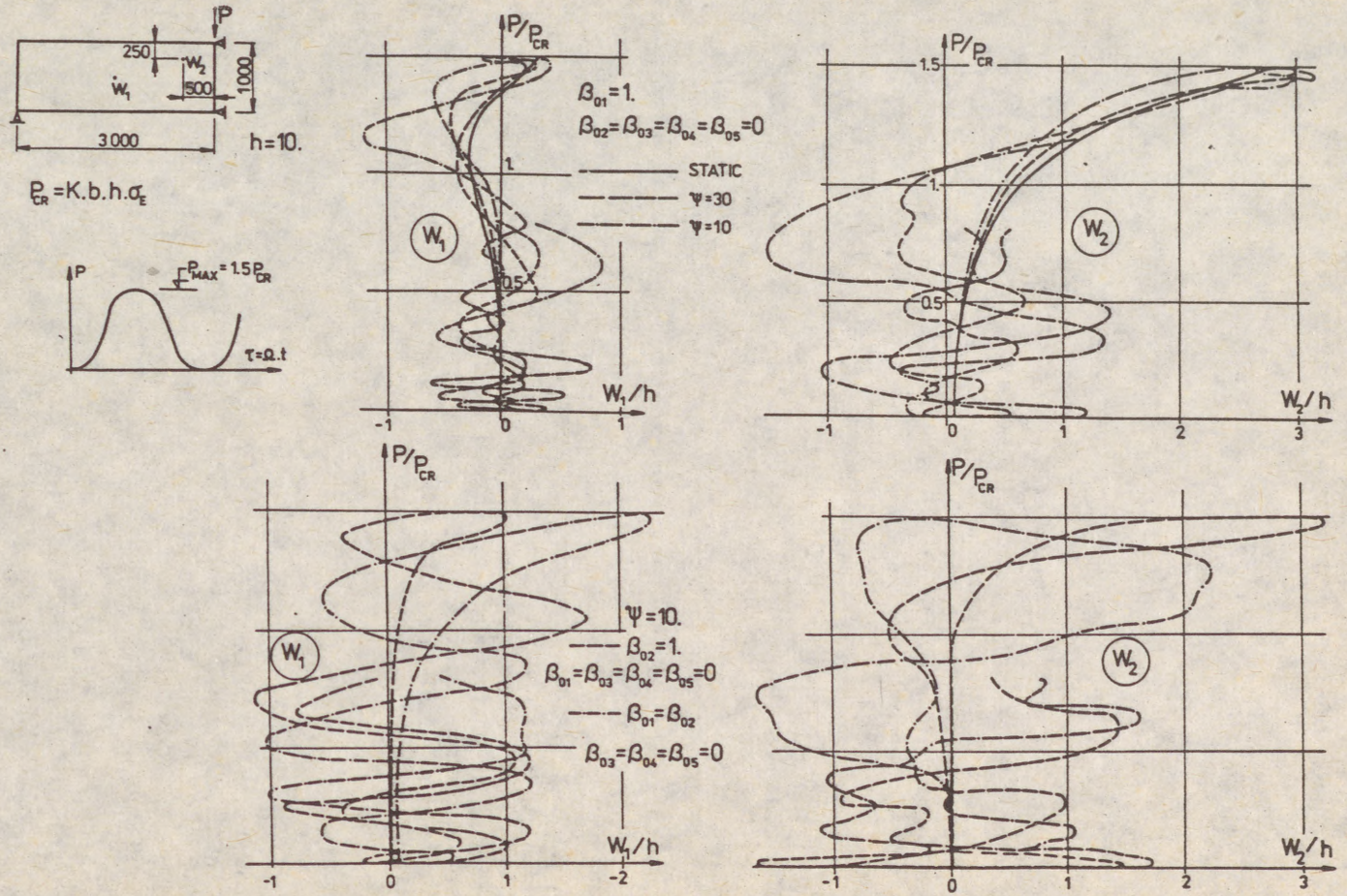

Fig. 3 Dynamic post-buckling behaviour of thin-walled panel, load vs displacements

(6)

The obtained eigenvectors that means the forms of buckling are used as basic functions of the plate displacements and the obtained system of conditional equations can be written in the form

$$M\ddot{\beta} + K(\beta)\beta = 0 \tag{6}$$

where

$$\beta = T \cdot \alpha_D \tag{7}$$

T is the transformation matrix characterized the forms of buckling,

M, K are the transformed mass and stiffness matrixes.

The stiffness matrix contains the cubic terms of the non-linear algebraic equations.

The system of differential equations has been solved by Newmark method. For one time increment we get the system of cubic algebraic equations which has been solved by the modified Newton-Raphson iteration.

Numerical example

The thin-walled panel (Fig. 1) represents a part of the thin-walled structure. Obtained results are presented at Figs. 2 and 3. where

Ω is the circular frequency of the applid load,

ω is the circular frequency of free vibration.

Conclusion

A number of examples of the post-buckling behaviour of thin-walled panels loaded by a harmonic load has been calculated. The results confirmed that for the thin-walled panel as a non-linear type of construction, the effect of the parametric resonance did not occur and the ratio between quadrates of the natural and applied frequencies is a suitable parameter for the evaluation of non-linear dynamic effects.

References

1. RAVINGER, J. 1987 : Dynamic Post-Buckling Behaviour of Slender Webs. ACTA TECHNICA ČSAV, No.1, 36-59.
2. RAVINGER, J. 1983 : Girders with Unstiffened Slender Webs. Journal of Constructional Steel Research, Vol.3, No.2, 14-22.
3. GALLAGHER, R,M. 1970 : The Finite Element Method in Shell Stability Analysis. Int. Journal Computer and Structures, Vol.3,
4. SYIGAL, S. and T.Y. YANG, 1985: Non-Linear Dynamic Analysis with 48 D.O.F Curved Thin Shell Element. Int. Journal for Numerical Methods in Engineering, Vol.21, 1115-1128.
5. BOLOTIN, V.V. 1956 : Dynamic Stability of Elastic Systems. Moskva, Nauka /in Russian/.

(1)
SEYRANIAN, Alexander P. (1)

INTERACTION OF EIGENVALUES AND STRUCTURAL STABILITY PROBLEMS

INTERNATIONAL COLLOQUIUM
STABILITY OF STEEL STRUCTURES
BUDAPEST, HUNGARY, 1990
PRELIMINARY REPORT

Summary: Vibration stability problems of autonomious systems depending on many parameters are considered. Both simple and multiple eigenvalues are analysed. The main attention is paid to the interaction of eigenvalues with the change of parameters. Strong and weak interactions of eigenvalues are distinguished. With the use of perturbation technique the main relations for expansion coefficients of eigenvalues are achieved. In the case of multiple eigenvalues directional derivatives are used. Dissipative, gyroscopic and circulatory systems are studied as examples. It is shown that strong interaction of eigenvalues leads to catastrophic changes in the system behaviour (loss of stability), while weak interaction does not mean qualitative change.

1. Due to the works by Nicolai, Ziegler and Bolotin in the theory of elastic stability dynamic approach was established. According to this principle stability of the structure must be studied by the analysis of small vibrations of the structure about equilibrium state. With the use of this approach both static (divergence) and dynamic (flutter) forms of the loss of stability can be found. Elastic stability problems as well as problems of vibrational stability of rotors, gyroscopes, panels in supersonic gas flow, wings of aircrafts lead to the study of linear vibrational equations

$$M\ddot{q} + G\dot{q} + Aq = 0 \qquad (1)$$

where M, G and A are real m x m matrices, smoothly depending on the vector of design parameters $h = (h_1, h_2 \ldots, h_n)$. As design parameters various geometric, stiffness and mass characteristics of the structure can be chosen.

Separating time with the use of transformation $q = X \cdot \exp(\lambda t)$ we get the generalized eigenvalue problem

$$[M\lambda^2 + G\lambda + A]X = 0 \qquad (2)$$

(1) D.Sc., Institute of Problems in Mechanics, Moscow 117526

(2)

where λ is an eigenvalue, and X is an eigenvector of dimension m. These quantities are complex quantities.

It is interesting to study dependence of eigenvalues λ on design parameters, especially, their penetration from the left to the right part of complex plane λ, i.e. study of the change of stability and instability regions, and calculation of the critical values. This is a general problem of stability theory.

Along with the eigenvector X let's consider the eigenvector Y of the adjoint operator

$$[\bar{\lambda}^2 M^T + \bar{\lambda} G^T + A^T] Y = 0 \qquad (3)$$

Here T designates transposition, and bar over symbol means complex conjugate quantity.

Let's calculate the increment of eigenvalue λ due to the change of design parameters assuming $\lambda(h_o) = \lambda_o$. For this purpose we take to the vector h_o an increment $h = h_o + \varepsilon k$. Here ε is a small positive number, and k is an arbitrary vector of dimension n, $|k| = 1$. As the result of this perturbation the matrices M, G and A will achieve the increments. For M we have

$$M(h) = M_o + \varepsilon M_1 , \qquad (4)$$

$$M_o = M(h_o),\ M_1 = \| (\nabla m_{ij}, k) \|,\ \nabla = (\partial/\partial h_1, \cdots, \partial/\partial h_n)$$

Similar relations are also valid for G and A.

Expansions of λ and X into a power series of ε depend on multiplicity of eigenvalue λ_o.

a) First we consider the case of the simple eigenvalue λ_o with the corresponding single eigenvector X_o. Then for λ and X expansions in integer powers of ε are valid

$$\lambda = \lambda_o + \varepsilon \lambda_1 + \cdots , \quad X = X_o + \varepsilon X_1 + \cdots \qquad (5)$$

With the use of (3) we obtain the relation for the first coefficient

$$\lambda_1 = - \frac{([A_1 + \lambda_o G_1 + \lambda_o^2 M_1] X_o, Y_o)}{([G_o + 2\lambda_o M] X_o, Y_o)} \qquad (6)$$

Round brackets mean the scalar product of vectors in complex space. The quantity λ_1 is a derivative of eigenvalue λ in direction k. Due to continuity property of the right hand side of (6) there exists also a traditional first derivative. Multiplying both sides of (6) by ε and designating $\delta\lambda = \varepsilon \lambda_1$, $\delta h = \varepsilon k$, we can write the increment of λ in traditional form

$$\delta\lambda = (\varphi, \delta h) , \qquad (7)$$

$$\varphi = - \frac{\sum_{ij=1}^{m} (\nabla a_{ij} + \lambda_o \nabla g_{ij} + \lambda_o^2 \nabla m_{ij}) x_j^o \bar{y}_i^o}{\sum_{ij=1}^{m} (g_{ij} + 2\lambda_o m_{ij}) x_j^o \bar{y}_i^o}$$

Vector φ is the gradient of λ with respect to parameters $h_1, h_2 \ldots h_n$. For its calculation it is necessary to know the

(3)

eigenvalue λ_0 and the corresponding eigenvectors X_0 and Y_0.

b) Consider now the case of double eigenvalue λ_0. It is assumed that the Jordan chain corresponding to λ_0 consists of single eigenvector and one adjoint vector. In this case it is necessary to use expansions in fractional powers of ε

$$\lambda = \lambda_0 + \sqrt{\varepsilon}\,\lambda_1 + \varepsilon\,\lambda_2 + \cdots ,$$
$$X = X_0 + \sqrt{\varepsilon}\,X_1 + \varepsilon\,X_2 + \cdots . \qquad (8)$$

Using relations (4),(8) we obtain expressions for the leading term coefficient λ_1

$$\lambda_1^2 = -\frac{([A_1 + \lambda_0 G_1 + \lambda_0^2 M_1]X_0, Y_0)}{([G_0 + 2\lambda_0 M_0]X_1, Y_0) + (M_0 X_0, Y_0)} \qquad (9)$$

Here X_0, Y_0 are eigenvalues in adjoint problems (2) and (3) at $h = h_0$, and X_1 is adjoint vector, defined by the equation

$$[\lambda_0^2 M_0 + \lambda_0 G_0 + A_0]X_1 = -[G_0 + 2\lambda_0 M_0]X_0 \qquad (10)$$

The denominator of (9) is not equal to zero.

Consider now the case when only one parameter p is varied. If $p - p_0 > 0$, then we take in (9) $k = 1$ (right hand derivative). Designating right hand side of (9) by $re^{i\varphi}$ we obtain $\lambda_1 = \pm\sqrt{r}\,e^{i\varphi/2}$, i is imagine unity. If now $p < p_0$, then we take $k = -1$ (left hand derivative) and achieve $\lambda_1 = \pm i\sqrt{r}\cdot e^{i\varphi/2}$. Four roots λ_1 are placed on the circle of radius $\sqrt{r}$, difference of arguments of adjacent roots is equal $\pi/2$, see Fig.1.

Combining these results, taking $\varepsilon = |p - p_0|$ and using (8) we get the expressions

$$\lambda = \lambda_0 \pm \sqrt{r}\,e^{i\varphi/2}\sqrt{p - p_0} + O(\Delta p), \quad p > p_0$$
$$\lambda = \lambda_0 \pm i\sqrt{r}\,e^{i\varphi/2}\sqrt{p_0 - p} + O(\Delta p), \quad p < p_0 \qquad (11)$$

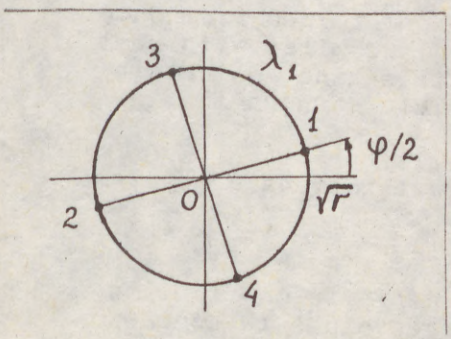

Fig. 1

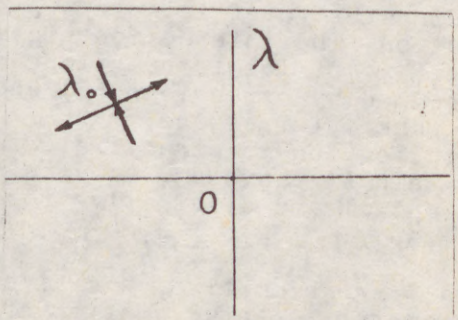

Fig. 2

Thus, when parameter $p < p_0$ increases two eigenvalues approach to each other on the straight line, merge at $p = p_0$, and then diverge, when $p > p_0$, in opposite directions on the line per-

(4)

pendicular to the line of approach, Fig. 2. Arrows show motion of λ when p increases. The eigenvalues as if collide, and then diverge at right angle. This is an interaction of eigenvalues if numerator of (9) is not zero. This kind of interaction we call strong interaction. It is characterized by the expansions (8),(11) and the interaction picture shown in Fig. 2. This is the case of nondifferentiable in common sense eigenvalues.

c) Let's consider other possible interactions of eigenvalues. For example, it takes place when double eigenvalue is characterized by two linearly independent eigenvectors. In this case λ and X are expanded in integer powers of ε as in the case of simple λ (5). The difference is that two roots λ_1 are found from the quadratic equation. For the case when only one parameter p is varied the interaction picture is shown in Fig. 3. Arrows show the motion of λ when p is increased. The eigenvalues approach, merge at $p = p_o$, and then diverge. The trajectories of λ don't change their directions through interaction. Nevertheless, the eigenvalues are not differentiable.

Consider now the case when the numerator of (9) is equal to zero. In this case the terms with $\sqrt{\varepsilon}$ in expansions (8) drop.

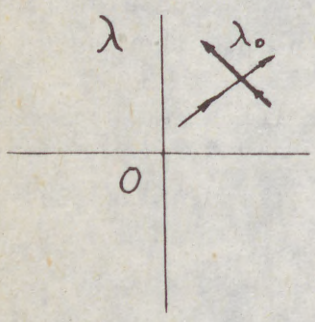

Fig. 3

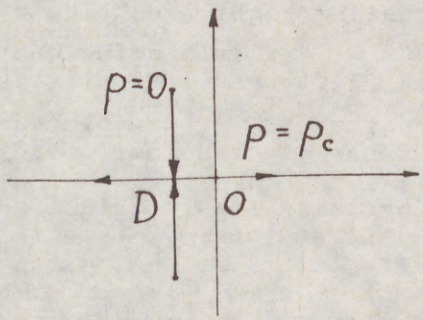

Fig. 4

The leading term coefficients λ_2 are determined from quadratic equation. The interaction picture is similar with that of shown in Fig. 3. The interactions of this kind, which are characterized by expansions (5) and picture shown in Fig. 3, we call weak interactions.

2. Application to structural stability problems.

a) Dissipative system. We consider vibrations of system with potential and dissipative forces

$$\ddot{X} + D\dot{X} + (A - pB)X = 0 \qquad (12)$$

A, B and D are symmetric, positively definite matrices, p is load parameter. We study motion of eigenvalues in complex plane λ with the change of load parameter, Fig. 4. For $p = 0$ all eigenvalues lie in the left half of complex plane, it means that the system is stable. When p increases then at the point D the strong interaction occurs. As a result one of the

(5)

eigenvalues becomes real and positive for $p > p_c$. The critical value p_c is equal to the first eigenvalue of the problem $AX = pBX$. It can be shown that dissipative system (12) losts its stability only statically ($\lambda = 0$ at $p = p_c$), and at the point D weak interaction is impossible.

b) Gyroscopic stabilization. We consider unstable potential system which is stabilized by gyroscopic forces

$$\ddot{X} + pG\dot{X} - AX = 0 \qquad (13)$$

Here A is symmetric, positively definite matrix, G is skew-symmetric matrix, p is load parameter, for example, angular velocity of rotation $p \geq 0$. For $p = 0$ we have $\lambda_i^2 > 0$ - the system is unstable. Behaviour of eigenvalues when p is increased is shown by arrows in Fig. 5. At the points F,F',S,S' the strong interaction occurs, as a result for $p > p_s$ the system is stabilized because λ become pure imagine and different quantities.

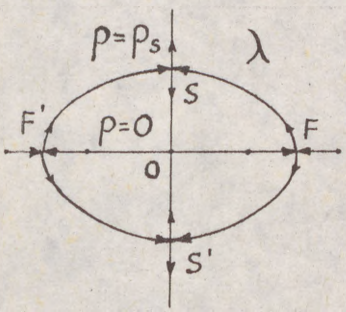

Fig. 5

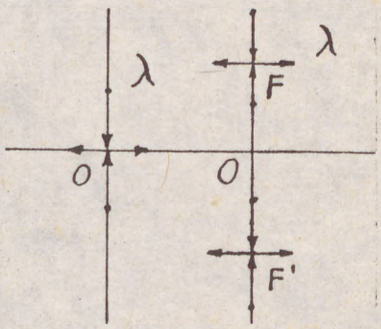

Fig. 6

c) Circulatory system. We consider the system with nonpotential positional forces. They are called circulatory forces. Vibrational equation for this system takes the form

$$\ddot{X} + (A - pC)X = 0 \qquad (14)$$

Here A is symmetric, positively definite matrix, p is load parameter, for example, magnitude of follower force. For $p = 0$ we have $\lambda_i^2 < 0$ - the system is stable, Fig. 6. When p is increased then at the points F or O the strong interaction takes place. As a result stability of the system is violated by static (divergence) or dynamic form (flutter). There are also examples of weak interaction when eigenvalues don't change their trajectories after collision, Fig. 7. It means that stability of the system is not violated.

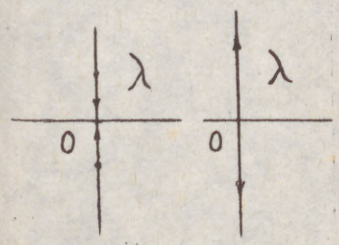

Fig. 7

(1)
TOMSKI, Lech (1)
KUKLA, Stanisław (2)
POSIADAŁA, Bogdan (3)
PRZYBYLSKI, Jacek (4)
SOCHACKI, Wojciech (5)

DIVERGENCE AND FLUTTER INSTABILITY OF COLUMN SUPPORTED BY A NONLINEAR SPRING AND LOADED BY A PARTIALLY FOLLOWER FORCE

INTERNATIONAL COLLOQUIUM
STABILITY OF STEEL STRUCTURES
BUDAPEST, HUNGARY, 1990
PRELIMINARY REPORT

Summary: In this work the effect of initial deflection of a nonlinear spring supporting a cantilever column loaded by a partially follower force on the regions of occurrence of divergence and flutter instability of this system is studied. In solving the problem the method of small parameter was used by expanding the lateral displacement and frequency of natural vibration of column into power series with respect to the amplitude parameter. The results of numerical calculation presented in the form of plots are the curves of the following relationships:

- load - supporting spring stiffness
- load - product of initial deflection of spring and nonlinear part of its characteristics for various follower parameters.

---

(1) Associate Professor, (3) Assistant Lecturer, (4) Lecturer,
(5) Assistant Lecturer, Częstochowa ,Institute of Technology,
(2) Lecturer, Częstochowa, Institute of Mathematics, Poland

(2)

List of symbols

A - area of column cross-section
E - modulus of elasticity (Young's modulus)
J - moment of inertia
P - force loading the column
w - lateral displacement of column
L - length of column
k_1 - spring stiffness (linear)
k_3 - spring stiffness (non-linear)
Ω - frequency of column vibration
Δ - initial deflection of spring
η - follower coefficient
ε - small parameter $\varepsilon \ll 1$
ϱ - density of column material
ν - correction factor of natural frequency

1. Introduction

In studies of stability of cantilever columns loaded by a partially follower force, the column is considered as a continuous or discrete system of two or three degrees of freedom . Such a column may loss the divergence or flutter stability depending on boundary conditions. In literature the effect of various parameters, which values decide on divergence or flutter, have been considered. Usually, external damping, distribution of concentrated masses, stiffness of supporting springs and follower parameter has been accepted as parameters.
In this work one considers a cantilever column (as a continuous system) supported by a spring of non-linear characteristics at its free end and loaded by a constant-in-time partially follower force.

One studies the joined effect of an initial deflection of spring and nonlinear part of its characteristics on instability of column. The characteristic of spring is assumed in such a way that the system is symmetric.

(3)

2. Formulation of the problem

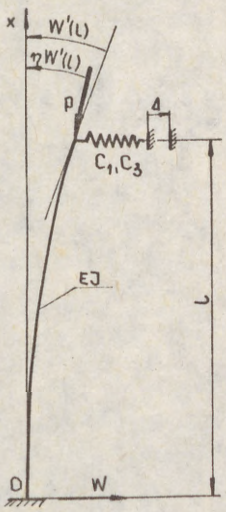

Fig.1.

Consider a homogeneous column (Fig. 1) of constant cross-section area, fixed at one end (x = 0) and supported on the other (x = 1) by a spring with non-linear characteristic. The initial deflection of spring is equal to Δ and the column is loaded by a partially follower force P.
By introducing the following dimensionless quantities:

$$\xi = \frac{x}{l} \quad , \quad w = \frac{W}{l} \quad , \tag{2.1}$$

$$c_1 = \frac{k_1 l^3}{EJ} \quad , \quad c_3 = \frac{k_3 l^5}{EJ}$$

the characteristic of spring may be expressed by the equation as below:

$$S(w_0) = c_1 w_0 + c_3 w_0^3 \tag{2.2}$$

where: W, EJ, l - denote the lateral displacement, bending stiffness and column length,

$w_0 = w(l), S(w_0)$ - is a dimensionless force in spring,

c_1, c_3 - present linear and nonlinear part of spring characteristics, respectively.

According to the Bernoulli-Euler theory, the differential equation of equilibrium in dimensionless form may be presented as follows:

$$w_i^{IV}(\xi,\tau) + q^2 w_i''(\xi,\tau) + \omega_n^{*2} \ddot{w}_i(\xi,\tau) = 0 \tag{2.3}$$

where:

$q^2 = \frac{Pl^2}{EJ}$, P - subtangential force loading the spring from $\eta = 0$ to $\eta = 1$ (Fig. 1),

(4) $\ddot{\omega}_n^2 = \frac{\varrho A \ddot{\Omega}^2 L^4}{EJ}$ - is dimensionless coefficient of vibration frequency.

By using the method of small parameter the expressions $w_i(\xi,\tau)$ and $\ddot{\omega}_n^2(\varepsilon)$ were expanded into power series with respect to amplitude parameter $\varepsilon, (\varepsilon \ll 1)$

$$w(\xi,\tau) = w_0(\xi) + \varepsilon w_1(\xi,\tau) + \varepsilon^2 w_2(\xi,\tau) + \varepsilon^3 w_3(\xi,\tau) + \ldots \quad (2.4)$$

$$\ddot{\omega}_n^2(\varepsilon) = \omega_n^2 (1 + \varepsilon \nu_1 + \varepsilon^2 \nu_2 + \ldots) \quad (2.4a)$$

where:

$$w_k(\xi,\tau) = \sum_{i=1}^{k} w_k^i(\xi) \cos i\tau \qquad k = 1,2,3,\ldots \quad (2.4b)$$

$$\omega_n^2 = \frac{\varrho A \Omega_n^2 L}{EJ} \quad (2.4c)$$

After introducing expansions (2.4) (2.4a-c) into equations of motion (2.3) and equating the terms with the same exponents ε, the infinite series of equations of motions were obtained:

$$(\varepsilon^0) \quad w_0^{IV}(\xi) + q^2 w_0''(\xi) = 0 \quad (2.5a)$$

$$(\varepsilon^1) \quad w_1^{IV}(\xi,\tau) + q^2 w_1''(\xi,\tau) + \omega_n^2 \ddot{w}_1(\xi,\tau) = 0 \quad (2.5b)$$

$$(\varepsilon^2) \quad w_2^{IV}(\xi,\tau) + q^2 w_2''(\xi,\tau) + \omega_n^2 \ddot{w}_2(\xi,\tau) + \omega_n^2 \nu_1 \ddot{w}_1(\xi,\tau) = 0 \quad (2.5c)$$

$$(\varepsilon^3) \quad w_3^{IV}(\xi,\tau) + q^2 w_3''(\xi,\tau) + \omega_n^2 \ddot{w}_3(\xi,\tau) + \omega_n^2 \nu_2 \ddot{w}_1(\xi,\tau) + \omega_n^2 \nu_1 \ddot{w}_2(\xi,\tau) = 0 \quad (2.5d)$$

where Roman numerals and dots denote the order of derivative with respect to variable ξ and time τ, respectively.
The above equations were solved by using the following boundary conditions:

$$w_i(0,\tau) = w_i'(0,\tau) = 0 \quad (2.6a\text{-}b)$$

$$w_i''(1,\tau) = 0 \quad (2.6c)$$

(5)

$$W_i'''(1,\tau) + (1-\eta)\Omega^2 W_i'(1,\tau) - C_1(W_0 - \Delta) - C_3(W_0-\Delta)^3 = 0 \qquad (2.6d)$$

for $i = 0, 1, 2, 3$.

and condition (2.6d) was also expanded into power series with respect to ε, and the following sequence of equations arranged according to exponent ε was obtained.

The sequences of equations of motion were solved by using conditions (2.6a-c). The integration constants appearing in solutions were determined from boundary conditions and by applying the normalization condition $W_1'(1) = 1$. (2.7)

From equation (2.5b), by using conditions (2.6a-c) and expansion of boundary condition (2.6d), the equation in the following form has been obtained for ε^1 :

$$F(\lambda_1, \bar{\lambda}_1) = \left[C_1 + 3C_3(W_0-\Delta)^2\right] F_1(\lambda_1, \bar{\lambda}_1) + F_2(\lambda_1, \bar{\lambda}_1) = 0 \qquad (2.8)$$

where:

$$F_1(\lambda_1, \bar{\lambda}_1) = -A_1 V_1'(1) - B_1 V_1(1) \qquad (2.8a)$$

$$F_2(\lambda_1, \bar{\lambda}_1) = -\eta\Omega^2\left[A_1 V_1''(1) + B_1 V_1'(1)\right] + A_1 V^{IV}(1) + B_1 V_1'''(1) + \Omega^2\left[A_1 V_1'(1) + B_1 V_1(1)\right] \qquad (2.8b)$$

A_1, B_1 - integration constants.

Equation (2.8) was used for calculation of vibration frequency, ω_n.

3. Divergence - type instability

By substituting solution of $W_0(\xi)$ into expansion of condition (2.6d) we get the following equation:

$$G(W_0, \Omega(W_0), \eta, C_1, C_3, \Delta) = W_0\left[C_1 + \frac{G_2(\Omega,\eta)}{G_1(\Omega)}\right] - C_1\Delta + C_3(W_0-\Delta)^3 = 0 \qquad (3.1)$$

where:

$$G_2(\Omega,\eta) = -\Omega^3\left[1 + (1-\eta)(\cos\Omega - 1)\right] \qquad (3.1a)$$

(6)

Generally, depending on the sign of C_3, the typical trajectories of equilibrium, presented primarily by Koiter, were obtained for the symmetrical system. According to the Koiter's theory the function $q(w_0)$ shows maximum for static elastic deflections of symmetrical systems. For a perfect system the maximum occurs at $w_0 = 0$. For an imperfect system this function shows maximum at the point $w_0 \neq 0$. In the second type of the load-displacement relationship, as has been noticed by Koiter, the minimum of function does not exist.

However, the trajectories of statical equilibrium for the perfect and imperfect systems exist and the increase in load is required for increasing the deflection.

3.1. The regions of divergence

Fig. 2. presents the curves of extrema of the function $C_1(q_c)$ given by equation:

$$D(q_c, C_1(q_c), \eta, \delta) = (G_1 C_1 + G_2)^3 + \frac{27}{4} \delta G_1 G_2^2 = 0 \qquad (3.2)$$

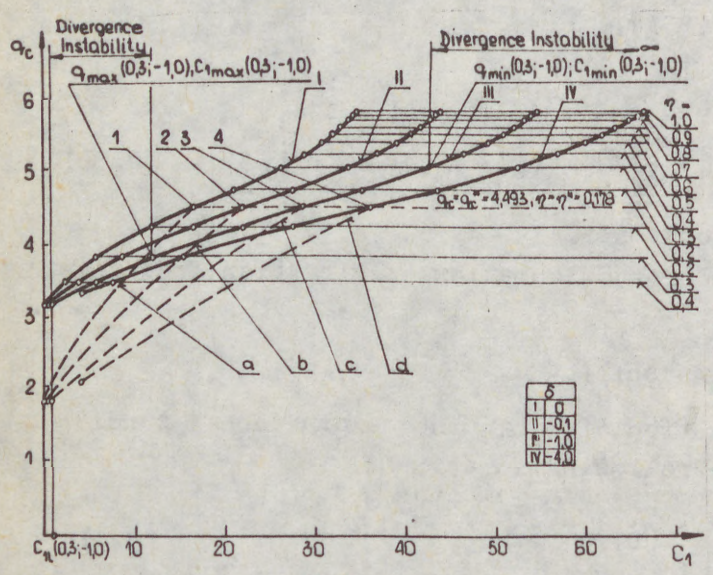

Fig. 2.

for various values of parameter δ.

The regions of existence of these curves are limited, on the LH side, by the points satisfying the condition

$$C_1 + C_3 w_0^2 > 0 \qquad (3,3)$$

(points 1,2,3,4).

The line $q = q^*$ divides two regions: above the curve ($\eta^* < \eta \leq 1$, δ - steady) the curves of family (3.2) are the plots of functions with minimum ($q > q^*$) whereas for ($q < q^*$) these functions have maximum. The curves a,b,c,d are the curves of family (3.2) for $\eta = \eta^*$ (with δ

(7)

taken according to the table in Fig. 2). These lines divide the regions in which the curves of family (3.2) correspond to the functions with extremum and to those without extremum. The region of divergence for the assigned values occurs for:

- $q > q^*$ rightwards from the points denoted by circles on curves I - IV.
- $q < q^*$ leftwards from these points.

There conditions are illustrated in Fig. 2 for exemplary data ($\eta = 0.3$ and $\delta = -1.0$). The extremum values of critical force of divergence q_c^{ex} are only dependent on parameter η, and are independent of the coefficient of stiffness C_1 and parameter δ, as illustrated by horizontal lines in this figure. The properties of function $C_1(q_c)$ given in the implicit form by equation (3.3) describing the critical force of divergence may be summarized as follows:

this function is determined for $0 \leq \eta \leq \eta_s$ (C_1, δ)

for $0 \leq \eta \leq \eta^*$ this function has no extrema

for $\eta^* < \eta \leq \eta_s$ $\begin{cases} q > q^* & \text{this function has minima,} \\ q > q^* & \text{this function has maxima.} \end{cases}$

for $\eta = \eta^*$ this function has a singular point.

4. Flutter and divergence instability

In analysing the relationship between the force loading column, q, and frequency of its natural vibration, ω_n, at various values of parameter η and various coefficients of spring stiffness C_1 and $\delta_1 (\delta = C_3 \Delta^2)$, the following form of equation (2.7) has been assumed:

$$(F_1 e_1 + F_2)\left(C_1 + \frac{3}{2}\frac{G_2}{G_1} - \frac{1}{2}\frac{F_2}{F_1}\right)^2 + \frac{27}{4}\delta G_2^2 / G_1 = 0 \qquad (4.1)$$

This form considers the relationship between the force q and static displacement $w_0(\xi)$, as determined by (3.1).

Fig. 3 illustrates the mutual location of the regions of flutter and divergence instability versus parameter δ.

(8)

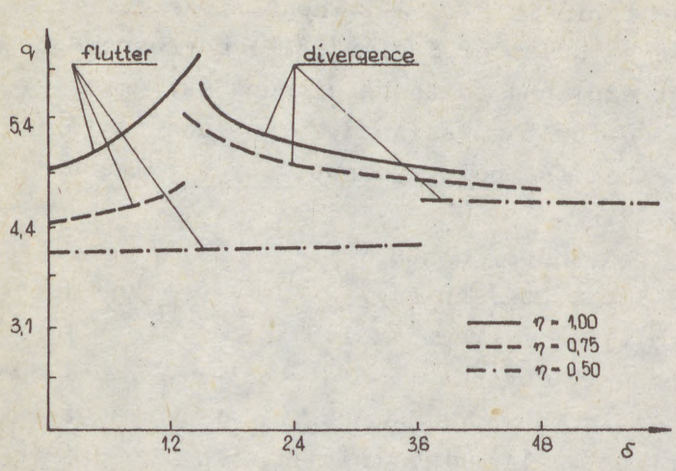

Fig. 3.

For follower coefficient $\eta = 1$, in the region of transition from one type of stability loss into another, the values of flutter force are higher than those of divergence force. This phenomenon is of reverse character for $\eta = 0.75$, ie., in the region of transition the values of flutter force are lower than those of divergence force (Fig. 3, dashed curves). For $\eta = 0.5$ the character of changes of the values of flutter and divergence forces is similar as for $\eta = 0.75$ (Fig. 3). For the decreased value of C_1 equal to 1.2 in the region examined δ ($\delta = 0 - 5$), the curves for $\eta = 1$ and $\eta = 0.75$ preserve their character and the change of the type of stability loss occurs at higher value of δ .
In this case, for $\eta = 0.5$, only the loss of stability of the flutter type occurs.

5. Final remarks

The nonlinearity of spring affects the critical force only in the case, in which the initial deflection exists. On the value of critical force, both of the divergence and flutter type, decides the parameter δ linking the effects of nonlinearity and initial deflection ($\delta = C_3 \Delta^2$).

(1)
TOMSKI, Lech (1)
PRZYBYLSKI, Jacek (2)

FLUTTER INSTABILITY OF A TWO MEMBER COMPOUND COLUMN

INTERNATIONAL COLLOQUIUM
STABILITY OF STEEL STRUCTURES
BUDAPEST, HUNGARY, 1990
PRELIMINARY REPORT

Summary: The flutter - type instability of a two member cantilever compound column loaded by a subfollower force and considered as a geometrically nonlinear system is studied. The effect of asymmetry of axial and flexural rigidities and unit masses of both bars as well as follower parameter on the value of critical force is discussed. The problem is solved with the use of the perturbation method. The results of numerical calculation are compared with those obtained for a single column. The existence of the smallest critical force was observed for a column composed of bars of asymmetric distribution of flexural rigidities.

Scope of the work

This work deals with the flutter type instability of a compound two-member cantilever structure loaded by a subfollower force (Fig.1). The members of the structure of different flexural ($E_i J_i$, $i = 1,2$) and axial ($E_i A_i$, $i = 1,2$) rigidities and different masses per unit length ($\varrho_i A_i$, $i = 1,2$) are rigidly

(1) Associate Professor, Częstochowa Institute of Technology, Poland
(2) Lecturer, Częstochowa Institute of Technology, Poland

(2)

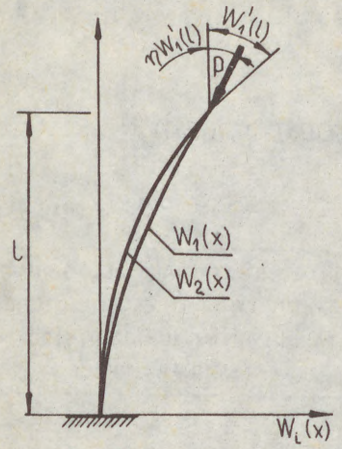

Fig. 1.

connected with each other, both in a displacement and rotational sense (E_i - modulus of elasticity, A_i - cross sectional area, J_i - moment of inertia of i-th bar).

A physical model of such a structure can be presented as a column made of two coaxial tubes or tube and bar or as a planar frame made of a strip located in the center of the structure in which the second is formed by two identical strips symmetrically located at both sides of the central strip. For the sake of the theory applied in this paper the members of column are called bars.

According to the moderately large bending theory the equations of motion of i-th bar of the column are the following:

$$\frac{\partial^4 w_i(\xi,\tau)}{\partial \xi^4} + k_i^2(\tau)\,\frac{\partial^2 w_i(\xi,\tau)}{\partial \xi^2} + \omega_{ni}^{*2}\,\frac{\partial^2 w_i(\xi,\tau)}{\partial \tau^2} = 0 \qquad (1a-b)$$

where:

$$w_i(\xi,\tau) = \frac{W(x,t)}{l}\,,\quad k_i^2(\tau) = \frac{S_i(\tau)\,l^2}{E_i J_i}\,,\quad \omega_{ni}^{*2} = \frac{\varrho_i A_i \Omega_n^{*2} l^4}{E_i J_i}\,,\quad \xi = \frac{x}{l}\,,\quad \tau = \Omega_n^{*} t \qquad (2a-h)$$

$W(x)$ - lateral displacement of i-th bar (i=1,2), $S_i(\tau)$ - axial force in i-th bar, Ω_n^{*} - vibration frequency of n-th order, x - axial coordinate, t - time, l - length of the column.

The equation of axial displacements in i-th bar after satisfying the boundary conditions $u_1(0,\tau) = u_2(0,\tau) = 0$ is as follows:

$$u_i(\xi,\tau) = -\frac{k_i^2(\tau)}{\lambda_i}\,\xi - \frac{1}{2}\int_0^{\xi}\left[\frac{\partial w_i(\xi,\tau)}{\partial \xi}\right]^2 d\xi \qquad (3a-b)$$

where:

$$\lambda_i = \frac{A_i l^2}{J_i} \qquad (4a-b)$$

By applying the perturbation method the terms $w_i(\xi,\tau)$, $k_i^2(\tau)$ and $\omega_{ni}^{*2}(\varepsilon)$ are expanded into exponential series with

(3)

respect to the amplitude parameter ε ($\varepsilon << 1$):

$$W_i(\xi,\tau) = \sum_{j=1}^{N} \varepsilon^{2j-1} W_{i2j-1}(\xi,\tau) + O(\varepsilon^{N+1}) \tag{5a}$$

$$k_i^2(\tau) = \sum_{j=0}^{N} \varepsilon^{2j} k_{i2j}^2(\tau) + O(\varepsilon^{N+1}) \tag{5b}$$

$$\omega_{ni}^{*2} = \omega_{ni}^2 \left(1 + \sum_{j=1}^{N} \varepsilon^{2j} \nu_{2j}\right) + O(\varepsilon^{N+1}) \tag{5c}$$

where:

$$W_{ij}(\xi,\tau) = \sum_{m=1}^{j} W_{ij}^{[2m-1]}(\xi) \cos(2m-1)\tau \qquad j = 1,3,5,\ldots \tag{6}$$

$$k_{ij}^2(\tau) = \sum_{m=0}^{j} \left(k_{ij}^{[2m]}\right)^2 \cos 2m\tau \qquad j = 2,4,6,\ldots \tag{7}$$

$$\omega_{ni}^2 = \frac{\varrho_i A_i \Omega_n^2 l^4}{E_i J_i} \tag{8}$$

By introducing expansions (5a-c) into equations of motion (1a-b) and axial displacement (3a-b) and then by equating the terms of the same exponents ε one derives the infinite sequence of equations of motion and displacements:

$O(\varepsilon^0)$ $$u_{i0}(\xi) = -\frac{k_{i0}^2}{\lambda_i}\xi \tag{9a-b}$$

$O(\varepsilon^1)$ $$w_{i1}^{IV}(\xi,\tau) + k_{i0}^2 w_{i1}''(\xi,\tau) + \omega_{ni}^2 \ddot{w}_{i1}(\xi,\tau) = 0 \tag{10a-b}$$

$O(\varepsilon^2)$ $$u_{i2}(\xi,\tau) = -\frac{k_{i2}^2(\tau)}{\lambda_i}\xi - \frac{1}{2}\int_0^{\xi} \left[w_{i1}'(\xi,\tau)\right]^2 d\xi \tag{11a-b}$$

$O(\varepsilon^3)$ $$w_{i3}^{IV}(\xi,\tau) + k_{i0}^2 w_{i3}''(\xi,\tau) + \omega_{ni}^2 \ddot{w}_{i3}(\xi,\tau) - \tag{12a-b}$$

$$= -k_{i2}^2(\tau) w_{i1}''(\xi,\tau) - \omega_{ni}^2 \nu_2 \ddot{w}_{i1}(\xi,\tau) \qquad (i = 1,2)$$

(4)

The Roman numerals and dots in the above equations denote the order of a deriviative with respect to ξ and τ .

The equations (9-12) may be solved at the following boundary conditions, in which expansions (5a-b) have previously been included:

$$w_1(0,\tau) = w_2(0,\tau) = w_1'(0,\tau) = w_2'(0,\tau) = 0 \quad , \quad w_1(1,\tau) = w_2(1,\tau) \; ; \; w_1'(1,\tau) = w_2'(1,\tau) \tag{13a-f}$$

$$\frac{1}{l^2} E_1 J_1 w_1'''(1,\tau) + \frac{1}{l^2} E_2 J_2 w_2'''(1,\tau) + P(1-\eta) w_1'(1,\tau) = 0 \tag{13g}$$

$$E_1 J_1 w_1''(1,\tau) + E_2 J_2 w_2''(1,\tau) = 0 \tag{13h}$$

$$u_1(1,\tau) = u_2(1,\tau) \quad , \quad k_1^2 + r k_2^2 = p^2 \tag{13i-j}$$

where:

$$r = \frac{E_2 J_2}{E_1 J_1} \quad , \quad p^2 = \frac{P l^2}{E_1 J_1}$$ and P is the load of column.

Results of numerical calculation

In order to study the effect of relationship occuring between axial and flexural rigidities and masses per unit length of the column bars on the value of flutter load the courses of variations of the first and second natural frequencies of the structure were determined at follower parameter $\eta = 1$ for columns characterized by data listed in Table 1 (column length l=4 m).

In selecting the data for this table one was governed by principle that the sum of flexural rigidities $(EJ = E_1 J_1 + E_2 J_2)$ and the sum of masses per unit length of both bars of structures $(\varrho A = \varrho_1 A_1 + \varrho_2 A_2)$ would have been constant and equal to corresponding sums for a column of asymmetric properties (data No 5). Data No 1 correspond to a structure composed of bars of the same flexural and axial rigidities and masses per unit length. Such a column resembles a single column of flexural

(5)

Table 1. Physical and geometrical data of the compound columns

	E_1A_1 [N]	E_2A_2 [N]	E_1J_1 [Nm^2]	E_2J_2 [Nm^2]	ϱ_1A_1 [kg/m]	ϱ_2A_2 [kg/m]
1	$21.42135\ 10^7$		$6.291\ 10^5$		21.42135	
2'	$21.42135\ 10^7$		$4.042\ 10^5$	$8.54\ 10^5$	21.42135	
2''	$21.42135\ 10^7$		$2.042\ 10^5$	$10.54\ 10^5$	21.42135	
3	$21.42135\ 10^7$		$6.291\ 10^5$		15.1971	27.6456
4	$5.0657\ 10^8$	$6.9114\ 10^8$	$6.291\ 10^5$		21.42135	
5	$5.0657\ 10^8$	$6.9114\ 10^8$	$2.042\ 10^5$	$10.54\ 10^5$	15.1971	27.6456

rigidity EJ and mass per unit length ϱA when vibrating at the same frequency and taking the identical form as a single bar column. Data Nos 2,3 and 4 were selected in such a way that one type of rigidities (ie. either flexural or axial ones) or masses per unit lengths of bars were the same for column 5 whereas the remaining data as for column 1. Column 2' have different distribution of flexural rigidity than column 2''. The curves of natural frequencies (of the first and second modes) for the data of Table 1 are presented in Fig 2. The curves are denoted according to data numeration.

For studies of the natural vibration mode the columns of data 3 and 5 were selected. For column 5 a fragment of characteristic of the third frequency was plotted additionally (Fig. 2 - curve 5 (III)). The vibration modes for this column were found for the force $P = 3.465 \times 10^5$ N and natural frequencies defined at the points A, B, C (Fig. 2). Column 3, when loaded by the force $P = 8 \times 10^5$ N vibrates according to the first and second modes (point D and E respectively - Fig. 2) taking the forms presented in Fig. 3. In the case of asymmetric distribution of flexural rigidity (column 5) there appe-

(6)

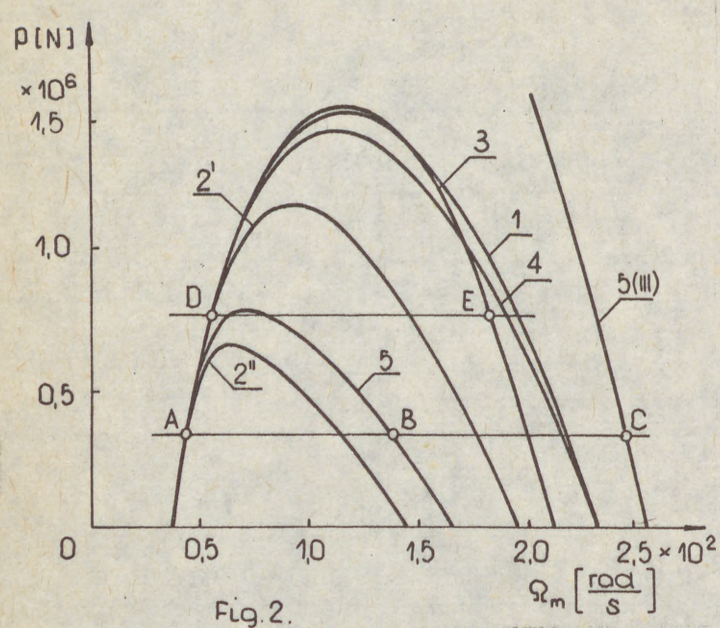

Fig. 2.

ars an additional mode of vibration (cf.Fig. 3) corresponding to a lower-value of frequency as compared with the second frequency of column 3. At symmetric distribution of flexural rigidity the frequencies and modes of free vibration of a compound column correspond to those of a single column.

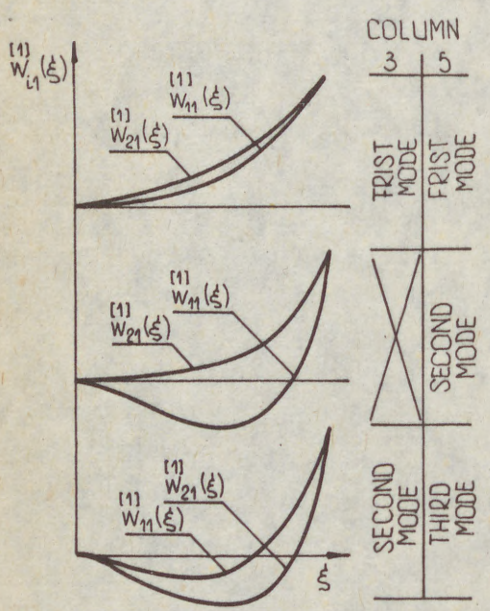

Fig. 3.

The courses of changes of the first and second natural frequencies of the two - bar and single - bar columns of the flexural rigidity EJ and unit mass ϱA up to the moment at which flutter occurs ($\Omega_1 = \Omega_2$) are presented in Fig.4 for η = 0.6, 0.8 and 1.0. The value of flutter force for a single column increases with the rise of the value of follower parameter η , whereas for the column 5 the opposite phenomenon occurs, ie. the value of critical force decreases with the increase of the follower parameter η .

Fig. 5 illustrates the cur-

(7)

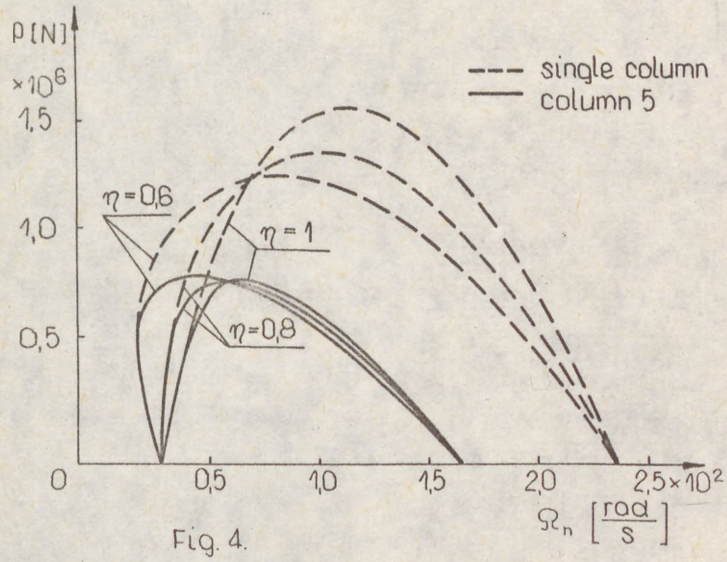

Fig. 4.

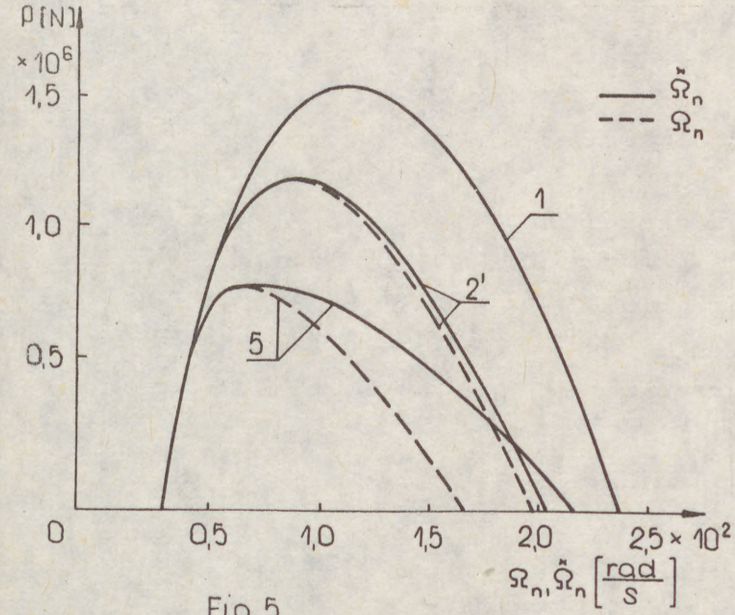

Fig. 5.

ves of the first and second natural frequency $\tilde{\Omega}_n$ for column Nos 1, 2' and 5 (with consideration of frequency correction factor ν_2). For the first natural frequency of the columns considered the correction factor value is $\nu_2 \approx 0$, whereas for the second frequency the value of ν_2 depends on the relationship between the flexural rigidities of both bars. The more asymmetric distribution of rigidity (higher geometrical nonlinearity), the larger value of correction ν_2.

The courses of curves Ω_2 and $\tilde{\Omega}_2$ prove that the correction ν_2 does not affect the value of flutter forces of two - bar columns and the flutter force determined from the condition $\Omega_1 = \Omega_2$ has a precisely defined value.

(8)

Conclusions

The value of flutter force for a two - bar column of constant values of flexural rigidities of its bars and masses per unit length, $EJ = E_1J_1 + E_2J_2$ and $\varrho A = \varrho_1 A_1 + \varrho_2 A_2$ respectively, depends mainly on the flexural rigidity distribution into individual bars. The highest value of flutter load occurs when the quotient of flexural rigidities $E_1J_1 / E_2J_2 = 1$ and the lowest one in the case of the most asymmetrical distribution of stiffness. The asymmetry of distribution of mass per unit length and axial rigidity into individual bars of a compound column only slightly affects the value of flutter force with respect to the structures of symmetrical mass and axial rigidity distribution.

For the compound column with asymmetric distribution of flexural rigidity an additional mode of vibration appears, wich does not exist for the single column or for the compound column with symmetric distribution of this rigidity.

For single - bar columns, with the increase of the value of follower parameter from 0.5 to 1, the value of critical flutter forces increases, whereas for compound columns, depending on the distribution of flexural rigidity into both bars of the structure, the relationship between the follower parameter and flutter force may be inverse, ie. to the higher value of follower parameter (from the range $< 0{,}6,\ 1 >$) a smaller critical force may correspond.

SESSION 15

SPECIAL PROBLEMS

(1)
BOJA, Nicolae (1)
IVAN, Marin (2)

A GEOMETRICAL APPROACH TO THE THEORY OF DEFORMATIONS FOR CURVED SHELLS RELATED TO THEIR CURVATURE LINES.

INTERNATIONAL COLLOQUIUM
STABILITY OF STEEL STRUCTURES
BUDAPEST, HUNGARY, 1990
PRELIMINARY REPORT

Summary: In the paper we establish some preparatory geometrical elements for the study of elastic deformations of the curved shells related to their curvature lines and we determine, in the generalized Love-Kirchhoff hypotheses, the displacement gradients of such a type of shells function only of the following elements of the undeformed middle surface: the components of the metric tensor, the principal curvatures, the distance of an arbitrary point of the shell to its projection on the middle surface and, obviously, the components of the displacement vector.

Our purpose is to obtain simplified results for this type of shells, which occur frequently in many technical problems (cylindrical, spherical, conical, curly, flat, etc. elastic shells), as againts the general case [Koiter - 1966, Batoz - 1977, Moreau - 1979].

1. Curved shells. The geometry of the middle surface and of the parallel foils.

By curved shell we understand a conex continuous material medium delimited by two surfaces (parallel or not),

(1) Professor of Mathematics, Timişoara, Polytechnical Institute
(2) Professor of Civil Engineering, Timişoara, Polytechnical Institute

(2)

named "faces of the shell", and by a union of surfaces which constitute the lateral frontier of the shell.

Also, we suppose that on the C shell is defined a 3-dimensional differentiable manifold structure for which one of the dimensions - the h thickness (constant or variable) is much smaller than the other two.

A placement of the shell in the 3-dimensional Euclidean space $\mathcal{E}^3$, i.e. the map $p:C \longrightarrow \mathcal{E}^3$, is a diffeomorphism (of class C^k, $k \geq 1$); the $\mathcal{E}^3$ space is related to a fixed orthonormal frame $R^o = \{O; \bar{I}, \bar{J}, \bar{K}\}$. The map considered above is called initial placement and $\Sigma = p(C)$ its corresponding image - reference position of the shell. In fact, this means to attach to every material particle $x \in C$ the coordinates of the $p(x) = P$ point - its image in $\mathcal{E}^3$, relative to the R^o frame. Generally, p is an injective regular map in every point of C, so p is an embedding and Σ is a submanifold of $\mathcal{E}^3$, which also has the dimension 3.

The middle surface of the shell plays an important role in studying the curved shell, as knowing its geometry allows the extension of properties in an arbitrary neighborhood of shells.

The middle surface of a curved shell C is a 2-dimensional submanifold S of the image - manifold Σ, having the property that every point M is the middle of the normal segment to S which passes through this point and has the extremities on the faces of the shell.

We consider oriented the outer surfaces of the shell and call them "the lower face" and "the upper face", respectively, as the angle $\sphericalangle(\bar{e}_3^o \bar{k})$ is $> \frac{\pi}{2}$ or $< \frac{\pi}{2}$, respectively, $\bar{e}_3^o$ - being the normal unit vector at M to S.

If Σ has the h thickness constant, then the faces are parallel and have common normals with the middle surface S; but, generally, $h = h(M)$ is a positive real function of $M \in S$, i.e. of the pair $(u^1, u^2) \in \mathbb{D} (\subset \mathbb{R}^2)$ of Gaussian coordinates of the considered point.

The position of each point P of the shell is determined by the normal which passes through this point and the real number $z \in [-h/2, h/2]$ which represents the number $\pm d(P,M)$, where $M (= pr_S P)$ is the intersection of the S surface.

(3)

with the normal through P, and "+" or "-" corresponds to the fact that P is situated in the upper half shell (of S), or in the lower half shell, respectively. So, for $P(\bar{r}^*)$ the position vector relative to R^o is

$$\bar{r}^* = \bar{r}(u^1,u^2) + z\bar{e}_3^o , \quad ((u^1,u^2)\in\mathbb{D}) \qquad (1)$$

where $\bar{r} = \overrightarrow{OM}$; we say that the point P is situated "over" M if in (1) we have $z>o$ and "under" M, in the opposite case. The curvilinear coordinates of P are (u^1,u^2,u^3), where $|u^3| \leqslant \frac{1}{2}h(u^1,u^2)$ and (u^1,u^2) are the Gaussian coordinates of its projection on S.

We denote by S^z the set of all points of Σ situated at $|z|$ $(z\in\left[-\frac{h}{2},\frac{h}{2}\right] \doteq I)$ distance from its projections on S; for z fixed in the interval I the set S^z is a pair of surfaces parallel with S and called "foils" of the curved shell. For different values of the variable $z\in I$ correspond foils which do not have common points. We denote the set of all foils by $(S^z)_{z\in I}$.

Let $P(\bar{r}^*)$ be an arbitrary point which belongs to the shell. We denote by $S^*\in(S^z)_{z\in I}$ the foil which passes through the point P; the surfaces S^* and S have common normals in the pairs (P,M) of corresponding points, called "initial configurations" of the shell. Also, we denote by $(M;\bar{e}_1,\bar{e}_2,\bar{e}_3^o)$ the Darboux trihedron associated to S with $\bar{e}_i$ $(i=1,2)$ the tangent vectors to the coordinate lines u^i=const. and by $(P;\bar{e}_1^*,\bar{e}_2^*,\bar{e}_3^o)$ the corresponding trihedron associated to S^*.

We suppose that S is related to its curvature lines (the coordinate lines coincide with the curvature lines through M, $(\forall)M\in S$) and on S we consider the Levi-Civita connection. Let (U,φ) be a local system of coordinates in M on S and $\{X_1,X_2\}$ an orthonormal moving frame on the conex neighborhood of coordinates U $(\subset S)$ so that X_i are principal vectors (they define the directions of the curvature lines on S), with the associated principal curvatures k_i $(=1/R_i)$, $(i=1,2)$. This frame will be call I-orthonormal, because the first fundamental form of S is diagonalised in relation to it.

For the associated fundamental forms we have in this case the canonical expressions

(4)

$$I = \sum g_i du^i \otimes du^i \quad , \quad II = \sum {}^{+}_{-} b_i du^i \otimes du^i \qquad (2)$$

and

$$b_i = k_i g_i, \quad (i=1,2) \; ; \qquad (3)$$

in (2) we take "+" or "-" function of the S orientation. Denoting by $\theta^i = du^i$ the coordinate forms, they satisfy in this case the relations

$$\theta^i(X_j) = \delta^i_j \; , \quad (i,j = 1,2) \qquad (4)$$

and are in dependence with the 1-forms of Levi-Civita connection by

$$\omega_{3j} = k_j \theta_j \qquad (5)$$

where $\theta_j = \theta^j$, $\omega^i_j = \omega_{ij}$, because the manifold S is Riemannian.

The derivatives of the vectors of the Darboux trihedron in each point M of S contain the components of the connection forms which depend on the coordinate forms by general relations $\omega^i_j = \Gamma^i_{jk}\theta^k$. Because S is related to curvature lines, we obtain the following simple expressions of Christoffel symbols of the second kind

$$\begin{aligned} &\Gamma^1_{21} = -g_1, && \Gamma^1_{31} = -k_1, && \Gamma^2_{31} = o \\ &\Gamma^1_{22} = -g_2, && \Gamma^1_{32} = o \; , && \Gamma^2_{32} = -k_2 \end{aligned} \qquad (6)$$

with which we have determined the coefficients of the I^* form relative to the parallel foil S^* which passes through the point $P(r^*) \in \Sigma$ [Boja, Florescu, Ivan - 1985] :

$$\begin{aligned} g^*_{11} &= (1 - 2z\, k_1 + z^2 k_1^2) g_1 \doteq g^*_1, \quad g_1 = \langle \bar{r}_{,1}; \bar{r}_{,1} \rangle \\ g^*_{12} &= o \\ g^*_{22} &= (1 - 2zk_2 + z^2 k_2^2) g_2 \doteq g^*_2, \; g_2 = \langle \bar{r}_{,2}; \bar{r}_{,2} \rangle \; . \end{aligned} \qquad (7)$$

The exterior geometry of the surface S^* in a neighborhood of the P point can be obtained starting from the derivatives of (1) relative to the variables u^i (i=1,2), $\bar{r}^*_{,i} = \bar{r}_{,i} + z\bar{e}^o_{3,i}$ and from the coefficients of the second fundamental form $b^*_{ij} = - \langle \bar{e}^*_i; \bar{e}^o_{3,j} \rangle$, (i,j =1,2), and we have, successively, the relations [Boja, Ivan - 1986] :

$$\begin{bmatrix} \bar{e}^*_1 \\ \bar{e}^*_2 \\ \bar{e}^*_3 \end{bmatrix} = \begin{bmatrix} 1 - zk_1 & o & o \\ o & 1 - zk_2 & o \\ o & o & 1 \end{bmatrix} \cdot \begin{bmatrix} \bar{e}_1 \\ \bar{e}_2 \\ \bar{e}_3 \end{bmatrix}, \qquad (8)$$

which express the relationship between the two Darboux trihedrons at S^* and S surfaces in the pair of coorespondent points (P,M),

(5)

$$b_{11}^{*} = (1 - zk_1)k_1 g_1 \doteq b_1^{*}$$
$$b_{12}^{*} = 0 \qquad (9)$$
$$b_{22}^{*} = (1 - zk_2)k_2 g_2 \doteq b_2^{*} \ ,$$

the coefficients of the form II^{*} relative to S^{*} at the point P and

$$k_i^{*} = \frac{k_i}{1 - zk_i} \ , \quad (i = 1,2) \qquad (10)$$

the principal curvatures of S^{*} at P for which $z \neq 1/k_i = R_i$.

The latter condition is generally satisfied at all points of a thin elastic shell because in this case we have $|z| \leq h/2$ and $h \ll R_i$, $(i = 1,2)$.

Computing now the Gaussian and the mean curvatures of parallel foil S^{*} at P, we obtain the expressions

$$K^{*} = \frac{K}{|1 - 2zH + z^2K|} \ , \quad H^{*} = (\text{sign } H)\frac{|H - zK|}{|1 - 2zH + z^2H|}, \qquad (11)$$

where K and H denote the corresponding curvatures of S in M. With (11) we can determine the coefficients of the III^{*} fundamental form of S^{*} using the identity [Koiter - 1966] :

$$Kg_{ij} - 2Hb_{ij} + c_{ij} = 0$$

and we obtain

$$c_{11}^{*} = k_1^2 g_1, \quad c_{12}^{*} = c_{21}^{*} = 0, \quad c_{22}^{*} = k_2^2 g_2 \ ; \qquad (12)$$

also, from the known relations $c_{ij} = - b_{ik}\Gamma_{j3}^{k}$, $(i,j = 1,2)$ there result the Christoffel symbols of the second kind for S^{*} in P:

$$\Gamma_{13}^{*1} = - \frac{k_1}{1 - zk_1}, \quad \Gamma_{13}^{*2} = \Gamma_{23}^{*1} = 0, \quad \Gamma_{23}^{*2} = - \frac{k_2}{1 - zk_2} \qquad (13)$$

2. Isometric deformations of curved shells.

In the first part we have described the initial placement Σ of a curved shell C related to curvature lines in $\mathcal{E}^3$ space.

Another placement $p: C \longrightarrow \mathcal{E}^3$ of the C curved shell in the Euclidean space can be the result of an exterior force action upon it.

The map $\delta : \mathcal{E}^3 \longrightarrow \mathcal{E}^3$, defined by $\delta = \tilde{p} \circ p^{-1}$ represents a displacement of the shell and we denote $\Sigma \longrightarrow \tilde{\Sigma}$ (where $\tilde{\Sigma} = \tilde{p}(C)$), consisting of a translation and a rotation in $\mathcal{E}^3$. That means it is an isometric deformation of the curved shell.

Any point $P(\in \Sigma)$ passes in a new position $\tilde{P} \in \tilde{\Sigma}$. If the $\delta|_{\Sigma}$ restriction map at each point of Σ is known, this

(6)
one defines a vector field of

$$v: \Sigma \longrightarrow V = E^3,$$

(E^3 being the 3-dimensional euclidian vector space), by

$$v(P) \doteq \bar{v}^* = \overrightarrow{P\tilde{P}}, \quad (\tilde{P} = \delta(P));$$

the $\bar{v}^*$ vector of the field at every point P is called the displacement vector of the respective point. Let $\bar{r}^*$ and $\tilde{r}^*$ be the position vectors of P and $\tilde{P}$ relative to the frame R^o. Also, let $\tilde{M} = \delta(M)$, ($M = pr_S P$), and $\bar{v} = \bar{v}(M)$ - the displacement vector of M. We have obviously, $\bar{v} = \overrightarrow{M\tilde{M}}, (\forall)\ M \in S$. We consider now the Darboux trihedrons to the S and $\tilde{S}$ middle surfaces at M and $\tilde{M}$, respectively, having the bases $(\bar{e}_1, \bar{e}_2, \bar{e}_3^o)$ and $(\tilde{e}_1, \tilde{e}_2, \tilde{e}_3^o)$, respectively, where ^{o} denotes the normal unit vectors.

Deriving function of the variables u^ρ ($\rho = 1,2$), the relation

$$\tilde{r} = \bar{r} + \bar{v}, \quad \bar{v} = v^\alpha \bar{e}_\alpha + v^3 \bar{e}_3^o$$

gives the tangent vectors to $\tilde{S}$ at $\tilde{M}$: $\tilde{e}_\beta = \bar{e}_\beta + \bar{v}_{,\beta}$, which can be expressed in the basis of Darboux frame at $\tilde{M}$ as follows:

$$\tilde{e}_\beta = (\delta_\beta^\alpha + d_\beta^\alpha)\bar{e}_\alpha + \phi_\beta \bar{e}_3^o, \tag{14}$$

where δ_β^α is the Kronecker tensor, and

$$d_\beta^\alpha = v^\alpha|_\beta - v^3 b_\beta^\alpha, \quad \phi_\beta = v^3{}_{,\beta} + v^\alpha b_{\alpha\beta} \tag{15}$$

are the displacement gradients [Batoz - 1977]: d_β^α -the mixed displacement tensor and ϕ_β-the covariant vector of the rotation around of the $\bar{e}_3^o$ normal to the $T_M(S)$ tangent plane. The covariant components of the displacement tensor are $d_{\alpha\beta} = g_{\alpha\gamma} d_\beta^\gamma$.

Further on we shall establish detailed analytic expressions for the gradients of the displacement of a curved shell C in the case in which it is related to the curvature lines. We can say about a curved shell that it is related to the curvature lines iff its middle surface has this property because, in this case, the foils parallel with this one will be also related to the curvature lines. This permits a study of deformations of the Σ shell starting from the deformations of foils $(S^z)_{z \in I}$, parallel with the middle surface S, in the sense that we shall analyze the displacement $P \longmapsto \tilde{P}$ of each point $P \in S^*$, ($S^* \in (S^z)$, $z \in I$), using the displacement vector $\bar{v}^* = v(P)$ of the respective points; shortlly, this manner to approach the problem follows the way: $S \longmapsto S^* \longmapsto \tilde{S}^*$, different from the usual way [Batoz - -1977] which analyzes the tract: $S \longmapsto \tilde{S} \longmapsto \tilde{S}^*$. Our choice has the advantage to avoid the stage of "lifting upon normal" after

(7)

deformation, $\tilde{S} \longrightarrow \tilde{S}^{*}$, according to the generalized Love-Kirchhoff hypothesis: the deformations $\Sigma \longrightarrow \tilde{\Sigma}$ are isometric, but the normals to the middle surface S remain straigh lines without being normals to the deformed surface $\tilde{S} = \delta(S)$ any longer. The stage $S \longmapsto S^{*}$ is completely described in the section 1. Here we describe the final stage $S^{*} \longmapsto \tilde{S}^{*}$ of the proposed chain.

Because the deformations are isometric, we have

$$\bar{v}^{*} = \bar{v} + z\bar{w} , \tag{16}$$

where $\bar{v} = v(M)$, $(M \in S)$ and $\bar{w} = \tilde{e}_3^0 - \bar{e}_3^0$ is the unit deviation vector of the normal vector to S, supposed known.

Utilizing the metric tensor of S^{*} and taking into account the fact that the mixed components of its curvature tensor coincide with the principal curvatures, we can expres the covariant components of the displacements tensor by the relations

$$\begin{aligned} d^{*}_{11} &= g^{*}_{1} d^{*1}_{1} = g^{*}_{1} v^{*1}|_{1} - v^{*3} k^{*}_{1}, \quad d^{*}_{12} = g^{*}_{1} d^{*1}_{2} = g^{*}_{1} v^{*1}|_{2} \\ d^{*}_{21} &= g^{*}_{2} d^{*2}_{1} = g^{*}_{2} v^{*2}|_{1}, \quad d^{*}_{22} = g^{*}_{2} d^{*2}_{2} = g^{*}_{2} v^{*2}|_{2} - v^{*3} k^{*}_{2} \end{aligned} \tag{17}$$

where $v^{*\alpha}|_{\beta}$ are covariant derivatives relative to S^{*} of the contravariant components of the displacement vector $\bar{v}^{*}$ given by (16) and have the following expressions:

$$v^{*\alpha}|_{\beta} = v^{*\alpha}{}_{,\beta} + \Gamma^{*\alpha}_{\gamma\beta} v^{*\gamma} , \tag{18}$$

in which the $\Gamma^{*\alpha}_{\gamma\beta}$ coefficients relative to S^{*} have the values

$$\begin{aligned} &\Gamma^{*1}_{11} = (\ln \sqrt{g^{*}_{1}})_{,1}; \quad \Gamma^{*1}_{21} = (\ln \sqrt{g^{*}_{1}})_{,2}; \quad \Gamma^{*1}_{22} = -\frac{1}{2} \frac{1}{g^{*}_{1}} g^{*}_{2,1} \\ &\Gamma^{*2}_{11} = -\frac{1}{2} \frac{1}{g^{*}_{2}} g^{*}_{1,2}; \quad \Gamma^{*2}_{12} = \Gamma^{*2}_{21} = (\ln \sqrt{g^{*}_{2}})_{,1}; \quad \Gamma^{*2}_{22} = (\ln \sqrt{g^{*}_{2}})_{,2} \end{aligned} \tag{19}$$

Passing now to the expressions of the ϕ^{*}_{β} $(\beta = 1,2)$ rotation components of the basis of $T_{\tilde{p}}(\tilde{S}^{*})$ around the normal vector $\bar{e}_3^{0*}$ $(= \tilde{e}_3^0)$ to $T_p(S^{*})$ we obtain the values

$$\phi^{*}_{1} = v^{*3}{}_{,1} + v^{*1} b^{*}_{1} , \qquad \phi^{*}_{2} = v^{*3}{}_{,2} + v^{*2} b^{*}_{2} , \tag{20}$$

where b^{*}_{α} are given by (9).

Finally, we can determine the components of the deformation tensor at the arbitrary point P of the deformed shell. We know as well this one is given by the general formula $\gamma_{\alpha\beta} = \frac{1}{2}(\tilde{g}_{\alpha\beta} - g_{\alpha\beta})$, where $g_{\alpha\beta} = \langle \bar{e}_{\alpha}; \bar{e}_{\beta} \rangle$ and $\tilde{g}_{\alpha\beta} = \langle \tilde{e}_{\alpha}; \tilde{e}_{\beta} \rangle$ and we compute with (14).

We write the (14) formulas in the $\tilde{P}(\in \tilde{\Sigma})$ point, utilizing the covectors of the basis of the tangent space, under

(8)

the form $$\bar{e}^{*}_{\alpha} = (g^{*}_{\alpha\lambda} + d^{*}_{\lambda\alpha})\bar{\theta}^{*\lambda} + \phi^{*}_{\alpha}\bar{e}^{3}_{0} \qquad (14')$$

in which we have used the known relations $\bar{e}_{\alpha} = g_{\alpha\lambda}\bar{e}^{\lambda}$, $\bar{e}^{3}_{0} = \bar{e}^{0}_{3}$.

We obtain the following components of the deformation tensor

$$\begin{aligned}
\gamma^{*}_{11} &= \theta^{*}_{11} + \tfrac{1}{2}(d^{*}_{11}d^{*1}_{1} + d^{*}_{21}d^{*2}_{21}) + \tfrac{1}{2}(\phi^{*}_{1})^{2}\\
\gamma^{*}_{12} &= \theta^{*}_{12} + \tfrac{1}{2}(d^{*}_{11}d^{*1}_{2} + d^{*}_{21}d^{*2}_{2}) + \tfrac{1}{2}\phi^{*}_{1}\phi^{*}_{2}\\
\gamma^{*}_{21} &= \theta^{*}_{21} + \tfrac{1}{2}(d^{*}_{12}d^{*1}_{1} + d^{*}_{22}d^{*2}_{1}) + \tfrac{1}{2}\phi^{*}_{1}\phi^{*}_{2}\\
\gamma^{*}_{22} &= \theta^{*}_{22} + \tfrac{1}{2}(d^{*}_{12}d^{*1}_{2} + d^{*}_{22}d^{*2}_{2}) + \tfrac{1}{2}(\phi^{*}_{2})^{2}
\end{aligned} \qquad (21)$$

The first terms from (21) are usually called "linearisation terms" of the tensor of deformations and represents the symmetric part of the $d^{*}_{\alpha\beta}$ tensor, being given by the expressions

$$\begin{aligned}
\theta^{*}_{11} &= g^{*}_{1}v^{*1}|_{1} - k^{*}_{1}v^{*3}\\
\theta^{*}_{12} &= \tfrac{1}{2}(g^{*}_{1}v^{*1}|_{2} + g^{*}_{2}v^{*2}|_{1}) = \theta^{*}_{21}\\
\theta^{*}_{22} &= g^{*}_{2}v^{*2}|_{2} - k^{*}_{2}v^{*3}
\end{aligned} \qquad (22)$$

where k^{*}_{α} have the values (1o) and g^{*}_{α} - the values (7).

References

1. Batoz, J.L. - 1977, Analyse non lineaire des coques minces elastiques des formes arbitraires par elements triangulaires courbes; These Univ.Laval, Quebec.

2. Boja, N., Florescu, D., Ivan, A. - 1985, Geometric elements associated to thin elastic shells for calculus of nonlinear deformations; Lucr.Conf.Naţ.de Mecanică Solidelor, Timişoara, 97-1oo.

3. Boja, N., Ivan, M. - 1986, Proprietăţi geometrice ale pînzelor subţiri raportate la liniile de curbură; Simpoz."Soluţii noi, eficiente în proiectarea structurilor", Timişoara, 1o9-114.

4. Boja, N., Ivan, M., Dănilescu, A. - 1988, Despre gradienţii deplasărilor plăcilor curbe raportate la liniile de curbură; 5th Conference on metal structures, Timişoara, 219-224.

5. Koiter, W.T. - 1966, On the nonlinear theory of thin elastic shells, I, II, III; Proceed.Koninkl.Akademie-Amsterdam, Mecanics, Serie B, 69, No.1, 1-54.

6. Moreau, J.J. - 1979, Lois d'elasticite en grande deformations; Sem.d'analyse convexe, Montpellier, No.12, 1-55.

Iacob Borş[1] and
Pavel Alexa[1]

ELASTICA OF A BEAM TAKING INTO ACCOUNT THE AXIAL AND SHEAR EFFECTS

INTERNATIONAL COLLOQUIUM
STABILITY OF STEEL STRUCTURES
BUDAPEST, HUNGARY, 1990
PRELIMINARY REPORT

Summary: The paper presents an original and efficient way of establishing the differential equation of a compressed straight beam in bending taking into account the shear effects. The equilibrium equations of an element of length dx in the deformed configuration to accounting for the axial effect are written. The component u_M of the transverse displacement u is then related to the bending moment via the usual curvature - bending moment constitutive relationship. A new component u_T of the transverse displacement due to shear effect is then introduced and related to the shear force via the constitutive relation. The total transverse displacement is the sum of the above two components. The differential equilibrium equation obtained is then integrated and the solution u(x) is used in two different ways: if the applied loads are end displacements and rotations of unit value, the stiffness coefficients are obtained and the beam stiffness matrix is ready for the wellknown stability analysis; if the applied loads on the beam are external forces, the end bending moments and shear forces obtained are ready to be used in second order analysis.

With the development of high capability computers the necessity of considering axial and shear effects on a beam in bending has to be dealt with from both, the point of view of solving the problem and establishing a criterion as to wether or not these effects should be accounted for in a given case.

---

(1) The Polytechnic Institute Cluj-Napoca, Romania

The paper is intended to present a way of dealing with shear effects in stability and second order analysis of skeletal structures. The first step is therefore the elastica of a compressed straight beam in bending accounting for shear effects. The next step would be the deriving of beam stiffness matrix using the differential equations of the deformed beam previously obtained (Borş,I., Alexa, P., 1986). The classic stability analysis may then be performed. If a second order analysis is required, the end bending moments and shear forces of the beam induced by external loads may also be computed using the above differential equation of equilibrium.

The differential equilibrium equation is obtained considering an infinitesimal element of the beam in the deformed state (Fig. 1).

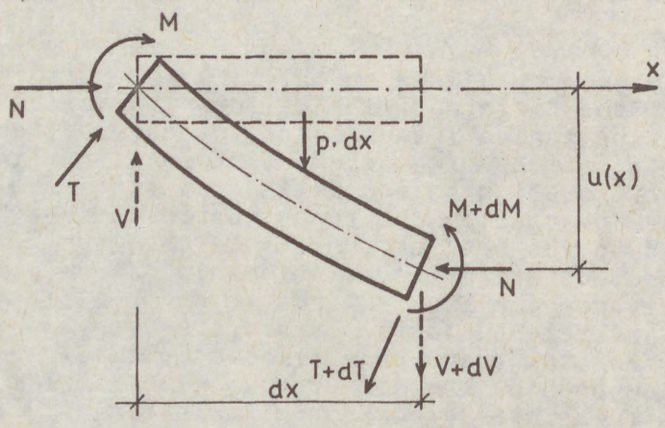

Fig. 1.

If x is the axis along the beam and u(x) is the transverse displacement under the applied loads p(x), the 3 equilibrium equations take, eventualy, the form

$$\frac{dV}{dx} = -p$$

$$\frac{dM}{dx} = T \qquad (1)$$

$$T = V + N\frac{du}{dx}$$

where M, T, N are the stress resultants of the deformed element and V is the shear force of the undeformed element. After some transforms equations (1) are equivalent with

$$\frac{d^2M}{dx^2} = -p + N\frac{d^2u}{dx^2} \qquad (2)$$

If $u_M(x)$ is the transverse displacement due to bending moment M only, the elastic constitutive relations assuming a linear elastic behaviour is

$$\frac{d^2u_M(x)}{dx^2} = -\frac{M}{EI} \qquad (3)$$

where E is the Young modulus and I is the second moment of inertia of the cross section.

The shear force T induces an average shear deformation

$$\gamma_m = \frac{kT}{GA} \qquad (4)$$

where k depends on the cross section shape, A is the cross section area and G is the shear elastic modulus.

If $u_T(x)$ is the transverse displacement due to shear force T only, the same shear deformation γ_m is

$$\gamma_m = \frac{du_T(x)}{dx} \qquad (5)$$

From (4) and (5), it yields

$$\frac{du_T(x)}{dx} = \frac{T}{GA'} \qquad (6)$$

where

$$A' = \frac{A}{k} .$$

The first and third equilibrium equations of (1) are equivalent to

$$\frac{dT}{dx} = -p + N\frac{d^2u}{dx^2}$$

and taking the first derivative in (6) one gets

$$\frac{d^2u_T(x)}{dx^2} = -\frac{p}{GA'} + \frac{N}{GA'} \cdot \frac{d^2u(x)}{dx^2} \qquad (7)$$

The total transverse displacement is

$u(x) = u_M(x) + u_T(x)$, i.e.

$$\frac{d^2u}{dx^2} = -\frac{M}{EI} - \frac{1}{GA'} p + \frac{N}{GA'} \cdot \frac{d^2u}{dx^2}$$

Using (2) and after two further derivation of the above relation the following form is obtained

$$\frac{d^4u(x)}{dx^4} + \frac{N}{EI(1 - N\gamma)} \cdot \frac{d^2u}{dx^2} = \frac{p}{EI(1 - N\gamma)} - \frac{\gamma}{1 - N\gamma} \cdot \frac{d^2p}{dx^2}$$

where $\gamma = \frac{1}{GA'}$ is the shear deformation due to T = 1.

Puting

$$n^2 = \frac{N}{EI} \; ; \qquad n_1^2 = \frac{n^2}{1 - N\gamma}$$

$$EI_1 = EI(1 - N\gamma); \qquad \gamma_1 = \frac{\gamma}{1 - N\gamma}$$

the above equation reads

$$\frac{d^4u(x)}{dx^4} + n_1^2 \frac{d^2u(x)}{dx^2} = \frac{p}{EI_1} - \gamma_1 \frac{d^2p}{dx^2} \qquad (8)$$

which is the equilibrium differential equation of the compressed beam in bending accounting for shear force.

Through the integration of (8) and using the end conditions, all the parameters related to the compressed beam behaviour in second order analysis allowing for shear effects could be computed.

For instance, if the load p is taken as some certain types of point-action (point rotations or point displacements), the stiffness coefficients of the beam are obtained. For the fixed end x = 0 the end conditions requiered by the solution of differential equation (8) are

$$x = 0; \qquad y_o = 0; \qquad y_o' = T_o \cdot \gamma \qquad (9)$$

which, after succesive transformations, lead to

$$x = 0; \quad y_o = 0; \quad (1 - \gamma N)y_o' = -EI\,\gamma y_o''' \qquad (10)$$

For the hinged end x = 0 the end conditions read

$$x = 0; \quad y_o = 0; \quad M_o = 0 \qquad (11)$$

that, through simple substitution become

$$x = 0; \quad y_o = 0; \quad y_o'' = -p\,\gamma_1 \qquad (12)$$

The equations (10) and (12) are used to compute the integration constants of the solution u(x) of the equation (8). Having u(x) and using (7) the stress resultants M(x) and T(x) = = dM/dx are computed. If the load p is unit end point displacement or rotation, the above stress resultants at the ends x = 0 and x = l are in fact the stiffness coefficients and, therefore, the stiffness matrix is obtained. The beam stability and structural stability analyses may then be performed in the usual way (Alexa P., - 1976).

In the second order analysis is to be performed, the load p is taken as the usual external loads. By integrating (8) and using the specific end conditions, the stress resultants M and T at the beam ends are obtained which,in turn, are - in the general displacement method equations - the right hand side terms. The static second order analysis allowing for shear effects is then ready formulated.

BIBLIOGRAPHY

Borş I. and Alexa P., 1986 - The Stability Analysis of Straight Bar Using Dirac's Distribution and Laplace Transform. Stability of Steel Structures. Vols.1-2, Akadémiai Kiadó, Budapest, Edited by M.Iványi, pp.483-489

Alexa P., 1976 - Geometrically Nonlinear Elasto-Plastic Analysis of Planar Frames by Mathematical Programming. Ph.D. Thesis, University of London.

(1)
BROŽ, Petr (1)

ON THE BUCKLING OF PLATE STRUCTURES

INTERNATIONAL COLLOQUIUM
STABILITY OF STEEL STRUCTURES
BUDAPEST, HUNGARY, 1990
PRELIMINARY REPORT

Summary: Well-known advantages of the Boundary Element Method have been proved in case of the submitted formulation for the nonlinear bending of plate problems, even in comparison with other sorts of problems; the shape functions for approximation present themselves rather complicated. That analysis serves as the preparatory phase for stability problems. The convergency of the given iteration procedure is connected with the solvability of the problem. It is qualified by the fulfilment of the condition of necessity that the transverse loading has to be bounded.
Further, a variant of BEM is sketched for the buckling problem of plate structures. This approach has proved competent being an effectual before. The introduced method is not limited by the number of plate components of the assembled structure.

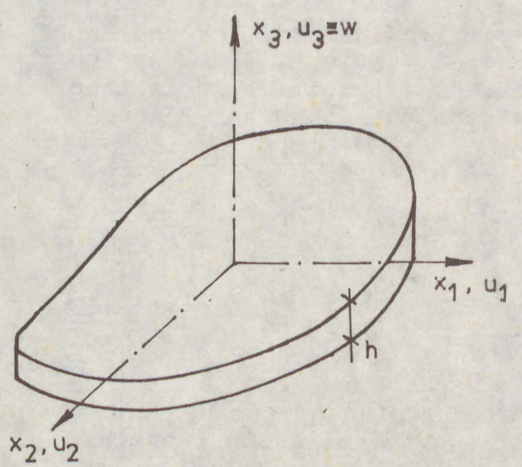

Fig. 1

Direct stresses applying in the middle plane of the thin-walled structure are considered throughout the finite deformation theory, they have an effect upon the deflection function. It is a case of the nonlinear formulation, for there are quadratic terms included in the starting equations.
First, basic relations of the mentioned theory will be derived. Let a plate in the three-dimensional space $Ox_1x_2x_3$ be given and its middle plane lies in Ox_1x_2, see Fig.1; u_1 and u_2 represent the displacement components in the middle plane,

(1) Senior Scientific Worker, Building Research Institute, Technical University of Prague

(2)
w is the transverse deflection and $\ell_1 = \varepsilon_{kk}$, $\ell_2 = \varepsilon_{11}\varepsilon_{22} - \varepsilon_{12}^2$. In case of the finite deformations, the energy functional of the principle of the minimum total potential energy (Lagrange) has the form:

$$\text{(1)} \qquad \Pi = \frac{D}{2}\int_\Omega \{(\Delta w)^2 + \frac{12}{h^2}\,\ell_1^2 - 2(1-\nu)\left[\frac{12}{h^2}\,\ell_2 + w_{,11}\,w_{,22} - w_{,12}^2\right]\}\,d\Omega - \int_\Omega p w\,d\Omega\,,$$

where we have denoted by D the flexural rigidity of the plate, h the plate thickness and Ω a region in Ox_1x_2 defining non-deformed state of the plate. After variating Eq. (1) with regard to both the deflection and the displacements we obtain the following system of equations:

$$\text{(2)} \qquad D\Delta^2 w = N_{ij}\,w_{,ij} + p = A(N,w) + p$$

$$\text{(3)} \qquad \Delta u_i + C\ell_{,i} = -C\,w_{,j}\,w_{,ij} - w_{,i}\,w_{,kk} = B_i(w), \quad i,j,k = 1,2,$$

where $C = \frac{1+\nu}{1-\nu}$, $\ell = u_{k,k}$.
Only the function p is dependent on the external loads - it describes the transverse forces acting on the plate. The system (2) and (3) has been formulated for three unknown functions of the deflection and displacements. The alternative procedure stems from the so called Airy´s function F defined in the manner:

$$N_{11} = \frac{\partial^2 F}{\partial x_2^2}\,, \quad N_{22} = \frac{\partial^2 F}{\partial x_1^2}\,, \quad N_{12} = -\frac{\partial^2 F}{\partial x_1\,\partial x_2}$$

Thus, in the system (3) being simplified in form, for the unknown F only one equation arises. Similarly, in Eq. (2) the right-hand side is converted. Instead (2) and (3) it is then possible to solve the following system for unknowns w and F:

$$\text{(4)} \qquad \begin{aligned} D\Delta^2 w &= [F, w] + p \\ \Delta^2 F &= -Eh\,[w, w] \end{aligned}$$

where $[a,b] = a_{,11}\,b_{,22} + a_{,22}\,b_{,11} - 2\,a_{,12}\,b_{,12}$

However, the integral form of the foregoing system has not proved suitable on a user´s behalf in view of known troubles with boundary conditions for F.
We will deal with solving of the system (2) and (3), the standard boundary conditions being determined at every point of the boundary P of the region Ω, viz. just one quantity

(3)
from those mentioned below in following brackets is prescribed along disjoint parts of the boundary Γ :

$$(5) \quad (w,\ V_n w);\ \left(\frac{\partial w}{\partial n},\ M_n w\right),\ (u_1,\ N_{11}),\ (u_2,\ N_{22}).$$

Let us modify the Eq. (2) into the integral form. After substituting for the function $w^* = \frac{1}{8\pi D} r^2 \ln r$, we get a system of two equations for the course of both w and its derivative as follows:

$$c(x)\, w(x) = \int_\Gamma \left[V_n w\, w^* - M_n w \frac{\partial w^*}{\partial n} + \frac{\partial w}{\partial n} M_n w^* - w V_n w^* \right] d\Gamma + \int A(N,w)\, w^*\, d\Omega + \int_\Omega p w^*\, d\Omega ,$$

$$(6) \quad c_1(x)\, w_{,1}(x) + c_2(x)\, w_{,2}(x) = \int_\Gamma \left\{ V_n w_1^* [w(x) - w(\xi)] + M w_1^* \frac{\partial w}{\partial n} - \frac{\partial w_1^*}{\partial n} M_n w + w_1^* V_n w \right\} d\Gamma + \int_\Omega A(N,w)\, w_1^*\, d\Omega + \int_\Omega p w_1^*\, d\Omega .$$

It holds about terms embracing $V_n w$ that in case of the free boundary considering that what is meant are zero tractions, the coincidence with the effective shear force is found. Then the integral representation is correct.
Now, let us attend to an integral formulation of Eqs. (3). There are familiar terms on the right-hand side governing the well-known problem of the two-dimensional theory of elasticity. The right-hand side represents a loading vector analogously to the body forces. After applying a standard line we obtain:

$$(7) \quad c(x)\, u_i(x) = \int_\Gamma u_{ji}^*\, t_j\, d\Gamma - \int_\Gamma q_{ji}^*\, u_j\, d\Gamma + \int_\Omega u_{ji}^*\, B_j(w)\, d\Omega , \qquad i,j = 1,2 ,$$

where the following source functions have been introduced:

(4)

$$u^*_{ij} = C_1 [C_2 \delta_{ij} \ell n r - \frac{\bar{x}_i \bar{x}_j}{r^2}] ,$$

$$q^*_{ij} = \frac{C_3}{r^2} [C_4 (n_j \bar{x}_i - n_i \bar{x}_j) + (C_4 \delta_{ij} + 2 \frac{\bar{x}_i \bar{x}_j}{r^2}) \bar{x}_k n_k] ,$$

$$\bar{x}_i = x_i - \xi_i , \quad r^2 = \bar{x}_k \bar{x}_k , \quad C_1 = - \frac{1+\nu}{8\pi} , \quad C_2 = 3 - \nu ,$$

$$C_3 = - \frac{1+\nu}{4\pi} , \quad C_4 = \frac{1-\nu}{1+\nu} = \frac{1}{C}$$

In Eqs. (7) we have denoted $t_j = N_{nj}$.
Let us now return to Eqs. (2) and (3). We express them in the incremental form for both sought-after functions and those induced by them. In so doing, the incremental quantities are denoted by dots. Let us assume, generally, a load-increment $\dot{p}$ to be nonzero. If p stands for a static loading, then the term with $\dot{p}$ disappears in the following relations. It is further possible to express the incremental form of Eqs. (2) and (3) in the manner:

(8) $$D \Delta^2 \dot{w} = A(\dot{N}, w) + A(N, \dot{w}) + \dot{p}$$

(9) $$\Delta u_i + C \dot{e}_{,i} = B_i (\dot{w})$$

The integral implication of (8) is similar to (6) for which it holds, viz.

$$c(x)\, \dot{w}(x) = \int_\Gamma [V_n \dot{w} w^* - M \frac{\partial w^*}{\partial n} + \frac{\partial \dot{w}}{\partial n} M^*_n +$$

$$+ \int_\Omega [A(\dot{N}, w) + A(N, \dot{w}) + p] \dot{w} \, d\Omega ,$$

(10)

$$c_1(x)\, \dot{w}_{,1}(x) + c_2(x)\, \dot{w}_{,2}(x) = \int_\Gamma \{ V_n w^* [\dot{w}(x) -$$

$$- \dot{w}(\xi)] + M_n w_1^* \frac{\partial \dot{w}}{\partial n} - \frac{\partial w_1^*}{\partial n} M_n \dot{w} + w_1^* V_n \dot{w} \} \, d\Gamma +$$

$$+ \int_\Omega [A(\dot{N}, w) + A(N, \dot{w}) + \dot{p}] w_1^* \, d\Omega .$$

(5)
The expression for (9) corresponds to (7) in the form:

$$c(x)\,\dot{u}_i(x) = \int_\Gamma \left[u^*_{ji}\, t_j - q^*_{ji}\, u_j \right] d\Gamma + \tag{11}$$

$$+ \int_\Omega w^*_{ji}\, B_j(\dot{w})\, d\Omega \qquad i,j = 1,2 .$$

Let us now approximate both the region boundary and a course of the functions u_1, u_2, w and $\frac{\partial w}{\partial n}$ just as $\dot{u}_1$, $\dot{u}_2$, $\dot{w}$ and $\frac{\partial \dot{w}}{\partial n}$ on the boundary and the functions $A(N,w)$, $A(N,w)$, $A(N,\dot{w})$, $B(w)$ and $B(\dot{w})$ in the region Ω. We choose polynomial approximations for both the deflection and its normal derivative, the linear interpolation on Γ appurtenant to the displacements. At a glance only, this approximation scheme seems to be complicated. The same kind of the approximations is selected for bending components and their increments and a routine problem of the thin plate is the point. Analogously, for membrane components we get to solve a web. It is also possible to simplify the calculation of surface integrals, approximations of the integrands being chosen with regard to the computer time minimization. At the same time only two sorts of the matrices will do and both the high effectiveness of algorithm and the solution exactness being kept.
The discrete form (6) and (7) may be rewritten as follows:

$$H^k u^k = G^k Q^k + B^k \quad ; \quad k = 1,2 \tag{12}$$

where

$$u^1 = \left\{ w^1, \frac{\partial w^1}{\partial n}, w^2, \dots, \frac{\partial w^S}{\partial n} \right\}^T, \quad u^2 = \left\{ u_1^1, u_2^1, u_1^2, \dots u_2^S \right\}^T$$

$$G^1 = \left\{ V_n w^1, M w^1, V_n w^2, \dots, M w^S \right\}^T, \quad G^2 = \left\{ t_1^1, t_2^1, t_1^2, \dots t_2^S \right\}^T$$

and S - number of boundary elements, the upper index of vector components denotes the node number of the boundary division. The surface integral contribution is expressed by the vector B^1 in (6) and similarly the vector B^2 is pertaining to (7).
Discretizating Eqs. (10) and (11) we get systems looking like (12)

$$H^k \dot{u}^k = G^k \dot{Q}^k + \dot{B}^k \quad ; \quad k = 1,2, \tag{13}$$

where

$$\dot{u}^1 = \left\{ \dot{w}^1, \frac{\partial \dot{w}^1}{\partial n}, \dot{w}^2, \dots \frac{\partial \dot{w}^S}{\partial n} \right\}^T, \quad \dot{u}^2 = \left\{ \dot{u}_1^1, \dot{u}_2^1, \dot{u}_1^2 \dots, \dot{u}_2^S \right\}^T$$

$$\dot{G}^1 = \left\{ V_n \dot{w}^1, M\dot{w}^1, V_n \dot{w}^2, \dots M\dot{w}^S \right\}^T, \quad \dot{G}^2 = \left\{ t_1^{\cdot 1}, t_2^{\cdot 1}, t_1^{\cdot 2}, \dots t_2^{\cdot S} \right\}^T,$$

$\dot{B}^1$, $\dot{B}^2$ represent vectors involving the surface integral influence in (10), (11), respectively.
Next, we can implement the numerical proceeding in the way:
1. After discretizating the boundary into elements as soon as matrices H^k and G^k being determined, we store them either in

(6)

the internal storage or in the data medium.

2. Performing the discretization of the region Ω into cells and approximating both the derivatives of the function w and the functions W_{ij} we calculate the vector B^2. If it is not possible to form a well-grounded estimate of the above functions, put B^2 equal to the zero vector.

3. After introducing the boundary conditions generally inhomogeneous into (12), the unknown vector components u^k as the case may be Q^k are being solved.

4. From the subdivision of the region Ω according to step 2. and by means of both the function values in the region derived in terms of step 3. and Eqs. (10) on condition $c(x) = c_i(x) = 1$, $i = 1, 2$, the vector B^1 may be specified.

5. Solve Eqs. (13) for $k = 1$, substitute $u^1 := u^1 + \dot{u}^1$, $Q^1 := Q^1 + \dot{Q}^1$ and the homogeneous boundary conditions being under consideration.

6. Calculate the vector $\dot{B}^2$ by means of the discretization conforming with step 2. and from both the function values in the region (step 5.) and Eqs. (11) for $c(x) = 1$.

7. After solving Eqs. (13) for $k = 2$ and putting $u^2 := u^2 + \dot{u}^2$, $Q^2 := Q^2 + \dot{Q}^2$ the homogeneous boundary conditions being introduced (possibly to make inhomogeneous conditions homogeneous ones).

8. Determine the vector B^1 for one thing by the discretization of the region Ω according to step 2., for another from the region function values in step 7. derived and Eqs. (10) with $c(x) = c_i(x) = 1$, $i = 1, 2$.

9. Test a criterion of convergency. If it is not fulfilled, we are under the necessity of iterating steps 5. - 8. It is possible to take out the following condition being a criterion

$$\max_{x \in \Omega} |\dot{u}_i(x)| < \varepsilon \quad , \quad i = 1, 2 \; ,$$

where ε is a positive number chosen.

In the case of the buckling problem, it is necessary to consider a combined action of in-plane and out-of-plane deformation. The biharmonic differential operator and also second-order partial differential operators are involved in the governing differential equation of the problem.

The integral equation formulation for the linear buckling problem of a single plate, according to /1/, by M.TANAKA, 1986, is discussed, using the biharmonic fundamental solution for the plate bending problem. The boundary element method is applied to the numerical solution of the set of integral equations. The total system of simultaneous equations is derived for nodal unknowns included in the whole region. These equations are then reduced to an algebraic system of eigenvalue equations by taking account of the prescribed boundary conditions.

When generalizing the method to the elastic buckling of assembled plate structures, emphasis is layed on the rigorous numerical of both the compatibility and equilibrium equations along the joint edges of plate parts. One example is demonstrated, namely the buckling problem of the structure consisting of two equal rectangular plates jointed at the right angle along one edge (see Fig.2). The upper and bottom boundaries of the structure are simply supported, the other sides being free. The aspect ratios are supposed $\frac{b}{a} = 0.5$ and $\frac{a}{h} = 240$ and a subdivision of the plate is shown in Fig. 3.

Results are given for the critical in-plane load N_{cr} in Table 1

(7)
including the comparison with the solution performed by S.P.Timoshenko.

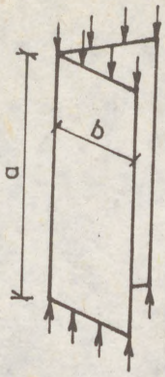

Fig. 2

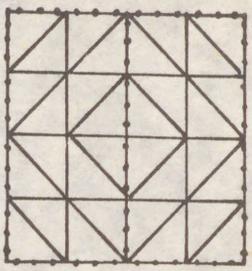

Fig. 3

Table 1

	$\frac{N_{cr}\, b^2}{\pi^2 D}$	
	BEM	Timoshenko´s solution
Assembled Plate Structure	0.67	0.7
Thin Plate	0.68	0.7

Reference

/1/ Tanaka, M. 1986, Elastic Buckling Analysis of Assembled Plate Structures by Boundary Element Method, Boundary Elements VIII Conference, ed. by C.A.Brebbia, Springer-Verlag, Berlin-New York-Tokyo, V1, pp. 547-59.

(1)

CLE
NIC
RAI

INT

SUM
to
kli
a m
or

asy
del
chi

sho
mod
1.

sel
obv
deg
(sp
the
ela
nal
str
may
so
F.E

tri

---

(1)
(2)

(1)

CLEMENTE, Paolo (1)
NICOLOSI, Giulio (2)
RAITHEL, Aldo (2)

INTRINSIC PROPERTIES OF RIGID-ELASTIC MODELS

INTERNATIONAL COLLOQUIUM
STABILITY OF STEEL STRUCTURES
BUDAPEST, HUNGARY, 1990
PRELIMINARY REPORT

SUMMARY : For a lot of years rigid-elastic models have been largely used to illustrate structural behaviour in problems regarding stability : buckling and limit loads. With particular reference to buckling loads in such a manner two types of bifurcation have been specified : symmetric (stable or unstable), asymmetric (stable-unstable).

Having these critical load been found, respectively, in symmetric and asymmetric structures it may appear that these intrinsic properties of models (symmetry or asymmetry) are strictly correleted to the type of branching they may exhibit.

At present, exemplifying the behaviour of a funicular arch, it is shown that this correlation is not always correct so that in a symmetrical model buckling loads of both types are possible.

1. INTRODUCTION

Rigid-elastic models are built-up with rigid bars linked among themselves, or to fixed space, by means of perfect restraints (fixed joint are obviously excluded) so that the system has n degrees of freedom. These degrees of freedom are balanced by an equal number of elastic elements (springs) connecting the rigid bars among themselves or to fixed space ; in the first event the ensemble of an internal restraint and of the relating elastic element is called elastic cell [1], in the second event an external elastic restraint is introduced. Because in such a way all types of strain may be simulated (flexural, axial ...) whichever elastic structure may be modelled with accuracy growing up with the number of elastic cells so that a structural analysis, C.E.M. [2], parallel or replaceable to F.E.M., is possible.

With reference to simple models of this kind branching points, symmetric and asymmetric, are usually explained through load-displacement dia-

---

(1) Student of Doctorate, Naples University
(2) Professor of Structural Engineering, Naples University

(2)

grams ; particularly, when the model exhibits more than one degree of free dom, the arbitrariness in the choise of the displacement (often just a lagrangian) considered in the diagram does not permit to have a clear idea about the problem. Later on, to avoid this difficulty, the behaviour of whichever model will be always shown in the diagram generalized load, F, generalized displacement, f ; this diagram is particularly significant as the product F f expresses the total work of external load proceeding from the initial configuration, Co, to the actual equilibrium configuration, C. This diagram has been suggested by Zanaboni [3] since 1961 and recently largely utilized, [4], because of its energetical meaning ; on it, as a matter of fact, point placed on a descendent path of the curve represent unstable configuration, points placed on an ascendent path represent stable configuration. When pre-critical deformation is neglected, various occurrences are represented as follows :

- 1. Symmetric buckling load

The secondary path is described by a curve starting from the point $F=F_c$, $f=0$ with horizontal tangent $(dF/df=0)$; it develops with crescent

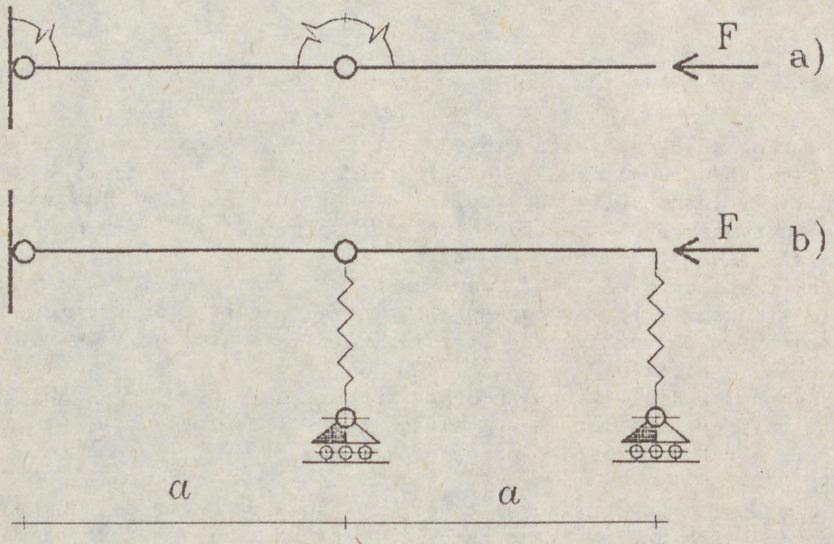

Fig. 1

derivative (stable behaviour) or with decrescent derivative (unstable behaviour). Following tables, relating to models of figures 1a and 1b, illustrate respectively the two previous behaviours.

a)	F=Fa/K	f=f/a	b)	F=F/Ka	f=f/a
	0.3820	0.0000		0.3820	0.0000
	0.3833	0.0180		0.3778	0.0181
	0.3875	0.0716		0.3649	0.0736
	0.3945	0.1592		0.3419	0.1703

(3)

- 2. Asymmetric buckling load

The caracteristic curve is described by two paths starting at the point F=Fc, f=0 with vertical tangent (dF/df=∞). The upper path is stable and cannot be followed by natural deformation of the structures which, on the contrary, is represented by lower path. Referring to the model in

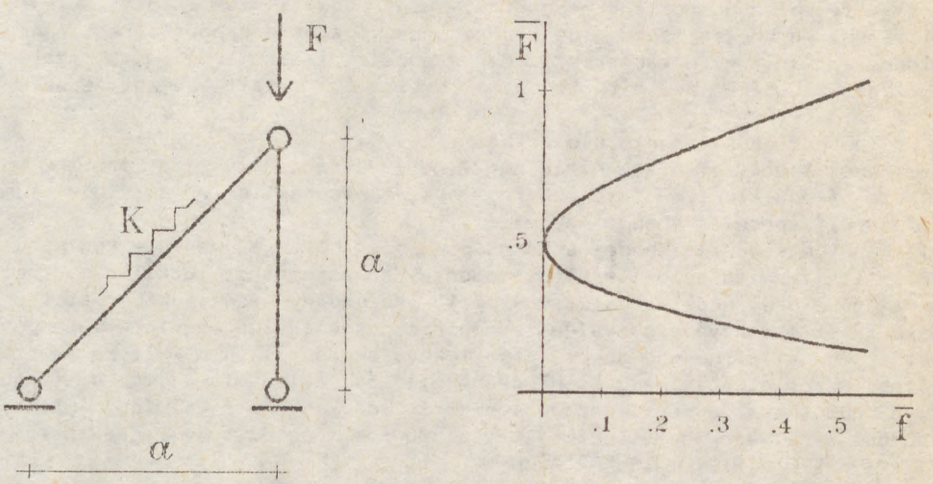

Fig. 2

figure 2 some points belonging to previous paths are indicated in the following table :

stable path		unstable path	
F=F/Ka	f=f/a	F=F/Ka	f=f/a
0.5000	0.0000	0.5000	0.0000
0.5065	0.0001	0.4934	0.0001
0.5198	0.0014	0.4805	0.0014
0.5332	0.0038	0.4677	0.0038
0.5675	0.0152	0.4363	0.0152

with the specification that the second path (unstable) is related to a clockwise rotation of the vertical bar.

2. CLASSIFICATION OF MODELS

The previous examples, referred to symmetric and asymmetric models, appear to support the assumption that the same denomination (symmetric and asymmetric) may be used as regards the type of the model and relating buckling load.

Because of the fact that the following example (a funicular symmetric arch) shows that it is possible to obtain post-critical behaviours of both types for distinct eigenvalues, it is necessary a more diligent investigation of the correlation between the structural types and the buckling loads.

The models shown in figure 1, and similar ones, (and symmetry is non really strictly necessary) exhibit two secondary equilibrium states which are one the mirror-image of the other. Therefore both states have the same

shape and the same value of potential energy. The two corresponding secondary paths, in the diagram F-f (characteristic curve) coincide because of the fact that f does not depend on the sign of the displacement.

The foregoing event is not verified in the example of figure 2 (and generally for asymmetric models) ; the change of the sign of the displacements, to which do not correspond specular equilibrium states, involves different energetic terms. The two secondary paths are therefore non coincident and in the characteristic curve appear distinct but with the same initial value (F_c) and with the same initial (vertical) tangent as said before.

The previous remarks clear that :

a) the existence of a symmetric buckling is essentially tied to the existence of equilibrium states having the same energetic terms ; this surely happens if specular shapes may exist.

b) when the specular shapes are not possible, but are possible two equilibrium states with opposite displacements, an asymmetric buckling may occur.

Structural models that may exhibit secondary equilibrium states of both types may have eigenvalues symmetric (usually the even ones) and asymmetric (usually the odd ones) ; the lowest among all them will be the buckling (or critical) load. Such models will be called mixed to distinguish them from those currently named symmetric and asymmetric, for which the confusion between the structural type and the type of buckling exists.

3. THE SYMMETRIC FUNICULAR ARCH

Among the mixed models the symmetric funicular arch is surely present. Both behaviours are thinkable for it :

a) equilibrium states developing from critical status (bifurcation with even eigenvectors) with skew-symmetric shapes. Because each of such equilibrium states grants the existence of its mirror-image (specular one) we have symmetric buckling.

b) equilibrium state developing from critical status (bifurcation with odd eigenvectors) with symmetry shapes. Since in this case specular equilibrium states are not possible buckling load is asymmetric.

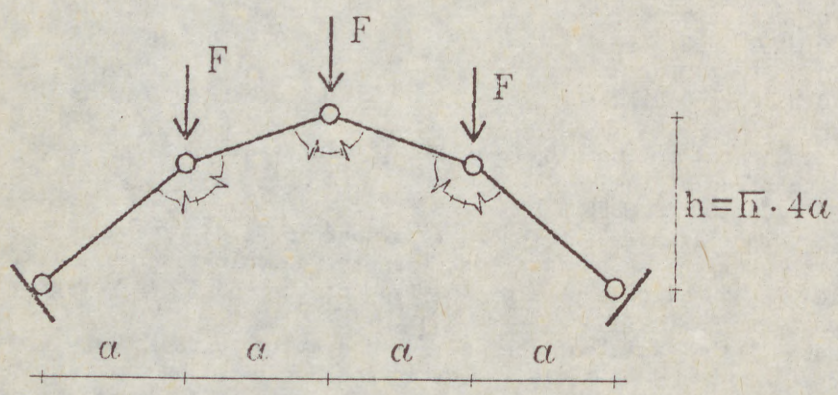

Fig. 3

With reference to the arch of figure 3 (in the assumption of constant

(5)

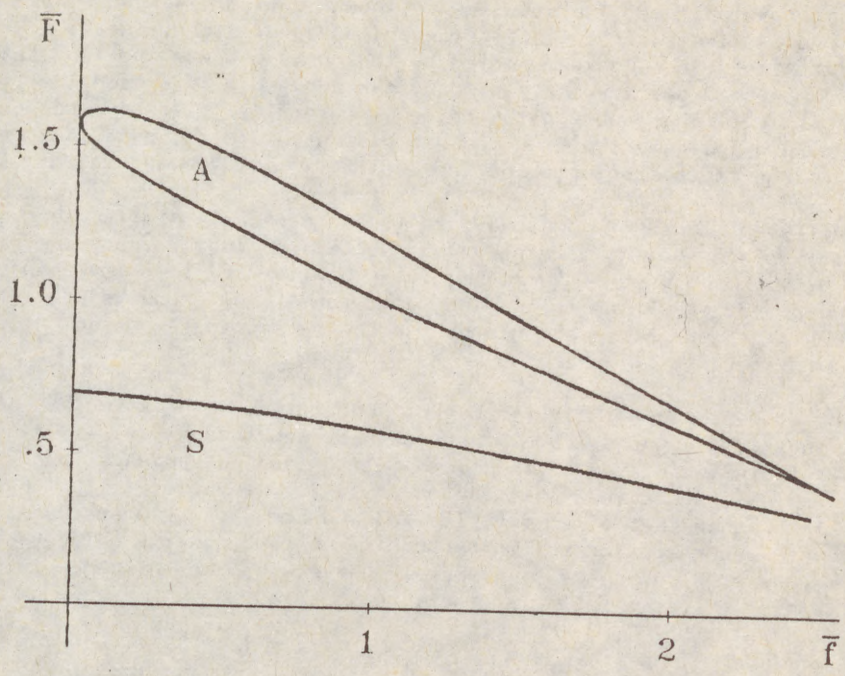

Fig.4

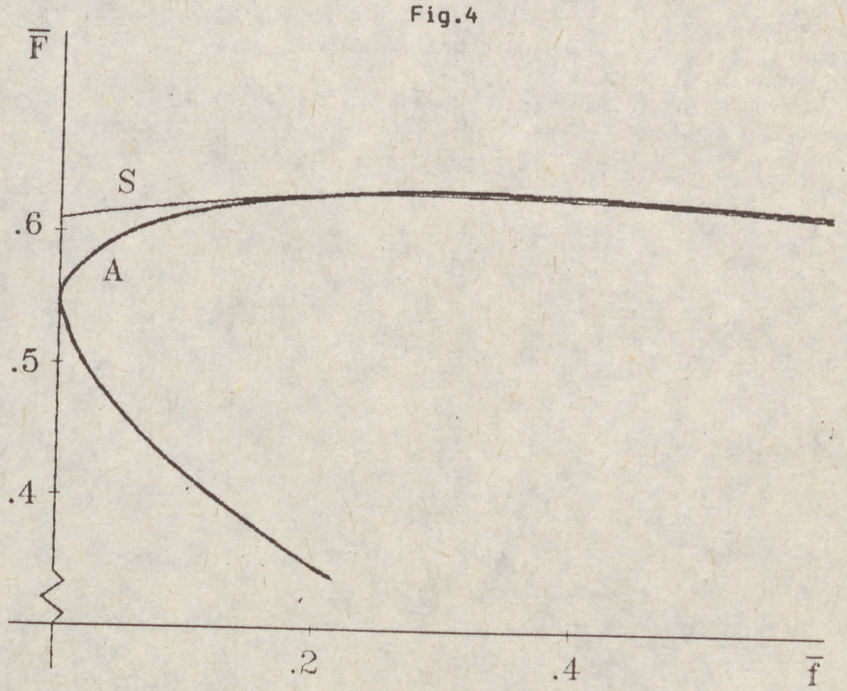

Fig. 5

(6)

cross-section and for h=0.3) an energetic analysis has been carried out with numeric developments. The results are shown in figure 4 where the curves start, respectively, from the first even, and odd, eigenvalue.

The first behaviour is represented by the curve S where the two paths coincide. The second one is represented by the curve A ; this time the two paths are distinct. The lowest path, which is naturally followed, conforms with an upward displacement of the crown of the arch and is unstable ; the other (starting stable) conforms, on the contrary, with the sagging at the crown.

For different types of arch the results are generally similar to those before analyzed and the lowest eigenvalue (buckling load) is symmetric-unstable. Only in the case of three-hinged arch with very low rise/span ratio the first odd eigenvalue is the most dangerous. The results obtained for the arch of figure 3, in absence of the central spring and for h=0.20 are shown in figure 5.

4. REMARK

In the present paper the influence of precritical deformation has been neglected that is, in the example, the arch has been thought axially rigid. If such hypotesis is removed asymmetric buckling load disappears and the buckling problem changes in a limit point one [4]. The value of limit load is always lower than that of asymmetric load and tends to it when the stiffness becomes larger and larger. On the contrary the quality of problem does not change with reference to symmetric buckling ; the influence is only quantitative and, as a matter of fact, negligible.

REFERENCES

[1] V.Franciosi, Il metodo delle celle ..., Giannini, Napoli 1988

[2] V.Franciosi,L.Adriani, Il metodo delle celle ..., La Sapienza,Roma 1988

[3] O.Zanaboni, Premesse allo studio della stabilita' ..., Giornale del Genio Civile, Roma 1961

[4] A.Raithel,N.Augenti,G.Nicolosi, Equilibrio e Stabilita' delle Strutture Elastiche, Cremonese, Roma 1989

(1)
GIZEJOWSKI, M.A. (1)
PARAMESWAR, H.C. (2)

A CONSISTENT NONLINEAR THEORY FOR THIN-WALLED MEMBERS OF OPEN CROSS-SECTION

INTERNATIONAL COLLOQUIUM
STABILITY OF STEEL STRUCTURES
BUDAPEST, HUNGARY, 1990
PRELIMINARY REPORT

Summary: A nonclassical model for the analysis of thin-walled members is presented. Starting from the equations of continuum mechanics, these are reduced to a form valid for one-dimensional problem in order to demonstrate effectively the displacement field for the Green-Lagrange strain tensor components. The approach presented here is of general nature, enabling its application to digital computers through incremental FEM formulation.

1. INTRODUCTION

In classical engineering theory of linear thin-walled members of open cross-sections, extended also to the range of nonlinear behaviour the following three basic assumptions are made,[2].

(1) The cross-section is treated as perfectly rigid in its plane (1st Vlasov hypothesis).

(2) The cross-section is free to warp out of its plane. As a result the shear strain in the middle surface may be neglected as it exists in the case of a uniform St.Venant's torsion (2nd Vlasov hypothesis).

(3) Normals to the middle surface of the member remain normal to it and undergo no change in length during deformation (the Kirchoff-Love hypothesis).

---

(1) Senior Lecturer of Civil Engineering, Univ. of Zimbabwe
(2) Senior Lecturer of Civil Engineering, Univ. of Zimbabwe

(2)

The approach on the basis of above assumptions using linear shear strain is usually referred to as Vlasov's theory and allows the displacement field to be determined in the form normally associated with one-dimensional problem of thin-walled open cross-section,[3,6]. The standard displacement matrix in such problems is of the form;

$$\begin{bmatrix} u_1 \\ u_2 \\ u_3 \end{bmatrix} = \begin{bmatrix} 1 & 0 & 0 & 0 & -(x_2-x_{2R}) & 0 & 0 \\ 0 & 0 & 1 & 0 & (x_1-x_{1R}) & 0 & 0 \\ 0 & -x_1 & 0 & -x_2 & 0 & w_R & 1 \end{bmatrix} \begin{bmatrix} u_{1R} \\ u'_{1R} \\ u_{2R} \\ u'_{2R} \\ \theta_3 \\ \theta'_3 \\ u_{30} \end{bmatrix} \qquad (1)$$

or simply as; $\mathbf{u} = \mathbf{A}\, \mathbf{u}_p$ (2)

where, referring to Fig.1, u_i(i=1,2,3) are the displacements of a point M arbitrarily taken on the cross-section and measured along the x_i axes of local Cartesian coordinate system, u_{iR} (i=1,2) are the displacements in the x_i directions at the rotation point $R(x_{1R},x_{2R})$ which is taken arbitrarily on the cross-section, u_{30} is the displacement in the x_3 direction at the origin O(0,0) of the local coordinate system, θ_3 is the rotation of cross-section about x_3 axis and finally w_R is the sectorial coordinate with respect to R

$$w_R = \left(\int_0^{\bar{x}_1} \bar{x}_{2R}\, d\bar{x}_1 \right) - \bar{x}_{1R}\, \bar{x}_2 \ . \qquad (3)$$

Coordinates $\bar{x}_i$(i=1,2) in Eq.(3) are measured along the axes of the other Cartesian coordinate system having its origin at point K, which lies at the middle line of the member cross-section and $\bar{x}_{iR}$(i=1,2) are the distances between the points K and R in the directions of $\bar{x}_i$.

The linear displacement field given by Eq.(1) is used then for geometrically nonlinear analysis since strain-displacement relationships consider nonlinear terms yielding directly from the definition of the Green-Lagrange strain tensor components. More consistent approach requires nonlinear displacement field relationships to be derived and then included in the Green's strain components. Using the assumptions cited at the beginning, such relationships were derived by Nishino et al. [5], Alwis et al. [1], Roberts [6]

(3)
and Maciejewski et al. [4]. However to deal with more accurate model for nonlinear analysis of thin-walled members requires to weaken the assumptions used to create the Vlasov's theory.

The purpose of this paper is twofold. The first is to develop an accurate nonlinear displacement field relationships for analysis of thin-walled members of open cross-section based on more realistic assumptions. The second is to point out that the developed model, after some simplifications, may be compared with those given by other authors, so that the conclusions concerning the source of errors in the classical analysis can be displayed.

2. ASSUMPTIONS AND GENERAL RELATIONSHIP FOR DESPLACEMENT FIELD

Let us consider a cross-section of a straight thin-walled member of open cross-section as shown in Fig.1.

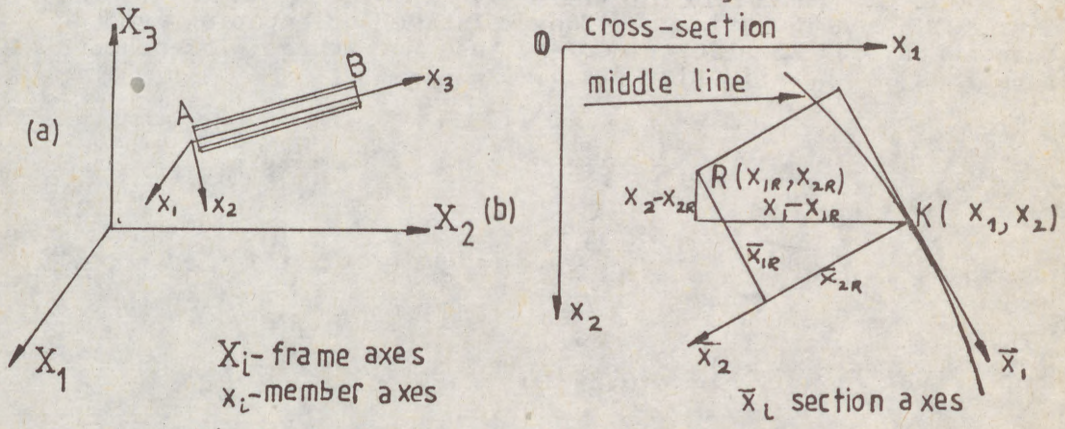

Fig.1 Cartesian coordinate systems

In order to determine the full description of the member geometry in the displaced configuration, two Cartesian coordinate systems are used, namely x_i and $\bar{x}_i$ (i=1,2,3). It is assumed here that the first Vlasov's hypothesis cited in Chap.1 will hold any longer while the other two are still valid. Thus the displacement vector can be extended for three components

$$\bar{u} = (\bar{u}_R - \bar{x}_R) + \bar{u}^{(1)} + \bar{u}^{(2)}, \qquad (4)$$

$$\bar{x}_R = < \bar{x}_{1R}, \bar{x}_{2R}, \bar{x}_{3R} >^T$$

where $\bar{u}$ is the vector of an arbitrary M point displacement field measured in coordinate system $\bar{x}_i$, $\bar{u}_R$ is the vector of the point R displacements due to rigid shifting along the $\bar{x}_i$ axes, $\bar{u}^{(1)}$ is the vector of the displacements due to rigid rotation about the $\bar{x}_i$ axes at the point R and finally $\bar{u}^{(2)}$ is the vector of displacements caused by warping effect. Because there is $x_3 \| \bar{x}_3$ between the coordinate systems x_i and $\bar{x}_i$, the axes x_1, x_2 are inclined to the $\bar{x}_1, \bar{x}_2$ with the angle α. Thus

(4)

$$\mathbf{u} = \mathbf{T}^T \bar{\mathbf{u}},$$

$$\bar{\mathbf{x}}_R = \mathbf{T} (\mathbf{x} - \mathbf{x}_R) \qquad (5)$$

where $\mathbf{T}$ is the transformation matrix in the plane of cross-section

$$\mathbf{T} = \begin{bmatrix} \mathbf{T}_{12} & \mathbf{0} \\ \mathbf{0}^T & 1 \end{bmatrix}, \qquad \mathbf{T}_{12} = \begin{bmatrix} c & s \\ -s & c \end{bmatrix} \qquad (6)$$

and $s=\sin\alpha$, $c=\cos\alpha$, $\alpha = \alpha(\bar{x}_1)$.

3. DISPLACEMENT VECTOR COMPONENT DUE TO RIGID ROTATION

To derive the displacement vector component due to the rigid rotation we consider the relative orientation between the $\bar{x}_i$ and $\bar{x}_i^{(3)}$ directions, where $\bar{x}_i^{(3)}$ are $\bar{x}_i$ axes in the displaced configuration. The relative orientation vector components can be described by use of three independent rotations as shown in Fig.2,[8].

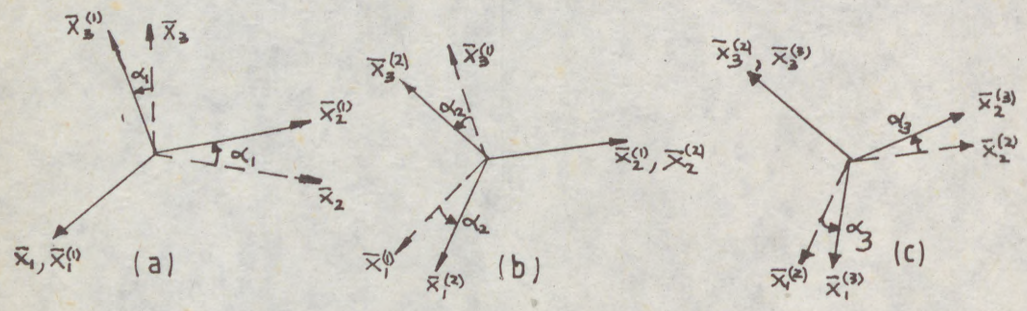

Fig.2 Relative orientation between coordinate axes before and after deformation

(1) Rotation α_1 about $\bar{x}_1$ axis for which the elementary rotation matrix is

$$\mathbf{T}_1 = \begin{bmatrix} 1 & 0 & 0 \\ 0 & c_1 & -s_1 \\ 0 & s_1 & c_1 \end{bmatrix} . \qquad (7)$$

(2) Rotation α_2 about $\bar{x}_2^{(1)}$ axis for which the elementary rotation matrix is

$$\mathbf{T}_2 = \begin{bmatrix} c_2 & 0 & s_2 \\ 0 & 1 & 0 \\ -s_2 & 0 & c_2 \end{bmatrix} . \qquad (8)$$

(5)
(3) Rotation α_3 about $\bar{x}_3^{(2)}$ axis for which the elementary rotation matrix is

$$T_3 = \begin{bmatrix} c_3 & -s_3 & 0 \\ s_3 & c_3 & 0 \\ 0 & 0 & 1 \end{bmatrix} . \qquad (9)$$

Considering the total rotation matrix as

$$T_R = \prod_{i=1}^{3} T_i \qquad (10)$$

we obtain

$$\bar{u}^{(1)} = T_R \, \bar{x}_R \qquad (11)$$

where

$$T_R = \begin{bmatrix} c_2 \, c_3 & -c_2 \, s_3 & s_2 \\ s_1 s_2 c_3 + c_1 s_3 & s_1 s_2 s_3 + c_1 c_3 & -s_1 c_2 \\ -c_1 s_2 c_3 + s_1 s_3 & c_1 s_2 s_3 + s_1 c_3 & c_1 c_2 \end{bmatrix} \qquad (12)$$

and $s_i = \sin \alpha_i$, $c_i = \cos \alpha_i$ $(i=1,2,3)$. To deal with one-dimensional problem it is necessary to cosider the member projections on x_i axes (Fig.3). Thus $\alpha_1 = -\bar{\theta}_1, \alpha_2 = \bar{\theta}_2, \alpha_3 = \bar{\theta}_3$

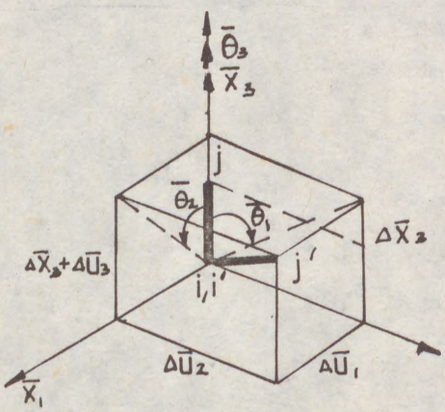

$$c_1 = \cos \bar{\theta}_1 = \frac{1 + \bar{u}'_{3R}}{\sqrt{1 + 2\,\bar{e}_2}} , \qquad (13)$$

$$s_1 = \sin \bar{\theta}_1 = \frac{\bar{u}'_{2R}}{\sqrt{1 + 2\,\bar{e}_2}} , \qquad (14)$$

$$c_2 = \cos \bar{\theta}_2 = \frac{1 + \bar{u}'_{3R}}{\sqrt{1 + 2\,\bar{e}_1}} , \qquad (15)$$

$$s_2 = \sin \bar{\theta}_2 = \frac{\bar{u}'_{1R}}{\sqrt{1 + 2\,\bar{e}_1}} \qquad (16)$$

Fig.3 Member projections and $\bar{x}_{3R} = 0$.

Hence the rotations $\bar{\theta}_1$ and $\bar{\theta}_2$ are related to the slopes $\bar{u}'_{1R}$, $\bar{u}'_{2R}$, $\bar{u}'_{3R}$ of the displaced axis passing through the

(6)
rotation point R and $\bar{\theta}_3$ remains as independent kinematic variable. Variables $\bar{e}_1, \bar{e}_2$ are the projections of the Green strain measure of the rotation axis on the planes $(\bar{x}_1, \bar{x}_3)$ and $(\bar{x}_2, \bar{x}_3)$, respectively. Thus

$$\bar{e}_1 = \bar{u}'_{3R} + \frac{1}{2} [(\bar{u}'_{3R})^2 + (\bar{u}'_{1R})^2], \tag{17}$$

$$\bar{e}_2 = \bar{u}'_{3R} + \frac{1}{2} [(\bar{u}'_{3R})^2 + (\bar{u}'_{2R})^2]. \tag{18}$$

In the following the symbol ()' will be used to denote $x_3 \doteq \bar{x}_3$ derivatives.

4. DISPLACEMENT VECTOR COMPONENT DUE TO WARPING EFFECT

To derive the displacement vector component due to a nonuniform torsion we consider the second and third assumptions cited in Chap.1 and recognize that warping effect may arise due to the rigid rotation only. Thus

$$\bar{u}^{(2)} = \bar{u}^{(21)} + \bar{u}^{(22)} \tag{19}$$

where

$$\bar{u}^{(21)} = < 0 , 0 , - \int [I_1 + \frac{\partial}{\partial \bar{x}_1} \bar{u}^{(1)}]^T \frac{\partial}{\partial \bar{x}_3} \bar{u}^{(1)} \, d\bar{x}_1 >^T, \tag{20}$$

$$\bar{u}^{(22)} = < 0 , 0 , - \int [I_2 + \frac{\partial}{\partial \bar{x}_2} \bar{u}^{(1)}]^T \frac{\partial}{\partial \bar{x}_3} \bar{u}^{(1)} \, d\bar{x}_2 >^T \tag{21}$$

and $I_1 = < 1 , 0 , 0 >^T$, $I_2 = < 0 , 1 , 0 >^T$.

The slope vector $\partial \bar{u}^{(1)} / \partial \bar{x}_3$ can be expressed as follows

$$\frac{\partial}{\partial \bar{x}_3} \bar{u}^{(1)} = T_{R1} \, \bar{x}_R \tag{22}$$

where

$$T_{R1} = \begin{bmatrix} d_{11} D t & d_{12} D t & d_{13} D t \\ d_{21} D t & d_{22} D t & d_{23} D t \\ d_{31} D t & d_{32} D t & d_{33} D t \end{bmatrix} \tag{23}$$

and

$$d_{11} = < - s_2 c_3 , 0 , - c_2 s_3 >, \tag{24}$$

$$d_{12} = < s_2 s_3 , 0 , - c_2 c_3 >, \tag{25}$$

$$d_{13} = < c_2 , 0 , 0 >, \tag{26}$$

(7)

$$\mathbf{d}_{21} = \langle -s_1c_2c_3 \,,\; -c_1s_2c_3 - s_1s_3 \,,\; s_1s_2s_3 + c_1c_3 \rangle, \tag{27}$$

$$\mathbf{d}_{22} = \langle \; s_1c_2s_3 \,,\; c_1s_2s_3 - s_1c_3 \,,\; s_1s_2c_3 - c_1s_3 \rangle, \tag{28}$$

$$\mathbf{d}_{23} = \langle - s_1s_2 \,,\; c_1c_2 \,,\; 0 \rangle, \tag{29}$$

$$\mathbf{d}_{31} = \langle -c_1c_2c_3 \,,\; s_1s_2c_3 - c_1s_3 \,,\; c_1s_2s_3 - s_1c_3 \rangle, \tag{30}$$

$$\mathbf{d}_{32} = \langle \; c_1c_2s_3 \,,\; -s_1s_2s_3 - c_1c_3 \,,\; c_1s_2c_3 + s_1s_3 \rangle, \tag{31}$$

$$\mathbf{d}_{33} = \langle - c_1s_2 \,,\; - s_1c_2 \,,\; 0 \rangle, \tag{32}$$

$$\mathbf{D} = \begin{bmatrix} (1 + 2\,\bar{e}_1)^{-1} & 0 & 0 \\ & (1 + 2\,\bar{e}_2)^{-1} & 0 \\ \text{symm.} & & 1 \end{bmatrix}, \tag{33}$$

$$\mathbf{t} = \begin{Bmatrix} \bar{u}''_{1R}\,(1+\bar{u}'_{3R}) - \bar{u}'_{1R}\,\bar{u}''_{3R} \\ \bar{u}''_{2R}\,(1+\bar{u}'_{3R}) - \bar{u}'_{2R}\,\bar{u}''_{3R} \\ \bar{\theta}'_3 \end{Bmatrix}. \tag{34}$$

The relations for $\partial\bar{\mathbf{u}}^{(1)}/\partial\bar{x}_1$ and $\partial\bar{\mathbf{u}}^{(1)}/\partial\bar{x}_2$ can be expressed as follows

$$\frac{\partial}{\partial x_1}\,\bar{\mathbf{u}}^{(1)} = \mathbf{T}_R\Big(\frac{\partial}{\partial\bar{x}_1}\,\bar{\mathbf{x}}_R\Big) + \Big(\frac{\partial}{\partial\bar{x}_1}\,\mathbf{T}_R\Big)\,\bar{\mathbf{x}}_R \,,\quad \frac{\partial}{\partial\bar{x}_2}\,\bar{\mathbf{u}}^{(1)} = 0. \tag{35}$$

From Eq.(35) it is obvious that for cross-sections composed of a series of plate segments both vectors are equal to zero. Thus

$$\bar{\mathbf{u}}^{(21)} = \langle \; 0 \,,\; 0 \,,\; -\mathbf{d}_{11}\,\mathbf{D}\,\mathbf{t}\,w_1 \; - \mathbf{d}_{12}\,\mathbf{D}\,\mathbf{t}\,w_2 \qquad \rangle^{\mathrm{T}}, \tag{36}$$

$$\bar{\mathbf{u}}^{(22)} = \langle \; 0 \,,\; 0 \,,(-\mathbf{d}_{21}\,\mathbf{D}\,\mathbf{t}\,\bar{\mathbf{x}}_{1R} - \mathbf{d}_{22}\,\mathbf{D}\,\mathbf{t}\,\bar{\mathbf{x}}_{2R})\,\bar{\mathbf{x}}_2 \rangle^{\mathrm{T}} \tag{37}$$

where

$$w_1 = \int_0^{\bar{x}_1} \bar{\mathbf{x}}_{1R}\,d\bar{x}_1 \,, \qquad w_2 = \int_0^{\bar{x}_1} \bar{\mathbf{x}}_{2R}\,d\bar{x}_1 \tag{38}$$

are the sectorial coordinates at the middle line of the member cross-section.

5. COMPARISON WITH THE CLASSICAL THEORY OF THIN-WALLED MEMBERS

The expressions derived here allow the member cross-section to be fully nonrigid. To explain inaccuracies of the classical theory of thin-walled members, a comparison between

(8)

components of displacement field is made with respect to some simplifications. In the expressions derived earlier it is assumed that the gradients of displacements $\bar{u}_{iR}(i=1,2,3)$, depending only on one coordinate variable, namely the longitudinal axis of the member, are of infinitesimal magnitude i.e. $0(\epsilon)$, where denotes quantity of such a magnitude. The approximate relationships for the slope vector $\mathbf{u}' = \partial \mathbf{u} / \partial x_3$ an arbitrary point M in the x_i directions are obtained considering only $0(\epsilon)$ terms in the gradients of transverse displacements u_1, u_2 and $0(\epsilon^2)$ terms in the gradient of longitudinal displacement u_3. The results of such a comparison is summarized below

(1) The classical theory, [1,4,5,6]

$$u'_1 = u'_{1R} - (x_2 - x_{2R}) \theta'_3 , \tag{39}$$

$$u'_2 = u'_{2R} + (x_1 - x_{1R}) \theta'_3 , \tag{40}$$

$$u'_3 = u'_{3R} - (x_1 - x_{1R})(u''_{1R} + u''_{2R}\,\theta_3 + u'_{2R}\,\theta'_3) + - (x_2 - x_{2R})(u''_{2R} - u''_{1R}\,\theta_3 - u'_{1R}\,\theta'_3) + w_2\,\theta''_3 . \tag{41}$$

(2) A nonclassical theory derived here; u'_1 and u'_2 as in Eqs.(40) and (41), respectively

$$u'_3 = u'_{3R} - (x_1-x_{1R})(u''_{1R}+u''_{1R}\,u'_{3R}-u'_{1R}\,u''_{3R}+u''_{2R}\,\theta_3 + u'_{2R}\,\theta'_3) - (x_2-x_{2R})(u''_{2R}+u''_{2R}\,u'_{3R}-u'_{2R}\,u''_{3R} + -u''_{1R}\,\theta_3-u'_{1R}\,\theta'_3)+w_1(u'_{1R}\,u''_{1R}+\theta_3\,\theta'_3)' + w_2\,\theta''_3 + \bar{x}_2\,[(\bar{u}'_{2R}\,\bar{u}''_{1R}+\bar{u}'_{1R}\,\bar{u}''_{2R}-\theta'_3)'\bar{x}_{1R} + (\bar{u}'_{2R}\,\bar{u}''_{2R} + \theta_3\,\theta'_3)'\,\bar{x}_{2R}] . \tag{42}$$

From the comparison made above it is clear that the significant differences may occur in the equation describing the gradient of the longitudinal displacement u_3. The error in the value of u'_3 derived in the classical theory can be attributed to the following two possible sources which are evident from Eqs.(41) and (42)

(1) The incorrect evaluation of the curvatures due to the omission of the terms $(u''_{1R}\,u'_{3R}-u'_{1R}\,u''_{3R})$ and $(u''_{2R}\,u'_{3R}-u'_{2R}\,u''_{3R})$.

(2) The omission of the terms associated with the sectorial coordinate w_1 and the linear coordinate $\bar{x}_2$.

The displacement field vector derived here may be used for exact fully geometrically nonlinear incremental analysis by FEM.

(9)
REFE
[1]
[2]
[3]
[4]
[5]
[6]
[7]
[8]

(9)

REFERENCES

[1] Alwis W.A.,Usami T., Elastic Lateral-Torsional Buckling of Unbraced and Braced Planar Frames. Comp.Struct.,10(1979), 517-529.

[2] Bradford M.A.,Cuk P.E.,Gizejowski M.A.,Trahair N.S., Inelastic Lateral Buckling of Beam-Columns. J.Struct.Eng.,113(1987), 2259-2276.

[3] Chan S.L.,Kitipornchai S., Geometric Nonlinear Analysis of Asymmetric Thin-Walled Beam-Columns. Eng.Struct.,9(1987), 243-254.

[4] Maciejewski M.,Osmolski W., Geometrically Nonlinear Theory of Thin-Walled Beams of Open Cross-Section. Wroclaw Tech. Univ.,Serie:Conferences No.34(1986),101-108 (in Polish).

[5] Nishino F.,Kurakata Y.,Hasegawa A.,Okumura T., Thin-Walled Members Under Axial Force, Bending and Torsion. Proc. Japan Soc.Civ.Engrs,225(1974),1-15.

[6] Roberts T.M., Second Order Strains and Instability of Thin-Walled Bars of Open Cross-Section. Int.J.Mech.Sci., 23(1981),297-306.

[7] Sekulovic M., Geometrically Nonlinear Analysis of Thin-Walled Members. In:Steel Structures.Ed.M.N.Pavlovic. Elsevier Appl.Sci.Publ.Ltd.(1986),219-243.

[8] Vacharajittiphan P.,Woolcock S.T.,Trahair N.S., Effect of In-Plane Deformation on Lateral Buckling. J.Struct.Mech., 3(1974),29-60.

GRUDEV I.D. (1)

SURVIVABILITY AS A FACTOR ENSURING FAILURE-FREE OPERATION OF STRUCTURES

INTERNATIONAL COLLOQUIUM
STABILITY OF STEEL STRUCTURES
BUDAPEST, HUNGARY, 1990
PRELIMINARY REPORT

Summary: Operating structures almost always have damages, however, failures take place relatively rarely and are always of an avalanche character. Hence, it follows that the cause of failures is loss of structural survivability. In this paper, a method of survivability design for one class of structures is proposed, which is characterized by uniform redistribution of additional forces after failure of one member. The results are compared with the experimental data.

At present, structures are designed according to many criteria: strength, stability, fatigue, deformability and sometimes the others. In most cases, however, the limiting parameters are strength and stability, and they will be considered below.

The check of load-carrying capacity is always carried out member by member / 1 /, irrespective of the fact if the structure is statically determinate or indeterminate, i.e., from the standpoint of reliability, the structural members are connected in series though, in practice, members working parallelly are met with rather often not only in physical but also in reliability context. It is these structures that are the subject of the present paper.

1. When there is a single-member failure in a statically indeterminate structure it is not necessary that the total failure of the structure occurs. Some redistribution of forces in members is possible at which the structure at the given loading does not lose its load-carrying capacity, i.e. it turns

(1) Professor of Civil Engineering, TSNIIProektstalkonstruktsiya named after Melnikov, Moscow, USSR

out to survive while the member considered fails. If the structure does not fail with the failure of any member, it means that the structure possesses survivability.

It is evident that in order to determine if a heterogeneous structure is survivable, it is necessary that the after-effects of each member failure be considered. In principle, this can be done numerically by considering the loads and properties of the structural members to be random variables and analysing a set of solutions, for example, by Monte-Carlo method. For homogeneous structures consisting of similar members, e.g. similar-wire ropes, multi-bolt joints, a considerably more profound theoretical analysis is possible. This particularly concerns structures with uniform redistribution of forces, when the failed member load is uniformly distributed among the rest of the member.

This situation arises when one wire of the parallel-wire rope breaks, because the wire stiffness is much less than that of the sockets in which the wire ends are sealed, and the sockets may be regarded as rigid ones (Sivachov 1978 / 2 /). The deformations of all operating wires will be always equal.

Another example is connection of two plates by means of self-tapping screws. The connection modulus per screw, according to measurements carried out by V.A. Checkalov (Checkalov 1984 / 3 /), turned out to be less than the plate modulus by a factor of 50, so the plate deformations may be neglected, and then deformations of all the bolts appear to be equal.

2. The problem on the load-carrying capacity of a structure with uniform redistribution of forces when one member is failed is solved in the following formulation.

The strength r of one member is a random variable and is characterized by the distribution density $p(r)$ and the distribution function $P(r)=\int_{-\infty}^{r} p(x)dx$ with the mean value of $\bar{r}$, variance d and standard $\hat{r}=\sqrt{d}$.

The strength of the n-member structure denoted as R_n and equal to the load at which failure of all the members occurs, is also a random variable. Of great interest is the specific strength $r_n = R_n/n$, characterized by the density $p_n(r_n)$ and the distribution function $P_n(r_n)$.

3. The solution of the problem on the load-carrying n-member structure with limited n is of a probabilistic character, i.e. the failure probability of all the members at the specified load may be found when one or a group of members fail.

For a parallel-member structure with uniform distribution of additional forces, at the failure of one member (rope, multi-bolt connection) the structural strength distribution is determined by the Daniels formula (Daniels 1945 / 4 /):

$$P_n(Q) = n! \sum_{B_n} \prod_{i=1}^{n} \frac{\delta_i^{m_i}}{m_i!} \qquad (1)$$

Here, δ_i is determined from the initial distribution:

$$\delta_i = P(q_i) - P(q_{i-1}), \tag{2}$$

q_i being a force in each of the other members at the failure of i members

$$q_i = Q/(n - i + 1), \; i = 1, \ldots, n \tag{3}$$

and the set B_n being defined by various collections of n integers $m_1, m_2, \ldots, m_n$ fulfilling the following conditions:

$$\begin{aligned} &m_1 + m_2 + \ldots + m_n = n, \\ &m_i \geqslant 0, \; m_1 + m_2 + \ldots + m_j \geqslant j, \; j = 1, \ldots, n-1 \end{aligned} \tag{4}$$

Formula (1) determines the failure probability of the whole structure; however, the problem of development of an avalanche failure is of no less interest. It is evident that there is a non-zero probability of such a situation when, at the given total load Q, failure of one or $k<n$ members will occur, and the load will be carried by the structure as a whole. This probability may be calculated by the formula obtained for the first time by Onischenko (Grudev, Onischenko 1988 / 5 /):

$$P_k(Q) = \frac{n!}{(n-k)!}\left[1 - P(q_{k+1})\right]^{n-k} \sum_{B_k} \prod_{i=1}^{k} \frac{\delta_i^{m_i}}{m_i!} \tag{5}$$

where the values of m_i, δ_i, B_k are determined by the formulae (2)-(4), if k is substituted for n in them.

It is not difficult to make sure that the Daniels formula (1) is a particular case of the Onischenko formula (5) at k=n and at $P(q_{n+1})=1$.

4. Calculations by formulae (1)-(5) are only possible when electronic computers are used, because they are of a combinatorial nature and have a great number of summands defined by the structure of sets B_k. This situation necessitates the search for optimal methods of summation, because a simple exhaustion of summands requires too much machine time even for modern electronic computers.

In this context, of great importance becomes the asymptotic analysis at $n \to \infty$. Naturally, a particular interest presents the specific strength r_n which shows how the load-carrying capacity of the member changes depending on the number of structural members. It was shown by Daniels (Daniels 1945 / 4 /) that, at unrestricted growth of n, the distribution function of the specific strength tends to normal distribution with the mean value

$$\bar{r}^a = q_a\left[1 - P(q_a)\right] \tag{6}$$

and the variance

$$d^a = q_a^2 P(q_a)\left[1 - P(q_a)\right]/n, \qquad (7)$$

the value of q_a maximizing the expression $q\left[1 - P(q)\right]$, i.e.

$$\bar{r}^a = \max\left\{ q\left[1 - P(q)\right]\right\}. \qquad (8)$$

The last formula gives the relationship for determining q_a (Rabotnov 1979 / 6 /):

$$q_a - \left[1 - P(q_a)\right]/p(q_a) = 0$$

Here and below, the asymptotic values are denoted by index a.

Formulae (6) and (7) are interesting in that respect that the variance d^a of the specific strength tends to zero with growth of n, and the variance D^a of the structural strength as a whole, on the contrary, increases because it is evaluated by the formula:

$$D^a = n^2 d^2 = q_a^2 P(q_a)\left[1 - P(q_a)\right] n$$

It follows that, though the specific strength in the range of $n \to \infty$ has no spread relative to the mean value of $\bar{r}^a$, the total structural strength has variance D^a increasing with growth of n.

5. The examples dealt with have shown that the loads per member corresponding to the failure probabilities ($P \sim 0.5$) decrease when the number of members increases and tend to a certain limit of qa. On the contrary, in the range of little failure probabilities ($P \sim 0.001$), structures with a large number of members appear to be more reliable.

For example, if the "rule of three sigmas" is used, the specific strength may be determined as follows:

$$r = \bar{r} - 3\hat{r} .$$

The standard value in this relationship may be calculated in terms of variance by formula (7) for given value of n, and the mean value of r calculated by formula (6) leads to considerable errors. It is due to the fact that the mean value of $\bar{r}_n$ varies as a function of n. The calculation of $\bar{r}_n$ by means of the exact formula (1) is rather awkward, therefore it is very attractive to obtain an analytical formula for this purpose.

6. To determine the mean value of $\bar{r}_n$ at not very large values of n the discrete analogue of formula (8) may be used. Let the n-member structure be considered as defined by a collection of members with deterministic values of strength: $r_1 < r_2 < \ldots < r_n$ chosen according to the following condition:

(5)

$$P(r_i) = i/(n+1),\ i = 1, \ldots, n \qquad (9)$$

If the connection members are arranged in order of their strength increase from i = 1 to i = n, the values of r_i will be approximate mean values of the i-th member strength. Their exact values may be found by means of the i-th member strength distribution specified by the following relationship (Ventsel 1973 /7/):

$$P_i^{(n)}(r) = \sum_{j=i}^{n} C_n^j P^j(r) \left[1 - P(r)\right]^{n-j},$$

where P(r) is the initial distribution.

For uniform distribution the approximate and exact values of r_i coincide, this being easily checked.

It is not difficult to note that the specific strength of the connection with deterministic elements is determined as follows (Grudev, Onischenko 1988 / 5 /):

$$\bar{r}_n = \max\left[r_i\left(1 - \frac{i-1}{n}\right)\right]. \qquad (10)$$

As an example, the specific strength values have been calculated for 9- and 20-member connections by formulae (9), (10), and the results obtained have been compared with the experimental data (Chekalov 1984 / 3 /) for 9- and 20-bolt connections.

There is a good agreement between the mean experimental and theoretical data despite the fact that the test sample was limited: there were 10 tests carried out for 9-bolt connections and only 5 ones for 20-bolt connections.

7. As a whole, the above numerical strength analysis of multimember structures allows the following conclusions to be drawn:

Effective asymptotic formulae have been proposed for survivability calculation of the structures considered or for choosing the specified values of loads.

The beginning of the "avalanche" process at any value of n is defined by a small distribution area in the vicinity of a point corresponding to the asymptotic approximation ($n \to \infty$).

REFERENCES

I. Строительные нормы и правила. Нормы проектирования. Стальные конструкции, СНиП II-23-81*.-М.: ЦИТП Госстроя СССР, 1987.-3-4 с.

2. Сивачев В.П. Гибкие высокопрочные элементы в строительных металлических конструкциях.-М.:ЦИНИС, 1978.

3. Чекалов В.А. Определение несущей способности многоболтовых соединений с помощью распределений прочности одноболтовых соединений по "условию слабейшего элемента". Разработка методов расчета и исследование действительной работы строительных металлоконструкций.-М.:ЦНИИПСК,1984.-132-136 с.

4. Daniels H.E. The statistical theory of the strength of bundle of threads//Proc.Roy.Soc.-London,1945.-183(A).-P. 405-435.

5. Грудев И.Д., Онищенко Д.А. Статическая оценка прочности многоэлементных соединений. Сб."Надежность и долговечность машин и сооружений"-"Наукова думка",Киев.:1988.-1-8 с.

6. Работнов Ю.Н. Механика деформируемого твердого тела. -М.: Наука, 1979.-744 с.

7. Вентцель Е.С., Овчаров Л.А. Теория вероятностей. Задачи и упражнения.- М.: Наука,1973.-368 с.

(1)
GVAMICHAVA A.S. (1)

INFLUENCE OF TECHNOLOGICAL INACCURACIES AT FABRICATION ON INITIAL STRESSED-STRAINED STATE OF STRUCTURES

INTERNATIONAL COLLOQUIUM
STABILITY OF STEEL STRUCTURES
BUDAPEST, HUNGARY, 1990
PRELIMINARY REPORT

Problems of theoretical determination of probable initial distortions of prefabricated structures shapes and initial forces, caused by technological errors at fabrication, are poorly described in our scientific literature. Initial distortions of bearing frames shapes play an important role at precision antenna structures, where they are often of a decisive importance. These also may be referred to reticulated domes, where they have a considerable influence on the critical load value.

Initial forces, caused by the errors in the members dimensions, play an important role at automatically deployable structures and sometimes at prefabricated structures. In the automatically deployable structures these forces are of the main factors, defining the deployment reliability; in the prefabricated structures the values of these forces permit to judge the assembly potentiality.

The report covers the initial stressed-strained state (SSS), caused by length deviations and misalignment of members to be joined.

At present, there are two methods of theoretical estimation of probable initial distortions of the structural shape: the first one (statical) is based on the statical analysis of the structure, the second one (geometrical) is based on the successive geometrical construction of the structural joints.

The statical method permits efficiently solve the problems in a linear approximation, but it is limited by the cases where

(1) D. Sc. (Eng.), TSNIIProektstalkonstruktsiya named after Melnikov

(2)
non-linear factors are to be considered. The geometrical method is efficient for statically determinate structures where geometrical non-linearity shall be considered. In statically indeterminate structures due to an excessive number of connections, geometrical equations are insufficient and their combination with the continuity equations leads to the system of non-linear equations, which makes this method non-efficient.

When using the statical method for initial stressed-strained state of structures estimation, each member is given its initial deviation from the theoretical dimension and the structure is designed as a whole.

In most cases, fabrication errors are variable values distributed in correspondence with the law similar to the normal one. For determining the probable initial imperfections of the structures various design methods were used (Savelyev, 1966 / 1 /), (Gvamichava et al., 1975 / 2 /), (Lombardo, 1973 / 3 /), in which fields of random deviations by means of a random-number generator were prescribed, corresponding to the established law of fabrication errors propagation. Numerous calculations of errors propagation for various fields were carried out as well as joints displacements and changing of rods inclination angles were determined. Statistical processing of the results gave mean and root-mean-square magnitudes of the required values.

The technique of separate joints or a group of joints probable initial forces and deviations from the theoretical position analysis has been worked out (Gvamichava, 1989 /4/), (Gvamichava, 1988 / 5 /), which allows to obtain probable magnitudes of the required values on the basis of one statical computation for unit or group excitation. This technique allows fairly simple to estimate probable values of initial forces and displacements for the structures operating in the linear field. Analytical expressions (Gvamichava, 1989 / 4 /) for some most widely used structural types have been obtained.

In those cases, when geometrical non-linearity has to be taken into account, a geometrical method developed in the work (Lebed et al., 1988 / 6 /) may be used. A complex of programmes for simulation a process of module erection and determination an initial profile of reticulated domes surface has been worked out. However, this method cannot be used for statically indeterminate structures.

An approximate method for determining initial deviations of structures operating in the fields of considerable geometrical non-linearity has been worked out, which may be used both for statically determinate and statically indeterminate structures.

Computations are to be performed in the following sequence: first, according to the above mentioned procedure, initial forces field in a linear approximation (when forces in a non-

(3)
deformed structure are found), then, the form of the structure distortion is prescribed and an arrow of deflection, corresponding to the minimum value of potential energy, is determined.

An accuracy of this method is characterised, mainly, by the accuracy of a form of the structure initial distortion presetting, which, in fact, coincides with the buckling form at the given distribution of initial stresses. In those cases, when the form is known, it is given with more accuracy, otherwise it may be preset approximately. Stringent evaluations of this method has not been yet developed. The main point of this method may be illustrated by the following example.

Let's take a square plate hingedly supported by its edges with initial stresses $\sigma_{0x} = \sigma_{0y} = \sigma_0$. Let's preset a deflection of the plate corresponding to the 1st form of the buckling

$$w = f \sin\frac{\pi x}{\ell} \sin\frac{\pi y}{\ell} \tag{1}$$

When the deflection appears, relative axial deformations at the plate middle surface will be as follows

$$\varepsilon_x = \frac{1}{2}\left(\frac{\partial w}{\partial x}\right)^2 = \frac{1}{2}\frac{\pi^2 f^2}{\ell^2}\cos^2\frac{\pi x}{\ell}\sin^2\frac{\pi y}{\ell}, \tag{2}$$

$$\varepsilon_y = \frac{1}{2}\left(\frac{\partial w}{\partial y}\right)^2 = \frac{1}{2}\frac{\pi^2 f^2}{\ell^2}\sin^2\frac{\pi x}{\ell}\sin^2\frac{\pi y}{\ell}, \tag{3}$$

and corresponding changing of the stresses will be equal to

$$\sigma_x = \frac{E}{1-\mu^2}(\varepsilon_x + \mu\varepsilon_y) = \frac{E\pi^2 f^2}{2(1-\mu^2)\ell^2}\left(\cos^2\frac{\pi x}{\ell}\sin^2\frac{\pi y}{\ell} + \mu\sin^2\frac{\pi x}{\ell}\cos^2\frac{\pi y}{\ell}\right) \tag{4}$$

Potential energy corresponding to the axial deformations will be

$$U_N = \frac{h}{2}\int_0^{\ell}\int_0^{\ell}\left[(\sigma_0 - \sigma_x)(\varepsilon_0 - \varepsilon_x) + (\sigma_0 - \sigma_y)(\varepsilon_0 - \varepsilon_y)\right] dx\,dy =$$

$$= \left[\frac{1-\mu}{E}\ell^2\sigma_0^2 - \frac{\pi^2 f^2}{4}\sigma_0 + \frac{E(9+\mu)\pi^4 f^4}{4(1-\mu)64\ell^2}\right]h \tag{5}$$

where h is the plate thickness.

Potential energy corresponding to the flexural deformations may be written as

$$U_M = \frac{1}{2}\int_0^{\ell}\int_0^{\ell} D\left\{\left(\frac{\partial^2 w}{\partial x^2} + \frac{\partial^2 w}{\partial y^2}\right)^2 + 2(1-\mu)\left[\left(\frac{\partial^2 w}{\partial x\,\partial y}\right)^2 - \frac{\partial^2 w}{\partial x^2}\cdot\frac{\partial^2 w}{\partial y^2}\right]\right\} dx\,dy \tag{6}$$

where D is the plate cylindrical rigidity.

Let's substitute Eq. (1) in Eq. (6) and after integrating we

(4)
get

$$U_M = \frac{\pi^4 f^2}{2\ell^2} D \tag{7}$$

The derivative of the plate total potential energy will be as follows

$$\frac{\partial U}{\partial f} = \frac{\partial (U_N + U_M)}{\partial f} = f\frac{\pi^4}{\ell^2} D - \frac{\pi^2 f}{2} \sigma_0 h + \frac{E(9+\mu)\pi^4 f^3 h}{1-\mu^2\, 64\ell^2} \tag{8}$$

By equating this expression to zero, we get the plate deflection value

$$f = \frac{4\ell}{\pi}\sqrt{\frac{2(1-\mu^2)}{(9+\mu)Eh}\left(\sigma_0 h - \frac{2\pi^4 D}{\ell^2}\right)} = \frac{4\ell}{\pi}\sqrt{\frac{2(1-\mu^2)}{(9+\mu)Eh}\left(\sigma_0 h - q_{кр}\right)} \tag{9}$$

where $q_{кр}$ is a critical longitudinal load for a rectangular load uniformly loaded in two directions.

At these computations, displacements in the plane of the plate were not taken into account. However, investigations showed that in the most cases their contribution to the total energy balance may be neglected.

Let's see how to determine the dispersion and the expectation of the initial deflection for the cases, when the initial stress is a random value. Let's write down Eq. (9) as:

$$\begin{aligned} y &= a\sqrt{\sigma(z) - b} \qquad \text{at} \quad \sigma(z) > b \\ y &= 0 \qquad\qquad\quad \text{at} \quad \sigma(z) \le b \end{aligned} \tag{10}$$

where σ_z is a root-mean-square of the random value, distributed according to the normal law; "a" and "b" are constant coefficients.

Using the methods of the probability theory we may demonstrate that the expectancy and the dispersion of the value "y" are determined as follows:

$$M(x) = \frac{a\sqrt{\sigma(z)}}{2\pi} \int_{\frac{b}{\sigma(z)}}^{\infty} \left[\sigma(z)\cdot u - b\right]^{\frac{1}{2}} e^{-\frac{u^2}{2}} \cdot du \tag{11}$$

$$D(x) = \frac{a^2\sqrt{\sigma(z)}}{2\pi} \int_{\frac{b}{\sigma(z)}}^{\infty} \left[\sigma(z)\cdot u - b\right]^{\frac{1}{2}} \cdot e^{-\frac{u^2}{2}} - M^2(x) \tag{12}$$

At deriving these expressions it was assumed that the expectancy of the random value "z" was equal to zero. Using Eqs (11) and (12) the values of the structure initial deflection expectancy and dispersion may be found. It should be noted that the deflection expectancy will be not equal to zero, though the expectancy of the initial force is equal to zero.

(5)

The suggested method may be used for designing of film structures. Works are now in progress on development of large film structures in space, formed by internal pressure forces, centrifugal forces, electrostatic forces etc. Such structures are glued, welded or sewed together from specially cut out members with the dimensions considerably less than those of the structure. Fabrication of the members and their joining are performed with deviations from the nominal dimensions, their values being defined by a concrete fabrication process.

Film structures peculiarity is that only tensioned members may take and transfer the forces. Until all the members are tensioned in the process of operation, the structure may be considered as a common momentless shell and in this case the surface distortions are characterized only by the members elastic deformations. When compressive stresses appear, the members under compression are no longer in operation which leads to dents appearance.

Transition from the first state (all members are tensioned) to the second one (compression appeared in some members) requires changing of the design scheme and the design method. In the first case, determining of the surface distortions due to fabrication process errors may be carried out according to the previously developed design method (Gvamichava, 1989 / 4/); in the second case, the design scheme and the design method should be changed. For many problems it is sufficient to determine the boundary between these states, because it defines the beginning of large distortions, which considerably exceed the first case distortions.

The technique of such problem solution may be illustrated at the example of a flat disk under centrifugal forces tension. Let's assume that this disk remains flat in service, in this case additional stresses may arise due to fabrication imperfections, their values may be found according to the method / 4 /. If the value of compressive stresses is less than that of tensile stresses caused by centrifugal forces, the disk remains flat. In the opposite case, folds may appear at the disk. On the basis of comparison of compressive and tensile stresses values fabrication accuracy values providing surface unfoldness may be determined. In practice, this problem is limited by this accuracy level estimation.

For the convenience of computation the disk may be either divided into finite elements or considered as a rod net of an equivalent rigidity; the rods sections are to be selected by a known method.

Let's analyse a disk of a radius R , rotating about an axis with an angle velocity ω . The modern fabrication technology of film surfaces ensures approximately similar fabrication accuracies in all directions. On this assumption, an equivalent transition from the regular rod net with the rod size corresponding to the typical size of the cut out pattern

(6)
member may be used.

According to the method / 4 /, the mean-root-square value of the expected force in the member is found from the expression

$$\sigma(N_\kappa) = \sigma(\delta_\kappa)(1-N_\kappa)^{\frac{1}{2}} \frac{EF_\kappa}{\ell_\kappa} \qquad (13)$$

where $\sigma(\delta_\kappa)$ is a mean-root-square value of the member fabrication value (a tolerance for fabrication may be taken equal to $3\sigma(\delta_\kappa)$); N_κ is a force in the member caused by mutually balanced unity forces applied to its ends; F_κ and ℓ_κ are the cross-section area and the member length, respectively.

At the transition from the solid disk to the equivalent rod system / 1 /

$$F_\kappa = \frac{\sqrt{3}}{2} \ell_\kappa t \qquad (14)$$

where t is the disk thickness.

In such a way,

$$\sigma(N_\kappa) = \sigma(\delta)(1-N_\kappa)^{\frac{1}{2}} \cdot \frac{\sqrt{3}}{2} Et \qquad (15)$$

Forces values from centrifugal forces may be found numerically by one of standard programmes.

The results for the disk made of some members of a typical size about 0.2 radius are given in Table 1. In the 4th column maximum values of a dimensionless mean-root-square error at members fabrication, which allows no folds to appear in the zone considered, are given. The sixth part of the design scheme used is given in Fig. 1.

Calculations show that the maximum fabrication accuracy is necessary in order to prevent folds along the disk contour.

The suggested methods of probable initial shape distortions and initial forces determination allow to analyse a wide range of structures. Statical method enables to analyse quite simply and efficiently the problems in a linear approximation. Combination of this method with the energetic methods allows to solve some problems in a non-linear approximation. In future, there should be developed more stringent errors estimations of the results obtained for more reasonable application of the suggested methods.

(7)

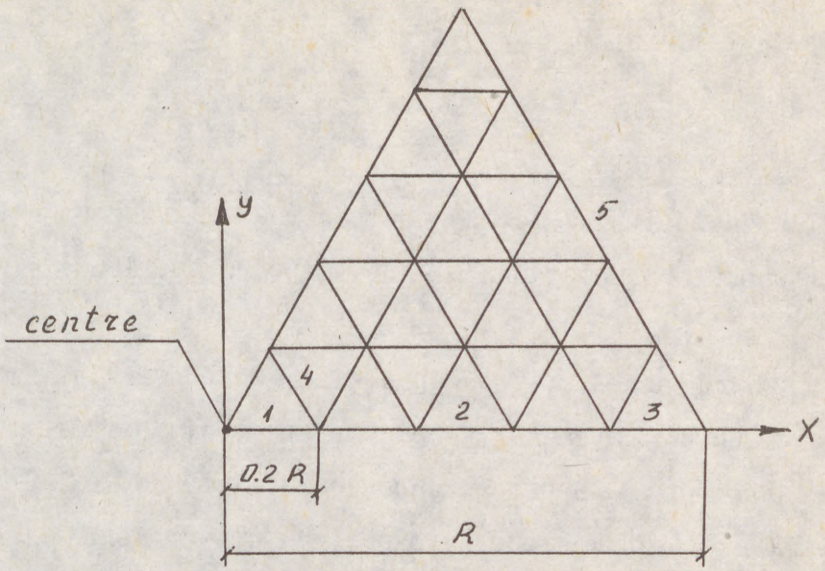

Fig. 1 Fragment (1/6 part) of the disk design scheme

Table 1

Member No.	N_K	$\frac{\sigma(N_K)}{\sigma(\delta_K) E t}$	$\frac{N_{u.l.}}{\rho \omega^2 R^3 t}$	$\frac{\sigma(\delta_K) E}{\rho \omega^2 R^3}$
1	0.6149	0.5373	0.0424	0.0789
2	0.6807	0.4892	0.0289	0.0591
3	0.8599	0.3241	0.	0
4	0.6664	0.5001	0.0424	0.0849
5	0.7333	0.4475	0.0323	0.0723

(8)
References

I. Савельев В.А. Устойчивость сетчатых куполов: - В кн. "Металлические конструкции". - М., Стройиздат, 1966. - с.325--340.

2. Гвамичава А.С., Ломбардо И.В., Савельев В.А. Статистический анализ случайных несовершенств формы сетчатых сферических оболочек: - Проблемы надежности в строит.мех.:Тез. докл. IУ Всесоюзн.конф.по надежности в строит.мех.-М., 1975. - с.55-56.

3. Ломбардо И.В. Исследование вопросов устойчивости металлических каркасов сферических односетчатых оболочек: - Автореф.дис.канд.техн.наук. - М., 1973. - 16 с.

4. Гвамичава А.С. Определение вероятных значений начальных усилий и искажений форм стержневых конструкций. - Строит. механика и расчет сооружений. - 1989. - № I, с.65-68.

5. Гвамичава А.С. Влияние технологических ошибок изготовления элементов на напряженно-деформированное состояние и собираемость пространственных конструкций: - ЦНИИПСК - Москва, 1988. - 18 с. - Деп. во ВНИИС в 1988 г. № 8239.

6. Лебедь Е.В., Савельев В.А. Математическое моделирование на ЭВМ процесса возведения пространственных сооружений. / ЦНИИПСК. - М., 1988. - 37 с. - Деп. во ВНИИС 23.12.88, № 9811.

(1)

IVAN, Marin (1)
BOJA, Nicolae (2)

ON THE DEFORMATIONS OF BARS WITH CURVED SECTION

INTERNATIONAL COLLOQUIUM
STABILITY OF STEEL STRUCTURES
BUDAPEST, HUNGARY, 1990
PRELIMINARY REPORT

Summary: In this paper, starting from some results established for the general case of curved shells related to its curvature lines by including curved bars in this class of shells, we give a geometrical formulation for its deformation state. This point of view permits to obtain the results for such a structure (partially) by an adaptation of the results relative to curved shells. This way, different from the known one [Brink and Krätzig - 1981], reveals that our results depend not only on the geometrical elements of the axial curve of the bar, considered as plane curve, but also on those of the middle surface on which the curve is situated.

The study is made only for displacements in the plane of the cross-section of the bar for which an expression of the vector of unit deviation is given.

1. Introduction.

In the nonlinear theory of the behaviour of the bars the knowledge their deformed state is indispensable. To make an analysis of its deformed positions means to investigate the displacements and the rotations of the points from which the points from which the bar is constituted. In the initial posi-

(1) Professor of Civil Engineering, Timişoara, Polytechnical Institute
(2) Professor of Mathematics, Timişoara, Polytechnical Institute

(2)

tion we consider the bar having the (Oy) axis situated along to the axis of the bar and the (Oxz) plane containing its cross--section.

The geometrical relations which express the deformations of the bar are useful to make up the calculus of the stress and strain state of this one.

We consider a bar made up of a homogeneous, isotropic and hyperelastic material.

2. Bars with curved section considered as curved shells.

In the following by a bar with curved section, or simply "curved bar", we understand a curved shell related to the curvature lines of constant thickness h, negligible as against its length, for which the longitudinal section is a rectangle and the cross-section a curvilinear trapeze.

Geometrically, that means that one of the family of coordinate lines of the middle surface S of the bar Σ is made up of arbitrary curvature lines and the others of straight lines. So, S is related to its curvature lines, which are, obviously, orthogonal.

Let P be an arbitrary point of Σ . We consider now the initial configuration $(M,P) \subset \Sigma$, so that M is the projection of the P point on the middle surface S of Σ and denote by $z \in [-h/2,h/2]$ the real number for which $|z| = \|\overrightarrow{MP}\|$ ($\|\cdot\|$ -being the euclidean norm of vectors), (fig.1).

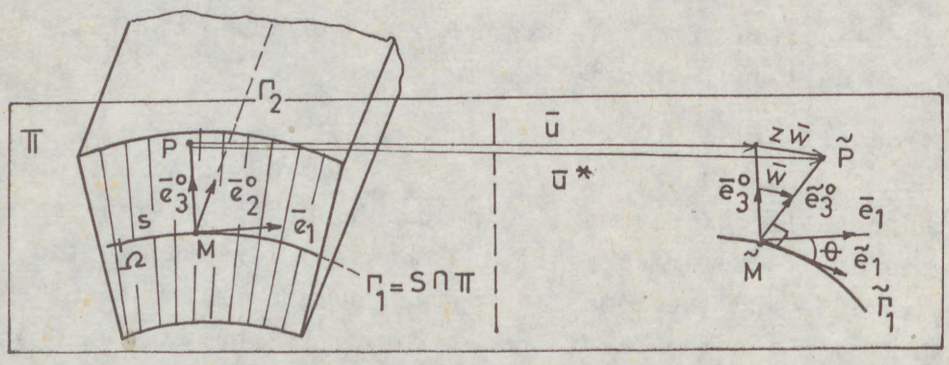

fig.1

(3)

Let $\bar{r}$ and $\bar{r}^{*}$ be the position vectors of M and P, respectively, relative to the orthonormal frame $\{O;\bar{i},\bar{j},\bar{k}\}$ of the euclidean space $\mathcal{E}^3$ and $(u^1,u^2)\in\mathbb{D}$ $(\subset\mathbb{R}^2)$ the Gaussian coordinates of M on S; thus we have the relation

$$\bar{r}^{*} = \bar{r}(u^1,u^2) + z\bar{e}_3^{o}, \qquad (1)$$

where $\bar{e}_3^{o}$ is a normal unit vector to S at M.

We denote by $(M;\bar{e}_1,\bar{e}_2,\bar{e}_3^{o})$ the Darboux trihedron to S, where $\bar{e}_i = \frac{\partial \bar{r}}{\partial u^i} \doteq \bar{r}_{,i}$, $(i=1,2)$, are the tangent vectors to the coordinate lines $u^i = const.$ on S; it results that they are tangent to the curvature lines of S which pass trough M.

A plane Π, which contains the M point and passes through the normal vector $\bar{e}_3^{o}$, intersects the middle surface S after a curve-section normal, having the curvature $k\in[o,k_1]$, k_1 being the principal curvature of S, i.e. the curvature of Γ_1, the curve of intersection of S with the plane which determines the transversal section of the bar.

Let S^{*} be a surface parallel with the middle surface S, which passes through the P point of the bar. The Darboux trihedron to S^{*} at P, $\{P;\bar{e}_1^{*},\bar{e}_2^{*},\bar{e}_3^{*o}\}$, is defined by the relations

$$\bar{e}_1^{*} = (1 - zk_1)\bar{e}_1, \quad \bar{e}_2^{*} = \bar{e}_2, \quad \bar{e}_3^{*o} = \bar{e}_3^{o}, \qquad (2)$$

obtained taking $k_2 = o$ in the corresponding relations for shell related to the curvature lines [Boja, Ivan, Brăiloiu - - 1988].

3. Deformations of the transversal section of the bar.

We consider now that the bar Σ of is exposed to some deformations which consist only of displacements along the cross-section plane. Geometrically, that means that normals to the axial curve Γ_1 remain normals to this one during and after deformation.

We shall mark by the "$\sim$" symbol elements of the deformed bar $\tilde{\Sigma}$, (fig.1).

By the above mentioned deformation the initial configuration $(M,P)\subset\Sigma$ becomes the final configuration $(\tilde{M},\tilde{P})\subset\tilde{\Sigma}$ with the displacement vectors $\bar{u}$ and $\bar{u}^{*}$, respectively.

Let $\bar{w}$ be the difference vector between the unit normal vectors at $\tilde{\Gamma}_1$ and Γ_1, in points $\tilde{M}$ and M, respectively.

(4)

This vector will be called "unit deviation"; thus the deviation of the P point (with vector $\bar{u}$) will be defined by the vector $z\bar{w}$. So, the deformed image of the $P(\in \Sigma)$ point has the following position vector and displacement vector

$$\tilde{\bar{r}}^{*} = \bar{r}^{*} + \bar{u}^{*}, \quad \bar{u}^{*} = \bar{u} + z\bar{w} , \tag{3}$$

whence, for vectors corresponding to $\tilde{M}$ belonging to the deformed axial curve, we obtain, in particular, $\tilde{\bar{r}} = \bar{r} + \bar{u}$, $\bar{u}^{*} = \bar{u}$.

We have the following decompositions of the displacement vectors

$$\bar{u} = a^{1}\bar{e}_1 + a^{3}\bar{e}_3^{o}, \quad \bar{u}^{*} = (a^{1}+zc^{1})\bar{e}_1 + (a^{3}+zc^{3})\bar{e}_3^{o} . \tag{4}$$

Computing the partial derivatives of the vector $\bar{r}^{*}$, given by (1), in relation to the u^{i} $(i = 1,2)$ variables and taking into account the (2) relations, we obtain

$$\bar{e}_{3,1}^{o} = -k_1\bar{e}_1 , \quad \bar{e}_{3,2}^{o} = \bar{o} . \tag{5}$$

On the other hand, if we derive in relation to the u^{1} variable the relation $\langle \bar{e}_1 ; \bar{e}_3^{o} \rangle = o$, and taking into account of (5) we obtain in the M point the relation

$$\langle \bar{e}_{1,1} ; \bar{e}_3^{o} \rangle = k_1 g_1 = b_1 , \tag{6}$$

and with the first Frenet formula relative to Γ_1, for which we identify the curvilinear coordinates $u^{1} = s$ (s being the arc of curve), we have

$$\bar{e}_{1,1} = \frac{d\lambda}{ds}\bar{e}_1^{o} + \lambda\frac{1}{R}\bar{e}_3^{o} , \tag{7}$$

where $\lambda(s)$ $(>o)$ is the factor of proportionality of the tangent vector $\bar{e}_1$ with the unit vector $\bar{e}_1^{o}$ and has the value $\lambda = \sqrt{g_1}$ relative to the middle surface S, and 1/R is the curvature of the plane curve Γ_1 (which represents in fact the curvature of the bar in the considered point).

From (6) and (7), for the principal curvature of S in the direction of the tangent vector $\bar{e}_1^{o}$ to the curvature line Γ_1, it results the expression

$$k_1 = \frac{1}{\sqrt{g_1}}\cdot\frac{1}{R} . \tag{8}$$

Deriving with respect to s the position vector $\tilde{\bar{r}}$ of $\tilde{M}$, given by (3) and taking into account (7) and (8), we obtain the decompositions of the Darboux frame vectors

$$\tilde{\bar{e}}_1 = \alpha_1^{1}\bar{e}_1 + \alpha_1^{3}\bar{e}_3^{o} , \quad \tilde{\bar{e}}_3^{o} = \alpha_3^{1}\bar{e}_1 + \alpha_3^{3}\bar{e}_3 , \tag{9}$$

which define the deformed position of the bar against the

(5)

initial state. In (9) the first two coefficients have the values

$$\alpha_1^1 = 1+a^1{}_{,1} - \frac{1}{\sqrt{g_1}}\frac{1}{R}a^3 + \frac{1}{2g_1}g_{1,1}a^1, \quad \alpha_1^3 = a^3{}_{,1} + \sqrt{g_1}\cdot\frac{1}{R}a^1 , \qquad (10)$$

and the others can be determined from the equations

$$g_1\alpha_1^1(\alpha_3^1) + \alpha_1^3(\alpha_3^3) = 0, \quad g_1(\alpha_3^1)^2 + (\alpha_3^3)^2 = 1 . \qquad (11)$$

The Darboux frame in the $\tilde{P}$ point is expressed with the one of the $\tilde{M}$ point by relations

$$\tilde{\bar{e}}_1^* = (1 - z\tilde{k}_1)\tilde{\bar{e}}_1, \quad \tilde{\bar{e}}_2^* = \bar{e}_2, \quad \tilde{\bar{e}}_3^{*0} = \tilde{\bar{e}}_3^0 ,$$

where $\tilde{k}_1$ has the (8) form in which only g_1 is replaced by

$$\tilde{g}_1 = g_1(\alpha_1^1)^2 + (\alpha_1^3)^2 , \qquad (12)$$

the curvature of the curve remaining the same.

4. The unit deviation of the normal vectors.

In the last part of the paper we determine a decomposition of the unit deviation vector with respect to the initial Darboux frame, which characterizes the transversal deformation of the bar by the (3) relations.

Let $\bar{n}$ be the unit vector normal to the plane $(\tilde{M};\bar{e}_3^0,\tilde{e}_3^0)$. We can take $\bar{n} = \bar{e}_2^0$ and let $\bar{a} = \bar{e}_3^0 \times \bar{e}_2^0 = -\mu\bar{e}_1$, $(\mu>0)$; decomposing the $\tilde{e}_3^0$ vector in the basis $(\bar{e}_3^0,\bar{a})$ of the E^2 euclidean space, containing the vectors of the Π plane, we find

$$\tilde{\bar{e}}_3^0 = \cos\theta\ \bar{e}_3^0 + \sin\theta\ (\bar{n}\times\bar{e}_3^0), \qquad (13)$$

where θ is the angle of the unit vectors $\bar{e}_3^0$ and $\tilde{e}_3^0$.

This angle can be considered as rotation angle in the section plane of bar and we notice it is the same with the angle of the tangent vectors to the Γ_1 and $\tilde{\Gamma}_1$ curves at the M and $\tilde{M}$ points.

Generally, the rotation is called moderate if $\theta \leq 20^0$; in this case the error is smaller than 0,06 [Batoz - 1977] for the approximations $\cos\theta \simeq 1$ and $\sin\theta \simeq \theta$. Thus, for the moderate rotations, the (13) relation becomes

$$\tilde{\bar{e}}_3^0 = \bar{e}_3^0 + \theta(\bar{e}_2^0 \times \bar{e}_3^0) \qquad (13')$$

and constitutes an approximate writing (with θ expressed in radians) of the deformation of the normal vector to the middle surface of the curved bar.

But in (13') we have a vectorial product of unit vectors which is also unitary, so that we must have the condition

(6)

$\|\mu \bar{e}_1\| = 1$, which gives the value $\mu = \frac{1}{\sqrt{g_1}}$. We obtain now the relations

$$\tilde{e}_3^o = \cos\theta \bar{e}_3^o + \sin\theta \frac{1}{\sqrt{g_1}} \bar{e}_1 \qquad (14)$$

and

$$\bar{w} = (\cos\theta - 1)\bar{e}_3^o + \sin\theta \frac{1}{\sqrt{g_1}} \bar{e}_1 , \qquad (15)$$

because $\bar{w}$ is the difference $\tilde{e}_3^o - \bar{e}_3^o$.

Comparing the decompositions (14) and (9), we obtain the relation

$$\operatorname{tg}\theta = -\frac{1}{\sqrt{g_1}} \cdot \frac{\alpha_1^3}{\alpha_1^1} , \quad (g_1 > o), \qquad (16)$$

where we make use of the first relation (11). This one gives the rotation angle θ.

Also, according to the previous statements, we can compute too

$$\cos\theta = (\sqrt{g_1}/\sqrt{\tilde{g}_1})\alpha_1^1 , \quad \sin\theta = -\frac{1}{\sqrt{\tilde{g}_1}} \cdot \alpha_1^3$$

which permits to express the unit deviation vector as follows

$$\bar{w} = -\frac{1}{\sqrt{g_1 \tilde{g}_1}} \alpha_1^3 \bar{e}_1 + (-1 + \frac{g_1}{\sqrt{g_1 \tilde{g}_1}} \alpha_1^1)\tilde{e}_3^o , \qquad (17)$$

in which $\tilde{g}_1$, α_1^1, α_1^3 are given by (12) and (1o), respectively.

Now, the calculus of deformation in the P point is made replacing the vectors of the basis of Darboux frame at the previous formula with the expressions of the vectors $\bar{e}_1^{\#}$ given by the (2) relations.

References

1. Batoz, I.L.-1977, Analyse non lineaire des coques minces elastiques de formes arbitraires par elements triangulaires courbes; These Univ.Laval, Quebec.
2. Boja, N., Ivan, M., Brăiloiu, G.-1988, Sur une expression geometrique de l'état déformé pour les barres à la section courbe; Proceedings of the Second Symposium of Mathematics and its applications, Timişoara, 282-286.
3. Brink, K., Krätzig, W.B.- 1981 , Geometrically correct formulations for curved finite bar; element under large deformations; Rhur-Univ.Bochum, Tehn.Rep., 236-256.
4. Gioncu, V., Ivan, M.-1983, Bazele calculului structurilor la stabilitate, Timişoara, Ed.Facla.

KURUTZ, Márta[1]

ON STRUCTURAL AND MATERIAL STABILITY BY VISUAL PRESENTATION

INTERNATIONAL COLLOQUIUM
STABILITY OF STEEL STRUCTURES
BUDAPEST, HUNGARY, 1990
PRELIMINARY REPORT

Summary

This paper gives the visual presentation of the variational principles relating to the stability of structures having structural and material imperfections. The analysis relates both to the stability of the equilibrium state and that of the equilibrium paths, inclusing problems of not everywhere differentiable potential energy functionals.

1 Introduction

It is wellknown that a stationary value of the total potential energy with respect to the generalized coordinates (the displacement parameters) is necessary and sufficent for the equilibrium of the system. Furthermore, a complete relative minimum of the total potential energy with respect to the generalized coordinates is necessary and sufficent for the stability of an equilibrium state of the system.

From the first condition we obtain one or more relations between the load and the displacement parameters. These functions are the equilibrium paths and the intersection of them is the point of bifurcation separating the fundamental and the post-buckling equilibrium paths.

From the second condition we obtain the stability coefficients which help us to qualify not only the stability of the equilibrium states but the stability of the equilibrium paths. Since

[1]Associate professor, Department of Civil Engineering Mechanics, Technical University, Budapest

the stability coefficients depend both on the load and the displacement parameters, they vary continuously along the equilibrium paths.

The total potential energy, namely the displacement function in it, is usually approximated by Taylor or power series. If the second variation of it is positive semi-definite we have no immediate decision about the stability of the equilibrium state and higher terms of the Taylor expansion must be examined.

In certain cases the material behaviour or the structural configuration involve a non-smooth function as the total potential energy. In such a case we have to apply the term of subdifferential and the extremum terminology of the convex analysis.

In this paper the effect of several structural and material imperfections or irregularities leading also to non-smooth functions and the order of the relating approximations will be analysed by a schematic visual representation. The numerical analysis of the stability problems of the non-smooth mechanics will be published elsewhere.

2 Visualization of the stability analysis

In a very simple and schematic illustration Fig.1 shows the total potential energy in the coordinate system of the displacements and the strains. Since the potential energy functional is linear with respect to the displacement functions and in most cases it is higher order in term of the strain functions, it can be illustrated as a cylindrical surface.

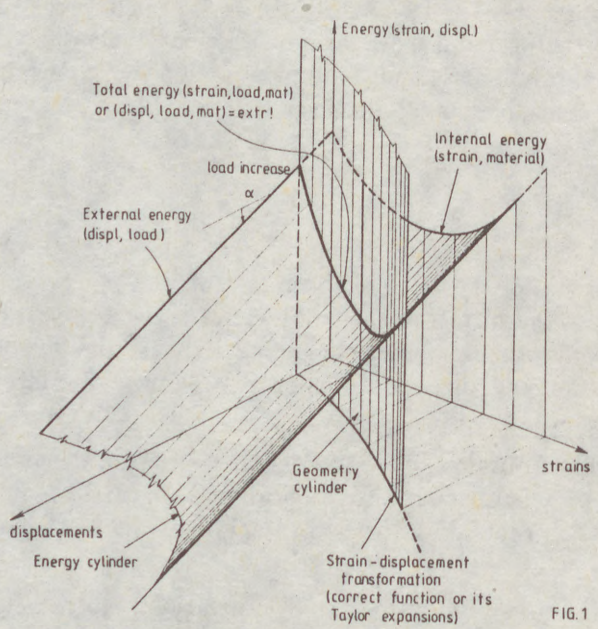

FIG. 1

Illustrating the potential energy with respect also to the loading parameter, we can say that the load level does not change the form of the energy surface in itself but it changes the position of it. Since in most problems of practical interest the total potential energy is a linear function of the chosen loading parameter, in the schematic illustration the load intensity can be signed by the slope angle of the axis of the parabolic cylinder. Increasing or decreasing the load parameter the slope angle of the axis of the cylinder will be increasad or decreased, respectively.

Thus, the section lines of the energy surface with the two vertical coordinate planes show the internal and the external energy functionals. Moreover, in the horizontal coordinate plane the transformations of the compatibility conditions can be visualised. Consequently, this transformation can illustrate the correct displacement function or its approximations, the chosen Taylor expansions, the (first, second os third) order of the analysis in itself. This transformation forms also a cylinder which has a vertical axis.

The final total potential energy function which contains the compatibility conditions of a chosen approximation level and whose extremum characteristics will qualify the stability of the equilibrium, can be seen as a curve in the space: as the section line of the two cylinders relating to the potential surface and the compatibility conditions.

It is easy to imagine that by changing the load parameter the cylinder of the energy surface will move while the cylinder of the geometry is motionless. This relative movement causes a change in the section line and consequently in its extrema which indicates a change in the state of the stability. So we can easy to identify and select the parameter of the critical load or to follow the paths of the equilibrium visually.

Through this schematic visual presentation we can easy to make perceptible all the other phenomena which can have ever any effect on the stability behaviour of a system. Namely, if the structural system or the material of it have any imperfection or irregularity, either the form or the position of the energy and geometry cylinder will change. For example, due to an imperfection in the strains the energy cylinder moves away in the direction of the strain axis while the geometry cylinder is fixed. A geometrical imperfection causes a change in the form of the geometry cylinder only. If there is any irregularity in the material characteristics or there is any change in the material behaviour in itself, the energy surface changes its form, causing sometimes the non-smooth character of the surface.

All the phenomena mentioned above can be analysed graphically. We can identify the stability of the equilibrium and the stability of the equilibrium paths at the same time visually. By changing the form of the surfaces or moving them relatively we can optimize the problem in a visual way.

3 Structural and material imperfections or irregularities

The visual presentation of stability problems will be introduced through the wellknown example of the hinged cantilever.

Fig.2 shows both the energy and the geometry cylinders of the perfect system in the case of a second order Taylor expansion. The load level is supposed to be lower than the critical one. The section line of the cylinders shows the stable state of the equilibrium at the mimimum point of $\vartheta=0$.

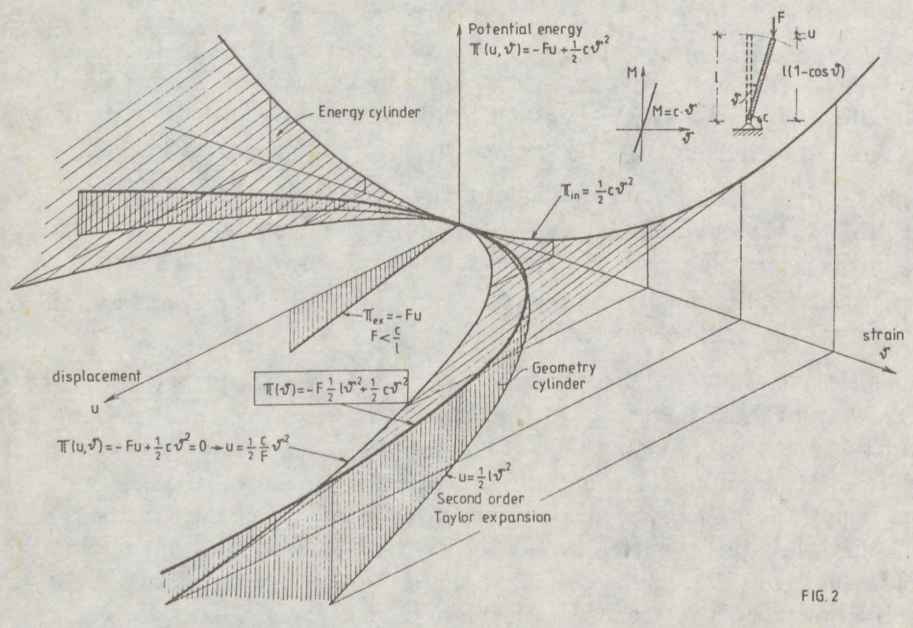

FIG. 2

Increasing the load the energy cylinder sinks, rotating through the axis of strains. Reaching the value of the critical load in Fig.3, the section line of the two cylinders coincides just in the horizontal coordinate plane so we have no information about the stability of the critical state. Consequently, to qualify the critical state we have to apply a higher order geometry approximation. Fig.3 shows also the fourth order Taylor expansion and the relating geometry cylinder, as well. The section line shows a character of minimum, thus the critical equilibrium state is stable at the point $\vartheta=0$.

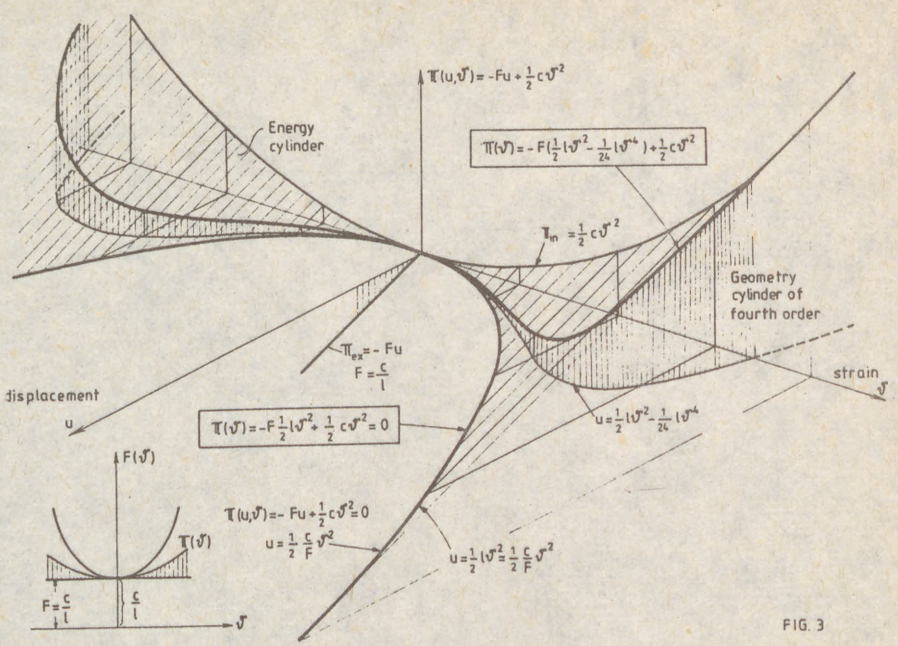

FIG. 3

Fig.4 shows a post-buckling state by sinking the energy surface due to a further load increasing. It is easy to prove visually that neither the stability of the post-buckling state can be analysed on the basis of a second order approximation. The fourth order section shows that the post-buckling equilibrium path is everywhere stable.

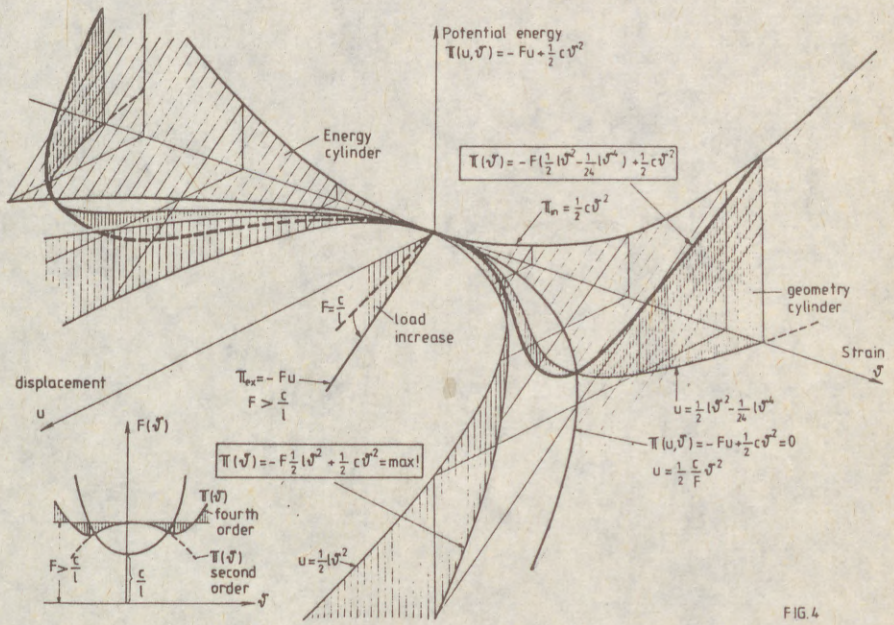

FIG. 4

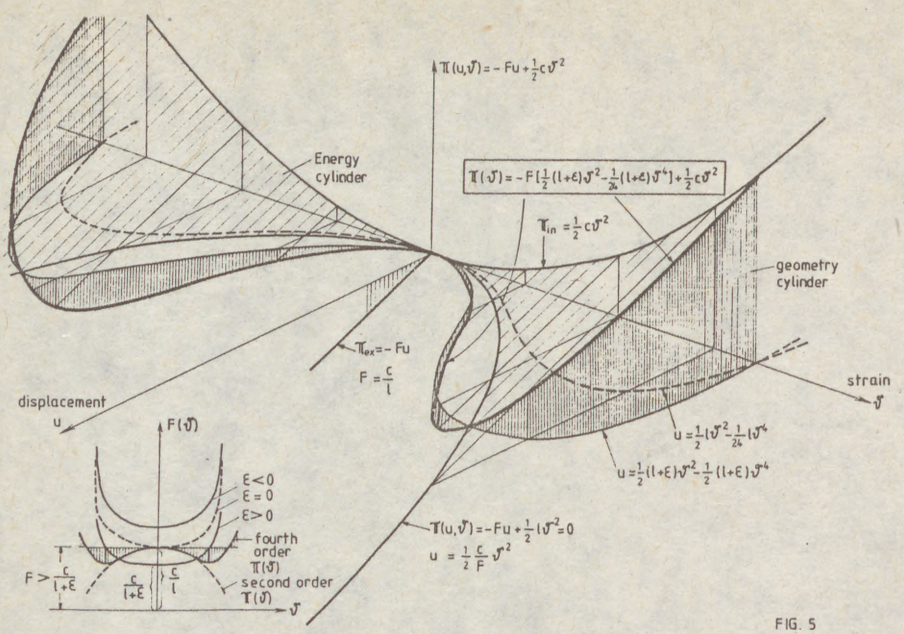

FIG. 5

Fig.5 illustrates a geometrical imperfection relating to the bar length. In this case the geometry cylinder is deformed causing an unstable state even at the critical load level of the perfect system. It can clearly be seen that on this load level the fundamental equilibrium path is unstable but the post-buckling one is stable.

Fig.6 shows a post-buckling state by a strain imperfection in the sense of an initial deviation. This type of imperfection moves the energy surface away along the strain axis, while the geometry cylinder is moveless, causing a stability situation of a non-symmetrical type.

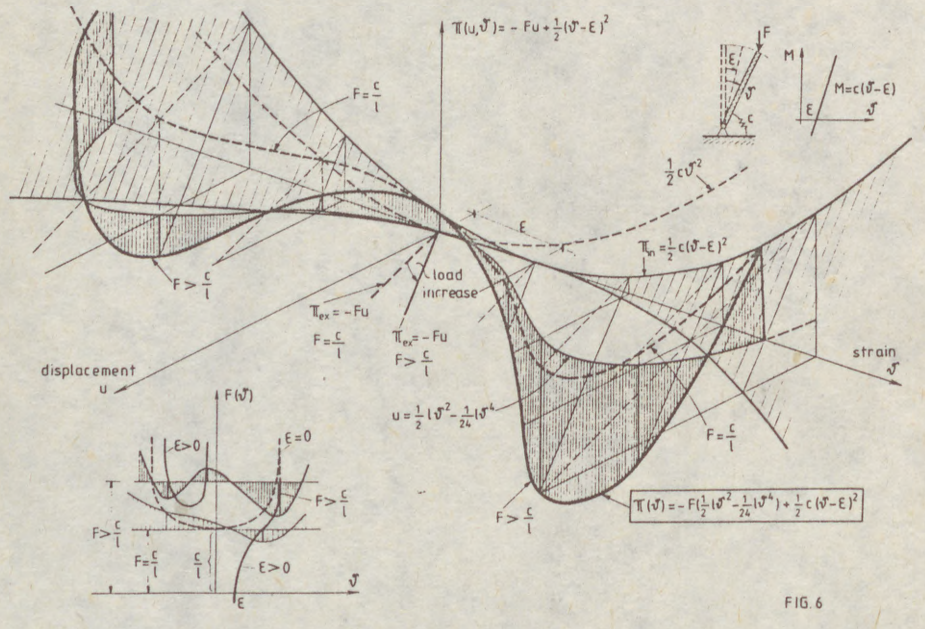

FIG. 6

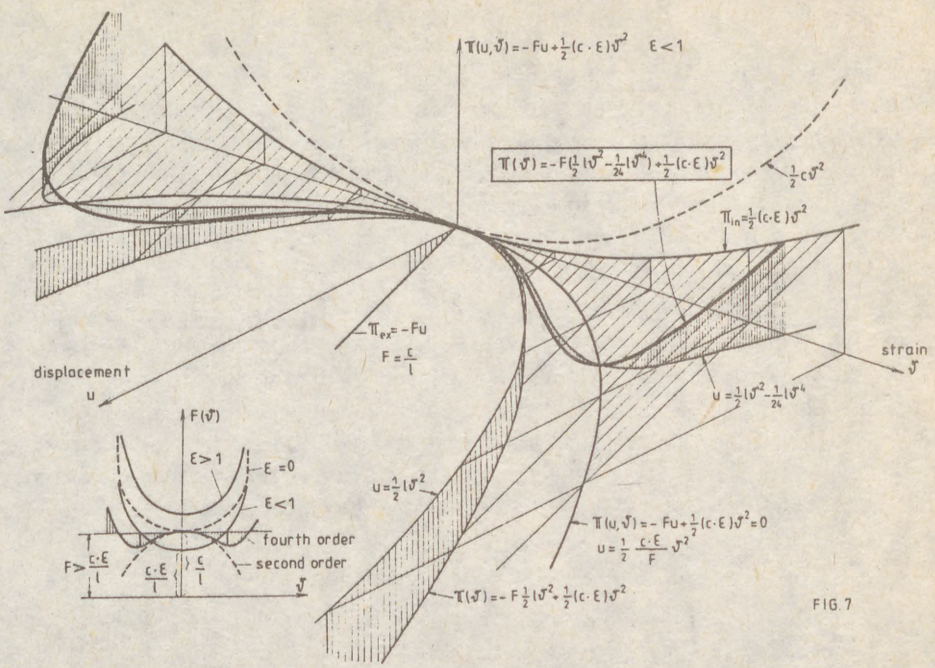

FIG. 7

Fig.7 illustrates an imperfection of material type, a strain-softening, which changes the form of the energy surface while the geometry cylinder is unchanged, leading to a post-buckling state. Concluded from this figure again we can state that on the basis of the fourth order geometry the equilibrium paths can satisfactorily be qualified.

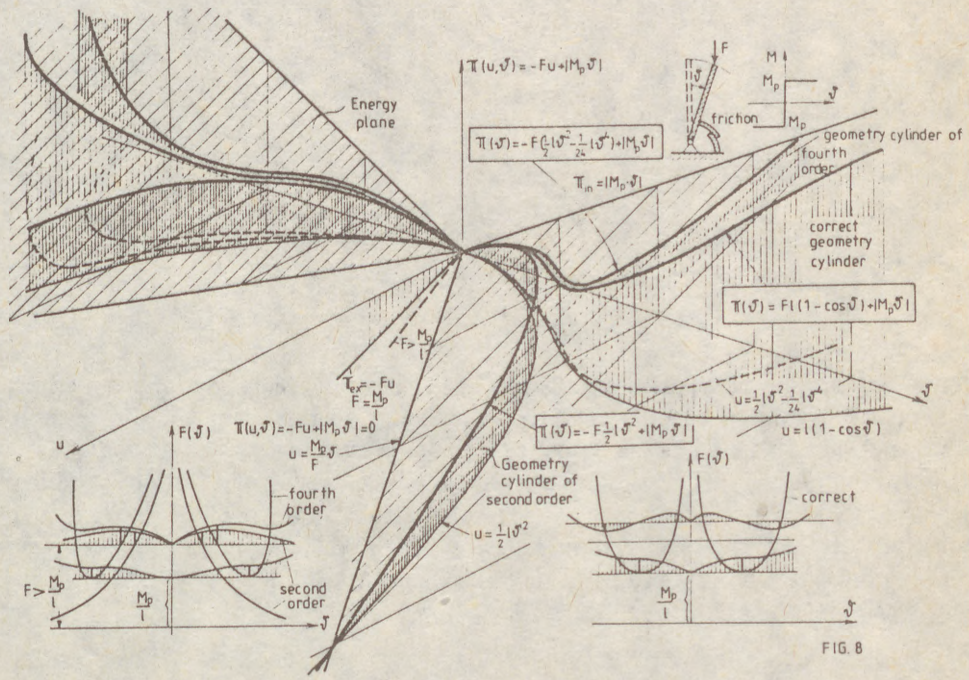

FIG. 8

Fig.8 indicates the rigid-plastic stability of the structure. In this case the cylinder of the energy degenerates: it consists of two planes having a break along their section line, causing the non-smoothness of the energy functional. It is easy to identify that the primary equilibrium path at the point of $\hat{\vartheta}=0$ is always stable undependently on the value of the load, but the secondary equilibrium path is unstable in any cases of the approximation level by small values of $\hat{\vartheta}$. Fig.8 shows the correct solution on the basis of the correct displacement function, as well.

If there is a strain imperfection in the case of the rigid-plastic material, the plane of the energy surface moves away along the strain axis in Fig.9, consequently the symmetry of the equilibrium paths disappears. The correct solution relates to the stable equilibrium state supposing the load to be under its critical value. The dotted line denotes a post-buckling case due to a load increase. In any cases the function of the section line is not everywhere differentiable just as in the following example, in the case of the so-called locking structures which can form a very important family of the stability problems.

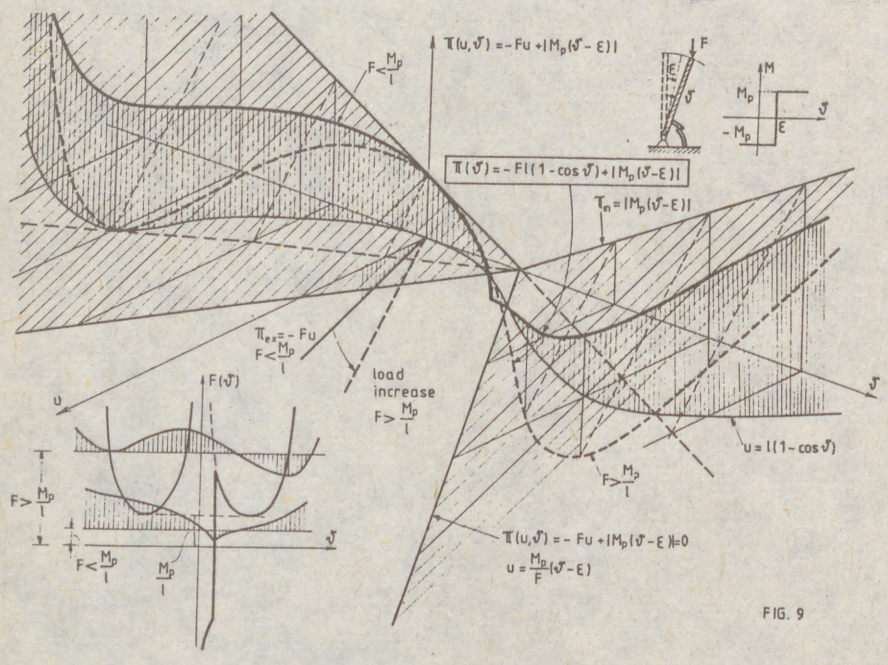

FIG. 9

Remaining at the rigid-plastic problems Fig.10 shows a case of a small imperfection of locking type relating to the strains. Here the energy surface also will be degenerated: it consists of thre planes while the geometry cylinder is unchanged. The section line is a non-smooth function, it contains non-differentiable points. Using the term of subdifferential we can describe the stability behaviour mathematically in a perfect way. We can identify visually that the primary equilibrium path at the point $\hat{\vartheta}=0$ is unstable but the post-buckling path at the point of the locking limit is always stable.

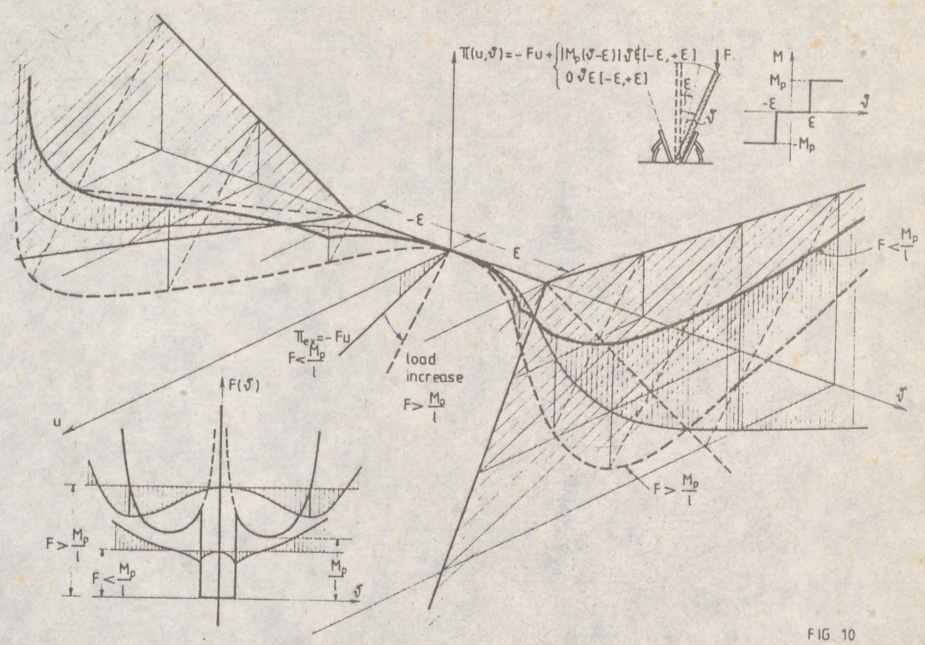

FIG. 10

Similar behaviour can be find in the case of a locking-elastic structure. Here we have to draw the attention to the fact that the locking structures or a locking joint in a structure can be very dangerous in the point of view of the stability. Namely, in this case the initial state is always unstable and the first deflections occur very quickly and rapidly. The systematical elaboration of the stability of the family of the locking structures is just going on and will soon be reported.

References

THOMPSON, J.M.T., HUNT, G.W. (1973): *A general theory of elastic stability* Wiley, London.

KOLLÁR, L. et al (to be published): *Special problems of structural stability* Akademiai Kiado, Budapest, (in Hungarian).

PANAGIOTOPOULOS, P.D. (1985): *Inequality problems in mechanics and applications. Convex and nonconvex energy functions* Birkhauser, Basel.

KURUTZ, M. (1987): *Analysis of generalized conditional joints as subdifferential constitutive models* Mech. of Struct. and Mach. **15** (2), 123-151

(1)

MILCHEV, Ewgeni

A GENERAL NUMERICAL METHOD FOR PLATES, MEMBERS WITH THIN-WALLED OPEN CROSS SECTIONS AND SHELLS STABILITY PROBLEMS

INTERNATIONAL COLLOQUIUM
STABILITY OF STEEL STRUCTURES
BUDAPEST, HUNGARY, 1990
PRELIMINARY REPORT

Summary:

The subject matter of this method is geometrical nonlinearity and buckling behavior of structural members limited to an intermediate class of deformations. For straight bars the kinematic relations used here are of the form $\varepsilon = u' + 1/2(w')^2$; $k = -w''$ The geometrical nonlinearity is taken into account step-by-step with not more then four linear solutions made with the usual programs based on the finite element method. Throughout the whole calculation process the stiffness matrix is unchanged. The user can solve all kinds of one- and two-dimensional structures with any kinds of boundary conditions, subjected to any kinds of loadings. Very important especially for shells is the possibility to prove their buckling behavior when they have initial imperfections in the geometry. The final results are all internal forces and displacements in every node of the mesh by geometrical nonlinearity and the critical value of the applied load.

Nowadays in every developed country the civil engineer can resolve his plane or space structural problems with sufficiently powerful programs based on the finite element method. Most of these programs have also great possibilities for solving quite difficult structural dynamics problems connected with wind or earthquake loads. It seems really strange that very few of these

---

Assistent Professor of Civil Engineering Centre of Electronics in Civil Engineering and Building Industry Sofia - 1000, Lenin sq. 6

powerful programs have modules for reasearching buckling problems or calculating structures by geometrical nonlinearity. For two dimensional structuctures we have not information that any such programpackage exists. So our basic goal was to develop such a numerical method for these two problems which uses existing powerful programs for finite elements in the range of linear mechanics. Of course,the more types of structures can be treated withit,the closer we will come to attaining our goals.

For plane frames structures this goal was realized some years ago (see [1]). In this paper the same idea is developed for all structures mentioned in the title.

So now let us look at a ractangular plane finite element which can belong to any two dimensional structure (plates, members with thin-walled open cross sections or shells) subjected to any kind of loading. The element on figure 1 is in equilibrium from the view point of linear mechanics and all internal forces and displasements of the four nodes are obtained on this base. For sake of simplicity, only the membrane forces (Nxi and Nyi) and the displacements (Ui,Vi,Wi) where i= 1÷4 are drawn on the figure.

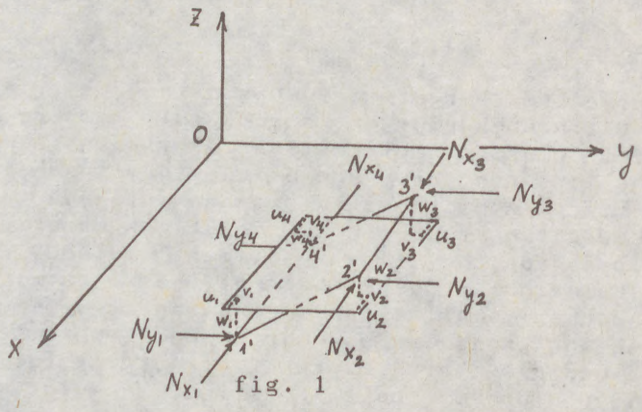

fig. 1

Let us try now to obtain in what kind of equilibrium is the finite element on fig. 1 with the help of wellknown criteria from physics. For this purpose the structure must be subjected only to the membrane forces and we give it a very small and possible displacement. Let this displacement be the same as that which the structure obtained by the load for wich we try its kind of equilibrium.In accordance with the criteria:

1) If the work done from the moments second order is enough to remove the structure in a slightly deformed configuration-the load has critical value.

2) If the structure subjected to the moments second order ret turns to its initial configuration we say that the equilibrium is stable.

3) If the structure deforms more and more it is in an unstable equilibrium.

(3)

The moments second order Mxi,Myi,Mzi are obtained from the membrane forces Nxi,Nyi and the displacements Ui,Vi,Wi. Again for simplicitis sake in the next text we shall discuss only the work done from the bending moments Mxi and Myi although Mzi which bends the element in its own plane has for members with thin-walled open cross sections the same importance as Mxi and Myi.

The problem of obtaining the final values of the displacements Ui,Vi,Wi is resolved step by step with linear statical solutions of the undeformed structure subjected only to the moments second order Mxi,Myi,Mzi. As the first step we calculate the structure for the moments which are obtained from the membrane forces Nxi,Nyi and the displacements Ui,Vi,Wi received from the real external load. As the second step we calculate the structure for the moments from the same membrane forces Nxi,Nyi but the displacements Ui',Vi',Wi' are obtained in the first step. In the same manner we have to do three, maximum four, steps to receive the final solution. It gives us two main results:

1) The kind of equilibrium;stable,unstable or critical
2) The internal forces and displacements by geometrical nonlinearity.

Of course the rectangular plane finite element on fig.1 taken from different zones of the structure can be deformed and subjected to different kinds of combinations. The analysis shows that all the combinations can be grouped in two main cases:

1) The nodes membrane forces* subjected one of the element's sides have opposite signs /that means the side is subjected either to compression or to extension/ and their values are different (see fig. 2).

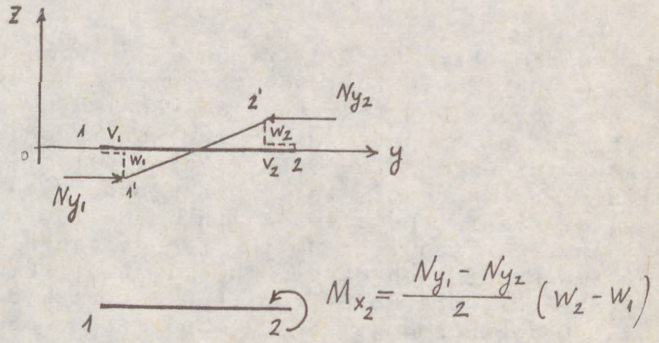

fig. 2

Now we do the moment equilibrium equation for node 2 and obtain the moment Mx1. Obviously from the moment equation for node 1 we can obtain the moment Mx2. Both moments,as it can be seen, do the same work. So it is of no importance which of the

moments we take into account. In the same manner we calculate the moments second order for the other sides of the element. All of them are either compressed or extended.

2) The element is subjected to shear forces see (fig. 3) In this case all membrane forces to which the element is subjected are equal one to another and on every element's side they have the same signs. This is true if the element is quadratic. If not /in exclusive cases/, the ratio between the two side's lengths of the rectangular element must be not bigger than 2.0, and we have to work with the average diagonal membrane force. So an element subjected to shears can be treated as an element subjected to compression or extention but in its diagonal directions.

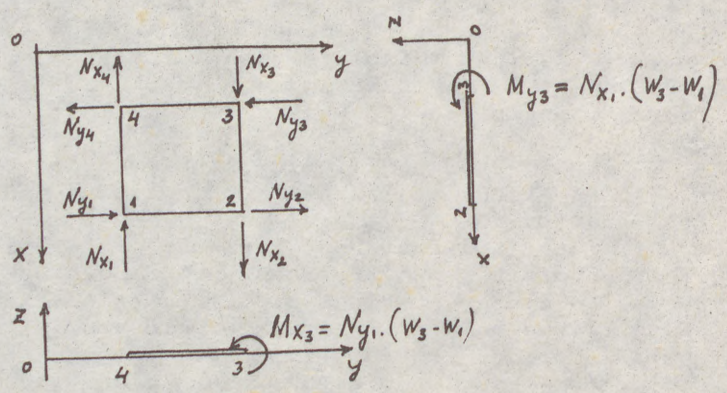

fig. 3

At the same time the difference between this case and the previous one is as follows: the work done by the compression membrane forces on the one diagonal of the element has the opposite sign compared with the work done by the extensive membrane forces on the other diagonal of the element. The physical relevance of this phenomenon is that by the critical values of shaers the element /the same is for the whole structure/ can be in equlibrium in two eigenvalue modes which are mirror images of each other. The first of these modes we obtain if we take the work done from the moments second order on the diagonal between nodes 1 and 3. The second mode we obtain if we take the work done from the moments second order on the diagonal between nodes 2 and 4.

On the basis of this simple algorithm we developed a program module for calculating the moments second order /Mxi,Myi,Mzi/ for every node of the structure and for every itteration step.

---

* Again for simplicity we shall deal now only with the bending of the side 1 2 outside the element's plane.

(5)

It was inserted in an usual program for linear statical calculations based on the finite element method with plane rectangular elements. A large number of examples for plates with different boundary conditions and loadings were calculated.The same was done for members with thin-walled open cross sections. For such members without an axis of symmetry we obtain the smallest critical value of the load for which the structure buckles in combined /bending and twisting/ eigenvalue.

In the field of shells we calculated cylindrical and conical shells with and without initial geometrical imperfections. Especially for cylinders we received results which are compared with the results of Koiter's analysis (see fig.4).

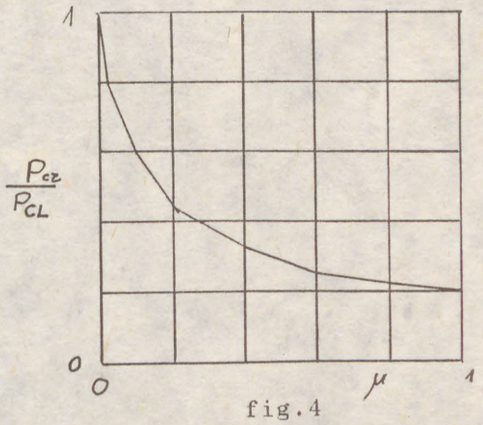

fig.4

μ is the ractio of imperfection amplitude to shell-wall thickness.

Concluding remarks

A general numerical method was developed for geometrical nonlinearity and buckling behavior of two-dimentional structures /plates, members with thin-walled open cross sections and shells/. Practical numerical calculations are very easy to realize for two reasons:

1) The method can use as a main calculator on every step every traditional program for finite elements based on the linear mechanics

2) The algorithm for the program-modul which have to be inserted in the traditional programs is very simple.

3) Outside its general possibilties for perfect structures the method can be used for researching geometrical nonlinearity and buckling bechavior for shells with initial imperfections.

References

[1] Milchev,E.M.: A Numerical Method for Solving Geometrical Nonlinear Elastic Frames and their Structural Stability with Computers. Thesis-Sofia 1976.
[2] Kollar and Dulacska: Buckling of Shells for Engineers Budapest 1984.
[3] Brush,D. and Almroth,B.: Buckling of Bars,Plates and Shells. McGraw Hill 1975.

(1)
POLYAK V.S. (1)

DESIGN CONCEPTS FOR PRECISION METAL STRUCTURES WITH DEFORMATION LIMITATIONS PLAYING A LEADING ROLE IN THEIR SHAPE FORMATION

INTERNATIONAL COLLOQUIUM
STABILITY OF STEEL STRUCTURES
BUDAPEST, HUNGARY, 1990
PRELIMINARY REPORT

Summary: Precision structures are called such structures for which limitation of deformation and shape changing is of decisive importance. Precision structures are characterized by some specific requirements to the marginal state when for the decisive violation a functional failure is taken, i.e. the reduction of the functional efficiency below the predetermined level under bearing capacity observing condition. Precision structures have their own requirements to a load, structural shape formation, materials, loaded structure behaviour, fabrication, erection, etc. Main aspects and principles of this new type of metal structures design are given in the report.

Problems of precision metal structures shape formation are basically new and have no analogues not only in the science of civil engineering but in the sciences dealing with mechanical engineering as well. It may be explained by the following reasons. The first reason lies in the fact that the deformativity took a primary position at development of structural shapes, which involved the problem of precision and, as a result, creation of a new class of precision structures (constructions). The second one lies in the fact that acquaintance with the practice of precision structures of various types development and ways of their structural shapes progress allows to define their effective shape formation as synthesizing of shape-stabilized systems with the given deformation law. Here the shape-stabilization is not static,

(1) Dr. Sc. (Eng.), Department Chief of TSNIIProektstalkonstruktsiya named after Melnikov

(2)

but a dynamic process of operational variations of the stressed-strained state of the structure. The third reason is formulation of the shape-stabilized systems synthesis problems as problems of precision structures optimization in terms of functional efficiency.

Giving the shape-stabilization the meaning of the structural characteristic, we define it as an artificially organized ability of the structure to maintain geometrical relationships for a group of typical structural nodal points under loading conditions.

Isolation of the precision structures into a separate class of building structures allows to oppose it to the existing classification of conventional building structures.

This isolation involves unification of structures of various types on the basis of their shape formation ideological unity, i.e. the precision is considered as a shape forming category - a decisive condition of designing.

Having in mind both a bearing capacity and a deformativity the structural solution is defined as a set of geometrical parameters: a span, a height and a rigidity. These parameters define also the volume of the metal consumed. Hence, there exists a relation of the above mentioned parameters at which the boundary conditions for the bearing capacity and for the deformativity are realized simultaneously at the threshold of applicability. It is suggested to consider this relation as a threshold of precision. Any building structure for which the relation of the above mentioned parameters exceeds this threshold shifts into the class of precision structures. If we use the term "theoretical characteristic of deflection" introduced by Streletsky N. and Streletsky D. (Streletsky, 1964 / 1 /), then the boundary condition of the structure transition to the precision structures category may be written as follows:

$$\lambda_{T\Delta} \leq \frac{E K \Delta_{np}}{R'' \nu m L},$$

where $\lambda_{T\Delta}$ is a theoretical characteristic of the deflection, E is a Young modulus, R'' is the proof strength of the material, K and m are the coefficients of working conditions and failure-free operations with the material; Δ_{np} and L are the limiting deflection and the structure span, ν is a coefficient characterizing the reduction of total stresses in the case of sole proof loads acting without taking into account any overloading factors.

An idea about the quantitative character of the phenomenon may be found on the example of such simple structures as beams or trusses (Table 1). As it is seen from this Table, the prevailing of the limiting state concerning deformativity, even for such simple conventional structures, may be found somewhere very close to the boundaries prescribed by the

(3)
Building Codes.

The analysis of the known progressive ideas of conventional metal structures shape formation reflecting the main point of the search of the best structural solution based on limiting states of the 1st group conditions (bearing capacity), from the point of view of their serviceability, when overcoming some technical violations, characteristic for the precision structures, shows not only their small efficiency, in this case, but also some negative effect from their realization.

Table 1. The precision threshold for beams

Structure	Load type	Structure type and height-to-span relation	Limiting relative deflection (a threshold)
A single-span beam with a constant height and rigidity	concentrated	beam, 1/20	1/450
		truss, 1/10	1/900
	uniformly distributed	beam, 1/20	1/360
		truss, 1/10	1/720
A multi-span beam with a constant height and rigidity	uniformly distributed	beam, 1/20	1/1200
		truss, 1/10	1/2400
A cantilever beam with a constant height and rigidity	concentrated	beam, 1/20	1/125
		truss, 1/10	1/250
	uniformly distributed	beam, 1/20	1/300
		truss, 1/10	1/600

According to all above mentioned, the main principles of the precision metal structures shape formation as shape-stabilized systems have been formulated based on the assumption of the problems of shape formation as problems of structures with given properties synthesis.

The 1st principle. When the decisive limiting state of the structure is the state according to the level of functional efficiency, then the best solution lies in the development of a shape-stabilized system, which is able to adapt to any effects in the process of operation in such a way that the structure deformation does not cause the efficiency reduction (the principle of adaptation to effects).

Adaptation of the system means the provision of the stability of certain relations between the displacements of some nodal points of the structure under changing of this structure stressed state conditions.

The possibility of this principle realization exists only because the requirements of the deformation law (the law of displacements relationship) are referred not to the system as

(4)
a whole, but only to a limited group of its points. Discrete (latticed) systems meet these requirements in the most degree, because continuous systems considerably restrict the possibility of directed force fluxes formation due to their continuum nature.

Stabilization of displacements according to their relations fits adequately to the limitation according to the law of derivative from displacements, which allows any scaling-up of the displacements themselves. In such a way, the above mentioned property allows to solve the main contradiction of the precision structures - the gap between the actual displacements and their admissible, from the point of view of functional efficiency, values.

The 2nd principle. If the search of structural solutions capable to adapt to the effects is carried out in the direction of a shape-stabilized system with a prescribed deformation law development, then the most effect may be obtained only at separation of the function by means of development of this system as a set of interconnected, but functionally different structural groups (the principle of functions separation).

The 3rd principle. The effect provided by the function separation principle will be more pronounced only when these functions realization by separate groups of structures is in a considerable extent localized, i.e. no substantial influence on other groups functioning is admitted (the principle of perturbations localization).

The 4th principle. When the shape-stabilized system is solved as a set of some functional structural groups, increasing in general the volume and the overall dimensions of the structure, which permits to improve the compactness of the construction, it is necessary to arrange these groups of structures in the same spatial volume (the principle of spacial compatibility).

The directive methods of shape formation allowing to realize the above mentioned principles are formulated on the basis of the structural analysis according to its typical structural shape, which enables to reveal the mechanism of structural damages and, as a result, the structure does not satisfy the predetermined conditions on operation.

In general, the spectrum of functional connections between separate functional groups of structures /FGS/, forming a precision structure, is comprehensively described by three types of connections: a) connections transmitting the forces /CF/; b) connections causing the distortion of geometrical shapes /CS/; c) connections causing the FGS position as a rigid body changing /CP/. Analysis of these connections permits to find a number of relationship:

- connections of CF type are always "directed" to FGS, playing a role of a supporting group and are an indispensable

(5)

indication of the structure existance stipulated by its geometrical invariability;

- connections of the CP type are always "directed" opposite to CF and are also an indispensable indication of the structure existance;
- connections of the CS type may have an arbitrary "direction" and be absent as well;
- connections of the CF and CP types form two equilink chains of a closed type, changing of the link CF_1 causes a respective changes of the link CP_1 and vica versa;
- connections of the CS type do not form a continuous chain and may be of a discrete and localized character.

Here, the term "direction" characterises solely a causely-consequential relationship between FGS, but never the direction of actual forces or displacements.

The mechanism of the phenomenon is essentially characterised by interaction of inner functional connections, inherent to one or another structural diagram. Changing the structural diagram by means of increasing the order of multilinking and determining for each FGS a set of connections of a certain type and a "direction", one may control the process of structural damages appearing. In this case, the equations of coupling chains may be used as criterial conditions.

Let's demonstrate the efficiency of application of the above mentioned design concepts of the precision metal structures at the example of reflectors of large radio astronomical radio telescopes being a complex three-dimensional latticed structure with a degree of statical indeterminace of about some thousands and their mass and dimensions being quite competitive with the conventional building structures: their overall dimensions are about dozens of meters and masses are about hundreds of tonnes. In spite of the specific character of shape formation, reflectors, as many other antenna-type structures, are referred to building structures. Their design is based on the well-known principles of structural science and production methods; traditional methods of structural mechanics, building materials and range of products, well-known solutions of structural steelworks (beams, trusses, joints and connections), methods of their fabrication and erection are used. However, such their peculiarities as mobility with inclinations to the horizon and exclusively stringent limitations on structural shape maintaining (2-3 orders exceeding the values specified in the Building Codes), verify the fact that these structures are referred to the class of precision structures, that is why they cannot be designed by traditional methods and require new design concepts (Polyak, Bervalds, 1989 / 2 /).

A two-member model is the lowest, not adopted to the problems of shape-stabilization, a trivial model of a reflector, where the reflecting surface may be considered as the first member, and the reflector frame as the second one. A coupling chain

(6)
equation is as follows:

$$f_{\Sigma}^2 = \sum_i (f_н)_i^2 + \sum_j [f_д(CS)]_j^2 ,$$

where $(f_н)_i$ are initial, and $[f_д(CS)]_j$ are deformation parameters of distortion of the reflecting surface contour, appearing as a result of CS functional connections interaction.

Minimization f_{Σ} possibilities in a two-member structure are considerably limited, because decreasing of any component f is restricted by one or another technical contradiction. They are as follows: unconformity of the required initial precision of the shape, corresponding to the 6th quality level according to ISO, and limiting tolerances specified by the Building Codes, but under the 13th quality level; the gap between the admissible (according to the effective behaviour at the given wave-length - shape distortions should not exceed 1/16 of the shape) and realized weight deformations of the structures inclined to the horizon; unconformity of the requirement of optimal conditions of the reflector frame supporting and the local perturbations due to reactive forces action in the places of engagement of the reflector; alternativity of the methods of the reflector initial precision improvement and mass decreasing as well as labour input reduction at the frame fabrication and erection, etc.

All these contradictions are solved on the basis of the above mentioned directive methods of shape formation. In the brief report it is difficult to describe how these methods are realized in practice. Let's see the realization of these methods at the example of the third contradiction solving, First, let's dismember the reflector frame into two FGS. The first one shall provide a prescribed deformation law under the normal operational conditions, but already under optimal support conditions and give it a name of a shape forming structure (SFS). The second one takes the role of an intermediate member between SFS and all the rest FGS, exerting local influences on the frame. On the one hand, it shall provide optimal conditions for SFS supporting conditions and on the other hand - the engaging of the reflector to the rotation device at simultaneous taking the whole effect from the local influences. Let's give this group the name of the intermediate structure (IS). Connection of SFS and IS shall be performed in such a way that any IS deformation caused only changing of SFS position without distortion of its shape. In other words, we realize one of the directive methods of the shape formation, involving introduction of the intermediate FGS into the CS member, the role of which plays IS, which transforms this member into a two-member CS-CP. As the base model for the shape-stabilized reflector which may solve all above mentioned technical contradictions, may serve a six-member, in the equation of the coupling chain of which enter already only three terms, unlike the two-member, where the number of terms

(7)
in the equation exceeds seven.

It should be noted that there are various ways of these contradictions overcoming. For example, the second contradiction may be solved not by introduction of the intermediate group, but by SFS transformation, giving it such a form at which the shape stabilization is achieved by means of an optimized choice of topology, geometry and rigidity distribution according to the functional efficiency criterion. In this case topology shall provide a control (at the design stage) at the mechanical compliance of SFS joints. That means that the new SFS structure results in the transformation of propriet SFS connections of CS type into connections of CP type.

The following results show the efficiency of the above described concept of the precision structures designing: the distortions of the reflecting surface contour of the 64-m reflector at its inclination to the horizon, wind effects and temperature influences did not exceed 0.5 mm, whereas the respective displacements exceeded 40 mm. In the 32-m reflector the deformational distortions were limited within 0.1 mm.

References

I. Стрелецкий Н.С., Стрелецкий Д.Н. Проектирование и изготовление экономичных металлических конструкций.- Москва: Стройиздат, 1964.
2. Поляк В.С., Бервалдс Э.Я. Прецизионные конструкции зеркальных радиотелескопов: Опыт создания, проблемы анализа и синтеза. - Рига: Зинатне, 1989.

(1)
RAITHEL, Aldo (1)
AUGENTI, Nicola (2)

INFLUENCE OF THE IMPERFECTIONS ON STABILITY PROBLEMS

INTERNATIONAL COLLOQUIUM
STABILITY OF STEEL STRUCTURES
BUDAPEST, HUNGARY, 1990
PRELIMINARY REPORT

Summary: First of all we want to remind you of the influence the imperfections can have on the behaviour of the ideal systems in the problems joined to the equilibrium stability. In particular nothing new comes out in relation to the well known cases of limit load and of symmetric buckling load (stable or unstable) of which we only mention the results of simple models. As for what concerns the asymmetric buckling load (stable-unstable) we'll show the different influence that has the sign of the imperfection that is to say the softening or the hardening of the structure depends on that sign. In the field in which there is an increasing hardening we define as "characteristic imperfection" the imperfection value, $\Delta=\Delta^*$, to which the highest values of the initial tangent stiffness as well as of the limit load correspond. Elementary models to which we refer in the text have been studied through an energetic method.We omit writing here the mathematic developments carried out, however, with great care.

1-INTRODUCTION: It is common knowledge the imperfection, that are introduced into the models to simulate in a more realistic way the structural behaviour, can modify, sometimes substantially, the equilibrium laws. In this report such laws are represen

(1) Professor of Structural Engineering, Naples University
(2) Professor of Structural Stability, Naples University

(2)

ted in a single diagram known as "characteristic curve" that permits to reduce complicated systems to systems with and only degree of freedom. On the axis of ordinates there is represented a common multiplier of loads, F, whose meaning is "generalized load"; on the axis of abscissas we represent the "generalized displacement", f, whose product by F is the potential of external loads: Fxf= -U.

2-POSSIBLE STRUCTURAL BEHAVIOUR: We'll describe here the influence the imperfections have on the behaviour of the corresponding perfect systems.

a)-Cases of limit load - The law F-f, representing in this case only the natural path, reaches a maximum corresponding to a limit state. Possible imperfections can cause only quantity modifications but not quality modifications (for example: Δ= length variation of the rise in an arch with a low rise/span ratio).

b)-Cases of symmetric buckling load - The imperfections can be divided into two classes. The imperfections that cause only a modification of the buckling load value but not the disappearing of the bifurcation point are less important (for example: Δ= length variation of Eulero's bar). The imperfections that make the bifurcation point disappear giving rise to the only natural equilibrium path are, instead, quite important. This path will always be stable in case of symmetric stable buckling load; it will be, instead, as in the problem of limit load in case of symmetric unstable buckling load (for example hinged rigid bar with elastic angular or linear restraint).

c)-Cases of asymmetric buckling load - Even though we don't exclude that such a type of buckling can take place for structurally symmetric systems too, we'll consider here the well-known possibility it can concern structurally asymmetric systems like, for instance, the well-known one represented in the following fig. 2. As for these systems, contrarily to what noticed in the b) case, the imperfections cannot be divided into two different classes because they produce always analogous modifications of the structural behaviour. Such modifications consist in changing the case of asymmetric buckling load into limit load even if, in case of asymmetric buckling load, it is always linked to ideal elastic-rigid schematizations of the model (as widely explained by the Authors elsewhere) and in the elastic reality it is must be replaced by a natural path with a limit state. As for these models the effect of the imperfections can: degrade the above mentioned natural path (soften-

(3)

ing), and in this case we will speak of "concordant imperfections", or produce an improvement (hardening) of the structural behaviour and in this case we will speak of "discordant imperfections"; such improvement (hardening) can be noted to a certain value, $\Delta=\Delta^*$, nomed "characteristic imperfection", beyond which the model, now substantially changed as to the initial one, presents again a tendency to degradation. This behaviour is represented in fig. 1 referring to a general case

fig. 1

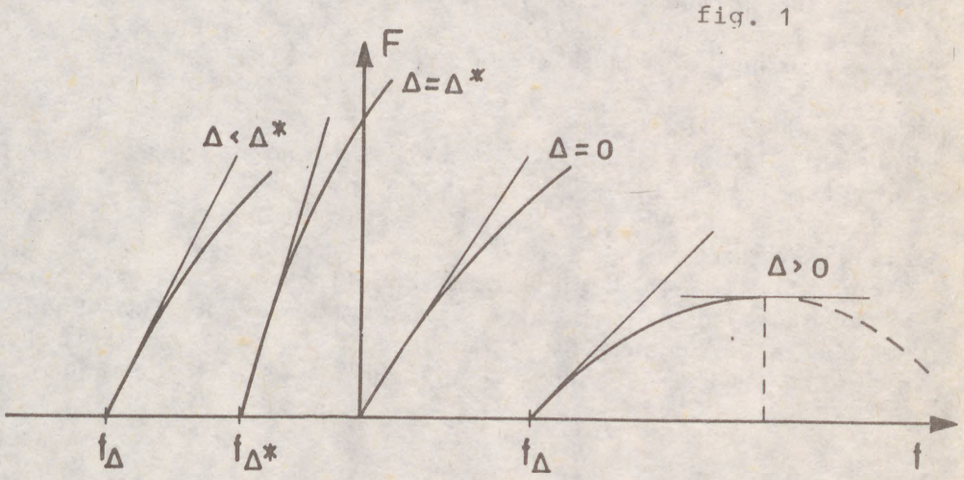

and in fig. 2 referring to a particular model in which every hypothesis about rigid bars is excluded ($\rho\neq\infty$); the positive imperfection corresponds to a shorter lenght of the bar.
The diagram represents the characteristic curves of models whose dimensionless imperfection, $\bar{\Delta}=\Delta/l$, has been varied between (-0.065, +0.045) and can be read as the abscissa in the initial points of the single caracteristic curves. A more immediate reading of how a limit load can vary with the imperfection is given in fig. 3 in which we have considered the different ratio between the stiffnesses of the two bars. In particular we see that, by varying the characteristic imperfection, we can reach nearly egual maximum F_{lim} values for models whose ρ values are very different. The extensive research done into models whose inclined bar sets itself with various angles (ε= angle between bars) has led, for ρ=100, to the results represented in the diagram of fig. 4. In particular we notice, besides, that the influence of the imperfections disappears as the angle between the bars increases.

(4)

3-CONCLUSIONS: What above said, shows the different way we must consider the imperfections in the field of the different problems of structural instability. In particular we have pointed out that the imperfections, generally harmful, can produce, as for the systems with an asymmetric behaviour, an improvement of the structural characteristics and that it happens when they are "discordant", that is when they are such as to oppose the natural deformation modalities of perfect system. It follows that in these cases the imperfections can be utilized using the same technique as the one of the "impressed distortions" with the limitations due to the necessity of keeping, appropriately, away from the "characteristic value".

ESSENTIAL REFERENCES

- Thompson J.M.T. & Hunt G.: (1973) "A general theory of elastic stability"; Wiley & Sons, London.
- Koiter W.T.: (1979) "Teory of elastic stability"; Mc Graw Hill, New York.
- Gioncu I.: (1984) "Teoria comportarii critice si postcritice a structurilor elastice"; Editura Academiei R.S.R., Bucaresti.
- Raithel A. & Augenti N. & Nicolosi G.: (1989) "Equilibrio e stabilità delle strutture elastiche"; E.S.A.C. Cremonese,Rome.

(5)

Fig. 2

Fig. 3

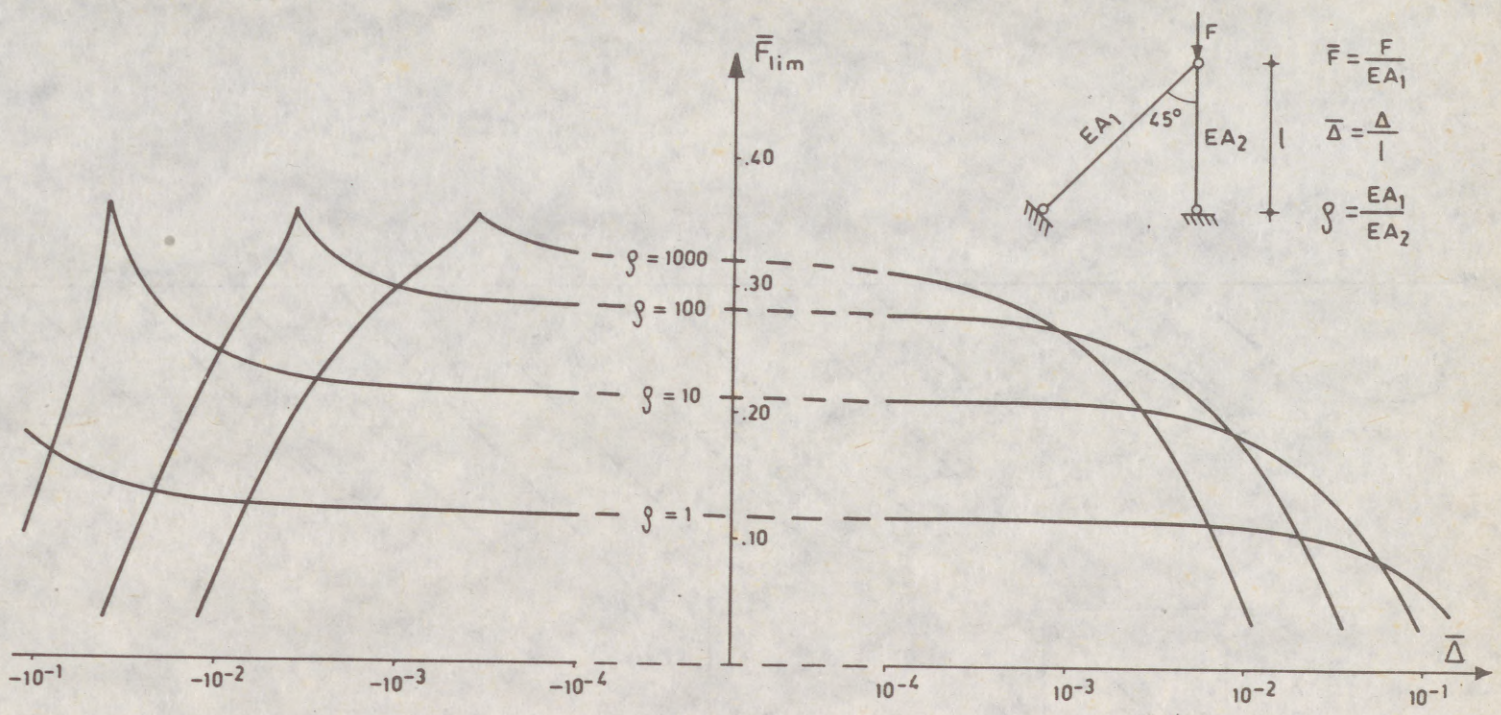
$\bar{F}_{lim}$
.40
.30
.20
.10
$\varrho = 1000$
$\varrho = 100$
$\varrho = 10$
$\varrho = 1$
-10^{-1}
-10^{-2}
-10^{-3}
-10^{-4}
10^{-4}
10^{-3}
10^{-2}
10^{-1}
$\bar{\Delta}$
F
EA_1
45°
EA_2
l
$\bar{F} = \frac{F}{EA_1}$
$\bar{\Delta} = \frac{\Delta}{l}$
$\varrho = \frac{EA_1}{EA_2}$

(6)

(7)

(7)

$\vartheta = 100$

Fig. 4

(1)

RAITHEL, ALDO (1)
NICOLOSI, GIULIO (1)

THE LOCAL POTENTIAL ENERGY IN THE POST-CRITICAL BEHAVIOUR

INTERNATIONAL COLLOQUIUM
STABILITY OF STEEL STRUCTURES
BUDAPEST, HUNGARY, 1990
PRELIMINARY REPORT

Summary :

With reference to elastic-rigid models of real structures, holonomic systems, the problem of buckling is considered and, in the aim to discuss about the critical status and the quality of equilibrium in its near field, the energetic procedure is considered.

Therefore the Total Potential Energy (T.P.E.) of the model is expressed and is shown how, to individuate and analize a critical status, may be useful to refer directly to a part of it, which is told Local Potential Energy (L.P.E.), so to avoid from the beginning the confusion, sometimes misleading, that in applications may occur beetween the two energies.

At the end a simple structure is considered to exemplify the previous results.

1. INTRODUCTION

Let C_o be the initial (or natural) state of an holonomic system built up with rigid bodies and linear elastic restraints whose number, and position, is assumed sufficient to balance the n degree of freedoms of the model.

The generic state that the model may assume is defined by the state-vector

$$q = [q_1 \ldots, q_i, \ldots . q_n] \qquad (1)$$

beeing q_i the lagrangians by which depend :

1. The strain and stress vectors having as components the strains and the stresses in the generic elastic restraint, be j, whose stiffness is told K_j :

$$s_j = s_j (\ldots . q_i \ldots .) \quad ; \quad S_j = K_j s_j \qquad j = 1 \ldots m \qquad (2)$$

---

(1) Professor of Structural Enginering, Naples University

2. The displacement-vector whose components are assumed to be the displacements corresponding to the external forces $F_k = \lambda_k F$

$$f_k = f_k (\ldots q_i \ldots) \qquad k=1\ldots s \qquad (3)$$

In the generic state C the T.P.E. is usually defined as :

$$T = \frac{1}{2} \sum_j S_j s_j - \sum_k F_k f_k = \frac{1}{2} \sum_j K_j s_j^2 - F_k \sum \lambda_k f_k = W - F f \qquad (4)$$

having called the strain energy W and assumed

$$f = \sum_k \lambda_k f_k \qquad (5)$$

as generalized displacement.

A general possible state C of the system, defined by a set of q_i, is notoriously an equilibrium one , C_e, if T is stationary otherwise if are satisfied the equations

$$T_i = W_i - F f_i = \emptyset \qquad i = 1\ldots n \qquad (6)$$

where the footer i means a derivative respect to q_i.

The proceding set of equations (6) describes at once the natural path and, if existing, secundary paths of equilibrium so that the complete solution of the problem may be investigated.

If the system possesses only the natural path the whole set of the q_i is active along it and no bifurcation may occur. In the aim to investigate just about bifurcation it is supposed that the lagrangians q_i may be divided in two subsets (at least)

$$q_r \quad r = 1,\ldots n' \quad ; \quad q_s \quad s = 1,..n'' \quad ; \quad n = n' + n'' \qquad (7)$$

so that :

- the first one describe the natural path satisfyng the equations

$$T_r = W_r - F f_r = \emptyset \qquad r = 1\ldots.n' \qquad (8)$$

obtained by the (6) imposing $q_s = \emptyset$.

- the two subsets together (that is the $\ldots q_i \ldots$) satisfy the sistem (6) giving solutions , secundary paths, that take their origins by states of the natural path for particular values of the loading parameter F the lowest of which is the critical value F_{crit}.

2. THE LOCAL POTENTIAL ENERGY

If the natural path is supposed already known, and the equilibrium state where the bifurcation occurs is told $C^*(...q^*...)$, the T.P.E. in any state C distinct from the natural ones may be written as follows

$$T(C) = T(C^*) + \sum S_j^* s_j + W - F^* f - (F - F^*)(f+f) \qquad (9)$$

In this formula the symbols have the following meaning :

- $T(C^*)$, S_j^*, F^* are, respectively, the values of the T.P.E., stresses in elastic restraints, generalized force, in C^*.
- s_j, f represent the strains and the generalized displacement in the transfer $C^* \Rightarrow C$.
- $W = \sum_j K_j s_j^2 / 2$ is the strain-energy connected to the s_j only.

Taking note of the fact that $T(C^*)$ and $F^* f$ are constant, and therefore inessential, the residual terms of (9) define the Local Potential Energy, L.P.E.

$$L(C) = L_s + W - F (f + f) \qquad (10)$$

where

$$L_s = \sum S_j^* s_j \qquad (11)$$

The (10) is currently used to individuate eigenvalues and eigenvectors in the hypotesis :

a) that F coincide with F^*, and therefore F f disappears beeing a constant
b) that precritical deformation is negligeable ($q_r = 0$) and therefore the strains s_j and the displacement f depend exclusively on the subset q_s ($C_o \equiv C^*$).

In such way the (10) becomes

$$L(C) = L_s + W - F^* f \qquad (12)$$

and terms of first order are absent; they might appear only in L_s and $F^* f$ but their algebraic sum is zero (principle of virtual work) beeing C^* an equilibrium state. Moreover L_s is usually zero when the lagrangians $..q_s..$ are chosen in such way that the strains s_j are zero in the elements where are present the pre-critical stresses S_j^* ; in this event the (12) becomes simply :

$$L(C) = W - F^* f \qquad (13)$$

The formal coincidence of the (4), T.P.E., and of the (13), L.P.E., justifies the confusion that often arises between the two energies specially when hypotesis of infinite stiffness are done.

3. SYMMETRIC BUCKLING

Except that for a quantitative error, which is introduced by the hypotesis b) of the former paragraph 2, the formulas (12) or (13) give results generally satisfactory and can be used to individuate eigenvalues (and eigenvectors) and to investigate about the quality of equilibrium at branching points.

The first aim is pursued in a analysis where only second order terms of L, set equal to zero, are considered. Well known properties of quadratic forms lead to the linear homogeneous system

$$L_s^{(2)} = \emptyset \qquad s = 1....n" \qquad (14)$$

which solves the problem.

The second aim, quality of equilibrium at critical state, is successively solved by the examen of the sign of the further terms of L , and precisely $L^{(4)}$($L^{(3)} = \emptyset$ because of the existence of two specular secundary paths whose energetical content must be the same).

At last we will enphatize that previous results are satisfactory[1] because of the fact that C_o (initial unstressed state) and C^* (bifurcation state) can, both, be of equilibrium when subjected to the same loads.

4. ASYMMETRIC BUCKLING

The possibility of previous behaviour is lost when the change of sign of the displacements leads to states in which the strains, and therefore $\mathcal{W}$, assume different values (terms of even order in the strain, and odd order in $\mathcal{W}$, by example $\mathcal{W}^{(3)}$,appear). This event surely occurs in the range of non symmetric structures and, for particular deformed shapes, also in that of symmetric ones so that an asymmetric buckling (stable-unstable) may be expected.

To discuss about the existence of the bifurcation attention is now called back to the (12) whose validity dependes just on the assumption that the bifurcation state exists and that, in it, the precritical deformation $(...q_r...)$ is negligeable to the extent that C_o and C^* may be considered coincident. Such a coincidence is, in reality, assumed from two different view-points :

- the well known geometrical one, thinking that the deformations due to the $...q_s...$ are nearly the same if expressed starting from the state C_o or C^*.
- the implicit one that the state C^* might be of equilibrium even though the $...q_r...$were assumed non zero.

Just because of the asymmetric behaviour formerly considered this last assumption is not true; as soon as the $...q_r...$ arise (for example they may represent axial desplacements) the $...q_s...$ must be present (and they may represent transversal displacements) though equilibrium may be respected. The complete set of lagrangians draws then the natural path and, on it, a limit point may exist.

---

(1) In the sense that the quality of the phenomena is respected in spite of the preliminary assumption b).

The difficulties connected to the investigation about the limit point widely justify the "asymptotic hipoteses" of infinite stiffness often assumed. Such hipoteses, in fact, may effectively make zero a subset of lagrangians so that the others may play the role of post-critical ones.

If in this way a critical value of F^* is found (stable-unstable because of the existence of odd energetical terms) it is proved that in the real problem a limit load exists. As surely results

$$F_{lim} < F^* \qquad (15)$$

the research, generally, must be continued to specify the real equilibrium (natural) path.

5. REMARKS

With reference to the previous shown necessity, research of the complete solution, the system (6) and therefore the T.P.E. may be utilized.

A lot of difficulties may be avoided making use of the L.P.E. computed, this time, not starting from an equilibrium state where, arbitrarily, some lagrangian,...q_s...,are assumed to be zero. In such conditions whichever

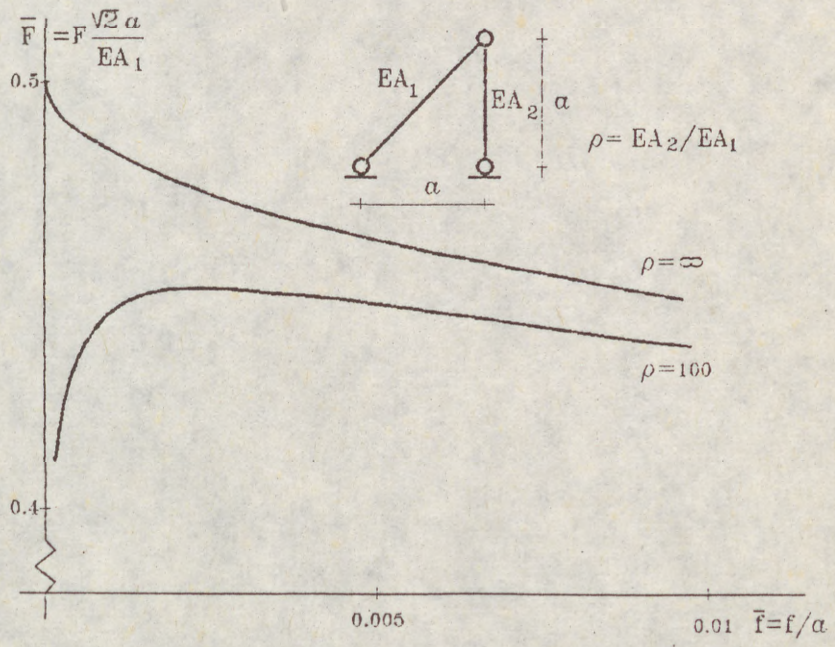

state, geometrically compatible with the remaining lagrangians (...q_r...),may be assumed to express, from it, the L.P.E. ; because of the

fact that such state is not an equilibrium one L ,also assuming an expression similar to the (12)

$$L = L_s + \mathcal{W} - F \not{\ell} \ , \qquad (16)$$

includes surely in L_s $(= \sum S_j s_j)$ first order terms[1].

Imposing the condition that L be stationary, a system of non homogeneous equations is found.

In this way the solution, beeing approximate too, has the advantage to lead to n'' equations instead of n (in the following example $n'' = 1$ while $n = 2$) .

In figure, where a well known example is considered, the asymptotic case of asymmetric buckling (upper curve) and the results obtained with the use of the (16) (curve below) are plotted.

REFERENCES

[1] W.T.Koiter, Teory of Elastic Stability, Mc Graw Hill, New York 1979
[2] H.H.E. leipholz, Stability theory , Academic Press, New York 1970
[3] A.raithel, N.Augenti,G.Nicolosi, Equilibrio e Stabilita' delle Strutture Elastiche, Cremonese Roma 1989

---

(1) When L is expressed (trough the $\ldots q_s \ldots$) the usual assumption that the reference state and C_o geometrically coincide is assumed.

(1)
SADOVSKÝ, Zoltán (1)

BUCKLING OF PLATES SUBJECTED TO COMPRESSION AT ELEVATED TEMPERATURES

INTERNATIONAL COLLOQUIUM
STABILITY OF STEEL STRUCTURES
BUDAPEST, HUNGARY, 1990
PRELIMINARY REPORT

Summary: Starting from the equations of uncoupled thermoelasticity the influence of a nonuniformly elevated temperature upon the critical compression buckling strength of plates is studied. The ranges of validity of the results obtained via the perturbation analysis are checked by means of a variational finite-difference method.

Introduction. Since the systematic exploatation of reference slenderness $\overline{\lambda}_p$

(1) $$\overline{\lambda}_p = \sqrt{f_y/\sigma_{cr}} = \sqrt{f_y/(k\sigma_E)} \quad \text{where} \quad \sigma_E = \frac{\pi^2 E t^2}{12(1-\nu^2)b^2}$$

for expressing the postbuckling strength of plates Dubas and Gehri 1986 the interest for the study of critical buckling strength again raises.

We consider a long plate uniformly compressed in a longitudinal direction x which is exposed to a temperature field $T = T(y)$ nonuniformly distributed in a transversal direction y ($y \in \langle 0, b \rangle$). The temperature is assumed not to raise above the threshold of the creep.

The equations of uncoupled thermoelasticity for the plate deflection w and Airy stress function Φ are (see e.g. Ogibalov Gribanov 1968)

(1) Senior research worker, Institute of Construction and Architecture of the Slovak Academy of Sciences,
842 20 Bratislava, ČSSR

$$(2)\quad \frac{t^3}{12(1-\nu^2)}\left\{\Delta(E\Delta w) - (1-\nu)\left[\frac{\partial^2}{\partial x^2}\left(E\frac{\partial w^2}{\partial y^2}\right)+\frac{\partial^2}{\partial y^2}\left(E\frac{\partial^2 w}{\partial x^2}\right) - 2\frac{\partial^2}{\partial x\partial y}\left(E\frac{\partial^2 w}{\partial x\partial y}\right)\right]\right\}$$

$$= t\left[\frac{\partial^2 w}{\partial x^2}\frac{\partial^2\Phi}{\partial y^2} + \frac{\partial^2 w}{\partial y^2}\frac{\partial^2\Phi}{\partial x^2} - 2\frac{\partial^2 w}{\partial x\partial y}\frac{\partial^2\Phi}{\partial x\partial y}\right],$$

$$(3)\quad \Delta\left(\frac{1}{E}\Delta\Phi\right) - (1+\nu)\left[\frac{\partial^2}{\partial x^2}\left(\frac{1}{E}\frac{\partial^2\Phi}{\partial y^2}\right)+\frac{\partial^2}{\partial y^2}\left(\frac{1}{E}\frac{\partial^2\Phi}{\partial x^2}\right) - 2\frac{\partial^2}{\partial x\partial y}\left(\frac{1}{E}\frac{\partial^2\Phi}{\partial x\partial y}\right)\right] = -\alpha_T\Delta T.$$

where the modulus of elasticity $E = E(^{o}t)$ is a function of the temperature ^{o}t, ν is Poisson's ratio, α_T the coefficient of thermal expansion and t the thickness of the plate. Since the plate is long, it suffices to study a part between two neighbouring nodal lines $x = 0, a$. The Airy stress function can be taken as a sum

$$(4)\quad \Phi = \Phi_T + \Phi_L$$

where the biharmonic function

$$(5)\quad \Phi_L = -p_L\frac{y^2}{2}$$

gives the load conditions and Φ_T satisfies

$$(6)\quad \Phi_{T,x} = \Phi_{T,xxx} = 0/_{x=0,a}\ .$$

The unloaded edges are assumed to be unrestrained which yields the boundary conditions

$$(7)\quad \Phi_T = \Phi_{T,y} = 0/_{y=0,b}.$$

As for the deflection w, the edges may be simply supported or clamped. The temperature field T we assume in the form

$$(8)\quad T(y) = \tau + \delta_1\cos\frac{\pi y}{b} + \delta_2\cos\frac{2\pi y}{b},$$

where δ_1, δ_2 are the parameters of skewsymmetric and symmetric perturbations, respectively, of the uniform temperature field given by the parameter τ .

Perturbation method. We employ variational forms of governing equations (2, 3). These can be obtained by multiplying (2) and (3) by test functions δw, $\delta\Phi$, respectively, which satisfy the same boundary conditions as w and Φ_T. Then integrating by parts we find

(3)

$$(9)\quad \frac{t^3}{12(1-\nu^2)} \int_0^b\int_0^a E(T)\left[\Delta w\Delta\delta w - (1-\nu)(w_{xx}\,\delta w_{yy} + w_{yy}\,\delta w_{xx} - 2\,w_{xy}\,\delta w_{xy})\right] dxdy$$

$$= -t \int_0^b\int_0^a \left[\Phi_{T,yy} w_x \delta w_x + \Phi_{T,xx} w_y \delta w_y - \Phi_{T,xy}(w_x \delta w_y + w_y \delta w_x)\right] dxdy$$

$$+ t\, p_L \int_0^b\int_0^a w_x \delta w_x \, dxdy,$$

$$(10)\quad \int_0^b\int_0^a \frac{1}{E(T)}\left[\Delta\Phi\Delta\delta\Phi - (1+\nu)\left(\Phi_{T,xx}\,\delta\Phi_{yy} + \Phi_{T,yy}\,\delta\Phi_{xx} - 2\,\Phi_{T,xy}\,\delta\Phi_{xy}\right)\right] dxdy$$

$$= -\alpha_T \int_0^b\int_0^a \Delta T\,\delta\Phi \, dxdy + p_L \int_0^b\int_0^a \frac{1}{E(T)}\,\delta\Phi_{yy}\, dxdy .$$

Now we introduce non-dimensional quantities

$$(11)\quad \alpha = \frac{a}{b},\ \bar{x} = \frac{x}{a},\ \bar{y} = \frac{y}{b},\ \bar{w} = \frac{w}{t},\ \bar{\Phi} = \frac{\Phi}{\sigma_E b^2},\ \bar{p}_L = \frac{p_L}{\sigma_E}$$

where σ_E is calculated with E corresponding to the uniform temperature field τ i.e.

$$(12)\quad \sigma_E = \frac{\pi^2 E(\tau)\, t^2}{12(1-\nu^2)\, b^2} .$$

In what follows we use only the non-dimensional form of the quantities (11) thereby, for simplicity, the bars over the symbols will be omitted.

Owing to the assumed temperature field (8) and boundary conditions (6,7) Φ_T is a function of y only. On seting

$$(13)\quad \Phi_T(x,y) = h(y), \qquad \delta\Phi(x,y) = \delta h(y),$$

we can find $h(y)$ in a form

$$(14)\quad h(y) = p_L\, h_L(y) + h_T(y)$$

where h_L, h_T are solutions of variational equations

$$(15)\quad \int_0^1 \frac{E(\tau)}{E(T)}\, h_{L,yy}\, \delta h_{yy}\, dy = \int_0^1 \frac{E(\tau)}{E(T)}\, \delta h_{yy}\, dy ,$$

and

$$(16)\quad \int_0^1 \frac{E(\tau)}{E(T)}\, h_{T,yy}\, \delta h_{yy}\, dy = -\alpha_T \frac{12(1-\nu^2)(b/t)^2}{\pi^2} \int_0^1 T_{yy}\, \delta h\, dy ,$$

respectively. The non-dimensional form of equilibrium equation (9) yields an eigenvalue problem

(4)

$$(17)\quad \frac{1}{\pi^4}\int_0^1\int_0^1 \frac{E(T)}{E(\tau)}\Big[\Big(\frac{1}{\alpha^2}w_{xx}+w_{yy}\Big)\Big(\frac{1}{\alpha^2}\delta w_{xx}+\delta w_{yy}\Big) - \frac{1-\nu}{\alpha^2}\left(w_{xx}\,\delta w_{yy}+w_{yy}\,\delta w_{xx}-2\,w_{xy}\,\delta w_{xy}\right)\Big]\,dxdy$$

$$+\frac{1}{\pi^2\alpha^2}\int_0^1\int_0^1 h_{T,yy}\,w_x\,\delta w_x\,dxdy - p_L\Big[\frac{1}{\pi^2\alpha^2}\int_0^1\int_0^1 (1-h_{L,yy})w_x\delta w_x\,dxdy\Big] = 0.$$

Equations (15-17) are a starting point of our perturbation analysis. Firstly, we expand $E(T)$, $1/E(T)$ in powers of the small parameter $\delta = (\delta_1,\delta_2)$

$$(18)\quad E(T) = E(\tau)\Big\{1+\frac{E'o_t(\tau)}{E(\tau)}\,T'_\delta(y)\delta+\ldots\Big\},$$

$$(19)\quad \frac{1}{E(T)} = \frac{1}{E(\tau)}\Big\{1-\frac{E'o_t(\tau)}{E(\tau)}\,T'_\delta(y)\delta+\ldots\Big\}$$

with

$$(20)\quad T'_\delta(y) = (\cos\pi y,\ \cos 2\pi y).$$

On employing boundary conditions (7) and introducing corresponding energy spaces, we subsequently obtain that h_L, h_T are of the order $O(|\delta|)$ and an operator equivalent to the equation (17) may be written as

$$(21)\quad (I+\delta M+\ldots)w - p_L\,(L+\delta N+\ldots)w = 0.$$

For $\delta=(0,0)$, there follows from (21) an equation

$$(22)\quad w - p_L\,Lw = 0$$

corresponding to the well known stability equation of thin elastic plate subjected to compression. Let us denote its critical buckling coefficient by p_{Lo} and the corresponding critical eigenvector φ_{cr}. A perturbation $p_{L\delta}$ of p_{Lo}, given by the equation (21), may be obtained by means of the classical perturbation theory. We treat (21) by a simple constructive approach following the proof of Lemma 2.1 Sadovský 1986 which employes the Liapunov-Schmidt reduction and the implicit function theorem. The resulting value $p_{L\delta}$ written up to the first order term in δ is

$$(23)\quad p_{L\delta} = p_{Lo} + \delta p_{Lo}\,((M - p_{Lo}\,N)\,\varphi_{cr}',\ \varphi_{cr}) + o(|\delta|).$$

where φ_{cr} satisfies $\|\varphi_{cr}\| = 1$ and

(5)

$$(24)\quad \|w\|^2 = \frac{1}{\pi^4}\int_0^1\int_0^1 \left(\frac{1}{\alpha^2} w_{xx} + w_{yy}\right)^2 dxdy ,$$

$$(25)\quad \delta(\underline{M}w, \delta w) = \frac{1}{\pi^4}\,\frac{E'o_t(\tau)}{E(\tau)} \int_0^1\int_0^1 T'_\delta(y)\delta\Big[\Big(\frac{1}{\alpha^2} w_{xx} + w_{yy}\Big)\Big(\frac{1}{\alpha^2}\delta w_{xx} + \delta w_{yy}\Big)$$

$$- \frac{1-\nu}{\alpha^2}\left(w_{xx}\delta w_{yy} + w_{yy}\delta w_{xx} - 2w_{xy}\delta w_{xy}\right)\Big] dxdy$$

$$-\alpha_T \frac{12(1-\nu^2)(b/t)^2}{\alpha^2\pi^4} \int_0^1\int_0^1 T'_\delta(y)\delta(w_x\delta w_x)\, dxdy,$$

$$(26)\quad \delta(Nw, \delta w) = \frac{1}{\pi^2\alpha^2}\,\frac{E'o_t(\tau)}{E(\tau)} \int_0^1\int_0^1 T'_\delta(y)\delta(w_x\delta w_x)\, dxdy.$$

Special case. On assuming that the plate is square and simply supported, we have

$$(27)\quad \alpha = 1, \quad p_{Lo} = 4, \quad \varphi_{cr} = \sin \pi x \sin \pi y.$$

Due to the symmetry of φ_{cr} the scalar product corresponding to δ_1 is zero, so the only first order contribution to $p_{L\delta}$ (23) is that one of δ_2. It can be easily calculated from (23), (25), (26) seting $T'_\delta(y)\delta = \delta_2 \cos 2\pi y$ on the right hand sides of (25), (26). Thus a simple approximate formula for $p_{L\delta}$ is obtained

$$(28)\quad p_{L\delta} \doteq 4 + \delta_2 \left\{ 2(1-\nu)\frac{E'o_t(\tau)}{E(\tau)} + \alpha_T \frac{6(1-\nu^2)}{\pi^2}(b/t)^2 \right\}.$$

In order to show a numerical results based upon (28) we take

$$(29)\quad \nu = 0.3, \quad \alpha_T = 0.000012\ (^oC)^{-1}.$$

Further, we assume $E(^ot)$ according to CTICM Provisions 1975 as

$$(30)\quad E(^ot) = E_o\left[1 + \frac{^ot}{A \ln(^ot/B)}\right], \qquad ^ot\ (^oC) > 0$$

$$E_o = 210 \text{ GPa}, \quad A = 2000, \quad B = 1100 .$$

Some of the calculated values of $p_{L\delta}$ (28) with τ, δ_2 given in ^oC are shown

(6)

$\tau = 100$:

$p_{L\delta}$ (28)	δ_2 = 40	20	0	-20	-40
b/t = 60	4.939	4.470	4.0	3.530	3.061
100	6.639	5.319		2.681	1.361

We see a high sensitivity of the critical buckling coefficient $p_{L\delta}$ to the parameter δ_2 of the symmetric perturbation of the uniform temperature field as well as its strong dependence upon the slenderness b/t. The influence of the level of the uniform temperature τ upon $p_{L\delta}$ is negligible: for τ =300, b/t =100 and δ_2 =-40 we obtain $p_{L\delta}$ =1.388.

Finite-difference check. The numerical results obtained by the perturbation analysis were checked by a variational finite- difference method applied to the equations (15 - 17). Equations were solved in a somewhat altered form, namely, the right hand side of equation (15) was transformed to

$$(31) \qquad \int_0^1 E(\tau)\,\frac{d^2}{dy^2}\left(\frac{1}{E(T)}\right)\delta h\,dy$$

and the second term of equation (17) containing mixed derivatives of w into:

$$(32) \qquad \frac{1-\nu}{\pi^4 \alpha^2 E(\tau)} \int_0^1\int_0^1 \frac{d\,E(T)}{dy}\left(w_{xx}\,\delta w_y + w_y\,\delta w_{xx}\right)dxdy$$

The following results, comparable with those ones presented in the foregoing section, are obtained for 5 x 5 unknowns on a quarter-plate

τ =100:

$p_{L\delta}$	δ_2 = 40	20	0	-20	-40
b/t = 60	4.922	4.467	4.002	3.527	3.042
100	6.542	5.298		2.656	1.265

We believe that the results justify a practical usefullnes of the approximate formula (28) in the displayed ranges of parameters. The value 4.002 of the buckling coefficient of a square plate in compression indicates the accuracy of the VFD results. In order to show that 5 x 5 unknowns are sufficient for $\delta_2 \neq 0$ as well, we computed $p_{L\delta}$ for b/t= 100, τ = 100, δ_2 = -40 on different meshes:

VFD	$p_{L\delta}$
5x5	1.26527
7x7	1.26825
9x9	1.26894

(7)

The influence of the skewsymmetric perturbation of uniform temperature field on $p_{L\delta}$ was studied on a halfplate with 5 x 9 unknowns. The value of $p_{L\delta} = 3.992$ for $b/t = 100$, $\tau = 100$, $\delta_1 = 40$ shows that it can be completely neglected.

Conclusions. A first order approximation to the perturbation of critical buckling load of a long plate subjected to compression with simply supported or clamped unrestrained unloaded edges, caused by the nonuniform temperature fields (8), was established in general terms.

The simple formula (28) obtained on evaluating the general expression (23) for the case of a simply supported square subplate showed that the critical buckling load is sensitive to the symmetric part of a nonuniform temperature field. The influence of its skewsymmetric part as well as the level of uniform temperature field (the averaged value) is negligible. As could be anticipated the decrease of the critical buckling load value takes place when the edges of the plate are less heated then its central parts. Another relevant parameter is that one of the plate slenderness.

References.

DUBAS, P. and GEHRI, E. /eds/ 1986: Behaviour and Design of Steel Plated Structures, ECCS-CECM-EKS, Zürich.

OGIBALOV, P.M. and GRIBANOV, V.F. 1968: Thermostability of Plates and Shells /in Russian/, Izd. Mosk. Univ. Moscow.

SADOVSKÝ, Z. 1986: Bifurcations near a multiple eigenvalue of the rectangular plate problem, Pr. of the Royal Society of Edinburgh, 103A, p. 35-62.

CTICM Prévision par le calcule du comportement au feu des structures en acier, 1975, Paris, CTICM.

(1)
SIDOROVITCH, Evgeni (1)

MULTIPARAMETRIC STABILITY AND POSTCRITICAL BEHAVIOUR OF NON-LINEAR SPACE STRUCTURES

INTERNATIONAL COLLOQUIUM
STABILITY OF STEEL STRUCTURES
BUDAPEST, HUNGARY, 1990
PRELIMINARY REPORT

Summary: The purpose of this report is to analyse the non-linear response and stability of various hyperstatic or hypostatic complex structural systems with large geometrical, material and constructive non-linearities. A structural system may be subjected to loading by several independent groups of external forces. The history of loading is supposed to be given definite. Some of elements or fragments of structural systems may be in a critical or postcritical equilibrium state and have zero or negative stiffness. Moreover, the zero stiffness of elements may be due to tension brace or push brace breaking and tension or compression failure of elements. The non-linear stability analysis purposes to obtain the ultimate equilibrium state characterized by the minimal critical load parameter value corresponding to the inferior ultimate or bifurcation point on the equilibrium state trajectory. A two-parametric loading of a gentle spherical dome truss has been analysed by the step-by-step method. The zone of stable and unstable equilibrium states have been derived. It has been ascertained that a one-sided unloading may cause instability in a stable loaded structure.

The non-linearities may be due to large displacements and large strains (geometrical non-linearity), non-linear and plastic material behaviour (material non-linearity), included or excluded unilateral constraints and other connections (constructive non-linearity). The destruction of several bars and other structural elements also causes non-linear response. In this report the all constructive non-linearities are considered to be special cases of the material non-linearity. In general case a material or constructive non-linearity may be described by an arbitrary function of the following type

---

(1) Assistant Professor of Structural Mechanics, Candidate of Science, Byelorussian Politechnical Institute

(2)
(fig. 1):

$$N = N (E) , \qquad (1)$$

where N and E are the total internal force and strain in a truss element, respectively. Thus, constructive non-linearity results the same effect as the material non-linearity. In the algorithm suggested the elements after destruction are supposed not to be restressed. However, the unilateral braces and others like conjonctions may be unloaded and reloaded. The strain of truss elements is calculated taking into account their lengths in the current equilibrium state and in the initial unloaded state:

$$E = L / L0 - 1 , \qquad (2)$$

where L is the current length and L0 is the initial length. The current truss element length is a function of nodal displacements:

$$L = L (V) , \qquad (3)$$

where V is the current nodal displacement vector. For a current equilibrium state the equilibrium equations are presented in the following form:

$$B N = Q , \qquad (4)$$

where B is the equilibrium matrix the elements of which depend on the nodal displacements, N is the internal force vector, and Q is the total external force vector.

So, taking into account the expression (1), (2), and (3) the non-linear equilibrium equations (4) are to be resolved with respect to the nodal displacements. The solution of the non- linear equation system is the main phase in the non-linear analysis. It is a method of parameter differentiation that is accepted for the solution of this problem. The parameter differentiation method reduces non-linear algebric or transcendental equations to ordinary differential equations which may be solved by a step-by-step method.

In that way the non-linear displacement equations (4) may be transformed into the linear algebraic equations with respect to displacement increments:

$$R U = P , \qquad (5)$$

where R is the tangent stiffness matrix of a structural system, U and P are the vectors of displacement increments and load increments, respectively. The step-by-step solution used permits to vary easily the structure loading character and history, and solve non-linear response and multiparametric stability problems. To increase the step-by-step solution accuracy, it is possible to use an integration method of high order accuracy or modified Newton iterations on every step.

The step-by-step method in the form (5) is applicable to

(3)

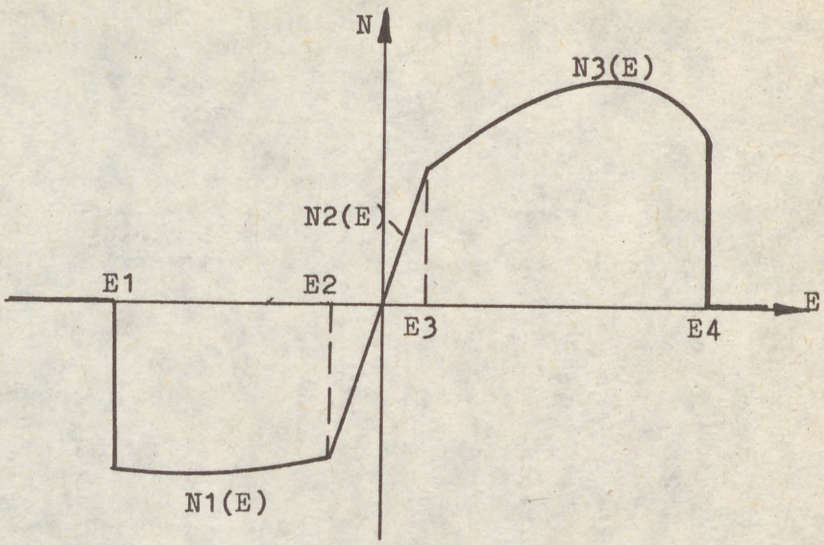
N
N3(E)
N2(E)
E1
E2
E3
E4
E
N1(E)

Fig. 1

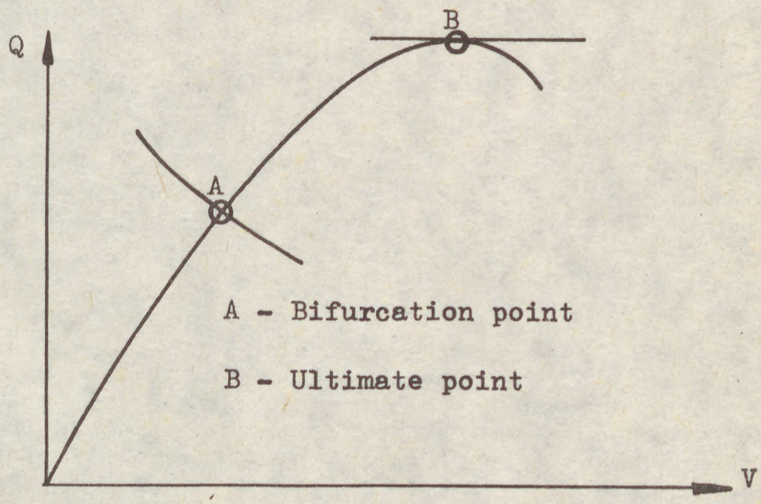
Q
B
A
A - Bifurcation point
B - Ultimate point
V

Fig. 2

(4)

the non-linear analysis of frame structures. In addition to the expression (1), a functional dependence is to be determined between bending moments and curvatures of sections:

$$M = M (C), \qquad (6)$$

where M and C are the vectors of the current bending moments and section curvatures, respectively. The elements of the frame stiffness matrix are calculated taking into account the transcendental functions caused by axial compressive or tensile internal forces.

The overall system of increment equations (5) is formed by the real finite element method procedure. The overall stiffness matrix is stored in the compact form. The solution of linear equations is obtained by the Cholesky square-root method. During the matrix factorization it is controled whether the current stiffness matrix is positive definite. The positive definition of the stiffness matrix confirms the structure equilibrium stability. In case of instability the current load step parameter is to be reduced, and the step-by-step procedure is continued until the critical load parameter value is calculated with a given accuracy.

To analyse the structure behaviour in the critical and postcritical equilibrium states the increment equations must be presented in the following form:

$$\begin{aligned} R\,U - P\,K &= 0 \\ U^T U + K^2 &= S^2 , \end{aligned} \qquad (7)$$

where K is the parameter in proportion to which the load increments are varied, S is an increment of the arc of the equilibrium state trajectory. In the equations (7) the load increment parameter K is an unknown variable. The trajectory arc increment S is the independent governing variable.

In the critical ultimate point of the equilibrium state trajectory (fig. 2) when

$$\mathrm{Det} (R) = 0 ,$$

the equations (7) have the definite solution, the load parameter increment K being equal to zero. In a postcritical point on the descending branch of the equilibrium state trajectory values of the load parameter increment are negative. Indefinite solutions take place in the bifurcation point where the trajectory has several branchs. The choice of a trajectory branch depends on supplementary conditions.

The suggested algorithm has been applied to a two-parametric loading of a gentle spherical dome truss composed with 110 bars, and 51 nodes including 20 supports. This structural system is 17 times hyperstatic. The system is subjected to an invariable dead load D1 and variable live loads SN1 and SN2 on

(5)

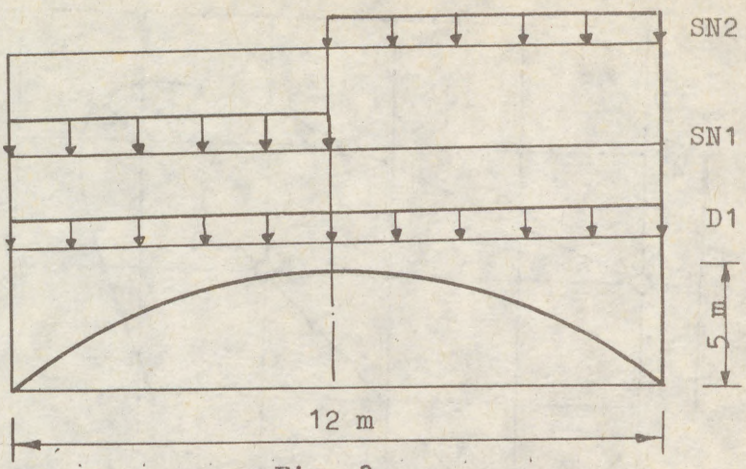

Fig. 3

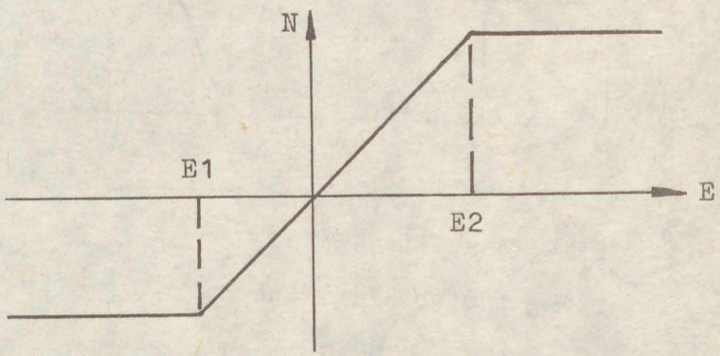

Fig. 4

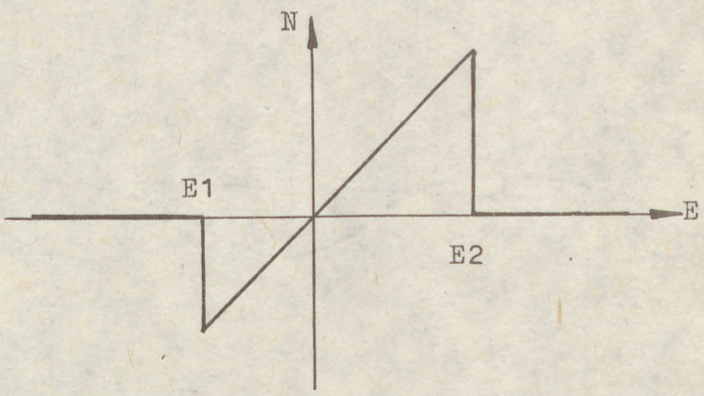

Fig. 5

(6)

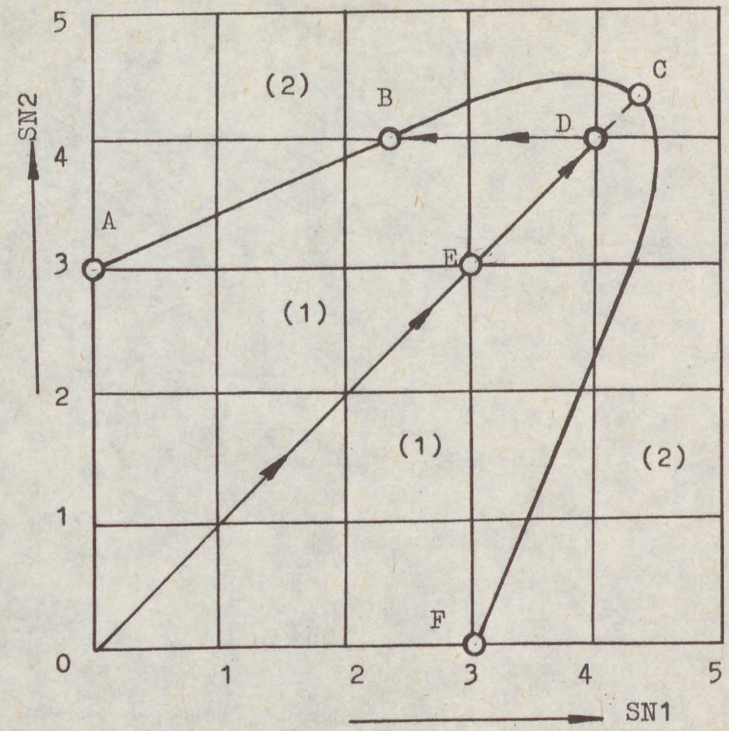

(1) _ Stability Zone

(2) _ Instability Zone

Fig. 6

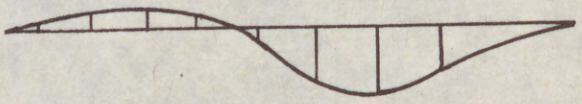

Fig. 7

(7)

both halves of the structure (fig. 3). The analysis of the dome truss has been accomplished taking into account the all non-linearities, truss element distruction included. Two stress-strain diagrams have been considered: elastic-plastic (fig.4) and elastic-destroyed (fig. 5). The difference of the values of the overall critical loads calculated for the two diagrams is negligible. The zone of the stable and unstable equilibrium states are represented in the figure 6. The boundary line ABCF determines the ultimate stable equilibrium states. The point A (or E) corresponds to the one-sided loading with the load SN2 (or SN1), only one truss element having been destroyed. The diagram of the total displacements in the state A is represented in the figure 7.

The point C corresponds to the symmetric live load (SN1+SN2), ten truss elements having been destroyed in this state. The total symmetric displacement diagram is given in the figure 8.

The zone ACFEA in the figure 6 embraces the formally stable equilibrium states. However, these stable equilibrium states are dangerous as an instability may be due to a non-symmetric unloading. For example, the way ODB corresponding to the symmetric loading (OD) and one-sided unloading (DB) causes instability in the point B. The displacement diagram for this point is given in the figure 9. Two truss elements have been destroyed in the state B, no destruction being in the state D.

So, non-linearly deformed and compressed space dome truss as well as geometrically non-linear suspended systems have a hightened sensibility to one-sided loadings.

Fig. 8

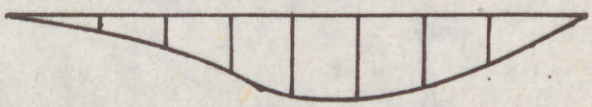

Fig. 9

(1)
SOBOTKA, Zdeněk (1)

STABILITY OF ORTHOTROPIC CYLINDRICAL TUBES AT THE THERMAL EFFECTS

INTERNATIONAL COLLOQUIUM
STABILITY OF STEEL STRUCTURES
BUDAPEST, HUNGARY, 1990
PRELIMINARY REPORT

Summary: The paper deals with the stability of the orthotropic viscoelastic tubes in the non-stationary temperature fields. There are on the whole three different thermal effects affecting the stability of the tubes, namely the direct thermoelastic effects, viscoelastic behaviour and the changes of mechanical parameters due to the temperature. It is assumed that the temperature varies linearly over the thickness of the tube. The author introduces the equivalent stresses, strains, displacements, internal forces and couples, pressures, loads and temperature in order to replace the time-varying relations by the equations of elasticity with the equivalent variables. In this manner, the author arrives at the separation of the solution with respect to the coordinates from that with respect to time. This leads to considerable simplification. The set of two non-linear differential equations is obtained, containing the equivalent stress function and displacement perpendicular to the tube axis. Finally, the formulae for the equivalent and actual time-dependent and temperature-dependent critical pressures are derived.

1. The Concept of Equivalent Variables

At high temperatures, the steel and other materials soften and the stability of tubes decreases. Many initially elastic materials become with increasing temperature viscoelastic. Their mechanical properties depend on temperature and time.

In order to simplify the analysis of structures with

(1) Scientific worker, Mathematical Institute of Czechoslovak Academy of Sciences, Prague

(2)

creep effects, the author introduces the concept of equivalent strains, displacements, stresses, internal forces and couples, loads, critical pressures and temperature. Replacing the non-stationary temperature by an equivalent variable, he reduces the non-stationary problems to those with the stationary temperature fields.

In this manner, the stability problems of viscoelastic tubes at the thermal effects can be solved by the methods of linear or non-linear thermoelasticity in equivalent variables and then the actual variables can be determined according to the individual rheological laws. In this way, the solution with respect to time is separated from that with respect to the coordinates.

The equivalent stress components are defined by

$$\bar{\sigma}_{ij} = \tilde{A}\sigma_{ij} = a_0(T,t)\sigma_{ij} + a_1(T,t)\frac{\partial \sigma_{ij}}{\partial t} + a_2(T,t)\frac{\partial^2 \sigma_{ij}}{\partial t^2} + \cdots + a_m(T,t)\frac{\partial^m \sigma_{ij}}{\partial t^m} + \\ + a_{-1}(T,t)\int_{t_0}^{t} K(t-\tau)\sigma_{ij}(\tau)\,d\tau \qquad (1)$$

while for the equivalent strain, we have the relation:

$$\bar{\varepsilon}_{ij} = \tilde{B}\varepsilon_{ij} = b_0(T,t)\varepsilon_{ij} + b_1(T,t)\frac{\partial \varepsilon_{ij}}{\partial t} + b_2(T,t)\frac{\partial^2 \varepsilon_{ij}}{\partial t^2} + \cdots + b_n(T,t)\frac{\partial^n \varepsilon_{ij}}{\partial t^n} + \\ + b_{-1}(T,t)\int_{t_0}^{t} L(t-\tau)\,\varepsilon_{ij}(\tau)\,d\tau, \qquad (2)$$

where $\tilde{A}$ and $\tilde{B}$ are linear integro-differential operators which have in special cases the differential or integral forms, respectively. The coefficients a_k and b_k are constants or functions of time and temperature but they cannot in any way depend on the coordinates.

The definition of equivalent temperature is expressed by

$$\bar{T} = \tilde{C}T = c_0(T,t)T + c_1(T,t)\frac{\partial T}{\partial t} + c_2(T,t)\frac{\partial^2 T}{\partial t^2} + \cdots + c_p(T,t)\frac{\partial^p T}{\partial t^p} + \\ + c_{-1}(T,t)\int_{t_0}^{t} M(t-\tau)\,T(\tau)\,d\tau. \qquad (3)$$

Assuming that the temperature varies linearly with the distance z from the middle surface of the tube, we can write

$$T = \frac{T_1 + T_2}{2} + \frac{T_1 - T_2}{h}z = \theta_0 + \theta z, \qquad (4)$$

where T_1 is the temperature of the inner surface, T_2 is that of the outer surface and h is the thicknees of the tube.

It is worthwile to emphasize that the definitions of equivalent variables include in their integral terms all integral transforms whose concrete forms can be obtained after substitution of the appropriate kernels and limits of integration.

(3)

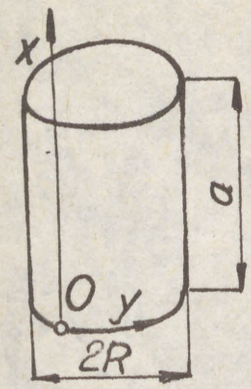

Fig. 1.

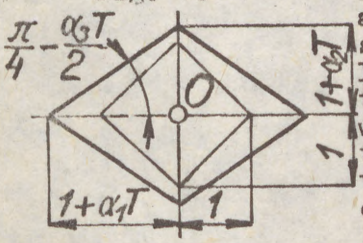

Fig. 2.

According to the notation of the scheme in Fig. 1, the equivalent strain-stress relations for the plane-stress state of the orthotropic viscoelastic tubes at the non-stationary thermal effects are expressed by

$$\bar{\varepsilon}_x = A_{11}\bar{\sigma}_x + A_{12}\bar{\sigma}_y + \alpha_1\bar{T}, \tag{5}$$

$$\bar{\varepsilon}_y = A_{21}\bar{\sigma}_x + A_{22}\bar{\sigma}_y + \alpha_2\bar{T}, \tag{6}$$

$$\bar{\varepsilon}_{xy} = A_{33}\bar{\sigma}_{xy} + \alpha_3\bar{T}. \tag{7}$$

In order to determine the relation between the coefficients α_1, α_2 and α_3, let us consider the thermal deformation of a prismatic element with the square cross-section shown in Fig. 2. This prismatic element is bounded by the planes parallel to the z-axis and forming the angles 45° with the x and y-axes. In the course of thermal deformation, the right angles between the sides of the initially square cross-section change for $\pi/2 - \alpha_3 T$ or $\pi/2 + \alpha_3 T$, respectively. From the geometrical relations in Fig. 2, we have

$$\tan\left(\frac{\pi}{4} + \frac{\alpha_3 T}{2}\right) = \frac{1+\alpha_1 T}{1+\alpha_2 T}, \quad \tan\left(\frac{\pi}{4} - \frac{\alpha_3 T}{2}\right) = \frac{1+\alpha_2 T}{1+\alpha_1 T}. \tag{8}$$

Replacing the tangents by the arcs of unit circle in radians, we get after rearranging the terms the resultant relation:

$$\alpha_3 = \alpha_1 - \alpha_2. \tag{9}$$

From Eqs. (5) to (7), we obtain the equivalent stress-strain relations:

$$\bar{\sigma}_x = \frac{1}{A_{11}A_{22} - A_{12}A_{21}}\left[A_{22}(\bar{\varepsilon}_x - \alpha_1\bar{T}) - A_{12}(\bar{\varepsilon}_y - \alpha_2\bar{T})\right], \tag{10}$$

$$\bar{\sigma}_y = \frac{1}{A_{11}A_{22} - A_{12}A_{21}}\left[A_{11}(\bar{\varepsilon}_y - \alpha_2\bar{T}) - A_{21}(\bar{\varepsilon}_x - \alpha_1\bar{T})\right], \tag{11}$$

$$\bar{\sigma}_{xy} = \frac{1}{A_{33}}(\bar{\varepsilon}_{xy} - \alpha_3\bar{T}), \tag{12}$$

i. e.

$$\bar{\sigma}_x = B_{11}\bar{\varepsilon}_x + B_{12}\bar{\varepsilon}_y + \beta_1\bar{T}, \tag{13}$$

$$\bar{\sigma}_y = B_{21}\bar{\varepsilon}_x + B_{22}\bar{\varepsilon}_y + \beta_2\bar{T}, \tag{14}$$

$$\bar{\sigma}_{xy} = B_{33}\bar{\varepsilon}_{xy} + \beta_3\bar{T}. \tag{15}$$

(4)

2. The Equivalent Equation of Compatibility

The equivalent strain-displacement relations in the case of large deformations of the circular tubes are expressed by

$$\bar{\varepsilon}_x = \frac{\partial \bar{u}}{\partial x} + \frac{1}{2}\left(\frac{\partial \bar{w}}{\partial x}\right)^2, \tag{16}$$

$$\bar{\varepsilon}_y = \frac{\partial \bar{v}}{\partial y} + \frac{1}{2}\left(\frac{\partial \bar{w}}{\partial y}\right)^2 - \frac{\bar{w}}{R}, \tag{17}$$

$$\bar{\varepsilon}_{xy} = \frac{\partial \bar{u}}{\partial y} + \frac{\partial \bar{v}}{\partial x} + \frac{\partial \bar{w}}{\partial x}\frac{\partial \bar{w}}{\partial y}, \tag{18}$$

where R is the radius of the tube and

$$\bar{u} = \tilde{B}u, \qquad \bar{v} = \tilde{B}v, \qquad \bar{w} = \tilde{B}w \tag{19}$$

are the equivalent displacements. The rheological operator $\tilde{B}$ has been introduced in Eq. (2).

Differentiating Eq. (16) twice by y, Eq. (17) twice by x and Eq. (18) by x and y, we get the equation of the equivalent compatibility:

$$\frac{\partial^2 \bar{\varepsilon}_x}{\partial y^2} + \frac{\partial^2 \bar{\varepsilon}_y}{\partial x^2} - \frac{\partial^2 \varepsilon_{xy}}{\partial x \partial y} = \left(\frac{\partial^2 \bar{w}}{\partial x \partial y}\right)^2 - \frac{\partial^2 \bar{w}}{\partial x^2}\frac{\partial^2 \bar{w}}{\partial y^2} - \frac{1}{R}\frac{\partial^2 w}{\partial x^2}. \tag{20}$$

Substituting for the equivalent strains Eqs. (5) to (7), we get

$$A_{11}\frac{\partial^2 \bar{\sigma}_x}{\partial y^2} + A_{33}\frac{\partial^2 \bar{\sigma}_{xy}}{\partial x \partial y} + A_{22}\frac{\partial^2 \bar{\sigma}_y}{\partial x^2} + A_{12}\frac{\partial^2 \bar{\sigma}_y}{\partial y^2} + A_{21}\frac{\partial^2 \bar{\sigma}_x}{\partial x^2} +$$

$$+ \alpha_1 \frac{\partial^2 \bar{\theta}_0}{\partial y^2} + \alpha_2 \frac{\partial^2 \bar{\theta}_0}{\partial x^2} + \alpha_3 \frac{\partial^2 \bar{\theta}_0}{\partial x \partial y} = \left(\frac{\partial^2 \bar{w}}{\partial x \partial y}\right)^2 - \frac{\partial^2 \bar{w}}{\partial x^2}\frac{\partial^2 \bar{w}}{\partial y^2} - \frac{1}{R}\frac{\partial^2 \bar{w}}{\partial x^2}. \tag{21}$$

Introducing the function of equivalent stresses expressed by

$$\bar{\sigma}_x = \frac{\partial^2 \bar{\Phi}}{\partial y^2}, \qquad \bar{\sigma}_y = \frac{\partial^2 \bar{\Phi}}{\partial x^2}, \qquad \bar{\sigma}_{xy} = -\frac{\partial^2 \bar{\Phi}}{\partial x \partial y}, \tag{22}$$

we finally obtain the first fundamental equation:

$$A_{22}\frac{\partial^4 \bar{\Phi}}{\partial x^4} + (2A_{12} + A_{33})\frac{\partial^4 \bar{\Phi}}{\partial x^2 \partial y^2} + A_{11}\frac{\partial^4 \bar{\Phi}}{\partial y^4} + \alpha_1 \frac{\partial^2 \bar{\theta}_0}{\partial y^2} + \alpha_2 \frac{\partial^2 \bar{\theta}_0}{\partial x^2} + \alpha_3 \frac{\partial^2 \bar{\theta}_0}{\partial x \partial y} =$$

$$= \left(\frac{\partial^2 \bar{w}}{\partial x \partial y}\right)^2 - \frac{\partial^2 \bar{w}}{\partial x^2}\frac{\partial^2 \bar{w}}{\partial y^2} - \frac{1}{R}\frac{\partial^2 \bar{w}}{\partial x^2}. \tag{23}$$

3. Equivalent Moments, Forces and Equilibrium

The equivalent strains due to the bending and twist are

(5)

$$\bar{\varepsilon}_{xB} = -z\frac{\partial^2 \bar{w}}{\partial x^2},\quad \bar{\varepsilon}_{yB} = -z\frac{\partial^2 \bar{w}}{\partial y^2},\quad \bar{\varepsilon}_{xyT} = -2z\frac{\partial^2 \bar{w}}{\partial x \partial y}. \tag{24}$$

The bending and twisting moments per unit length of the tube are in view of Eqs. (4), (13), (14), (15) and (24) given by

$$\bar{m}_x = \int_{-\frac{h}{2}}^{+\frac{h}{2}} \bar{\sigma}_x z\,dz = -\frac{h^3}{12}\left[B_{11}\frac{\partial^2 \bar{w}}{\partial x^2} + B_{12}\frac{\partial^2 \bar{w}}{\partial y^2} - \bar{\theta}(\beta_1+\beta_2)\right], \tag{25}$$

$$\bar{m}_y = \int_{-\frac{h}{2}}^{+\frac{h}{2}} \bar{\sigma}_y z\,dz = -\frac{h^3}{12}\left[B_{21}\frac{\partial^2 \bar{w}}{\partial x^2} + B_{22}\frac{\partial^2 \bar{w}}{\partial y^2} - \bar{\theta}(\beta_1+\beta_2)\right], \tag{26}$$

$$\bar{m}_{xy} = \int_{-\frac{h}{2}}^{+\frac{h}{2}} \bar{\sigma}_{xy} z\,dz = -\frac{h^3}{6}\left(B_{33}\frac{\partial^2 \bar{w}}{\partial x \partial y} - \bar{\theta}\beta_3\right). \tag{27}$$

The equivalent shear forces per unit length which are perpendicular to the middle surface of the tube are defined by

$$\bar{t}_x = \int_{-\frac{h}{2}}^{+\frac{h}{2}} \bar{\sigma}_{xz}\,dz, \qquad \bar{t}_y = \int_{-\frac{h}{2}}^{+\frac{h}{2}} \bar{\sigma}_{yz}\,dz. \tag{28}$$

The equations of the equivalent equilibrium have the form

$$\frac{\partial \bar{m}_x}{\partial x} + \frac{\partial \bar{m}_{yx}}{\partial y} - \bar{t}_x = 0, \tag{29}$$

$$\frac{\partial \bar{m}_{xy}}{\partial x} + \frac{\partial \bar{m}_y}{\partial y} - \bar{t}_y = 0. \tag{30}$$

From the sum of the projections of equivalent forces into the normal of the tube, we obtain (Volmir 1956, Sobotka 1986):

$$\frac{\partial \bar{t}_x}{\partial x} + \frac{\partial \bar{t}_y}{\partial y} + \bar{\sigma}_x h\frac{\partial^2 \bar{w}}{\partial x^2} + \bar{\sigma}_y h\left(\frac{1}{R} + \frac{\partial^2 w}{\partial y^2}\right) - 2\bar{\sigma}_{xy} h\frac{\partial^2 \bar{w}}{\partial x \partial y} + - \bar{q} = 0, \tag{31}$$

where

$$\bar{q} = \bar{A}q = a_0(T,t)q + a_1(T,t)\frac{\partial q}{\partial t} + \cdots + a_m(T,t)\frac{\partial^m q}{\partial t^m} + a_{-1}(T,t)\int_{t_0}^{t} K(t-\tau)q\,d\tau \tag{32}$$

is the time-varying internal pressure which is perpendicular to the middle surface of the tube.

Substituting for the equivalent stresses Eqs. (22) and for the equivalent shear forces their values from Eqs. (29) and (30), we obtain from Eq. (31) in view of Eqs. (25), (26) and (27) the second fundamental equation for the stability:

$$\frac{h^2}{12}\left[B_{11}\frac{\partial^4 \bar{w}}{\partial x^4} + 2(B_{12}+2B_{33})\frac{\partial^4 \bar{w}}{\partial x^2 \partial y^2} + B_{22}\frac{\partial^4 \bar{w}}{\partial y^4} -\right.$$

(6)

$$-(\beta_1+\beta_2)\left(\frac{\partial^2\bar{\theta}}{\partial x^2}+\frac{\partial^2\bar{\theta}}{\partial y^2}\right)-2\beta_3\frac{\partial^2\bar{\theta}}{\partial x\,\partial y}\Big]=$$

$$=\frac{\partial^2\bar{\phi}}{\partial y^2}\frac{\partial^2\bar{w}}{\partial x^2}-2\frac{\partial^2\bar{\phi}}{\partial x\,\partial y}\frac{\partial^2\bar{w}}{\partial x\,\partial y}+\frac{\partial^2\bar{\phi}}{\partial x^2}\left(\frac{1}{R}+\frac{\partial^2\bar{w}}{\partial y^2}\right)-\frac{\bar{q}}{h}. \tag{33}$$

4. The Equivalent Critical Pressures

Expressing approximately the equivalent deflection and temperature by

$$\bar{w}=\bar{w}_0\sin\frac{\pi x}{a}\sin\frac{y}{R},\qquad \bar{\theta}_0=\theta_i\sin\frac{\pi x}{a}\sin\frac{y}{R}, \tag{34}$$

where a is the length of the tube and substituting them into Eq. (23), we obtain after rearranging the terms:

$$A_{22}\frac{\partial^4\bar{\phi}}{\partial x^4}+(2A_{12}+A_{33})\frac{\partial^4\bar{\phi}}{\partial x^2\partial y^2}+A_{11}\frac{\partial^4\bar{\phi}}{\partial y^4}=$$

$$=\frac{\pi^2\bar{w}_0^2}{2a^2R^2}\left(\cos\frac{2\pi x}{a}+\cos\frac{2y}{R}\right)+\frac{\pi^2\bar{w}_0}{a^2R}\sin\frac{\pi x}{a}\sin\frac{y}{R}-$$

$$-\bar{\theta}_i\left[\left(\frac{\pi^2\alpha_2}{a^2}+\frac{\alpha_1}{R^2}\right)\sin\frac{\pi x}{a}\sin\frac{y}{R}-\frac{\pi\alpha_3}{aR}\cos\frac{\pi x}{a}\cos\frac{y}{R}\right]. \tag{35}$$

The particular solution of the foregoing equation can be sought in the following form

$$\bar{\phi}_1=C_1\cos\frac{2\pi x}{a}+C_2\cos\frac{2y}{R}+C_3\sin\frac{\pi x}{a}\sin\frac{y}{R}+C_4\cos\frac{\pi x}{a}\cos\frac{y}{R}. \tag{36}$$

Substituting it into Eq. (35) and comparing the coefficients of trigonometric functions, we obtain the constants:

$$C_1=\frac{\bar{w}_0^2a^2}{32\pi^2A_{22}R^2},\qquad C_2=\frac{\pi^2\bar{w}_0^2R^2}{32A_{11}a^2}, \tag{37}$$

$$C_3=\frac{a^2\left[\bar{w}_0-\bar{\theta}_i(\alpha_2R+\alpha_1\frac{a^2}{\pi^2R})\right]}{\pi^2R\left[A_{22}+2(A_{12}+A_{33})\frac{a^2}{\pi^2R^2}+A_{11}\frac{a^4}{\pi^4R^4}\right]},\quad C_4=-\frac{\alpha_3\bar{\theta}_ia^3}{\pi^3R\left[A_{22}+(2A_{12}+A_{33})\frac{a^2}{\pi^2R^2}+A_{11}\frac{a^4}{\pi^4R^4}\right]}. \tag{38}$$

The integral of the homogeneous equation can be expres- in the form

$$\bar{\phi}_2=-\frac{1}{2}py^2, \tag{39}$$

where p is the equivalent longitudinal pressure acting on the circular boundaries.

The general integral of Eq. (35) is then given by

$$\bar{\phi}=\frac{\bar{w}_0^2}{32}\left(\frac{a^2}{\pi^2A_{22}R^2}\cos\frac{2\pi x}{a}+\frac{\pi^2R^2}{A_{11}a^2}\cos\frac{2y}{R}\right)+$$

(7)

$$+\frac{a^2}{\pi^2 R\left[A_{22}+\left(2A_{12}+A_{33}\right)\frac{a^2}{\pi^2R^2}+A_{11}\frac{a^4}{\pi^4R^4}\right]}\left\{\left[\overline{w}_0-\right.\right.$$

$$\left.\left.-\bar{\theta}_i\left(\alpha_2 R+\alpha_1\frac{a^2}{\pi^2R}\right)\right]\sin\frac{\pi x}{a}\sin\frac{y}{R}-\frac{\alpha_3\bar{\theta}_i a}{\pi}\cos\frac{\pi x}{a}\cos\frac{y}{R}\right\}-\frac{1}{2}\bar{p}y^2. \quad (40)$$

Denoting by $\overline{\Psi}$ the function from Eq. (33):

$$\overline{\Psi}=\frac{h^2}{12}\left[B_{11}\frac{\partial^4\overline{w}}{\partial x^4}+2\left(B_{12}+2B_{33}\right)\frac{\partial^4\overline{w}}{\partial x^2\partial y^2}+B_{22}\frac{\partial^4\overline{w}}{\partial y^4}-\right.$$

$$\left.-\left(\beta_1+\beta_2\right)\left(\frac{\partial^2\bar{\theta}}{\partial x^2}+\frac{\partial^2\bar{\theta}}{\partial y^2}\right)-2\beta_3\frac{\partial^2\bar{\theta}}{\partial x\partial y}\right]-$$

$$-\frac{\partial^2\bar{\Phi}}{\partial y^2}\frac{\partial^2\overline{w}}{\partial x^2}+2\frac{\partial^2\bar{\Phi}}{\partial x\partial y}\frac{\partial^2\overline{w}}{\partial x\partial y}-\frac{\partial^2\bar{\Phi}}{\partial x^2}\left(\frac{1}{R}+\frac{\partial^2\overline{w}}{\partial y^2}\right)+\frac{\bar{q}}{h}. \quad (41)$$

we can express the Bubnov-Galerkin equation in the form:

$$\int_0^a\int_0^{2\pi R}\overline{\Psi}\sin\frac{\pi x}{a}\sin\frac{y}{R}\,dx\,dy=0. \quad (42)$$

Substituting Eqs. (34), (39) and (40) and integrating, we have

$$\frac{\pi aRh^2\overline{w}_0}{24}\left[\frac{\pi^4B_{11}}{a^4}+\frac{2\pi^2}{a^2R^2}\left(B_{12}+2B_{33}\right)+\frac{B_{22}}{R^4}\right]+$$

$$+\frac{\pi a\overline{w}_0}{R^2\left[A_{22}+\left(2A_{12}+A_{33}\right)\frac{a^2}{\pi^2R^2}+A_{11}\frac{a^4}{\pi^4R^4}\right]}\left[\overline{w}_0-\right.$$

$$\left.-\bar{\theta}_i\left(\alpha_2R+\alpha_1\frac{a^2}{\pi^2R}\right)\right]=\frac{\pi^2\bar{p}\,\overline{w}_0R}{2a}. \quad (43)$$

The equivalent critical longitudinal pressure follows from this relation in the following form:

$$\overline{p}_c=\frac{a^2h^2}{12\pi^2}\left[\frac{\pi^4B_{11}}{a^4}+\frac{2\pi^2}{a^2R^2}\left(B_{12}+2B_{33}\right)+\frac{B_{22}}{R^4}\right]+$$

$$+\frac{2a^2}{\pi^2R^3\left[A_{22}+\left(2A_{12}+A_{33}\right)\frac{a^2}{\pi^2R^2}+A_{11}\frac{a^4}{\pi^4R^4}\right]}\left[\overline{w}_0-\right.$$

$$\left.-\bar{\theta}_i\left(\alpha_2R+\alpha_1\frac{a^2}{\pi^2R}\right)\right]. \quad (44)$$

We can then see how the temperature decreases the stability.

(8)

5. The Actual Critical Pressures

The first-order rheological differential equation with variable coefficients

$$\overline{p_c} = a_0(T,t)p_c + a_1(T,t)\frac{\partial p_c}{\partial t} \tag{45}$$

yields the following expression for the actual critical longitudinal pressure

$$p_c = e^{-\int_{t_0}^{t}\frac{a_0(T,\tau)}{a_1(T,\tau)}d\tau}\left[\int_{t_0}^{t}\overline{p_c}(\tau)e^{\int_{t_0}^{\tau}\frac{a_0(T,\tau_1)}{a_1(T,\tau_1)}d\tau_1}d\tau + p_{c0}\right], \tag{46}$$

where p_{c0} is the initial critical pressure at the time t_0.

From the second-order rheological differential equation

$$\overline{p_c} = a_0 p_c + a_1\frac{\partial p_c}{\partial t} + a_2\frac{\partial^2 p_c}{\partial t^2}, \tag{47}$$

we obtain the actual critical pressure given by (Sobotka 1984)

$$p_c = \frac{e^{-\chi_1 t}}{\chi_2-\chi_1}\int_{t_0}^{t}\overline{p_c}(\tau)e^{\chi_1\tau}d\tau + \frac{e^{-\chi_2 t}}{\chi_1-\chi_2}\int_{t_0}^{t}\overline{p_c}(\tau)e^{\chi_2\tau}d\tau +$$

$$+\frac{p_{c0}e^{-\chi_2 t_A}-p_{cA}e^{-\chi_2 t_0}}{e^{-(\chi_1 t_0+\chi_2 t_A)}-e^{-(\chi_1 t_A+\chi_2 t_0)}}e^{-\chi_1 t} + \frac{p_{cA}e^{\chi_1 t_0}-p_{c0}e^{-\chi_1 t_A}}{e^{-(\chi_1 t_0+\chi_2 t_A)}-e^{-(\chi_1 t_A+\chi_2 t_0)}}e^{-\chi_2 t}, \tag{48}$$

where p_{cA} is the critical pressure at the time t_A and χ_1 and χ_2 are the reciprocal times of relaxation represented by the roots of the characteristic equation which are taken with opposite signs.

From the foregoing relations, we can see that the viscoelastic behaviour and temperature may sometimes affect the stability to a considerable extent.

References

[1] Sobotka, Z., 1984, Rheology of Materials and Engineering Structures. Elsevier, Amsterdam, Oxford, New York, Tokyo, pp. 552.

[2] Sobotka, Z., 1986, Stability of Orthotropic Cylindrical Shells. Second Regional Colloquium on Stability of Steel Structures, Hungary, Proceedings, Vol. II/1, pp. 195-202.

[3] Vol'mir, A. S., 1956, Flexible Plates and Shells (in Russian), Gostechteorizdat, Moskva, pp. 419.

(1)
TOCHÁČEK, Miloslav (1)
FERJENČÍK, Pavel (2)

FURTHER STABILITY PROBLEMS OF PRESTRESSED STEEL STRUCTURES

INTERNATIONAL COLLOQUIUM
STABILITY OF STEEL STRUCTURES
BUDAPEST, HUNGARY, 1990
PRELIMINARY REPORT

Summary: In the connection with the revision of the Czechoslovak national standard for designing prestressed steel structures /ON 73 1405/1989/ there were proposed and in the present paper are presented new formulae for checking stability and/or strength of (i) centrally compressed strut prestressed by concentric tendon; (ii) compressed flange of loaded plate girder prestressed by straight tendon; (iii) anchor zone of prestressed plate girder.

1. CENTRALLY COMPRESSED STRUT PRESTRESSED BY CONCENTRIC TENDON

An in-plane, Euler buckling is considered. Fig. 1a, b depicts the buckled shapes and the critical lengths L_{cr} of a pinned prestressed strut subject to two limit loading situations: (a) $N = 0$, $P > 0$; (b) $N > 0$, $P = 0$. Because of the play in the holes of the stabilization diaphragms, the theoretical critical length is to be increased to $L_{cr} = Ka$ in the case (a), usually with $K = 1.1$ to 1.2. For the intermediate case (c) $N > 0$, $P - X > 0$, the critical length $Ka < L_{cr} < L$ can be derived by the aid of the interaction diagram, Fig. 1c: The conditions that the actual forces in the situations (a) and (b) must not exceed the corresponding Euler loads are observed on the coordinate axes. The line connecting the terminal points 1-1 confines from above the safe region for the case (c). The linear border $m = 1$ is the most strict one and, at the buckling load $(N+P-X)_{cr}$, yields the critical length

---

(1) Principal Research Officer, Ing. CSc., Building Research Institute, Czech Technical University, Prague, Czechoslovakia
(2) Professor of Metal a. Timber Structures, Prof. Ing. CSc., Faculty of Civil Engineering, Slovak Technical University, Bratislava, Czechoslovakia

(2)
$$L_{cr} = a\sqrt{\frac{n^2 + K^2\varkappa}{1+\varkappa}} \quad ; \quad \varkappa = \frac{P_{-}X}{N} \quad ; \quad X = \frac{A_p E_p}{AE + A_p E_p} \quad . (1),(2),(3)$$

The ratio $\varkappa$ is calculated from the service loads, X is the statically indeterminate force in tendon from the load N.

Form. (1) can be obtained also analytically, by means of the principle of virtual work /Tocháček 1989/. A rigorous, but more complex solution /Tocháček-Ferjenčík 1977/ renders results which differ from Form. (1) less than by 3 %.

Rationally spaced stabilization diaphragms divide the length of a prestressed bar into segments with a uniform slenderness. A pinned bar of a constant cross-section has the diaphragms in equal distances a = (35 to 50) i. If the cross-section of a bar varies along its length, larger spacings $a = a_{min}\sqrt{I/I_{min}}$ correspond to larger moments of inertia. In a fixed-ended prestressed bar with a uniform cross-section, it should be $a_{ex} \doteq (1/0.7)\, a_{in} \doteq 1.4\, a_{in}$; here ex/in relate to the external/internal segments.

As follows from Form. (1), the prestressed tendon substantionally reduces critical length of a compressed bar even at small prestressing forces, e.g., at K = 1, $\varkappa$ = 1, n = 2 down to $L_{cr}/L = 0.791$, whilst an increase of the amount of the stabilization diaphragms has only a small effect: with n = 10 we obtain $L_{cr}/L = 0.711$. A favourable influence of their increased number is marked only at larger prestressing forces: at $\varkappa$ = 100, n = 2 we get $L_{cr}/L = 0.507$, but at n = 10 as little as $L_{cr}/L = 0.141$.

2. PLATE GIRDER PRESTRESSED BY STRAIGHT TENDON AT TENSION FLANGE

When the girder with a unisymmetrical cross-section, Fig. 2a right, is subjected only to the force from prestressing P, the latter may assume one of three critical values which correspond to (i) the loss of stability of Euler type, when the girder buckles like a bar, perpendicularly to the plane of its web; (ii) torsional buckling; (iii) lateral-torsional buckling /Tocháček-Ferjenčík 1977/. The most common type of buckling of an unloaded plate girder prestressed by a straight tendon at the tension flange 2 is similar to that one of a centrally prestressed bar.

A loaded girder without the prestressing cable represents the other limit case. This situation is characterized by the respective critical bending moment and treated in agreement with the standards for unprestressed steel structures by the aid of the coefficient of lateral-torsional buckling, /ČSN 73 1401/1985, cl. 38/.

The intermediate case is a prestressed and loaded girder. While the use of an interaction diagram relating both limit cases, similarly to Fig. 1c, gives some insight into this situation, two other, more instructive ways of calculation

(3)

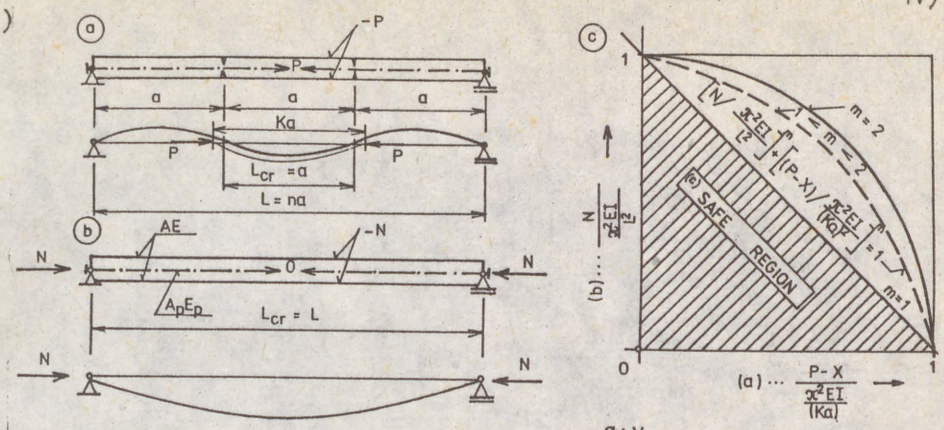

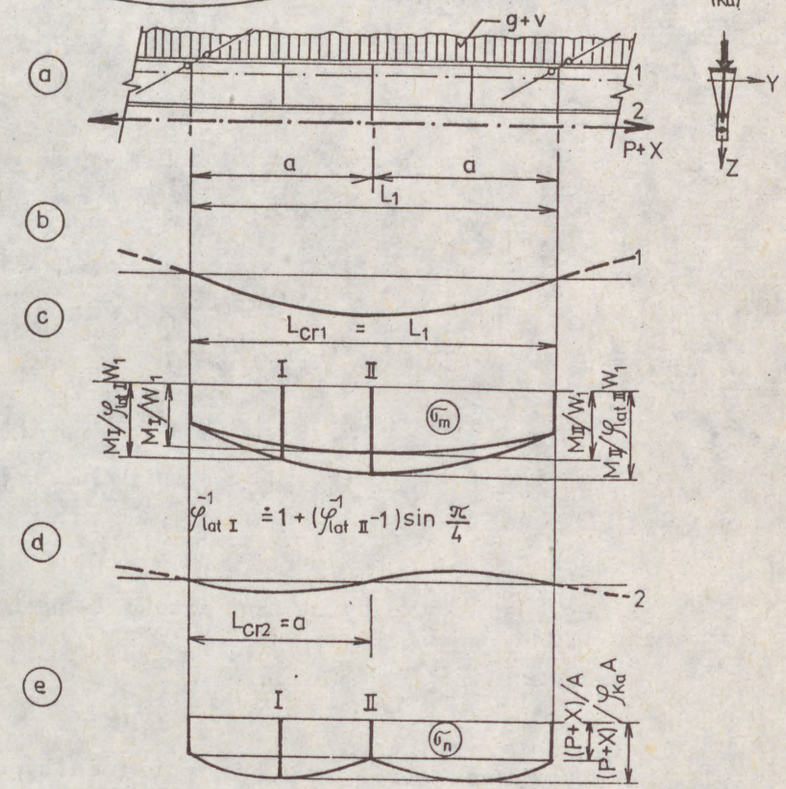

(I) $\sigma_{1I} = \frac{P+X}{\varphi_{Ka}\,A} + \frac{M_I}{\varphi_{lat\,I}W_1}$ (II) $\sigma_{1II} = \frac{P+X}{1 \cdot A} + \frac{M_{II}}{\varphi_{lat\,II}W_1}$

Fig. 1 Centrally compressed strut prestressed by concentric tendon; loading cases:
(a) N=0, P>0; (b) N>0, P = 0; (c) N>0, P-X>0

Fig. 2 (a) Plate girder prestressed by straight tendon at tension flange; (b), (d) buckled top, bottom flange; (c), (e) stress from bending, from normal force

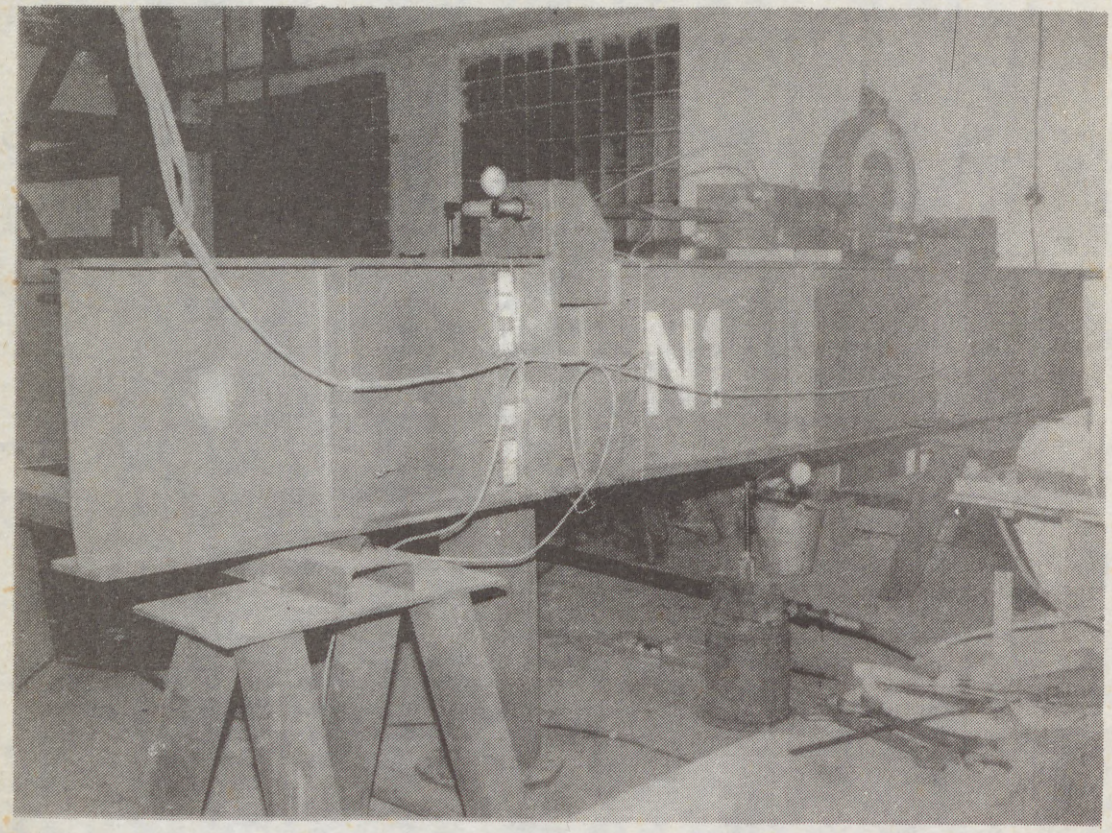

Fig. 3 Test girder N1 for verifying the actual behaviour of anchor zone

are preferred:

1st method: The compressed girder boom is replaced by a centrally compressed bar. Its cross-section with the area $A_T = A_1 + 15\ t_w$ consists of the compression flange 1 and 15 web thicknesses. The extreme design stress σ_T at the controid of the considered T-section due to load and total force P+X in tendon is calculated. The fictitious strut is checked for the compression force $A_T\ \sigma_T$; the critical length L_{cr} equals the distance of the laterally restrained sections being reduced with respect to the stress variation along the girder length /ČSN 73 1401/1985, Form. (II.11)/. The normal stress σ_T is considered in the most loaded section of the respective length segment between the lateral restraints of the compression flange 1.

2nd method: Form. (30) of /ČSN 73 1401/1985/, observing

(5)
a combined effect of normal force and bending, can be adopted for the examined case,

$$\frac{P+X}{\varphi_{Ka}(x).A} + \frac{M}{\varphi_{lat}(x).W_1} \leq R_d \quad . \qquad (4)$$

Extreme design loads are to be considered. The statically indeterminate force X due to external loading follows from the compatibility condition of deformations. The buckling or lateral buckling coefficients for the critical section (in Fig. 2: section I or II) may be calculated from an approximate relationship

$$\varphi^{-1}(x) = 1 + [\varphi^{-1}(L_{cr}/2) - 1] \sin \frac{\pi x}{L_{cr}} \quad ; \qquad (5)$$

the origin of the x-coordinate is at the beginning of the buckled segment.

3. ANCHOR ZONE OF PRESTRESSED PLATE GIRDER

Stability and strength of the anchor zone of a prestressed plate girder, where large concentrated forces are transmitted from the tendon through the bracket into the girder, represent a special group of problem. Normal and shear stresses σ_x, σ_z and τ_{xz} vary nonlinearly along the girder web within the length of approximately two web depths $2h_w$. The analysis may be based on various approaches /Ferjenčík et al. 1983, 1985, 1988/, as on the Vlasov s theory of warping torsion of thin-walled sections for calculating the elementary stresses; mathematical theory of elasticity for analyzing local stresses /Lampsi 1987/; FEM; theory of folded plates /Scordelis 1961/, etc.

Theoretical findings were verified experimentally on the test girders 4000 mm long and 464 mm deep, with the anchoring brackets 2000 mm apart, Fig. 3 /Ferjenčík et al. 1985, 1988/. The anchoring brackets were either single-webbed, connected by friction-grip bolts (N2, 4, 6, 8) or double-webbed and welded (N1, 3, 5, 7), Fig. 4. The girder web was provided by 2 (N1, 2, 3, 4, 5, 7), or 1 (N8), or 0 (N6) stiffeners. - It was the arrangement with a welded, double-webbed bracket and with a pair of vertical stiffeners of the girder web (N1 and 3) which rendered optimal results, both from the constructional and statical views. The type with a single-webbed bracket and FG bolts (N4) granted less satisfaction, while the remaining constructional solutions (N2, 5, 6, 7, 8) cannot be recommended. Increasing the bracket length e leads to smaller stresses; best results were achieved with the lengths e = (0.5 to 1) h_w and e = (2 to 4) f. Welding of the bracket end plate to the girder flange should be avoided.

(6)

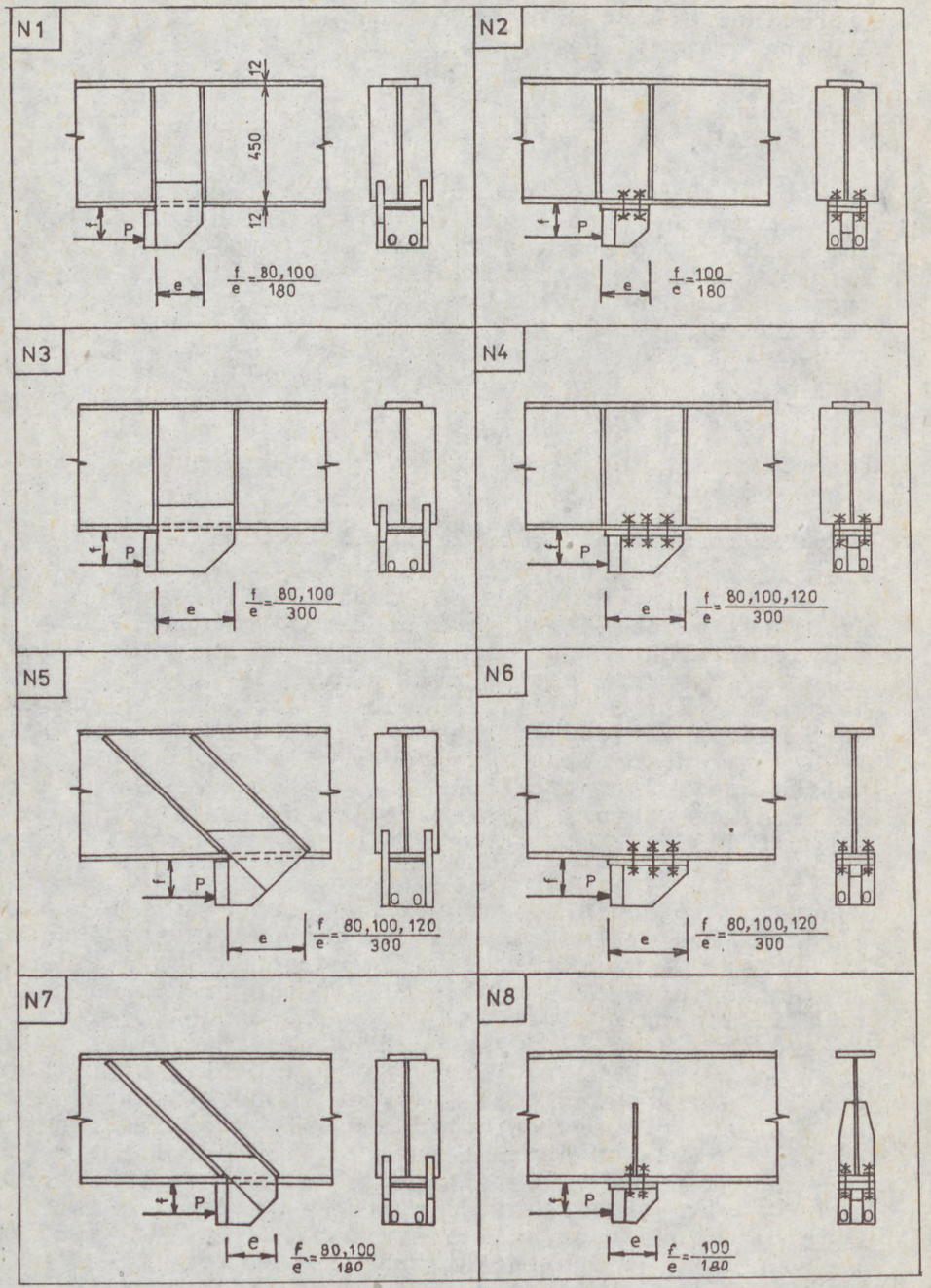

Fig. 4 Various arrangements of anchor zone

(7)

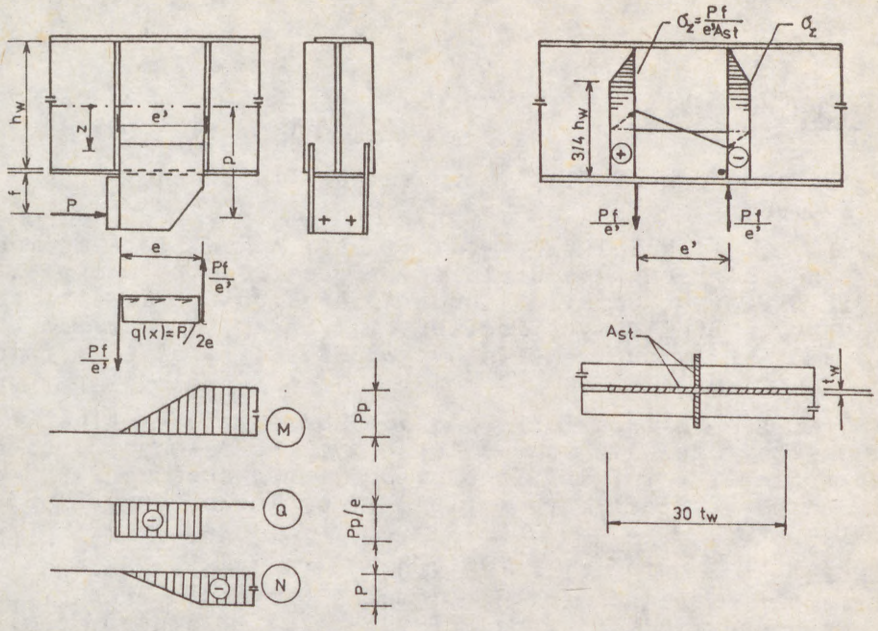

Fig. 5 Anchor zone, type N1 or N3: linearized distribution of internal forces M, Q, N and of stress

Fig. 5 portrays the linearized distribution of internal forces and stresses in the anchor zone of the type N1 or N3. The most stressed is that spot of the web, which is marked by a dot • :

$$\sigma_{eq} = \sqrt{\sigma_x^2 + \sigma_z^2 - \sigma_x \sigma_z + 3\tau^2} \leq 1.1 R_d \,, \qquad (6)$$

where

$$\sigma_x = \frac{P}{A} + \frac{P_{pz}}{I} \,; \quad \sigma_z = \frac{P_f}{A_{st} e} \,; \quad \tau_{xz} = \frac{P_p}{et} \frac{S}{I} \,. \quad (7),(8),(9)$$

The stability of the girder web and stiffeners in the anchor zone is to be checked in accordance with Chapt. VII of /ČSN 73 1401/1985/.

(8)

REFERENCES

ČSN 73 1401 Design of Steel Structures. (In Czech.) Praha, Vyd. ÚNM 1985

FERJENČÍK, P. - ARJESTOVIČ, A.I. et al.: Actual Behaviour of Anchor Zone of Prestressed Plate Girders from the Viewpoint of Their Different Constructional Arrangements. (Res. report, in Slovak.) = Bratislava, Fac. of Civ. Engng, Slovak Tech. Univ. 1988. (Previous reports by FERJENČÍK, P. et al.: ibid 1980, 1983, 1985)

FERJENČÍK, P. - BALÁŽ, I.: Predeĺnoe sostoyanie v oblasti lokaĺnogo zagruzheniya sosredotochennymi normaĺnoy i tangentsiaĺnoy silami. = In: 1st Intern. Correspondence Conf. "Design Limit States of Steel Structures". Brno, Techn. Univ. 1983, Vol. II

FERJENČÍK, P. - BALÁŽ, I. - KRIVÁČEK, J.: Theoretical and Experimental Ascertainment of State of Stress in Anchor Zone of Prestressed Plate Girders. (In Slovak.) = "Staveb. Čas." 33, 1985, No 8

LAMPSI, B.B.: Prochnosť tenkostennykh metallicheskikh konstruktsiy. Moscow, Stroyizdat 1987

ON 73 1405 Design of Prestressed Steel Structures. (In Czech.) Praha, Vyd. norem 1989

SCORDELIS, A.C.: Experimental and Analytical Study of a Folded Plate. = "Proc. ASCE, Struct. Div.", Dec. 1961

TOCHÁČEK, M.: Steel Trusses with Independently Prestressed Members. =In: "VII międzynarodowa konferencja naukowotechniczna Konstrukcje metalowe", Gdansk 1989

TOCHÁČEK, M. - FERJENČÍK, P.: The Stability Problems of Prestressed Steel Structures. = In: "Regional Colloquium on Stability of Steel Structures". Theme 7, Prepared Discussion. Budapest-Balatonfüred 1977.


Insignia Liberæ Regiæ Me
=icopolit ana Civitatis Budensis

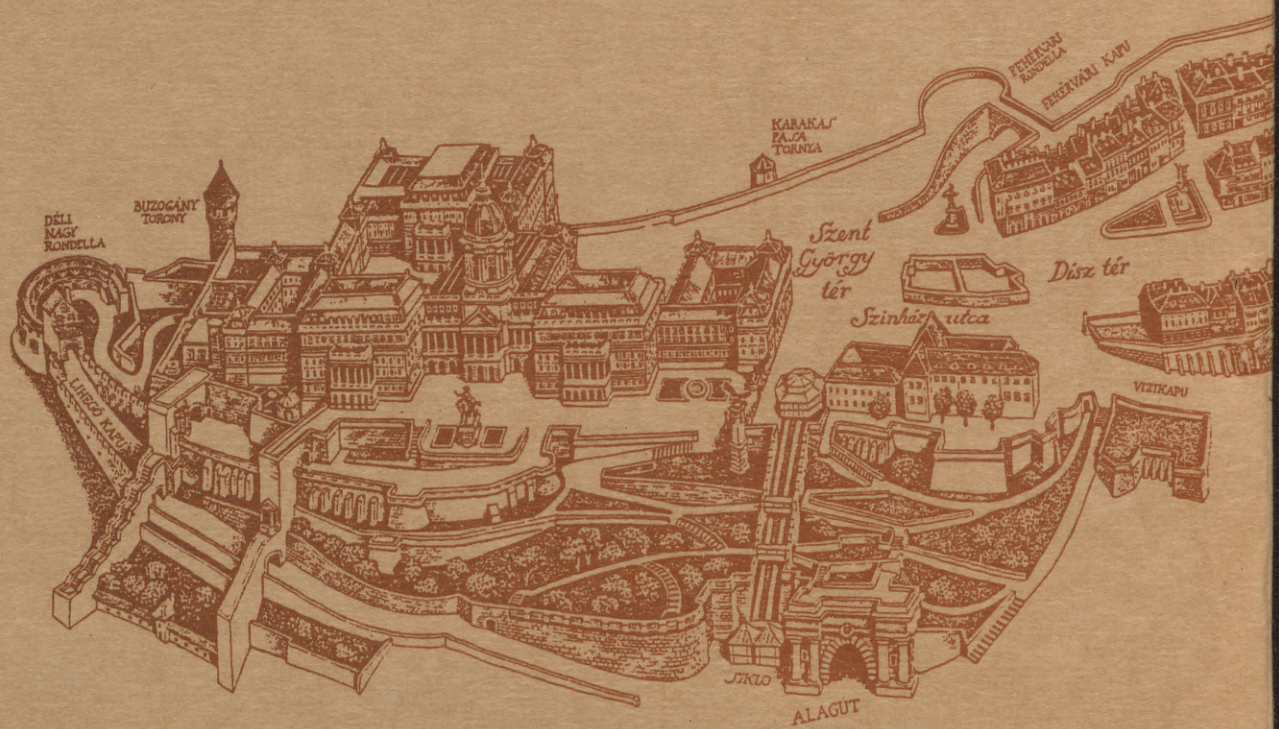
DÉLI NAGY RONDELLA
BUZOGÁNY TORONY
KARAKAS PAJZA TORNYA
FEHÉRVÁRI RONDELLA
FEHÉRVÁRI KAPU
Szent György tér
Dísz tér
Színház utca
VÍZIKAPU
LIONGÓ KAPU
SIKLÓ
ALAGÚT

INTERNATIONAL COLLOQUIUM

STABILITY OF STEEL STRUCTUR

HUNGARY, BUDAPEST 19

PRELIMINARY REPORT

VOLUME IV.